Simulation, testing and design of a fully adhesive bonded flat plate solar collector for highly automated production

Hermann Riess

A thesis submitted in partial fulfilment
of the requirements of De Montfort University
for the degree of Doctor of Philosophy (PhD)

February 2017

Institute of Energy and Sustainable Development
De Montfort University Leicester

Institute of new Energy Systems
Technische Hochschule Ingolstadt

Declaration

I declare that the content of this submission is my own work. The contents of the work have not been submitted for any other academic or professional award. I acknowledge that this thesis is submitted according to the conditions laid down in the regulations. Furthermore, I declare that the work was carried out as part of the course for which I was registered at *De Montfort University*, United Kingdom from January 2012 until February 2017. I draw attention to any relevant considerations of rights of third parties.

Abstract

This thesis presents simulation results and experimental data for a collector type with an all-round supported absorber and a fully adhesive edge bond that is produced on a highly automated production line. A literature review discussing measures to reduce the convective heat loss in flat plate collectors as well as on the status quo of the collector production was conducted. It was determined that an adaption of an existing automated production technique from the insulated glazing industry opens new paths towards a collector design allowing a mass production and an improved thermal collector efficiency. Within the thesis, the thermal and mechanical behaviour as well as the applied production method for this collector type are discussed.

By implementing and validating a finite element model of the collector, the absorber deflection was analysed, different calculation approaches compared and conclusions drawn on the pressure change in the cavity of gas-filled collectors. Unlike stated in the literature, it was found that the thermal elongation of an all-round supported absorber has a considerable effect on the overall collector performance. Based on these conclusions, an optimised sheet-pipe absorber structure is introduced allowing a predictable absorber deflection and, thus, reduced chance of contact between absorber and glazing in collectors. The findings of the thermal simulation and, in particular, on the convective heat transfer confirmed the reliability of a recently extended convection calculation approach for solar collectors. Even though the gas-filled collector is capable of a superior thermal performance, simulation and testing results could not confirm the calculated efficiency increase given in recent literature. In comprehensive testing, the strengths and weaknesses of different batches of prototypes are discussed. Based on an economic analysis considering the collector production costs and the solar yield, the new approach was compared to a conventional solar collector.

Acknowledgements

I would like to express my gratitude to Prof Rick Greenough and Prof Wilfried Zörner. Rick guided me with his constructive criticism and positive manner in an ideal way through this work. Wilfried initiated this work and gave me support whenever needed. Without their support, this work would have not been possible.

Moreover, I am very grateful for the friends who accompanied and supported me since my first day at the research institute, particularly Dr Christoph Trinkl, Dr Sebastian Brandmayr, Dr Holger Müller, Matthias Sonnleitner and Dr Christoph Reiter.

I would also like to thank the ‘newer’ colleagues, which made the institute much more than just a place to work: Daniel Beckenbauer, Jonas Busch, Mathias Ehrenwirth, Thomas Duschner, Dr Michael Klärner and Matthias Stark.

The patience, motivation and support from my whole family helped me to carry on with my work and made things much easier.

Most importantly, I want to express my heartfelt thanks to my wife Veronika for her unconditional and enduring support, her encouragement and love. In the end, this helped me to accomplish my work and I cannot thank you enough for this.

Table of Contents

List of Figures

List of Tables

Abbreviations

Al	Aluminium
Ar	Argon
ARC	Anti-reflective coating
CAD	Computer aided design
CARNOT	Conventional and renewable energy systems optimisation block set
CPC	Compound parabolic collector
Cu	Copper
ETFE	Ethylene tetrafluoroethylene
FE	Finite element
FEM	Finite element method
FEP	Fluorinated ethylene propylene
IEA	International energy agency
IGU	Insulated glazing unit
ISE	Institute for solar energy
Kr	Krypton
low-e	Low-emissivity
NREAPs	National renewable energy action plans
PET	Polyethylene terephthalate
RB	Roll bond

Ref	Reference
SAH	Solar assisted heating
TPS	Thermoplastic spacer
UV	Ultraviolet
Xe	Xenon

Symbols

a	Distance neutral axis	mm
A	Area	m^2
a_1	Linear heat loss coefficient	W/m^2K
a_2	Quadratic heat loss coefficient	W/m^2K^2
b	Width	mm
c_p	Specific heat capacity	J/kgK
D	Diameter	mm
d	Distance, gap size	mm
E	Young's modulus	MPa
F'	Plate efficiency factor	-
g	Gravity	m/s^2
G	Solar irradiance	W/m^2
Gr	Grashoff number	-
h	Heat transfer coefficient, height	W/m^2K / mm
J	2^{nd} moment of area	mm^4
$\dot{m}$	Mass flow	kg/s
n	Number of points	
Nu	Nusselt number	-
p	Pressure	Pa
Pr	Prandtl number	-

Symbols

$\dot{q}$	Heat transfer rate	W
Ra	Rayleigh number	-
s	Gap size, standard deviation	mm
s^2	Variance	
S	Steiner's theorem	m^4
t	Thickness, student t's parameter	mm
U	Loss coefficient	W/m^2K
v	Velocity	m/s
V	Volume	m^3
W	Section modulus	m^3
w	Deflection	mm
x	Coordinate	mm
z	Coordinate	mm
α	Absorption	-
β'	Volume expansion coefficient	1/K
γ	Collector costs	€
Δ	Difference / Change	-
ε	Emission coefficient	-
η	Efficiency	-
η_0	Zero loss coefficient	-
ϑ	Relative collector costs	-
λ	Heat conductance	W/mK
ν	Poisson's ratio, kinematic viscosity	- / Pa s

μ	Confidence level	
ρ	Density	kg/m^3
τ	Transmission coefficient	-
ϕ	Collector slope	°
φ	Beading degree	-

Subscripts

abs	Absorber
amb	Ambient
back	Backside
bottom chord	Bottom chord
c	Convection
col	Collector
con	Convection
concept	Concept
conv	Convection
convFPP	Conventional flat plate collector production
critical	Critical
design	Design
diff	Difference
displ	Displacement
e	Edge
exp	Expansion
f	Front, fluid
g	Glazing
glazing	Glazing
i	Placeholder
init	Initial

ins	Insulation
irr	Irradiation
lts	Long-term service
max	Maximum
mean	Mean
R	Rectangular
sheet	Sheet
steiner	Steiner
sts	Short-term service
t	Total
T	T-beam
top chord	Top chord
use	Useful
wind	Wind
z	Coordinate

1 Introduction

1.1 Research background

Assuming a further growth of the solar thermal collector sector by tapping new markets, the industry will be confronted with increasing sales, higher quality demands and rising competition. However, industry analyses show that currently available collectors are suboptimal with respect to mass production (Müller and Zörner 2009, 2010). According to industry experts, this is due to the present collector design (Müller and Zörner 2010, Epp and Berner 2010, Epp 2012). To overcome this and to manage the changeover to an industrialised collector production, new collector designs suitable for high volume automated production need to be evaluated. Against this backdrop, a great potential is seen in adhesive technologies (Epp and Berner 2010, Epp 2012). Production technologies based on the use of adhesive bonding provide a considerable degree of production flexibility and can be highly automated. Beyond that, the application of new production methods can allow new collector designs. Collector advancements need to combine higher efficiencies at a competitive price structure, which are, ultimately, target properties in this thesis.

1.2 Objective of the research

The objective of the thesis is to spread knowledge gained throughout the design, testing and simulation of a flat plate collector with an all-round supported absorber that is bonded via a fully adhesive edge bond to the cover and manufactured on a highly automated production line. Figure 1.1 shows a schematic cross section of a sheet-pipe absorber, which is bonded via an adhesive edge bond to the glazing.

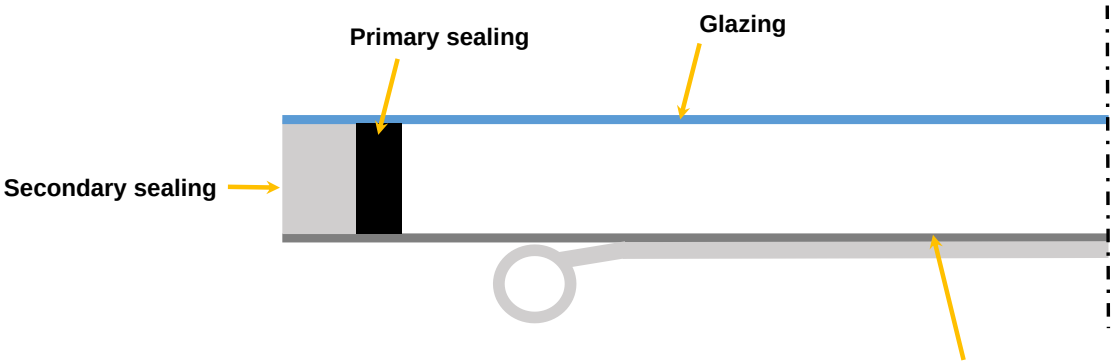

Figure 1.1: Schematic cross section of a fully adhesive edge bond for a collector with an all-round supported absorber

An adhesive gluing technique, widely used in the glazing industry, was investigated for its application to solar collectors. Using the adhesive production technique, collector prototypes were assembled and analysed in laboratory tests. As the research focussed on a collector type with a fully adhesive edge bond, the ‘interspace’ or ‘gap’ between absorber and glazing is hermetically sealed and filled with an inert gas. However, given in the nature of this collector type, the superposition of various influences led to considerable elastic absorber buckling. Thus, a finite element (FE) model was set up to analyse the mechanical behaviour of the collector. Based on the validated FE model, measures for a predictable absorber deflection were derived allowing a collector design with short distances between absorber and glazing. In addition, the research discusses the overall performance of a gas-filled solar collector. In laboratory and outdoor testing as well as in numerical simulations, the collector usability, efficiency and the convective heat transfer for such a collector type were thoroughly investigated. By comprehensive testing, the thermal collector simulation model was validated and the outcomes were compared with recent research results in this field. The experiences with this collector type and collector production are summarised and can be used as basis for further research or development.

1.3 Methodology and identified research gaps

The thesis focuses on the evaluation of gas-filled solar collectors at ambient pressure, which can be produced on a highly automated production line. Figure 1.2 shows the applied methodology in the thesis.

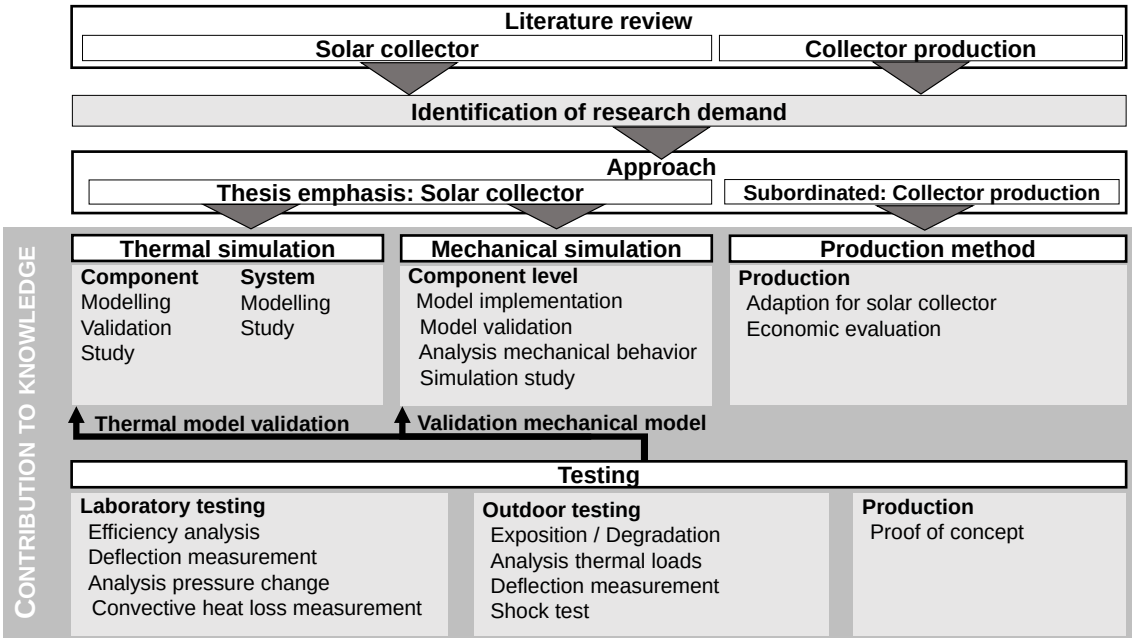

Figure 1.2: Research methodology

The following methodology has been applied to achieve the research objectives:

- Literature review on solar collectors with a focus on convective heat loss reducing measures and the status-quo of the collector production
    - Justification of the need for research in the field of gas-filled solar collectors and collector production
    - Identification of the research gaps
- Introduction of the followed approach of both collector design and production method
- Implementation of a thermal and mechanical collector model for analysing the research gaps
- Validation of the models by extensive prototype testing
- Deduction of insights for the collector design and production method
- Summary of the deduced knowledge on gas-filled solar collector and an adapted production method for solar collector in the conclusions

Within this thesis, research gaps concerning gas-filled collectors at ambient pressure were identified; however, certain research gaps and findings are applicable for conventional flat plate collectors as well. The thesis addresses those gaps, whereas the outcomes of this research programme represent the contribution to knowledge. Figure 1.3 summarises the identified research gaps.

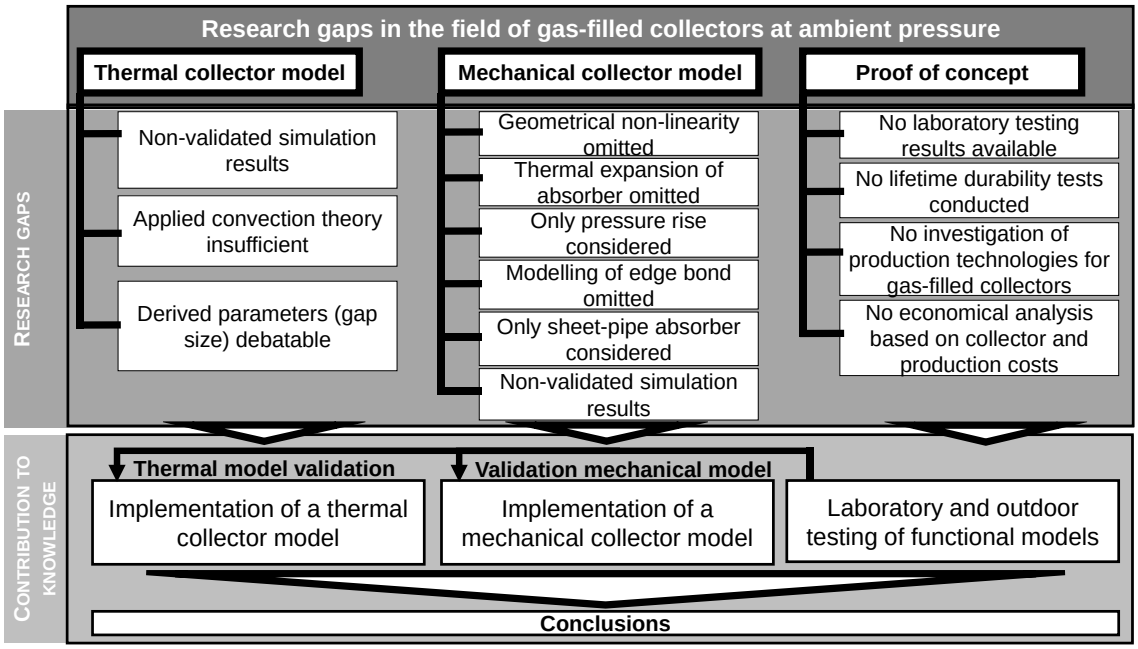

Figure 1.3: Identified research gaps within the thesis for gas-filled collector and the anticipated fields of the contribution to knowledge

Eventually, the literature review and the identification of the research gaps led to three research questions that are dealt with in this thesis:

- Is there a more suitable design of solar thermal collectors for mass production?
    - Addressed in chapter 3, 6 and 8
- How would such a design perform mechanically?
    - Addressed in chapter 4, 6 and 7
- How would such a design perform thermally?
    - Addressed in chapter 5 and 6

In the following, the relation between these three research questions and the chapters in this thesis are explained in brief.

Suitable design for solar thermal collectors for mass production

The question concerning a suitable mass production technology as well as the adaption of the collector design to it is discussed in chapter 3. In chapter 6, the assembly of the proposed collector design on the adapted production method for insulating glazing units is documented as a proof of concept. Finally, the applied production method is in terms of economically aspects compared and evaluated to a conventional flat plate collector production in chapter 8.

Mechanical analysis of hermetically sealed collector with a fully adhesive edge bond

Chapter 4 and 6 cover the mechanical performance of the proposed collector design. A case study that introduces possible ways to optimise a sheet-pipe absorber in terms of reducing deflection and buckling is presented in chapter 7.

Thermal analysis of a hermetically sealed collector with a fully adhesive edge bond

Chapter 5 addresses the thermal performance of a hermetically sealed collector with a gas-filled cavity between absorber and glazing. The extensive analysis comprises a simulation part as well as several laboratory tests of prototypes and is further extended with results from outdoor testing in chapter 6.

2 Literature review

2.1 Flat plate solar collectors

In the early 80s, solar thermal collectors were primarily utilised for domestic hot water preparation. During the last two decades, solar collectors have been more and more embedded as solar assisted heating (SAH) systems which have become popular for reasons of rising energy costs and environmentalism. Because of these circumstances, new markets for solar systems will be tapped. In particular, the provision of solar energy in district heating networks, industrial processes and cooling will be of greater importance.

For the various applications of solar collectors their optimal collector operation point have to be considered. Solar collectors can be divided in four major temperature operating ranges (Table 2.1).

Table 2.1: Categorisation of four major operating temperature ranges for solar thermal collectors

Operation range in °C	Application	Collector type
0 to 40	Pool heating, heat pump application	Mostly unglazed collectors (Pool absorber)
40 to 90	Domestic hot water preparation, SAH, low temperature processes (e.g. desiccation), solar cooling, water desalination	Flat plate collectors or evacuated tube collectors
70 to 150	Process heat (solar cooling, steam generation)	High efficiency flat plate collectors (anti-reflective coated glazing, excellently insulated) or evacuated tube collectors
90 to 250	High temperature process heat applications	Tracking and concentrating collectors (parabolic trough or Fresnel collectors)

Since the very beginning of the production of solar collectors, only minor changes in the design were implemented. Casings of solar thermal collectors are either designed as a frame configuration or a deep-drawn trough as shown in Figure 2.1.

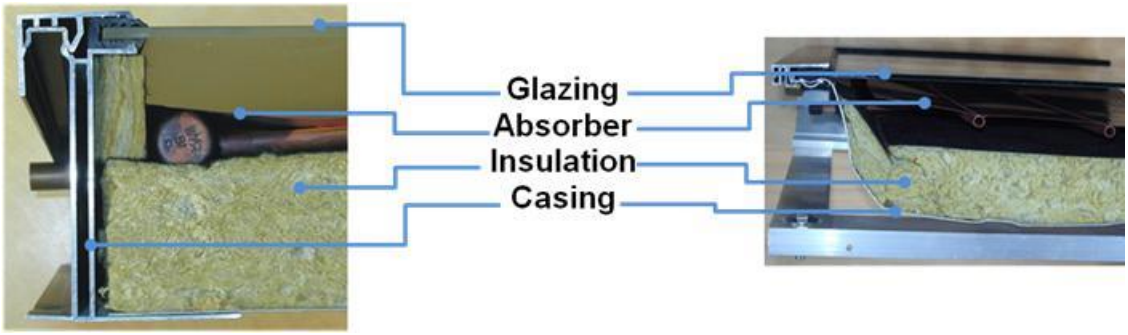

Figure 2.1: Components of a flat plate solar collector

The common casing material for framed collectors is aluminium. For integrated roof collectors wood frames are also applied. Trough collectors are made of aluminium, polymers or stainless steel (Figure 2.2).

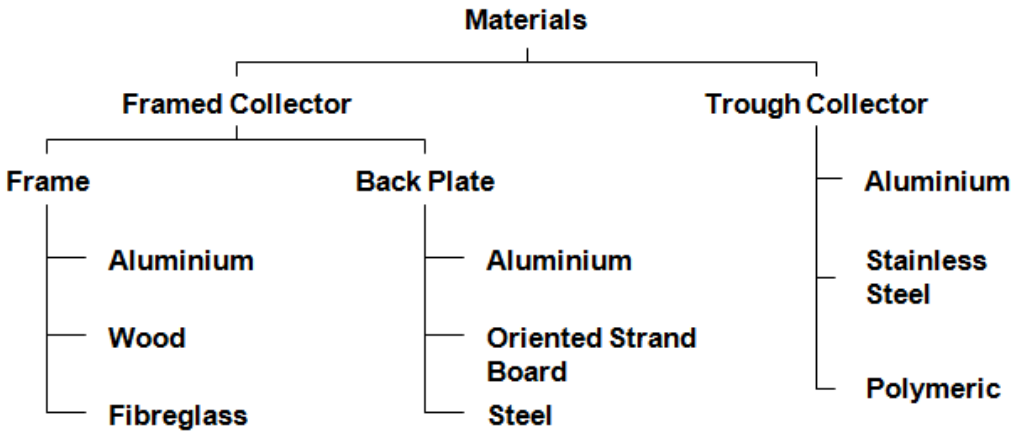

Figure 2.2: Overview of materials for the collector casing

The biggest market share for solar collectors is held by framed collectors. This is a result of the inflexible size of trough collectors and the high investment costs for the tools, such as the moulding die.

Table 2.2 characterizes the significant advantages and disadvantages of the different solar collector configurations.

Table 2.2: Summary of the assets and drawbacks of different collector designs

	Frame design	**Trough design**	**Wooden frame design**
Advantages	↑ High flexibility ↑ Low investment (Tools)	↑↑ Simple assembly ↑↑ Low weight ↑ Few sealing points	↑↑↑ Low investment ↑↑↑ Low material costs ↑ Ecological material
Disadvantages	↓ Complex assembly ↓ Many sealing points	↓↓ No flexibility in size ↓↓ High investment (moulding die)	↓ Complex assembly ↓ Many sealing points ↓↓↓ No weather exposure possible

To reduce the heat loss thermal insulation is inserted into the casing. The layer thickness varies depending on the application from 30 mm to 60 mm at the back of the collector and up to 30 mm along the sides. Some binders of insulation materials are known to degas at high temperatures. Consequently, a film on the glazing caused by the binding material can worsen the transmission property of the glazing. The used insulation material is chosen by its thermal conductivity, density, temperature stability and costs. In most cases mineral wool is used.

Table 2.3 shows an extract of some parameters of common insulation materials.

Table 2.3: Parameters of different insulation materials

Material	Density in kg/m³ (range)		Thermal conductivity in W/mK	Temperature operating range in °C
Glass wool	20	153	0.035 to 0.045	> 1000
Rock wool	22	200	0.035 to 0.045	> 1000
Foam glass	100	165	0.040 to 0.060	430
Expanded Polystyrene	10	35	0.035 to 0.040	100

The absorber is, ultimately, an array of pipes welded to a sheet metal. Its main function is collecting solar radiation and converting it into heat. The stored heat in the absorber is transferred to a fluid circulating through the pipe array on the back of the absorber sheet. Usually, the heat exchanger fluid is a water-based freeze resistant liquid; however, there are also applications using thermal oil or even air. In this work, the focus is put on conventional non-concentrating solar flat plate collectors with a water based heat transfer medium.

In the following sections, the principle equations of solar collectors are elucidated. A comprehensive compendium of solar thermal collectors can be found in Duffie and Beckmann (1991), Goswami et al. (2000), Eisenmann (2003) or Eicker (2001).

The conversion of sun light into thermal energy comes along with different loss mechanisms (Figure 2.3).

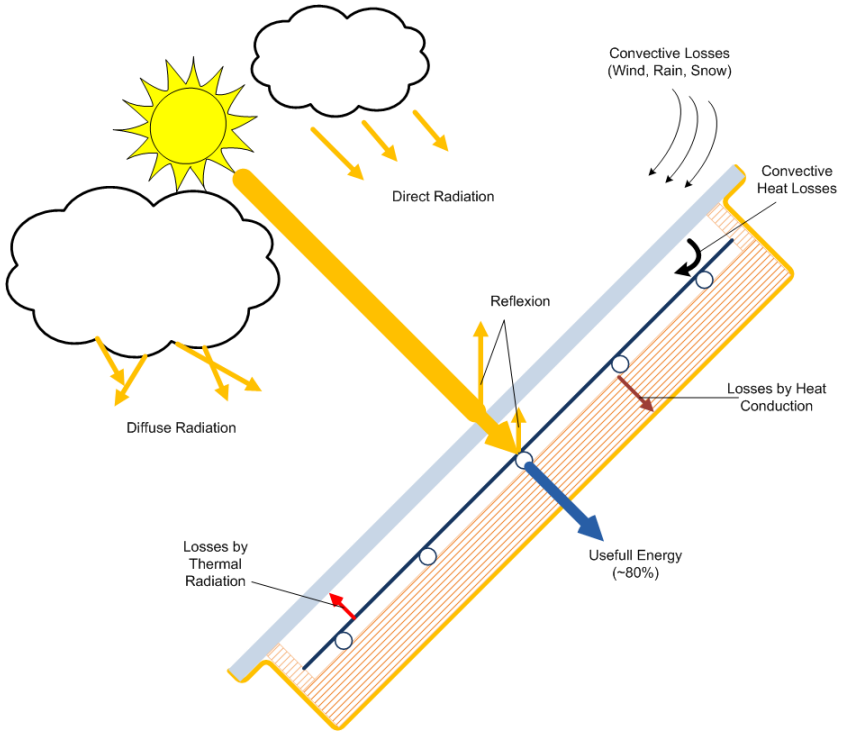

Figure 2.3: Thermal and optical losses on a flat plate solar collector (Brandmayr 2012)

The loss mechanisms can be divided into a thermal and an optical part. The absorbed solar radiation on the absorber surface is dependent on the transmission coefficient τ of the glazing and the absorption coefficient α of the absorber:

$$G = I \cdot (\tau\alpha) \qquad \text{Equation 2-1}$$

The thermal losses of a flat plate collector can be subdivided into conductive, radiative and convective mechanisms resulting in the network shown in Figure 2.4.

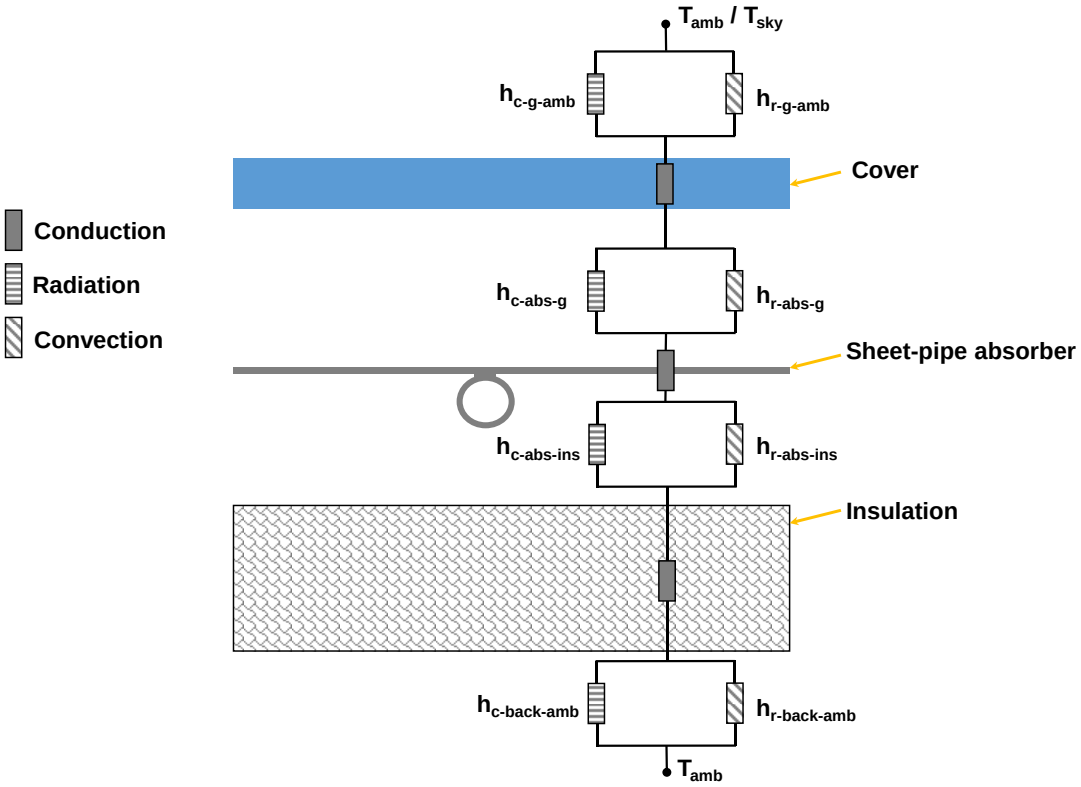

Figure 2.4: Principal thermal losses in a schematic flat plate solar collector

Forced Convection occurs between ambient and the outer surface of the glazing ($h_{c\text{-}g\text{-}amb}$) whereas free convection takes place between absorber and inner surface of the glazing ($h_{c\text{-}abs\text{-}g}$).

Radiative heat losses appear between the outer surface of the glazing and the sky ($h_{r\text{-}g\text{-}amb}$) and between absorber and inner surface of the glazing ($h_{r\text{-}abs\text{-}g}$). The radiative heat loss of the surface facing the surrounding of the glazing is driven by the sky temperature, which is below the ambient temperature. In analogy, the same applies for the backside of the absorber: A radiation exchange exists within the back of the absorber and the insulation material ($h_{r\text{-}abs\text{-}ins}$) as well as between the back plate of the collector and ambient ($h_{r\text{-}back\text{-}amb}$).

There is convection between the back of the absorber and the insulation ($h_{c\text{-}abs\text{-}ins}$) and forced convection between the back plate of the collector and ambient ($h_{c\text{-}back\text{-}amb}$).

The thermal losses are summarised in the total heat loss coefficient U_t, which is driven by the difference of the absorber temperature T_{abs} and ambient

temperature T_{amb}. Consequently, the collector performance per aperture surface $\dot{q}_{col}$ can be expressed as:

$$\dot{q}_{col} = G - U_t(T_{\mathrm{abs}} - T_{amb}) \qquad \text{Equation 2-2}$$

The collector efficiency is defined by the relation of the current collector performance $\dot{q}_{col}$ and the global solar radiation G:

$$\eta = \frac{\dot{q}_{col}}{G} = (\tau\alpha) - \mathrm{U_t}\frac{T_{\mathrm{abs}} - \mathrm{T_{amb}}}{\mathrm{G}} \qquad \text{Equation 2-3}$$

The total heat loss coefficient U_t (Equation (2-4)) is the sum of the top losses U_f, the edge losses U_e and the losses of the back of the collector U_b. The edge losses are usually small, i.e. around 10 % of the total losses (Tabor 1958). Thus, the edge loss can be included in the front and back loss coefficient. In Duffie and Beckman (2006) it is suggested to reference the edge losses to the collector area.

$$U_t = U_f + U_e + U_b \qquad \text{Equation 2-4}$$

2.2 Convective heat loss reducing measures in solar flat plate collectors

An essential design criterion for flat plate solar collectors is the thermal performance. This is in particular important for areas with a low irradiation or a colder climate such as central or northern Europe. Typically, the thermal performance is increased by minimising the heat losses of the collector. The overall heat loss U_t is the sum of the edge, back and front losses. In a standard flat plate solar collector the highest heat loss is caused by U_f (Tabor 1959, Beikircher 2009). Edge losses in conventional collectors are comparatively low due to the small surface area of the edge. A further reduction of this loss mechanism can be achieved by a thicker insulation along the absorber. Thicker insulation can also be used to reduce back losses. However, there have also been other measures tested to lower the heat transfer of the backside insulation (Beikircher et al. 2013).

U_f, in turn, can be split up into a radiative and convective part. Nowadays, modern collectors are equipped with a high selective coating with absorbance values of

0.95 and emission values of less than 0.05. This means 95 % of the short-wave sunlight is absorbed but only 5 % of the black body heat radiation (long-wave) emitted. Therefore, the highest loss in a flat plate collector with a high selective coated absorber is caused by the convection between absorber and glazing, whereas the convective heat loss is prevailing (Tabor 1959, Platzer 1988, Beikircher 2009). The qualitative graph in Figure 2.5 shows the fractions of the thermal losses in a glazed flat plate collector (Reiter 2014).

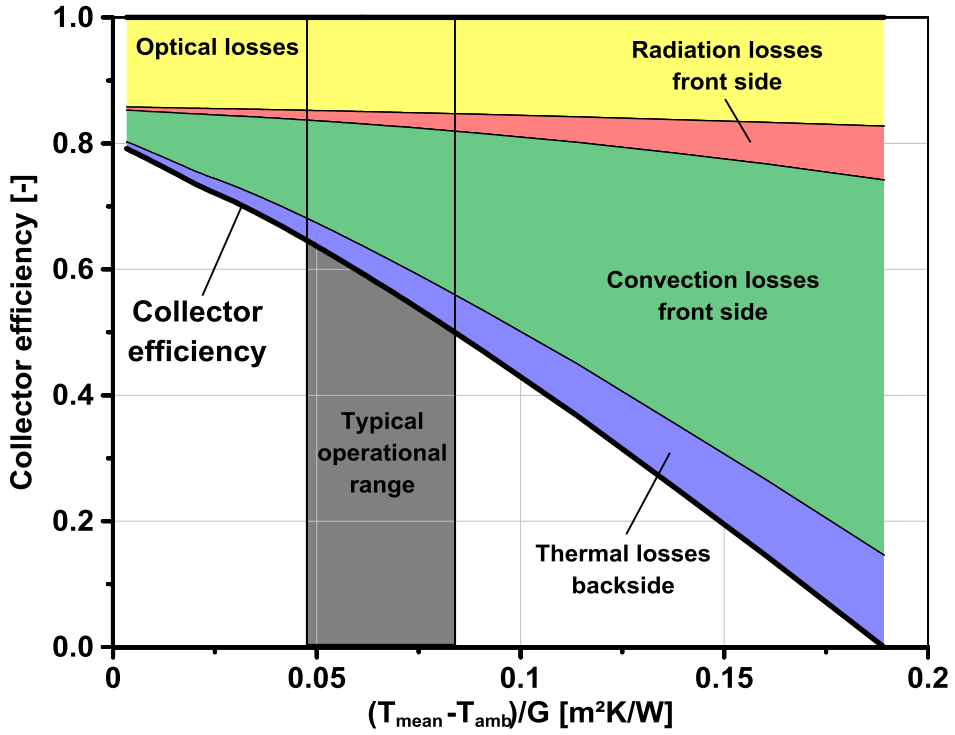

Figure 2.5: Collector efficiency and fractions of heat loss mechanisms shown for a glazed solar thermal collector (Reiter 2014)

This, in turn, means that reducing the convective heat transfer is the most promising approach to increase the efficiency.

Over the decades a vast number of measures have been analysed and evaluated to reduce the convective top heat loss. The following subchapter discusses an extract of this wide field to give an overview of the conducted research. However, the review focuses on convection reducing structures. Radiation and reflection losses, which may be affected by some of the convection reducing measures, are not discussed in detail.

2.2.1 Transparent front insulation in solar flat plate collectors

A common and successful method to reduce the top heat loss is the use of transparent insulation material. In particular, a transparent component is put between absorber and the ambient retarding the convection process. An adverse effect of this is the lowered radiation energy input from the sun, the increasing reflection loss, increased conduction loss and in some cases increased radiation losses from the structure itself.

The measures can be classified according to their geometrical position to the absorber (Figure 2.6) (Platzer 1988, Voss 1991, Kaltenbach 2003).

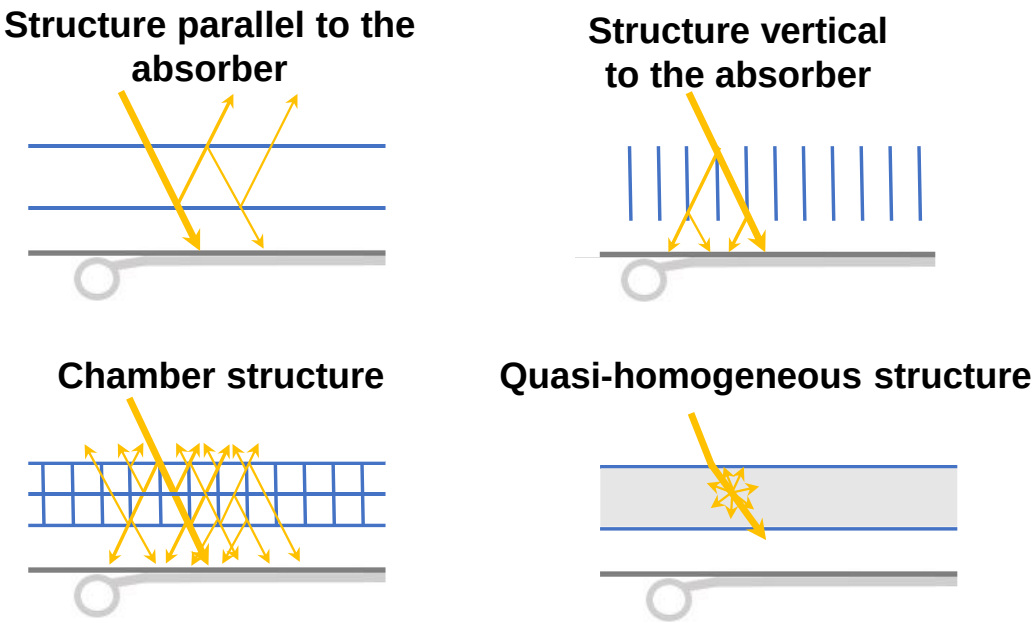

Figure 2.6: Classification of different transparent front insulation

In the upcoming subchapters, these convective heat loss reducing measures are reviewed more in detail.

2.2.1.1 Insulation parallel to the absorber

At least one layer between absorber and environment defines an absorber parallel structure. The archetype of this design is the ordinary glazed flat plate collector. Yet, there are several approaches to use two or more layers to suppress free convection in the interspace. As layer material, usually, plastic foils or glasses are used.

By inserting a further cover, the air layer is separated in to two layers. The cover is considered opaque to long-wave thermal radiation. The convective heat transfer between absorber and the covers is as shown in Figure 2.7.

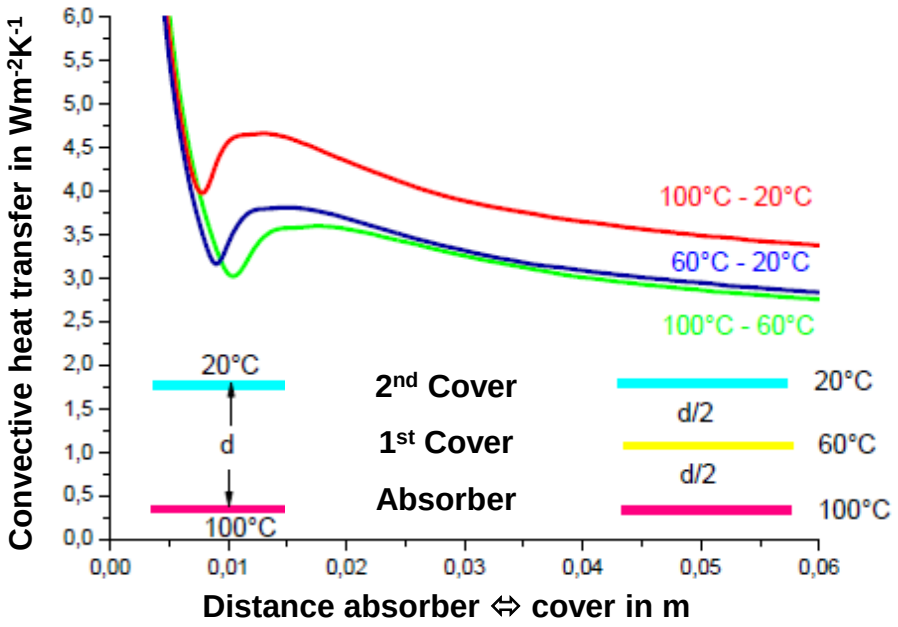

Figure 2.7: Comparison of the convective heat transfer in a single-glazed collector (red line) and a double glazed collector (blue and green line) for a total temperature difference of 80 K (cf. Beikircher 2010)

The red curve represents the convective heat transfer of a single-glazed flat plate collector whereas the blue and green line show the convective heat transfer of each enclosure of a double-glazed collector. If the multiple covers separate the initial gap of 30 mm in to two equidistant enclosures with a gap size of 15 mm, the temperature difference in each enclosure is halved. This results in a lower convective heat transfer for each layer. As a consequence of the series connection of the thermal resistances, the total resistance of the double-glazed type is twice as high as for the single-glazed collector.

In principle, the use of more covers is adverse as the reflection loss increases and, thus, the optical efficiency decreases. Another disadvantage becoming more dominant with multiple covers is the growing heat conductance through the structure to the ambient and the collector weight.

Rommel et al. (2003) conducted a study on the impact of an anti-reflective coated double-glazed cover. In experimental tests, an efficiency increase compared to a single glazed collector was shown. The authors concluded that a double-glazed

collector with anti-reflective coating has a significant higher efficiency potential in the collector operation range between 80 and 120 °C over a conventional solar collector. Furthermore, a development potential was seen in the choice of material to overcome problems such as degassing. Unfortunately, the authors did not state more details or figures.

In the work of Beikircher (2010), an approach from the early 1980s is described whereby a PET foil was mounted between absorber and glazing to reduce the convective heat transfer. Back then, the poor optical efficiency and the insufficient long-term stability of this approach prevented a further application in flat plate solar collectors. According to Symons (1979), FEP is a material that is very suitable for designing a convection barrier in solar collectors. These plastics have an acceptable temperature durability even at higher thermal loads as well as a suitable solar transmittance. However, the high pricing of the material limited its utilisation in solar collectors. Nevertheless, nowadays, a Danish collector producer is selling a foil-insulated collector with an aperture of 12 m² for heating plants (Beirkicher 2010, Vejen 2004). The Danish company is using a FEP foil that is highly temperature and UV resistant as well as highly transparent (τ = 0.95 to 0.96). A negative effect is the thermal expansion of the polymer that leads to creasing or even to tearing (Figure 2.8).

Figure 2.8: Torn foil in a foil-insulated flat plate collector in a district heating system near Palma de Mallorca (Spain)

In case of creasing, this effect is reversible and more of an aesthetic issue. Nonetheless, the foil needs a stretching mechanism to prevent it from sagging – otherwise the convection barrier is out of function. As an alternative to PET, ETFE was analysed (Beikricher 2010). The material shows almost an equal solar transmission (τ = 0.93 to 0.94) as PET and, at the same time, a lower thermal expansion. Ultimately, this reduces the clamp loads and, thus, the risk of tearing the foil. The drawbacks of this approach are a more complicated production, additional costs for the clamping jig and in some cases the long-term stability.

Between 2011 and 2013, Föste et al. (2011, 2013) analysed the principles of selective coated high performance glazing for the application in solar collectors. Their study focussed on the realisation and usability test of a low emissivity (low-e) coating on the collector glazing in laboratory scale. In addition to that, a gas-filled double glazed insulated glazing unit was used as collector cover. The insulated glazing unit (IGU) is coated with a low-e and an anti-reflective coating (Figure 2.9).

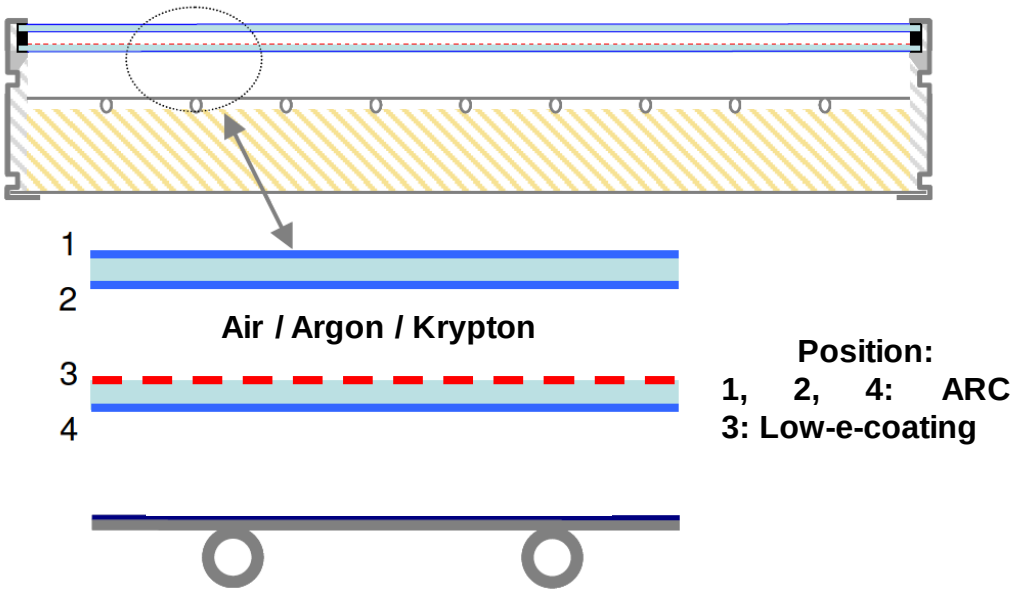

Figure 2.9: Collector setup of Föste's approach (cf. Föste 2013)

In a follow-up project, Föste (2013) continued with the research on the IGU collector. His focus was to design a solar collector on a performance level of a vacuum tube collector but keeping the advantages of flat plate collectors, such as lower costs or hail resistance. In simulations a boost of the solar annual yield of up to 20 % compared to conventional collectors for collector inlet temperatures of 100 °C were shown. As the low-e coating was applied only in a bench scale testing, further research is needed to determine whether it is possible to coat collector sized glazing, i.e. 2 to 2.5 m² in an industrial scaled production (Föste 2013). The higher costs (+ 20 to 30 %), the higher weight and, thus, a more difficult handling impede the utilisation of this approach. Due to its higher pricing, an economic use of this collector type is limited to solar process applications.

2.2.1.2 Insulation perpendicular to the absorber

The most popular insulation amongst perpendicular structures to the absorber are honeycomb structures. Already in the 19th century, Russian engineers were testing the use of honeycomb structures in flat plate collectors. Ever since, a wide field of valuable publications on the convective heat transfer itself and on honeycomb structures have been published. Hollands (1965) studied the application of honeycomb structures between absorber and glazing in flat plate

solar collectors in theory. It was concluded that an economic solar collector design on a superior performance level within a temperature range between 90 °C to 150 °C would be realisable. At this time, the author conducted no tests with solar collectors. Nevertheless, fundamental relations such as the dimensions, i.e. aspect ratio (length to diameter) of the cell structures were analysed. Another crucial contribution was made by Tabor (1969) with his analysis of cellular insulations for solar collectors. A focus in this paper was the investigation of suitable materials and the discussion of design aspects for this insulation. As a result, Tabor saw an application for cellular insulations in concentrating collectors rather than in conventional flat plate collectors, i.e. honeycombs structures. The main reason for this conclusion was the high pricing of suitable materials for the insulation. Eventually, the following design requirements were stated (Tabor 1969):

- High stability to UV and maximum temperatures,
- High transparency to solar radiation,
- High opacity to thermal radiation.

Buchberg and Edward (1976) published a paper on design considerations for solar collectors with cylindrical glass honeycombs. Beside the consideration of the convective heat loss, the radiative as well as the optical influence of those structures play a significant role in their study. All those aspects were thoroughly discussed in their work. Based on their results, nomograms were derived to optimise the cellular structure in regards of convective and radiative heat transfer, optical aspects as well as cost effectiveness. Subsequently to this publication, Buchberg et al. (1976) released a review of natural convection in enclosed spaces for the application in solar collectors. This comprehensive study treats the dimensioning of high aspect ratios of enclosed spaces and deals with the suppression of convection by cellular structures. As a conclusion, the authors recommend a gap distance between absorber and glazing of 40 to 80 mm to reduce the convective heat transfer for conventional collectors. However, the drawbacks of these measures are higher casing costs and an increased shadowing of the aperture area along the edges (Figure 2.10).

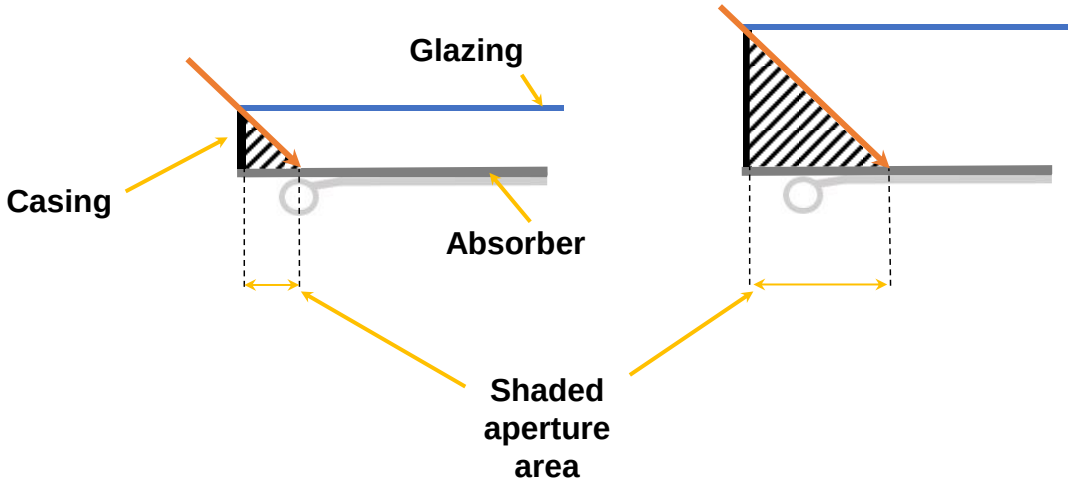

Figure 2.10: Shaded aperture area due to higher side walls of the casing

To overcome the disadvantages, the application of honeycomb structures were recommended.

Hollands and Iynkaran (1984) made another relevant observation. The authors proposed a separation of the honeycombs from the absorber plate to achieve a compound honeycomb with an air layer (Figure 2.11).

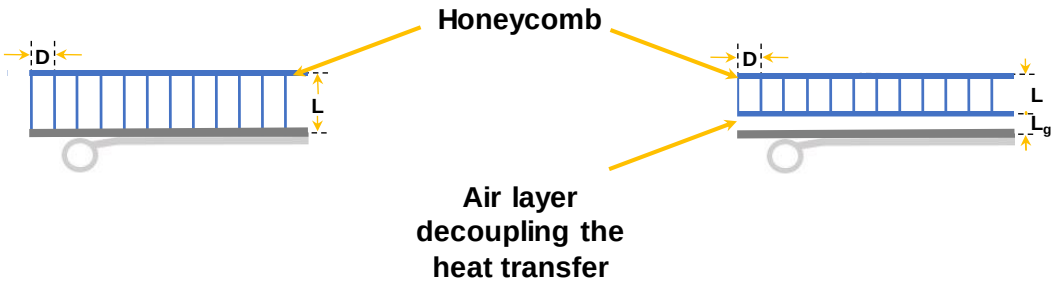

Figure 2.11: Decoupled heat transfer between absorber and honeycomb structure

As there was no gap between absorber plate and cell structure in former studies, the convection barrier was heating up by conduction and emitting the heat and, thus, reducing its efficiency.

The use of a single and double honeycomb structure in flat plat solar collectors was analysed by Abdullah et al. (2003). In their large-scale experimental tests, single layered and double layered structures were put in between absorber and glazing of a specially prepared collector on a test facility. The authors concluded that a well-designed setting of the honeycomb structure increases the thermal efficiency; however, the optical efficiency was always decreased. As their work

solely focussed on the performance of such a collector no conclusions were drawn concerning long-term stability or suitable materials.

Giovanetti et al. (2011) experimented with the application of a hexagonal structure made out of acetyl cellulose as a convection barrier in solar collectors. The benefits of the material are the low costs as well as the good optical properties. It was shown that the thermal loss coefficient could be decreased by this approach. Giovanetti et al. (2011) proved a reduction of the linear thermal loss coefficient at T_{mean}-T_{amb} = 60 K of 45 % compared to a conventional flat plate collector. Yet, the usability is strongly limited as the material degases at temperatures of about 80 °C. The fog deposits on the glazing and lowers the solar transmission. Another negative aspect is the embrittlement of the polymer due to ageing. This ageing effect is further magnified by UV radiation. In consequence, Giovanetti's research programme was not viable and discontinued.

Recently, the work in this field was taken up again. As a consequence of the insufficient long-term stability of practical transparent insulation materials, Kessentini et al. (2013) implemented an over-heating system, i.e. thermally controlled ventilation, to lower the temperature loads on the plastic structure. Again, the honeycomb structure showed a high thermal performance at an acceptable optical efficiency. However, the focus of this paper was rather the development of a new type of solar collector model as well as a suitable approach to investigate the vast number of different configurations. Unfortunately, there was only one stagnation test conducted; nevertheless, the over-heating protection was working properly in this case. Further testing is recommended by Kessentini et al. (2013) to ensure the function of the over-heating protection. According to the authors, the expected costs are lower than that of a conventional flat plate collector. Regrettably, no further details were given in this publication.

An alternative to polymers is the use of glass for absorber perpendicular structures. Rommel (1992) investigated a thin-walled and, thus, fragile structure to reduce the heat transfer from the absorber through the glazing to the ambient. The structure needs to be embedded in a double glazing, which results in higher costs, a more difficult collector assembly and handling as well as in a poor optical efficiency compared to single glazed solar collectors. These circumstances prevented this approach from further applications.

During the same time, many others contributed with their work to the understanding of convection in solar collectors – especially with honeycomb devices (Hollands 1973, Cormack et al. 1974a and 1974b, Arnold et al 1976, Hollands et al. 1976, Cane et al. 1977, Wittwer 1983). The principles and analyses of the convective heat transfer are dealt with in more detail in chapter 0.

Despite of all the various analyses and application studies there was no successful breakthrough with this measure. The high thermal collector loads, the poor UV resistance of the material, the material's long-term stability and the cost pressure are preventing the utilisation in flat plate solar collectors.

2.2.1.3 Chamber structures

Chamber structures are closely linked to absorber perpendicular and parallel structures and are usually made out of multiple wall sheets. The method retards convection in a similar way to the other structures mentioned above. Even though the convection can be suppressed the high material use results in a higher heat conductance (Voss 1991). More importantly, this measure results again in a deterioration of the solar transmission coefficient. Since the chambers are made out of plastics the negative effects of ageing and long-term stability applies here as well.

2.2.1.4 Quasi-homogenous structures

Svendsen and Jensen (1987), Svendsen (1992) as well as Nordgaard and Beckman (1992) have all investigated collectors filled with monolithic silica aerogel. Aerogel is a highly porous solid body in which more than 95 % of the volume is air. As the pore size is in the nanometre region, 1 to 100 nm, the mean free path is comparable with the molecules in the air resulting in a transparent behaviour. Due to this, the material has superior insulation properties and is an outstanding material for insulation in solar collectors. Svendsen (1992) calculated for high collector operation temperatures (80 °C) a doubling of the energy yield compared to conventional collectors. Nordgaard and Beckman (1992) followed a similar approach as Svendsen did. In their collector design, the absorber was plain and black with copper risers wrapped in copper foil. The casing consisted of a 4 mm tempered low-iron glass on the front, a back plate and steel frame achieving the gap between front and back cover. In between, the absorber and

the monolithic silica aerogel were put. Throughout the research work, a simulation model was implemented to predict the efficiency of such a collector type. The transparent insulation material lowered the optical efficiency in comparison to conventional collector types by about 8 % (absolute) but increased the efficiency at temperature difference (T_{mean}-T_{amb}) of 120 K by more than 30 % (absolute) (Nordgaard and Beckman 1992). An application was, from the view of the authors, not feasible due to the high costs of the insulation material.

Up to date, the use of aerogel insulation in solar collectors is impractical, as the material costs are exorbitant.

2.2.2 Evacuated collectors

In the 1970s, scientists were analysing the impact of a vacuum in the collector casing on the efficiency of evacuated flat plate solar collectors. The aim is to reduce the pressure between absorber and glazing and in the complete casing to suppress the natural convection, which in turn increases the efficiency. One of the first scientists to analyse an evacuated flat plate solar collector were Eaton and Blum (1975). They showed that convection was suppressed in relation to the gap distance between absorber and glazing and the prevalent pressure in the casing (Eaton and Blum 1975). In their theoretical study, an efficiency of 41 % at an operating temperature of 150 °C was calculated. According to the authors, critical points in the design of an evacuated solar collector were the sealing of the housing and the mechanical loads on the collector components – such as the glazing. In particular, a deflection of the glass towards the absorber or towards the back plate due to the low pressure needs to be prevented. As there were insufficient cost data available, the authors conducted no further cost analyses.

Benz and Beikircher (1996, 1999) deduced that a pressure reduction below the continuum range (< 10^2 Pa) avoids the convective heat transfer (Figure 2.12).

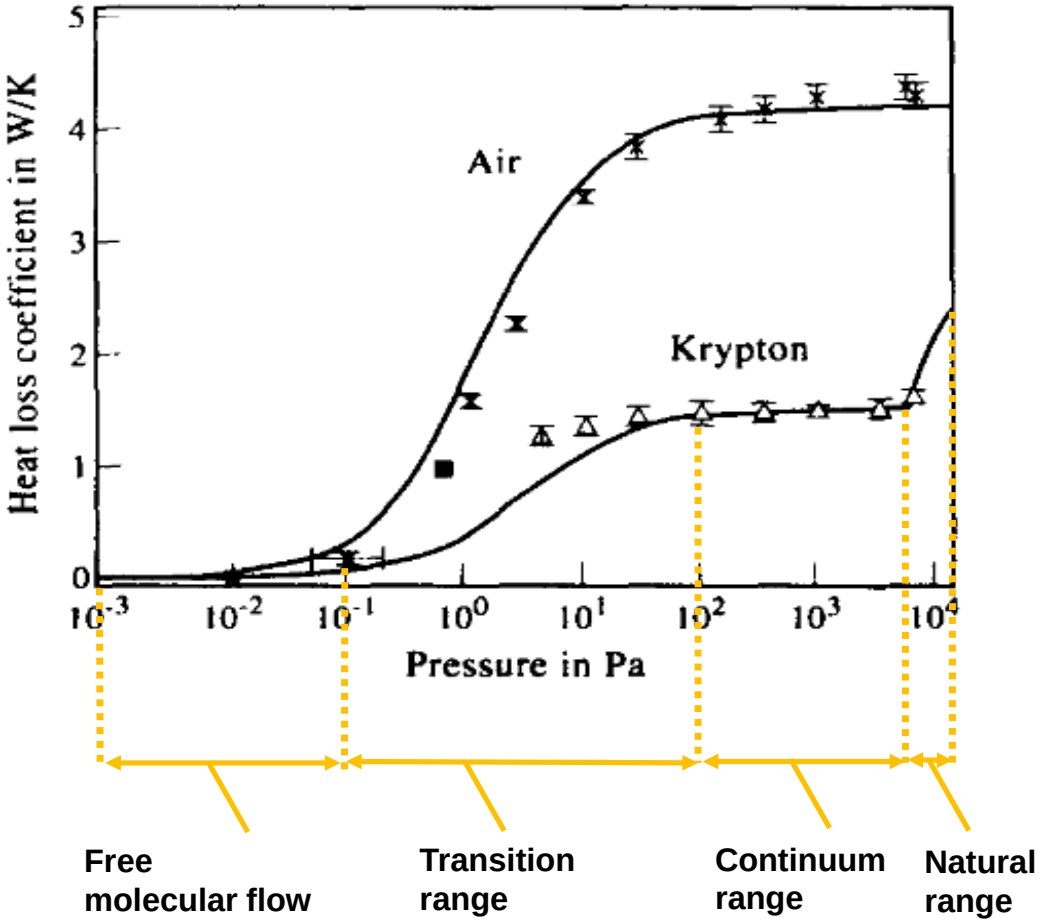

Figure 2.12: Pressure dependency of gas heat conduction and its different states marked for krypton (cf. Benz and Beikircher 1999)

This approach, however, is economically infeasible as it is too costly to achieve such a low pressure. Therefore, a moderate vacuum was used suppressing the convective heat transfer. By reducing the pressure to 10^3 to 10^4 Pa, the heat transfer is mostly driven by gas conduction, i.e. molecule collisions. A further minimisation of the convection is achieved by replacing the remaining air with a more suitable gas – such as krypton. Benz and Beikircher (1999) concluded in laboratory testing that the convective heat coefficient is reduced by up to 65 % in the continuum range compared to air. As a result of their previous research, Benz and Beikircher introduced a high efficiency evacuated flat plate collector for process steam production.

Following the approach of Benz and Beikricher, Buttinger et al. (2009, 2010) combined their design with a compound parabolic concentrator (CPC). An important aspect of the design of such collectors is the consideration of the

mechanical loads on the collector casing. Due to the low pressure, loads of more than 98 kN/m² occurred on the trough structure. Hence, its wall thickness as well as the glazing thickness were analysed in a FE study. It was concluded that the best way to apply the loads is via an equally spaced support (Figure 2.13).

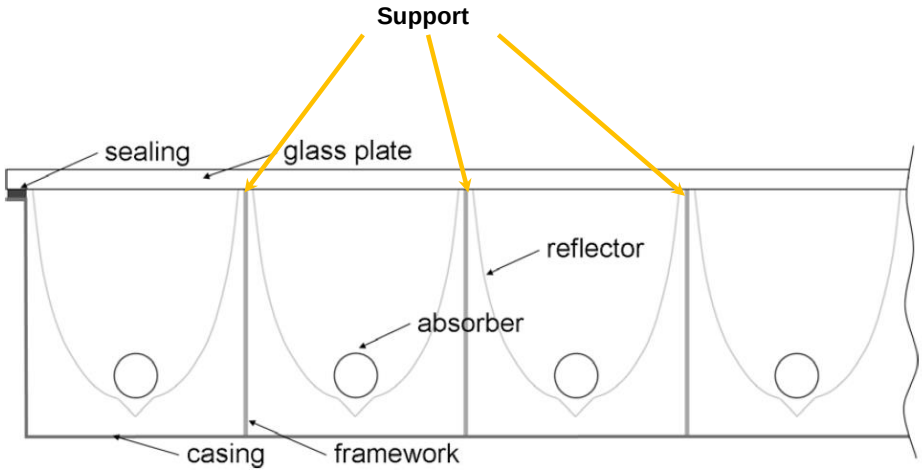

Figure 2.13: Cross section of an evacuated CPC collector (cf. Buttinger et al. 2010)

In contrast to the other studies, sealing methods were discussed by Buttinger (2009). Over a typical collector lifetime of more than 20 years, the sealing needs to meet high demands that are magnified by the vacuum inside the collector. In the approach, a double connected sealing method was applied. The inner seal was a butyl based adhesive whereas the outer seal was silicone. However, according to the authors, further experiments are necessary to ensure trouble-free operation below 100 Pa. Nevertheless, the evacuated CPC collector showed an excellent thermal performance – especially at higher collector inlet temperatures. Tests confirmed efficiencies above 50 % for collector working temperatures of more than 150 °C (Buttinger 2009).

Shire et al. (2016) introduced a slim design approach for an evacuated flat plate collector. In their approach, a novel absorber type was put in the interspace between two glass panes. For the edge bond, a profile was used, which was sealed to the upper and lower glazing. To avoid a deflection of the glasses by the low pressure, an array of spacers is perforating the absorber. The absorber is positioned in between the glazing unit by well-insulated support pillars to minimise the conductive absorber heat loss to the ambient. As a consequence of the superior insulation properties of the vacuum, a typical backside insulation is not necessary and a total collector depth of only 20 to 25 mm is possible. In terms of

efficiency, the authors estimated a reduction of the total loss coefficient U_t between a conventional (3.9 W/m²K) and evacuated (0.8 W/m²K) flat plate collector of 80 %. Details on costs, suitable production methods or experiences of field-tests results were not given. However, Henshall et al. (2016) analysed the mechanical stress in the glazing of this collector type. In contrast to the approach after Shire et al. (2016), Henshall et al. (2016) used a sheet-pipe absorber with a meander piping in a metal housing instead of a full glass collector. The authors used a FE model to conclude on the stress level of the evacuated flat plate collector and validated their results by a digital image correlation strain measurement. Due to different material pairings in a collector, different thermal elongations could lead to a critical stress level for the components. Therefore, the authors included the thermal expansion coefficient of the components in their modelling and analysed the thermal induced stress. It was concluded that the introduced collector design is capable to withstand typical loads during collector operation. Henshall et al. (2016) reviewed possible sealant methods for evacuated enclosures. Contrary to Buttinger's (2009) approach, the authors recommended suitable sealant methods for vacuum applications, which are also temperature resistant.

The biggest drawbacks of an evacuated collector design are the costs for the hydraulics and – where applicable – valves and the complex casing design compared to conventional approaches. For instance, the concave deflection of the glazing is usually avoided by an array of spacers to the keep the constant distance between absorber and glazing (Figure 2.14).

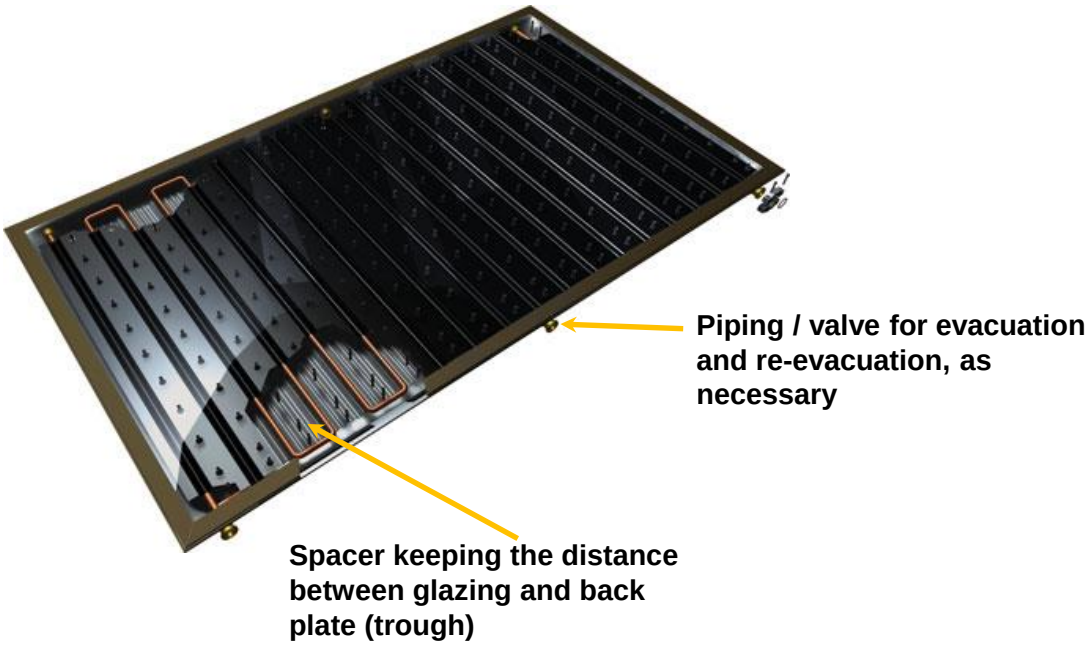

Figure 2.14: Evacuated and krypton filled flat plate solar collector (cf. Thermo|Solar 2011)

The spacers need to be mounted on the back side of the collector casing and are most often perforating the absorber. Eventually, this leads to a considerable manufacturing effort and higher costs.

Flat plate collectors are known to need no maintenance and incur little or no cost during the lifetime, unlike some evacuated flat plate collectors. These collectors have to be periodically re-evacuated and re-filled with krypton (Thermo|Solar 2015).

Finally, evacuated collectors are most suitable for solar process applications. From an economic point of view, this kind of collector is of little interest for solar domestic hot water or space heating which still provides the greatest market share for solar collectors (Renewables 2016 Global Status Report 2016).

2.2.3 Gas-filled collectors at ambient pressure

Between the cavities of an insulated glazing unit is dry air or a more suitable gas than air to lower the heat transfer between the glass panes (Cuce and Riffat 2015). To achieve a higher thermal insulation effect modern glazing units are usually either filled with argon, more seldom with krypton and in very exceptional cases with xenon. Over the years, this technology got more and more useable and is by now a long-term tested and reliable method to lower the heat

loss in glazing units. From this perspective, a gas-filled interspace between glazing and absorber is a promising approach in reducing the convective heat loss.

Vestlund et al. (2009) analysed the thermal performance of a gas-filled solar collector at ambient pressure. In their work, a parameter analysis was carried out including the variation of the inclination angle and the type of gas. Based on simulations a considerable reduction of the overall heat loss by 20 % was shown. According to the convection theory for inclined air layers (Hollands et al. 1976), Vestlund et al. (2009) deduced that a short distance between absorber and glazing would not only offer aesthetic advantages but also a better thermal performance. Beside the medium in the collector's interspace, the top heat loss is strongly dependent on the distance between absorber and glazing.

As the collector is assembled and gas-filled at ambient conditions, the pressure will vary according to the medium temperature in the interspace. The pressure change follows the ideal gas law, i.e. linear to the temperature rise. This results in mechanical loads as the stagnation temperature can reach more than 500 K with a gas temperature slightly below that. Vestlund et al. (2009) claimed that further investigations were required to analyse the mechanical loads caused by the pressure rise on the collector design. They intended to use the glazing and absorber as a kind of membrane. Due to the components deflection an extra volume is created lowering the pressure rise. Another alternative would be to integrate an expansion vessel. However, this is seen as an inferior solution as an additional component is needed (Vestlund et al. 2009).

2.2.4 Summary of the use of convective heat loss reducing measures

There have been great efforts to lower the convective heat loss via the top in solar collectors. The application of honeycomb structures in solar collectors was very well analysed. Remarkable boosts in efficiency were calculated and demonstrated. Still, to date the author has no ensured knowledge of a market-ready or even available application of this measure. This fact is, ultimately, due to the demanding requirements in solar collectors concerning the long-term stability and costs.

In contrast to this, absorber parallel structures such as multi-covers in solar collectors are finding infrequent use in solar collectors. There might be still some challenges concerning the long-term stability as well as problems during stagnation but an acceptable performance level was demonstrated. The disadvantages are the higher costs and weight, a more complex manufacturing as well as the extra care needed when handling during installation.

Quasi-homogenous insulations will remain an exotic approach as long as the very high pricing hinders further utilisation in solar collectors. The increased thermal efficiency cannot be justified by the insulation material costs.

Vacuum flat plate solar collectors are proven to provide a significantly higher thermal efficiency than conventional collectors do. A significant drawback can be seen in the complex design, the high requirements concerning mechanical loads and sealing methods preventing a low-maintenance lifetime. Due to the complexity of the collector design, the collector production becomes more intricate in terms of working steps and automation. Ultimately, the higher costs for both collector components and production make such designs less suitable for the domestic heating sector.

Despite of the discussed paths, gas-filled collectors at ambient pressure are not yet as explicitly analysed as the other approaches discussed– though this approach is at least to some extent similar to evacuated collectors. The benefit of this measure is that there is no additional hardware needed. Yet, an efficiency on the level of a well-designed collector with a honeycomb structure or even an evacuated flat plate collector needs to be proven.

For future findings, the aim should lie in a collector design with an adequate thermal performance level and a cost structure competitive to a conventional solar collector that is also suitable for a highly automated production.

2.3 Collector production

In 2008, a market survey on the current state of collector production was conducted for the German Solar Thermal Technology Platform (Müller and Zörner 2008). By means of established appraisal criteria, the situation of the assembly of flat plate solar collectors was investigated. The survey proved that a large number of collector producers are running a workshop operation instead of

a mass production system. By judging the manufacturer sales figures, the authors concluded that some of the examined collector producers are on the threshold to a ‘serial production’ (Figure 2.15).

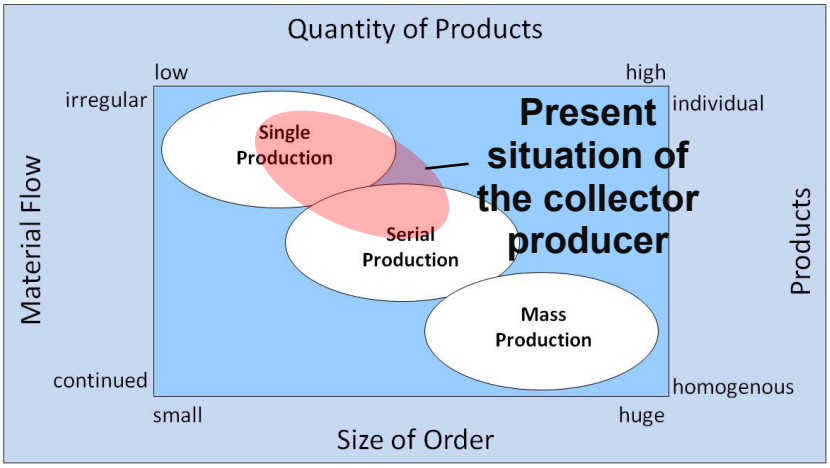

Figure 2.15: Current situation in the collector production in Germany (cf. Müller and Zörner 2008)

It was emphasised that collector producers tend to simply duplicate a single collector assembly line to increase the production capacity. However, based on their inquiry, Müller and Zörner (2008) queried whether a collector production at an industrial scale is feasible with the current production technique.

In a further study, Müller and Zörner (2010) extended the original study by including further collector producers from Germany and Austria. This time, their focus lay on the evaluation of the automation level of eight different collector manufacturers. To evaluate the collector assembly, the production process was divided into the main work steps:

- Cleaning of the glass cover
- Assembly of the frame
- Assembly of the back plate
- Assembly of the absorber and insulation
- Application of the adhesive
- Assembly of the glass cover
- Curing of the adhesive

Finally, the automation grade for each work step was analysed for eight German and Austrian companies and compiled in a matrix (Figure 2.16).

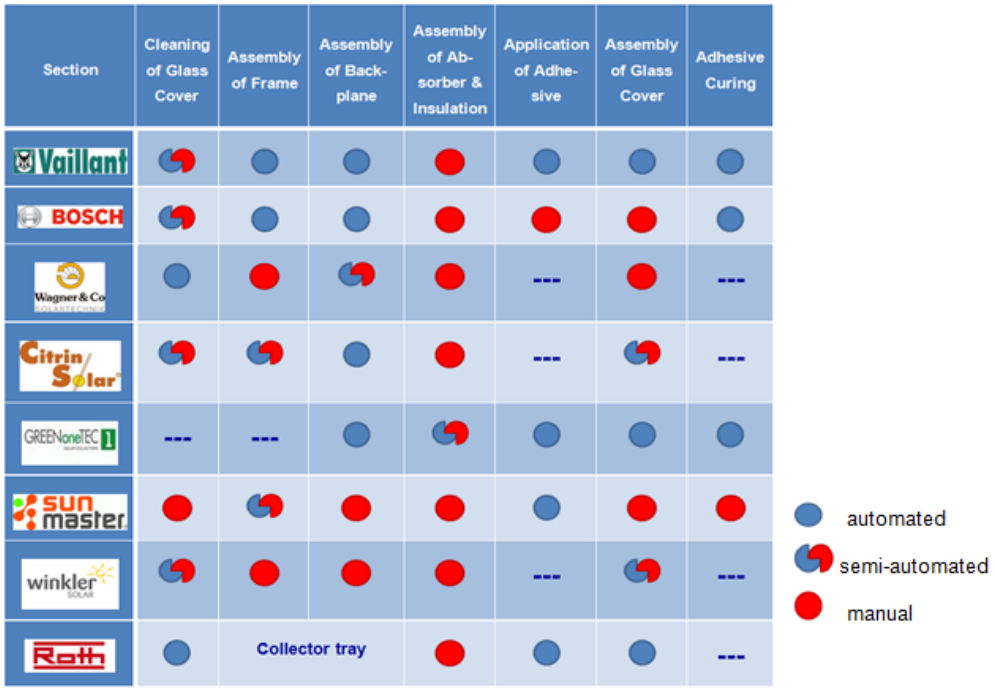

Figure 2.16: Overview of the automation level of German and Austrian collector manufacturer (Müller and Zörner 2010)

Even though there are some automated sections, such as the adhesive application, the evaluation matrix shows there is no continuously automated produced collector.

Furthermore, no common strategy among the manufacturers to standardise the production for the same product type was identified: For instance, the assembly of the back plate may be done manually, semi-automatically, automatically or not at all (if a tray is used). This leads to different approaches to a single process (Figure 2.17).

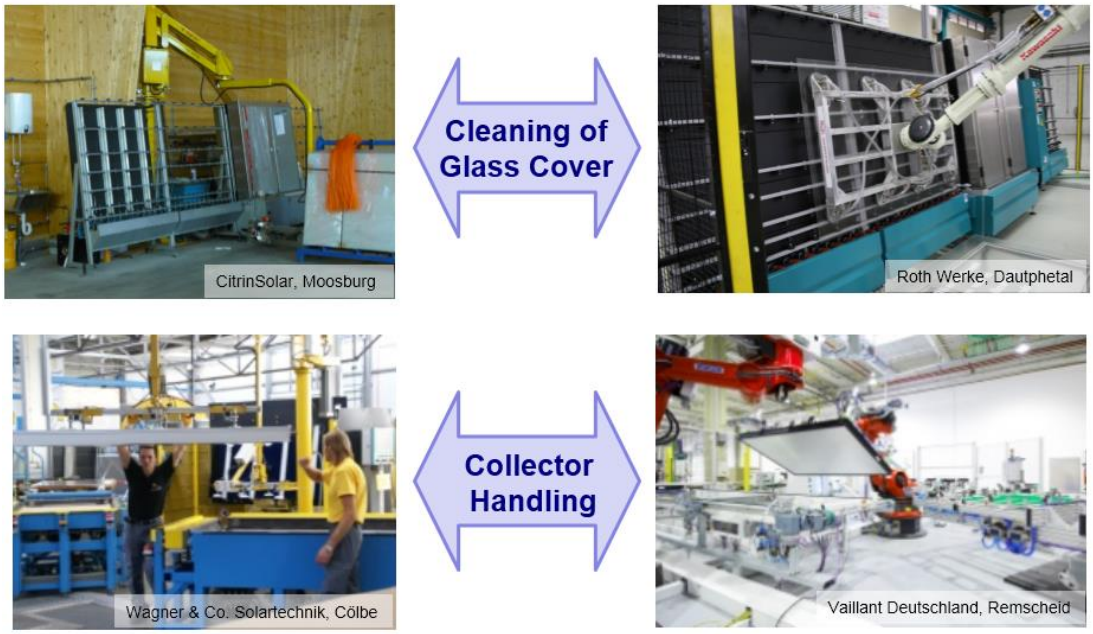

Figure 2.17: Different approaches for an identical assembly step (Müller and Zörner 2010)

The collector producers stated an amount of investment from 0.3 to 3 million € per production line. However, no correlation between the degree of automation and the cycle time or deployed employees and the investment was found (Müller and Zörner 2010) (Figure 2.18).

	Company A	Company B	Company C	Company D	Company E	Company F	Demon-stration
Cycle Time [sec]	600	420	240	180	180	90	240 / 144
Collectors per Shift	50	70	120	160	160	320	112 / 187
Personnel	3 *	2 *, **	3 *, **	?	3 *, **	5 *, **	6 / 10 *, **
Planning and Imple-mentation	internal	*Dtec*	*EEP-Maschinen-bau*	*Reis Maschinen-fabrik*	*Fix Maschinen-bau*	internal	*Minitec*
Investment [Mio. €]	0.3	1.5	0.9	2…3	1.5	?	0.4

* without glass cover cleaning ** without packaging

Figure 2.18: Parameters of six different collector production lines (Müller and Zörner 2010)

Berner (2012) published an overview of the situation in the German solar thermal industry. He found the absorber production to be a highly automated process whereas the assembly of the solar collector seems to be difficult to automate. According to Berner (2012), the reason for this is the current collector design. In addition to this, the author also claimed that a higher degree of automation would limit the producer's flexibility.

2.3.1 Conventional collector production line

For a better understanding of this situation, an example of a production line for a flat plate collector is described more in detail. Figure 2.19 shows the schematic production process of a German collector manufacturer.

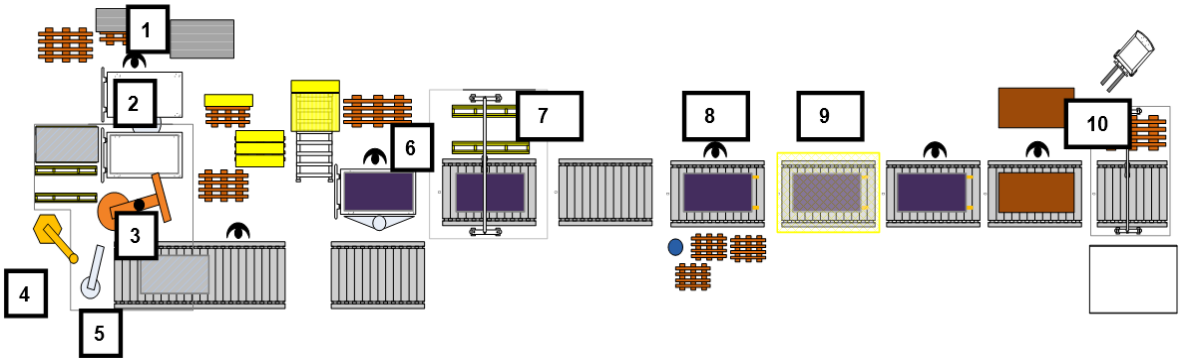

Figure 2.19: The major steps of a flat plate collector production

At the first step, a worker positions the frame profiles (1) on a rotatable assembly bench (2). To join the frame parts and for extra stability, angle pieces are put into the corners of the frame. The frame is then rotated into the automated production area. A robot picks up the back plate (3) and moves it to the gluing station (4) where an adhesive bead is applied. Subsequently, the robot assembles the back plate and the frame. The frame is clinched (5) and put down on a roller conveyor. At the next station (6), a worker manually inserts the side wall and back insulation in the casing. Before the absorber is manually inserted, the insulation is vacuumed off to avoid pollution on the absorber surface. After that a linear robot mounts the glazing (7). At station (9), the collector is equipped with glazing ledges by a worker. Then the glazing ledges are fixed on the collector frame (10). Finally, the collector is packed and palletised (11).

The cycle time for a conventional framed collector on this production is about ten minutes. Altogether, six people are working on the production line.

There are some advantages of this production method for the manufacturer that needs to be considered: Given in the nature of the collector frame design, a wide range of collector dimensions can be produced on the same production line. Many manufacturers are producing at least two different collector types on the same production line. The low overhead costs allow a matched production according to the current market demand.

A highly automated production line causes higher capital costs than a line as described in the example. However, to fulfil the targets set by the national renewable energy action plans (NREAPs) a high growth of the collector market is predicted (Figure 2.20) (ESTIF 2012).

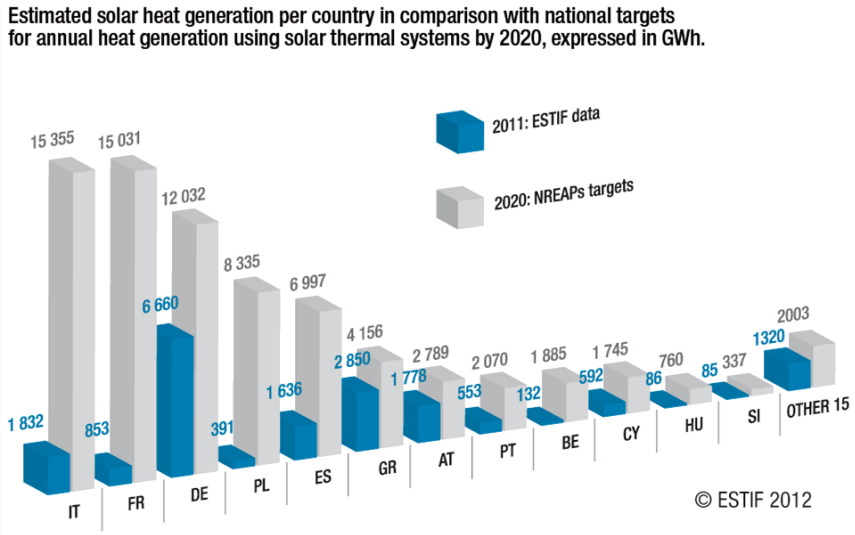

Figure 2.20: The installed solar heat generation is behind schedule indicating a necessary market growth (ESTIF 2012)

Taking this market growth into account, the costs of a highly automated production line could be quickly amortised.

2.3.2 Current use of adhesive in the collector production

To meet the expectations of the manufacturer regarding a flexible and automated production, which is inevitable when designing a successful product, certain aspects need to be considered: A new production technology needs to be at least as flexible as the current technique. At the same time, the automation degree needs to be higher, scalable and expandable.

A great potential is seen in the use of adhesives to increase both the automation level and the collector design (Epp and Berner 2010; Berner 2012). Adhesive technology is rapidly developing and is well established in other sectors already, such as the glazing industry. However, there are collector manufacturers that use adhesive for the joints between the frame and back plate. Berner (2012) found adhesive technology to be the most frequently used method of joining the collector frame parts. In fact, more than half of all the collectors sold in Germany have the glazing bonded onto to the frame by adhesives. In 2008, more than 62 % of the producers were still using mechanical bonding methods, such as clinching (Berner 2012). Figure 2.21 illustrates areas in solar collectors in which adhesives are commonly used.

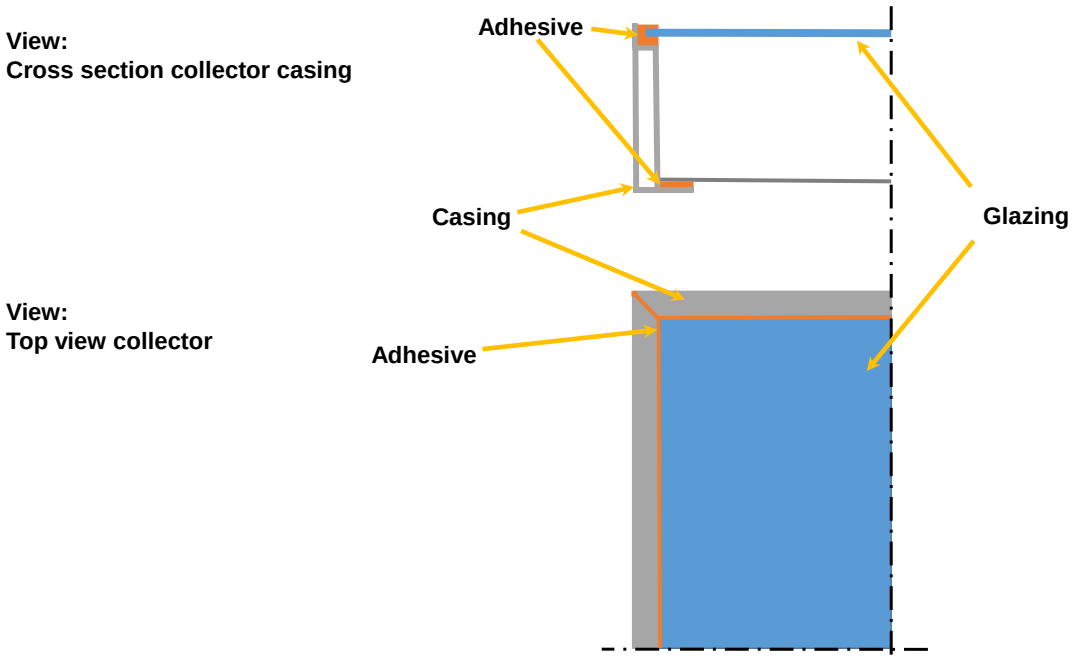

Figure 2.21: Typical areas in flat plate solar collectors in which adhesives (orange inked) are commonly used

Some collector producers are using fixing ledges in addition to adhesives to fix the glazing to the frame. This is actually not necessary but a result of a product recall by a manufacturer in 2008 after the glazing came off the collector frame. The use of adhesive in collector production has several advantages. Beside the suitability for automation of adhesive techniques, materials such as the upper sealant, cover strips and aluminium profiles can be saved and, thus, costs could be reduced. However, compared to other industry sectors the adhesive technology for solar thermal applications is still in its infancy.

2.3.3 Summary of the situation in the collector production

In summary, Müller and Zörner (2009, 2010) concluded that there is no dominant strategy in the production of solar collectors. Although some of the producers in the survey are among the largest three collector producers in Europe, none of them is producing a collector on a continuously automated assembly line.

The reasons for this situation in the solar thermal industry are manifold and can be found among others in its history. In the 1980s, the first solar collectors were hand made in very low quantities. During the following decades, solar collector sales increased but the basic design of a flat plate solar collector did not change much.

Another reason for the patchy production situation is the unsteady European market. Since this work is focussed on technical aspects of collectors and their production, this circumstance is not further discussed.

In the medium term, the European collector producers will be confronted with increasing sales and an increasing competition from Middle East, Asia and South America. To tackle this challenge, great potential is seen in a more standardised and automated production process. Consequently, the development of both a new solar collector and its production process should be carried out in parallel. New production techniques and materials should be analysed to allow the production of innovative collector designs.

3 Proposed production method and collector design

Adhesive bonding is increasingly being adopted in the design of flat plate solar collectors. This enables highly automated production in a cost effective manner opening the path towards new design approaches for flat plate solar collectors.

The basic designs of an IGU and a flat plate solar collector are similar in that two or more layers are joined by an adhesive. The use of adhesive technology allows a higher level of automation than in current collector production lines, resulting in a production process with consistently high quality and low cycle times.

In the upcoming subchapters, the proposed collector production as well as the collector design are presented.

3.1 Proposed collector production

Modern insulated glazing units consist of at least two glass panes in which the interspace between the panes is usually flooded with an inert gas. Different spacers are used to keep a constant distance between the panes (Figure 3.1).

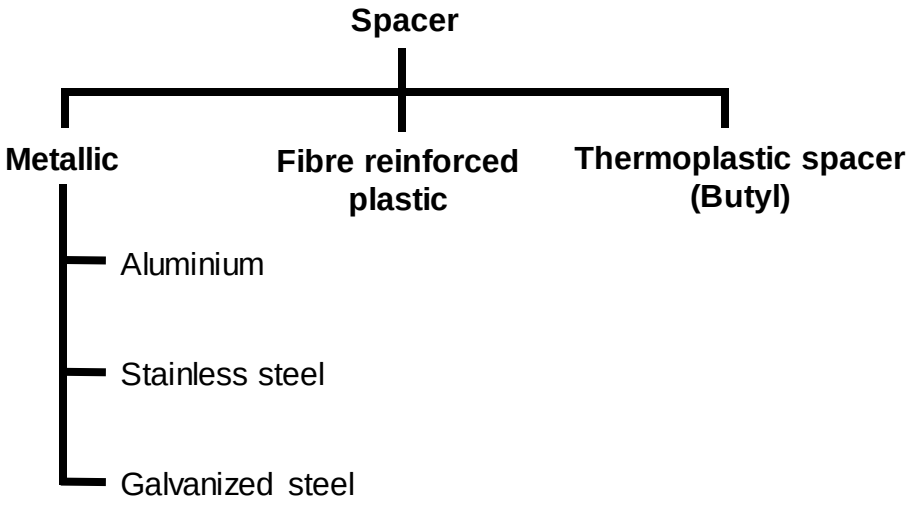

Figure 3.1: Different type of spacers in insulated glazing units

A disadvantage of metallic or fibre reinforced plastic spacers are a more time-consuming production preparation. As those spacers are manufactured in an upstream production, there might be idle or retooling times in the actual insulated glazing unit (IGU) production. Over the last decade, thermoplastic spacer (TPS) are increasingly used for IGU substituting the conventional spacers. Beside the

lower heat conductivity of the TPS, there are no upstream processes needed. Within the interspace of hermetically sealed glazing units, temperature fluctuations cause pressure changes that lead to varying mechanical loads on the edge bond and glazing. As a fully adhesive edge bond – such as TPS – is more elastic than a stainless steel spacer, insulated glazing units with an adhesive edge bond are more capable of compensating the pressure induced movement of the glass panes and, thus, ensure a higher lifetime of the sealed interspace. Figure 3.2 shows the typical setup of an IGU.

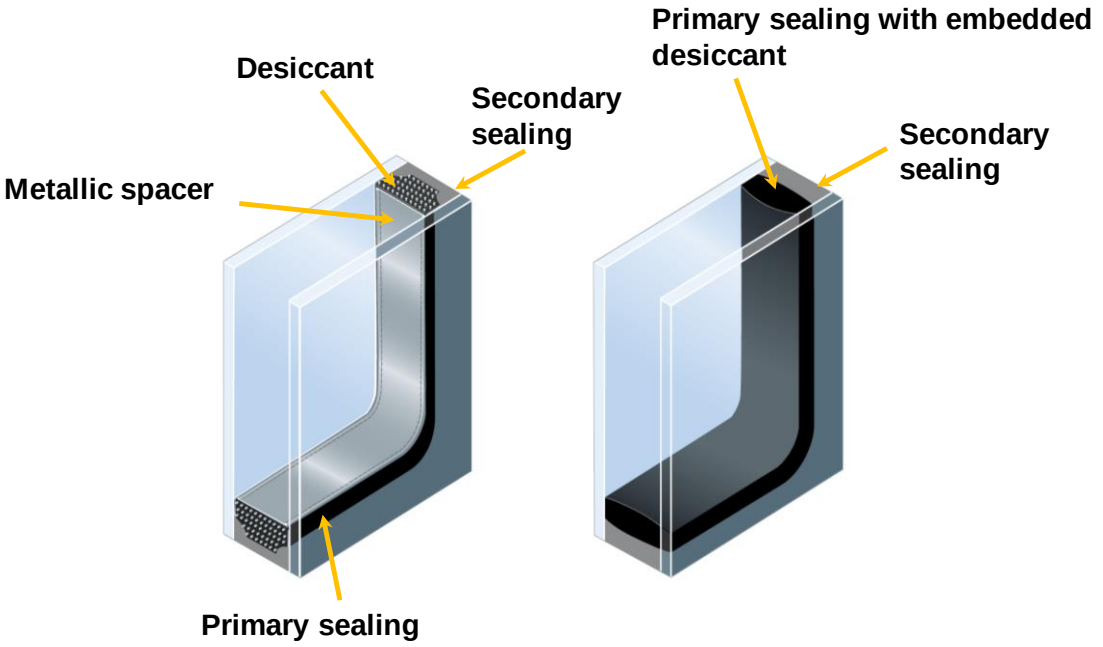

Figure 3.2: Schematic setup of an insulated glazing unit with a metallic spacer (left) and a thermoplastic spacer (right) (cf. Bystronic Lenhardt GmbH)

In contrast to the collector production, the insulated glazing unit production is highly automated allowing cycle times of less than 60 s for a double glazed window. Figure 3.3 shows a production line for insulated glazing units with a thermoplastic spacer.

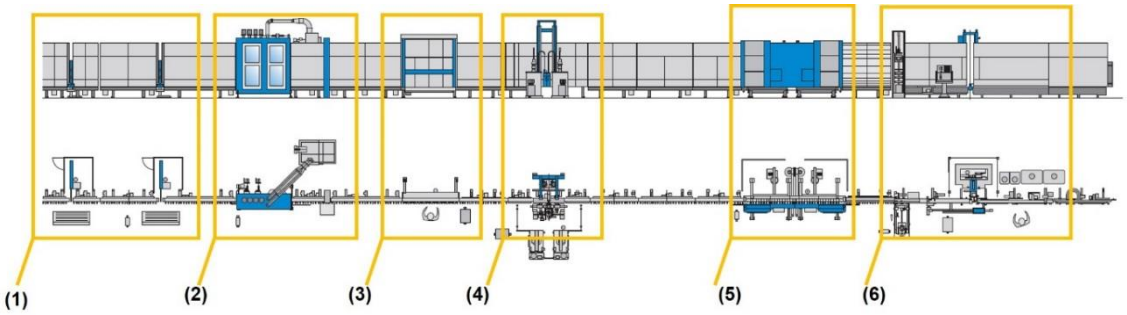

Figure 3.3: Layout of the 'tps'line' (cf. Bystronic Lenhardt GmbH)

In the following, the production of a double glazed window with a thermoplastic spacer is described:

The first glass pane is put on the roller conveyor by a robot or a worker (1). To stabilise the components during the production process the glass panes are handled in a vertical position avoiding a bending of the glass panes (up to 5 m² and more). The glass panes are separated from the production line plate by an air stream to assure a frictionless transport without scratches. At station (2), the glass is cleaned and, subsequently, transferred to the inspection station (3). Before the glass pane gets to the adhesive applicator its dimensions have been measured by light barriers (3). A robot is applying the primary sealing on the glass at station (4). This butyl-based adhesive keeps the distance between the glass panes and ensures a hermetically sealed interspace. At the same time, the second glazing is already washed, inspected and ready to be assembled with the first glass in the press (5). Without any idle time both panes are transported into the press. During the press process, the interspace is flooded with an inert gas lowering the convective heat loss of the IGU. Before the IGU gets to cure, the secondary sealing is applied. This sealing is a silicone based adhesive ensuring a high mechanical load capacity – for example in structural glazing applications.

Throughout this research programme, the described manufacturing process was adapted for the production of flat plate solar collectors.

3.2 Proposed collector design

An all-round adhesive supported absorber and, thus, sealed collector has several technical advantages over more conventional designs. In the following subchapter, the possible assets of such a collector type are discussed in more detail.

3.2.1 Advantages of a hermetically sealed collector design

Unlike vented collector designs, environmental contaminants such as moisture and dust have no negative effects on the absorber surface of the proposed design. The residual moisture in the hermetically sealed interspace is removed by the primary sealing, which contains a desiccant material. Ultimately, this leads to less degradation on a coated glazing or the absorber surface.

In 1998, an International Energy Agency (IEA) task force was set up to analyse ageing effects in solar thermal collectors. The task force was split up into four sectors:

- Ageing effects on absorbers
- Ageing effects on AR coated glazing
- Micro climates in vented solar collectors
- Ageing of polymeric glazing

The Fraunhofer Institute for Solar Energy (ISE) was assigned with the task of analysing the microclimate in vented solar collectors (Köhl 1998). During this work, a simulation model was developed to analyse the processes caused by the ventilation in conventional collectors (Holck et al. 2003) in order to deduce design guidelines for ventilation in solar collectors. According to Holck et al. (2003) and Köhl (1998), the microclimate inside the collector has a considerable effect on the ageing of the collector components, such as on the glazing, coating or insulation. Beside high temperature loads during stagnation, a main factor for the degradation of the collector materials is a high humidity level in the collector. This can lead to condensation on the glazing and in some cases on the absorber surface. At first, this might appear to be merely an aesthetic issue; however, humidity is a driving factor for corrosion, which is in particular damaging the coated collector surfaces – such as an anti-reflective coating glazing or the sensitive absorber surface – or even the metal components. Corrosion on the absorber surface causes a loss in the thermal performance as the thermal emissivity rises (Holck et al. 2003). A correctly designed ventilation can prevent this ageing. In contrast, corrosion due to high humidity or pollution is eliminated in sealed collectors.

During the work of the task force, it was discovered that high moisture levels also increase the back loss of the collector. This is caused by the heat conduction of

the insulation (in most cases mineral wool), which increases with rising humidity. Beikricher (2013) showed the effect of soaked insulation material in solar collectors. In fact, the author determined an increase of the thermal conductivity of mineral wool of more than 3,000 % at a moisture content of 30 Vol.-%. Despite the fact that imbued insulation increases the back loss of the collector; the material itself starts to clump and loses its shape increasing its conductivity further (Beikricher 2013).

Vestlund et al. (2009) analysed the thermal performance of a gas-filled solar collector theoretically and derived by their simulation model a significant boost of the thermal efficiency. In 2012, Vestlund et al. (2012a) followed the approach to design a gas-filled collector with an acceptable thermal performance and at the same time reduce the use of the absorber material. In fact, the absorber holds the biggest cost share in a collector. Figure 3.4 shows the cost structure of a typical flat plate solar collector (author's own data).

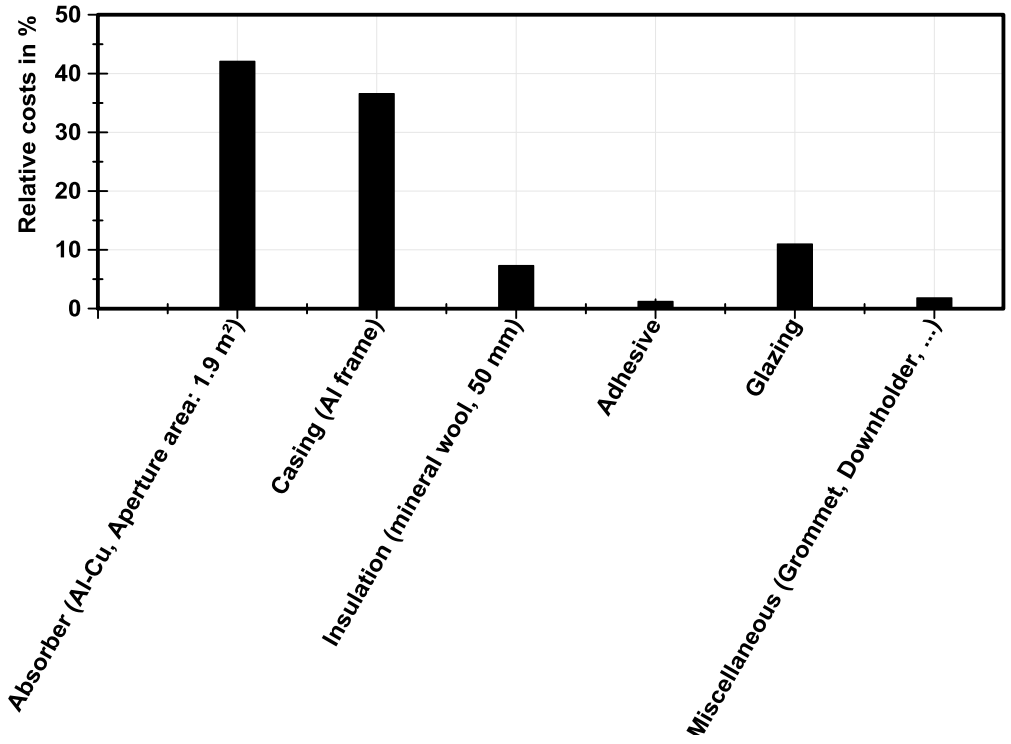

Figure 3.4: Cost structure of a conventional flat plate collector with an aluminium absorber sheet and copper piping (aperture area: 1.9 m²)

As the applied production method within this research programme allows a gas-filled cavity, it was plausible to investigate this concept more in detail.

3.2.2 Design of a fully adhesive edge bond for a collector with an all-round supported absorber

The basic collector construction was intended to be simple and as similar to an insulated glazing unit as possible. Hence, the butyl sealant (primary sealing) was applied directly on the absorber sheet. Subsequently, it was bonded to the glazing to achieve a gastight cavity. During the assembly process of the absorber and the glazing, the gap can be filled with an inert gas, which lowers the convective heat loss (Figure 3.5).

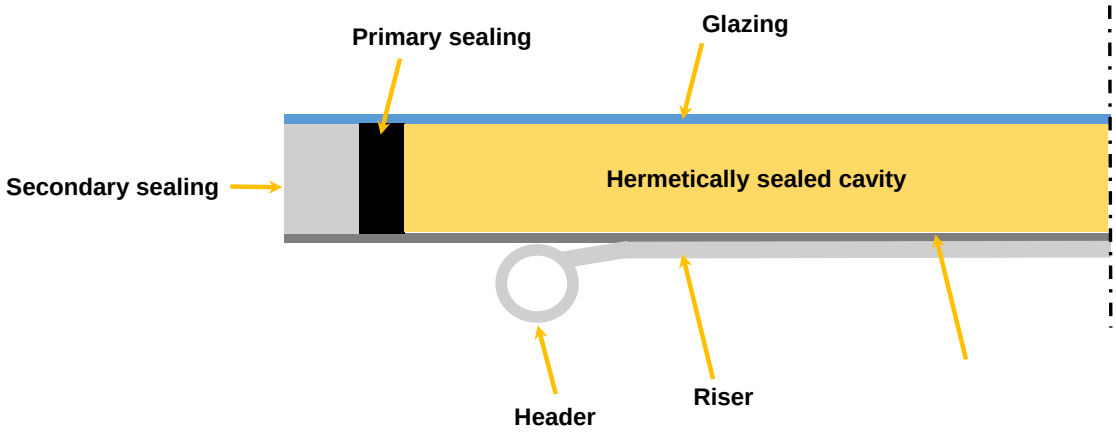

Figure 3.5: Schematic cross section of the fully adhesive edge bond for a collector with an all-round supported sheet-pipe absorber (laser welded)

3.3 Summary

The adaption of the highly automated production technology for insulated glazing units for the assembly of solar collectors has the potential to improve the automation degree of current collector production. However, a collector design that is fitted to the production method and uses new materials needs to be designed and analysed in terms of thermal and mechanical aspects as well as durability. Beyond that, literature shows that a hermetically sealed collector could profit from less degradation and an efficiency uprating.

Nevertheless, challenges concerning the collector design need to be thoroughly analysed and tackled.

4 Experimental setup and procedure

This chapter includes the used measurement devices, the sensors and their accuracy as well as a description of the applied measurement procedures.

4.1 Data reduction

This subchapter describes the calculation of important parameters in this thesis.

Mean absorber temperature

The mean absorber temperature was calculated based on all applied absorber sensors in the measurement or used nodes in the thermal simulation model:

$$T_{mean\ abs} = \frac{\sum_{i=1}^{n} T_{abs}}{n}$$ Equation 4-1

Mean glazing temperature

The mean glazing temperature was derived by the following equeation:

$$T_{mean\ glazing} = \frac{\sum_{i=1}^{n} T_{glazing}}{n}$$ Equation 4-2

Mean fluid temperature

The mean fluid temperature was estimated based on the average value between inlet and outlet temperature:

$$T_{mean\ fluid} = \frac{T_{in} + T_{out}}{2}$$ Equation 4-3

Collector heat flux

The collector heat flux was calculated based on the following equation:

$$\dot{q}_{collector} = \dot{m} \cdot c_p \cdot (T_{out} - T_{in})$$ Equation 4-4

Expansion volume

The expansion volume of the absorber deflection was estimated with equation 4-5:

$$\Delta V_{exp} = z_{mean\ displ} \cdot A_{abs} \qquad \text{Equation 4-5}$$

Where $z_{mean\ displ}$ is the mean value of all derived displacements in Z direction:

$$z_{mean\ displ} = \frac{\sum_{i=1}^{n} z_{displ}}{n} \qquad \text{Equation 4-6}$$

4.2 Data logging unit

Throughout the complete research programme, two data loggers were used. The data from indoor tests were recorded with the TopMessage data logger from Delphin. The 34970A from Agilent is a handy and portable data acquisition unit. Therefore, it was convenient to log the outdoor tests. The short-term tests were logged with a one or five-second data logging interval. For the long-term tests, i.e. several days up to months, an interval of 30 seconds was chosen.

4.3 Solar simulator setup

For the collector efficiency tests, the university's indoor solar simulator was used (Figure 4.1).

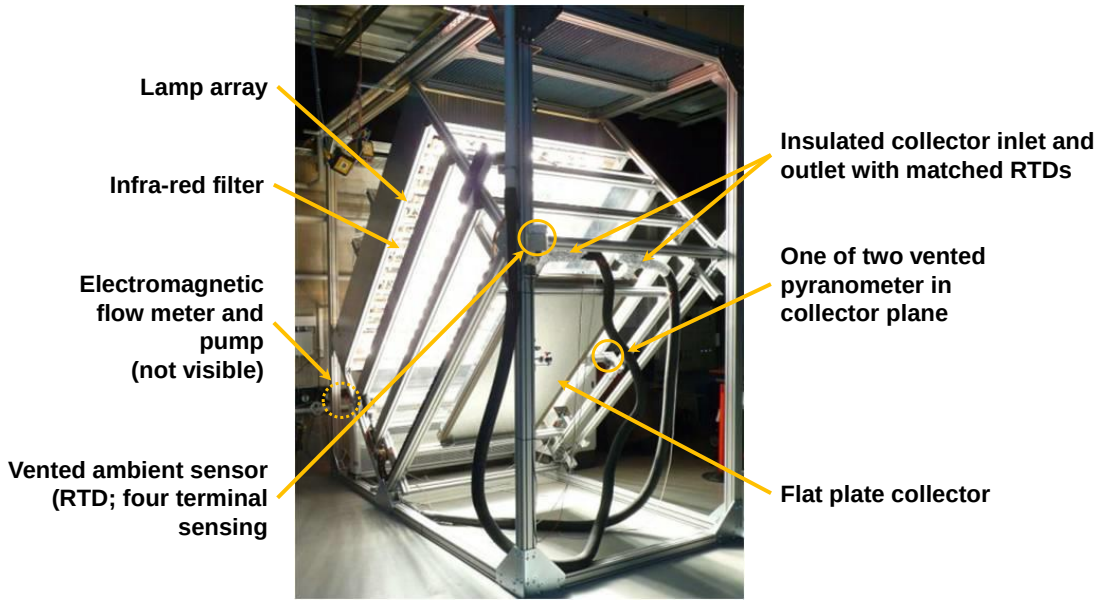

Figure 4.1: Setup of the university's solar simulator used during the research project

All efficiency tests were conducted according the standard DIN EN 12975-2. The irradiance of the lamp array is measured by two pyranometers (CMP 11 secondary standard according to ISO 9060). The wind speed is checked before each collector test with a hand held anemometer. An electromagnetic flow meter logs the mass flow during the test procedure. Two matched resistance temperature detectors (RTD) (four terminal sensing) measure the temperature difference between collector inlet and outlet to determine the mean collector temperature. A vented and irradiation shielded RTD is used to log the ambient temperature. Table 4.1 comprises the specification of the used pyranometer.

Table 4.1: Specifications of the used pyranometers

Parameter	**Value**
Spectral range in nm	285 to 2,800
Sensitivity in µV/W/m²	7 to 14
Response time in s	< 5
Zero offset A in W/m²	< 7
Zero offset B in W/m²	< 2
Directional response in W/m²	< 10
Temperature dependence (-10 °C to +40 °C) in %	< 1
Operational temperature range in °C	-40 to +80
Maximum solar irradiance in W/m²	4,000
Field of view in °	180

Table 4.2 shows the specifications of the used RTD sensors used in the collector efficiency tests.

Table 4.2: Sensor type, range and accuracy of the used temperature sensors

Parameter	**Value**
Sensor type	Resistance temperature detector RTD (four terminal sensing)
Measuring range in °C	-30 to 250
Accuracy in K	±(0.03 + 0.0005 · measured value in °C)

In Table 4.3 the accuracy of the electromagnetic flow meter is compiled.

Table 4.3: Specifications of the electromagnetic flow meter

Parameter	**Value**
Sensor type	Electromagnetic flow meter
Range in m/s	-12 to 12
Accuracy in mm/s	0.15 % of the measured value in mm/s + 1 mm/s

The anemometer's technical specifications are summarised in Table 4.4.

Table 4.4: Specifications of the used anemometer

Parameter	**Value**
Measuring range in m/s	0.1 to 25
Accuracy in %	± 5 of the measured value
Functional principle	Hot-wire
Volume flow rate range in m³/min	0.001 to 999,000

4.4 Deflection measurement

For the analysis of the mechanical deflection of the absorber, an optical measurement device called PONTOS (GOM 2013) was used (Figure 4.2).

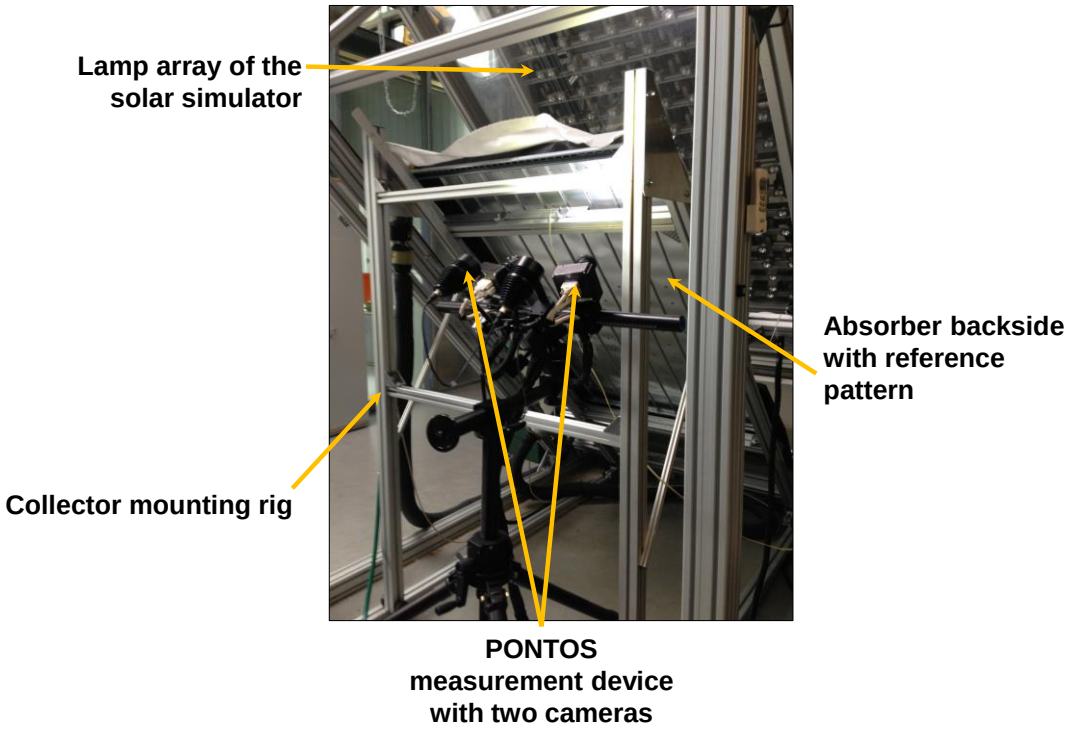

Figure 4.2: PONTOS setup to determine the absorber deflection

This device needs a reference pattern to process the deflection. The pattern was applied on the backside of the absorber (Figure 4.3).

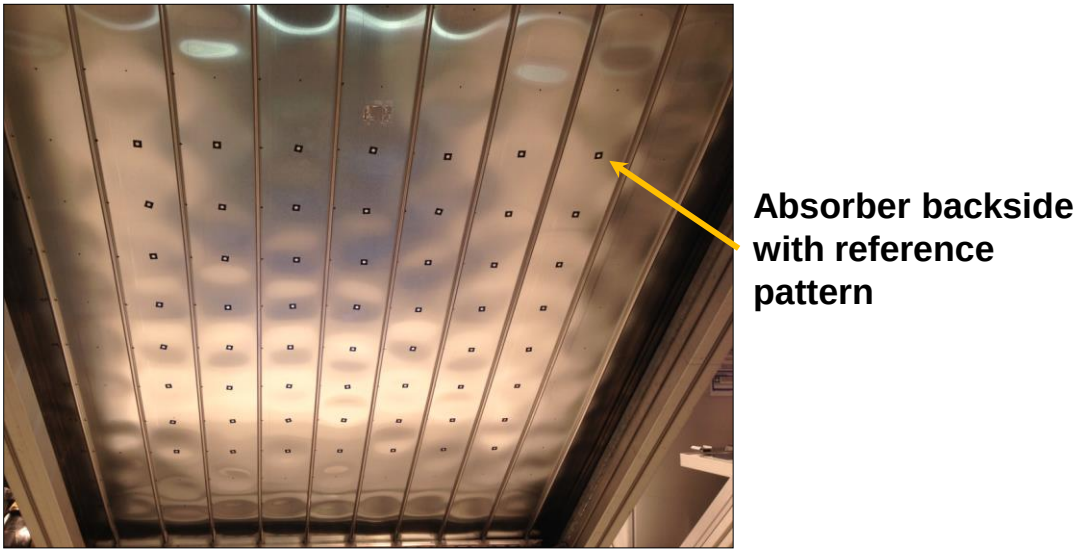

Figure 4.3: Backside of the absorber with the reference pattern (0.6 m²) for the PONTOS measurement device

The camera captures the pattern while the absorber is at ambient temperature and during stagnation or collector operation. After the collector test, the captured pictures are processed with the included software package (Figure 4.4).

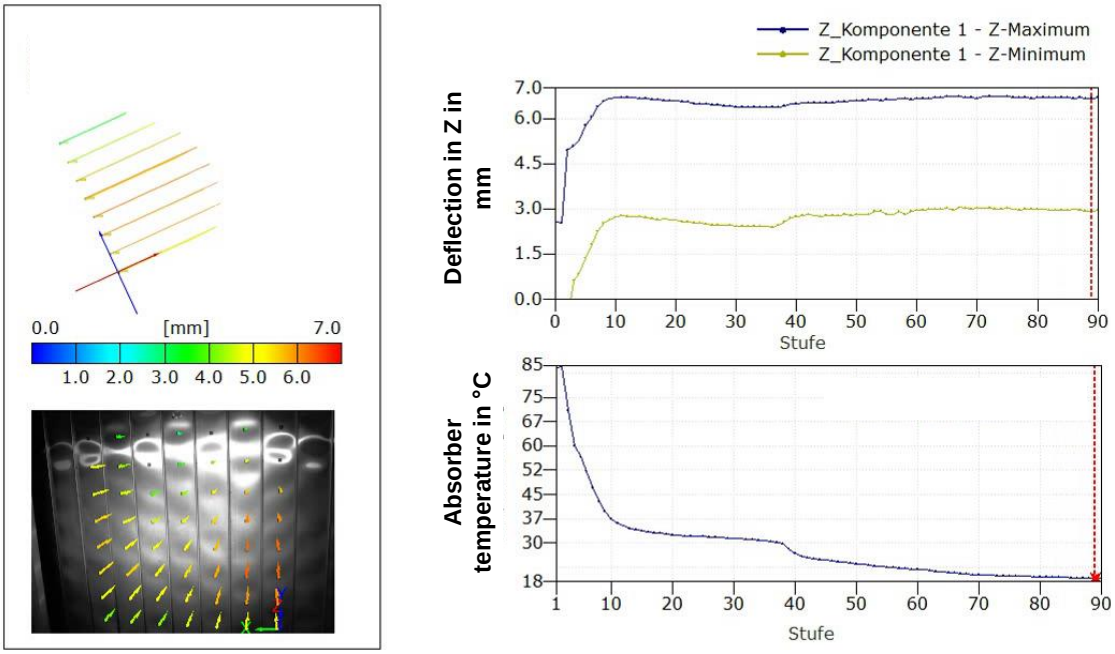

Figure 4.4: Example of the post processing in the PONTOS software environment for an absorber cool down

The manufacturer states that the accuracy for deflection measurements is 0.01 % for a strain range of 0.02 to 100 % (GOM 2013).

Figure 4.5 shows the procedure of the manual deflection measurement.

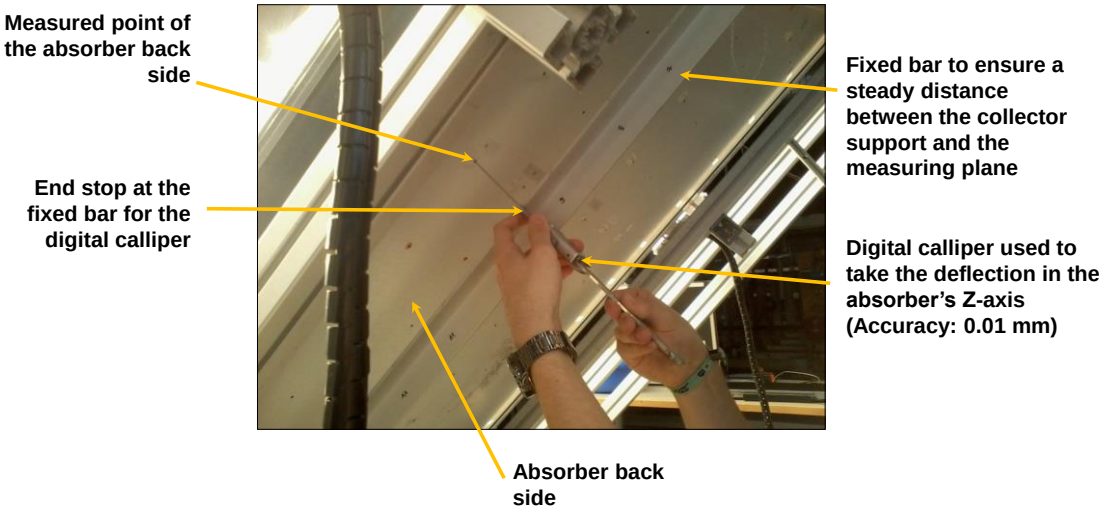

Figure 4.5: Manual deflection measurement taken with a digital calliper

A digital calliper rule with a display accuracy of 0.01 mm was used to take the absorber deflection. The collector's back plate was removed and the collector was put on the mounting rig. To ensure a steady measuring plane, an L-shaped bar was used, which was fixed on the collector-mounting rig. The L-shaped bar functioned as a reference for the digital calliper. From this end stop, the calliper's rule was moved until the rule tip touched the absorber back. This procedure was conducted thrice for each test – at ambient temperature, during collector operation or stagnation and after the test again at ambient temperature. In total, 323 measuring points were applied on the absorber back. The measurements before and after each test run were compared to ensure that the absorber was again at its initial shape, i.e. excluding remaining deformations of the absorber. Once this was done, the initial coordinates at ambient temperature were subtracted from the values taken during the test run under the solar simulator's lamp array.

The deflection measurements were taken just beside the risers and midway between two risers (Figure 4.6).

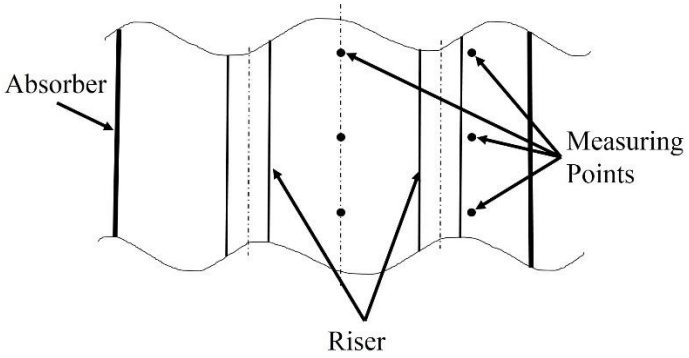

Figure 4.6: Detail view of the taken measurements

Before the measurement procedures started, it was ensured that the collector was at a steady state. This means the collector gains equalled the collector losses, which was indicated by a constant absorber temperature at a certain ambient temperature (Figure 4.7).

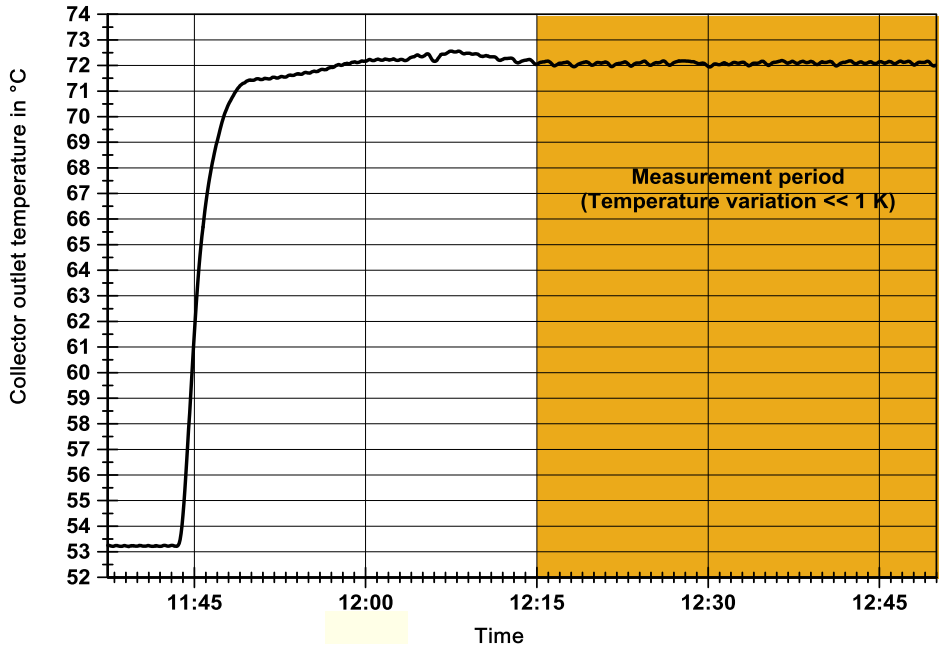

Figure 4.7: Collector outlet temperature on a steady level to conduct measurements (orange inked area; T_{amb} = 26 °C)

After the computer-controlled thermostat was set to a certain inlet temperature, it took about 30 minutes until a steady collector outlet temperature was reached.

Figure 4.8 shows the variation of the outlet temperature between 12:15 and 12:50.

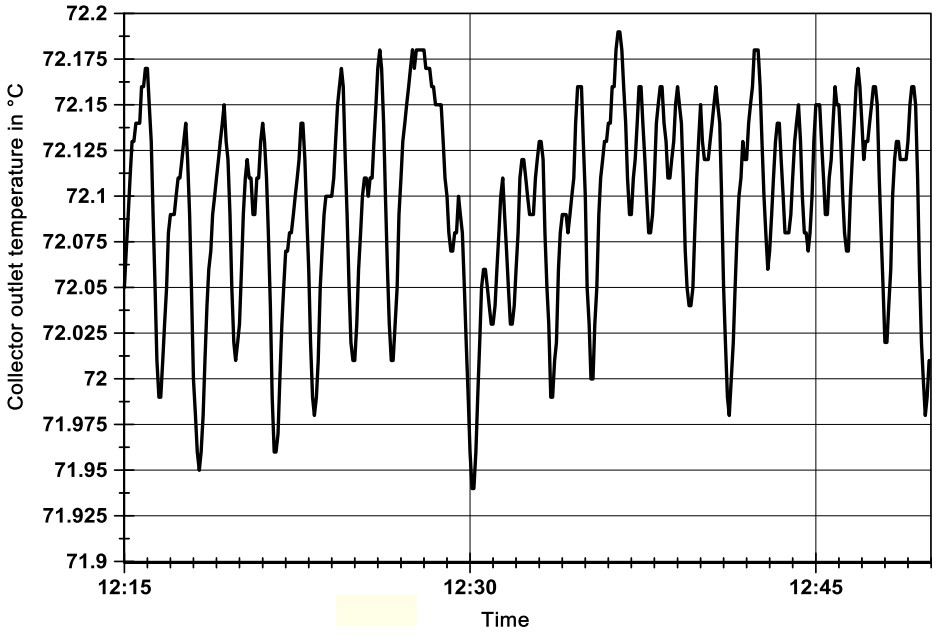

Figure 4.8: Steady collector operating state for measurements

The collector inlet temperature was immediately on a steady level due to the computer-controlled thermostat.

During the test runs, the ambient temperature in the laboratory was kept steady by the facility's ventilation system. Unless otherwise stated, all temperature sensors were fixed to the collector components, e.g. glazing, absorber or casing, by heat-resistant aluminium duct tape. This ensured a tight contact between sensor and component and shielded the sensors from solar radiation.

Figure 4.9 shows the deviation between the optical and manual measurement procedure.

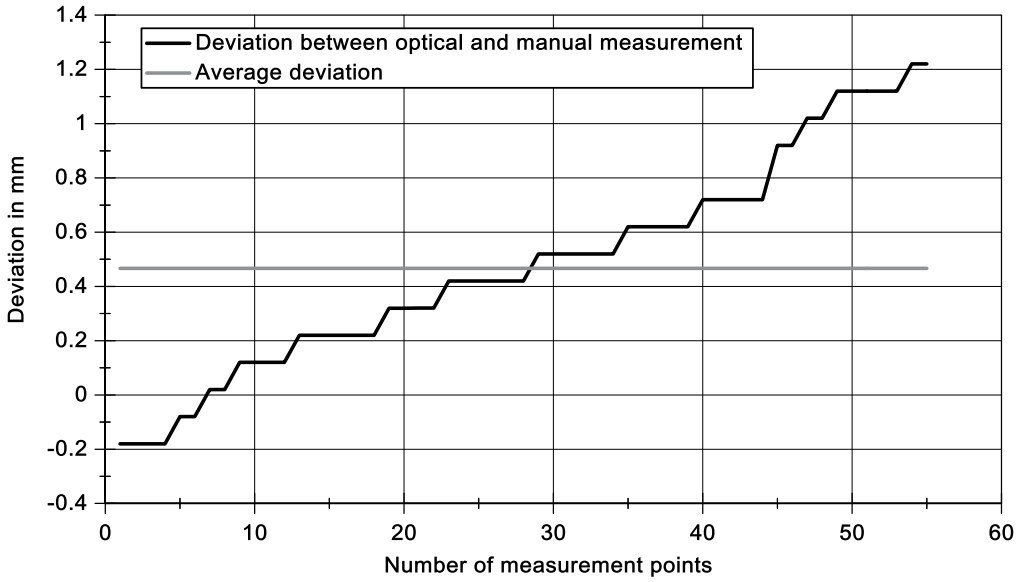

Figure 4.9: Comparison between optical and manual measurement showed an average deviation of 0.466 mm (rounded to 0.5 mm)

The optical measurement device was capable of capturing 0.6 m² of the absorber back. On this size, a pattern with 55 reference points (see Figure 4.3) was applied. The graph (Figure 4.9) shows the deviation between a deflection measurement taken with the optical measurement device and the calliper. This difference was sorted by size (ordinate) and plotted over the number of measured points (abscissa). From this plot, the minimum and maximum deviation can be derived, which were -0.2 mm (minimum) and 1.2 mm (maximum). The average deviation of all 55 points was 0.467 mm, which was rounded to 0.5 mm. This value was assumed to be representative for the total absorber area (2 m²). Based on this result, a certainty margin for the expansion volume of ±1 litre was calculated.

4.5 Pressure measurement

To detect the pressure between absorber and glazing, a differential pressure transmitter was used. The sensor data is summarised in Table 4.5.

Table 4.5: Technical specifications of the used differential pressure transmitter

Parameter	**Value**
Reaction time in ms	250
Measuring range in Pa	±400
Accuracy in Pa	0.25 % of the measured value in Pa

4.6 Outdoor testing

Figure 4.10 represents the outdoor testing rig scheme with the attached sensors and their signals.

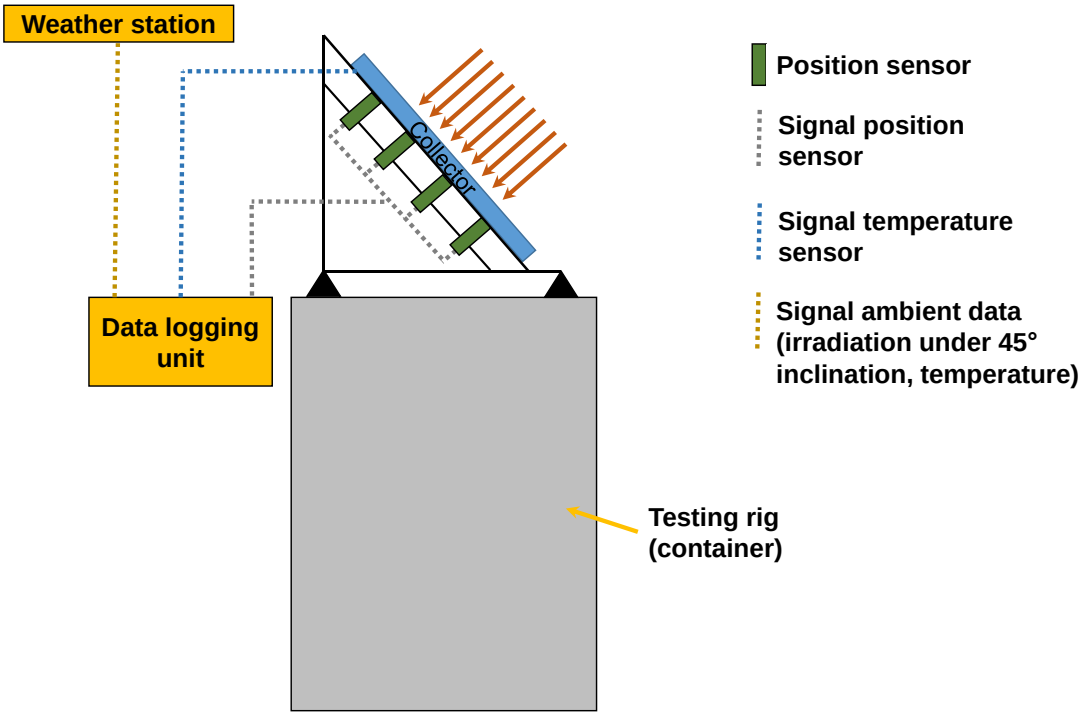

Figure 4.10: Scheme of the outdoor testing rig

For the temperature measurement during the outdoor tests, thermocouple sensors of the type T were used. Table 4.6 comprises the relevant specifications of the sensors.

Table 4.6: Summary of the technical data of the applied temperature sensors for the outdoor testing

Parameter	**Value**
Type / material	T / Cu-CuNi
Temperature range in °C	-40 to 250
Accuracy in K	max. 0.5 or 0.004 · measured value in °C

The same pyranometer type, i.e. CMP 11 secondary standard, which was used in the solar simulator, measured the solar radiation in the collector plane during the outdoor tests. Four potentiometric position sensors were attached on the collector back with a direct connection between sensor tip and absorber. Table 4.7 comprises the specifications of the position sensors.

Table 4.7: Relevant parameter of the position sensors

Parameter	**Value**
Measuring range in mm	0 to 100
Accuracy in mm	< 0.01

The position sensors were attached to a collector parallel bar to ensure a fixed position.

4.7 Calibration

The solar simulator's homogeneity of the irradiation in the collector plane was controlled before each test run. A movable pyranometer, controlled by a computer numerical control, screens the irradiated collector area and takes a 10 s measurement of the irradiation for 200 equally distributed positions. Subsequently, a script is used to plot the irradiation homogeneity. If necessary, a correction factor is calculated for the measurement.

The installed sensors, i.e. temperature sensors, pyranometers and flow meter, are checked on a regular basis by the researchers or university's laboratory staff in dedicated testing rigs.

Beyond that, the university's laboratory staff conduct the calibration of the solar simulator at regular intervals. Therefore, a reference collector is used, which was tested at a certified laboratory under an identical solar simulator.

4.7.1 Calibration of the flow meter

Figure 4.11 shows the calibration procedure used for the flow meter.

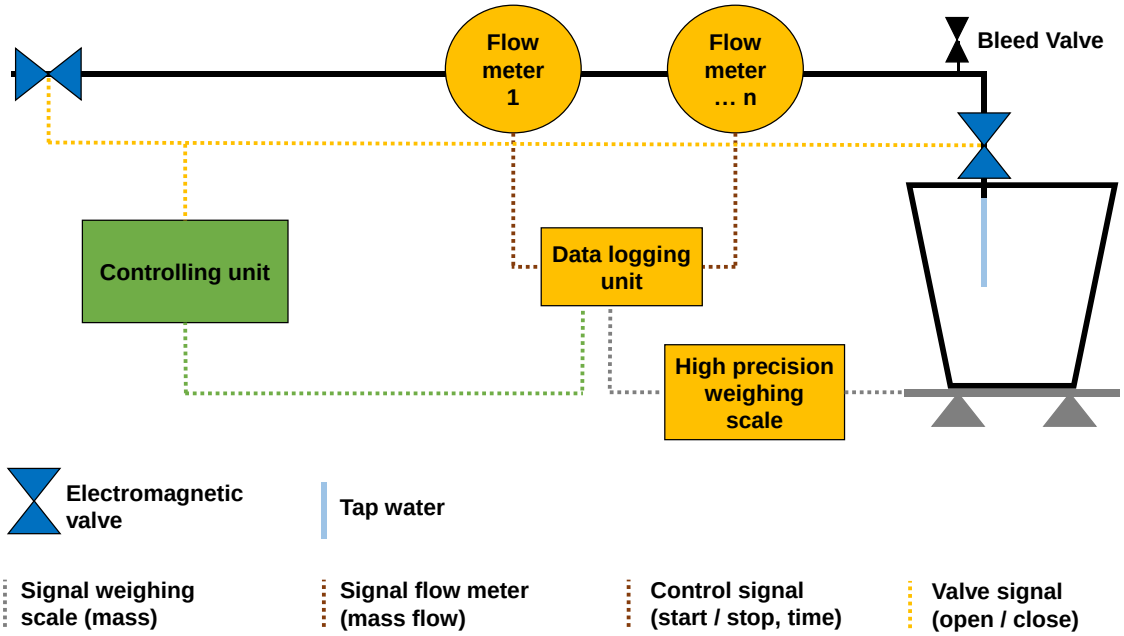

Figure 4.11: Schematic illustration of the calibration procedure for flow meters

The testing rig is connected to a tap water valve. Electromagnetic valves are put at the start and the end of the testing rig circuit. Between the valves, one or more flow meters can be tested. A vessel is put on a high precision weighing scale (±1 gram). Subsequently, the scale is zeroed. The digital output of the scale is connected to the data logging unit. By activating, a switch at the controlling unit, the valves open and a mass flow is established. The flow meter detects the mass flow and the tap water fills up the vessel. At the time, the switch activates this procedure, the data logging unit starts logging the volume flow and the duration. As soon as the vessel is filled up, the valves are closed by the controlling unit and the measurement is stopped. Based on the test duration and the current volume flow, the flow meter is compared with the value of the high precision weighing scale by integrating the volume flow. To calculate the mass flow, additional temperature sensors (RTD, four terminal sensing) are used to determine the density of the water.

Table 4.8 shows the deviation between the high precision weighing scale and the integrated mass flow over the time.

Table 4.8: Results of the mass flow meter calibration for a volume flow of 150.9 litre per hour at a mean fluid temperature of 18.08 °C

Parameter	**Value**
Mass of weigh scaling in kg	119.1
Integrated mass flow in kg	119.2
Deviation in kg	0.1
Relative deviation of flow meter in %	0.084

4.7.2 Temperature sensor calibration

Figure 4.12 shows the setup for the temperature sensor calibration.

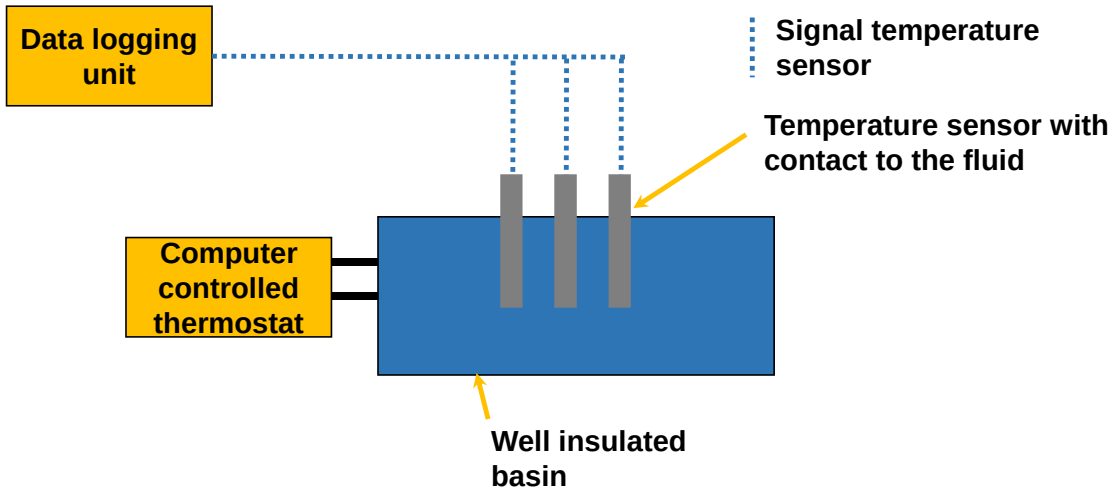

Figure 4.12: Schematic setup of the calibration procedure for temperature sensors

A very well insulated basin with a computer-controlled thermostat connected to it was used to calibrate the temperature sensors. The computer-controlled thermostat is set to different temperature levels and heats up the fluid in the calibration basin. At the same time, the temperature sensors are logging the temperature in the basin. The logging data is displayed in real-time. If there is no further temperature change for 5 minutes in the basin and the fluid temperature is close to the temperature adjusted at the computer-controlled thermostat, the next temperature level is set. After several temperature stages, the collected data is processed and the sensors are compared. A calibrated temperature sensor (RTD, four terminal sensing, 1/10 DIN class B, Platinum 100 Ohm) is used as reference for this type of procedure.

Figure 4.13 shows the correlation for the thermocouples before the calibration procedure.

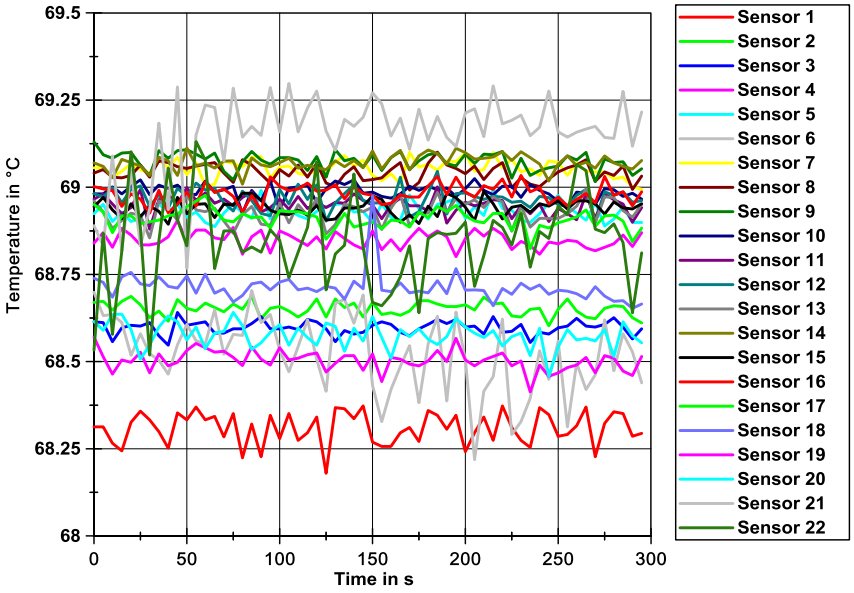

Figure 4.13: Sensor correlation without calibration

The sensors differed by up to ±0.5 K before the calibration. The data logging unit includes a separate menu for sensor calibration, which was used to achieve a better correlation of the temperature sensors. In Figure 4.14 the logged temperatures after the calibration is shown.

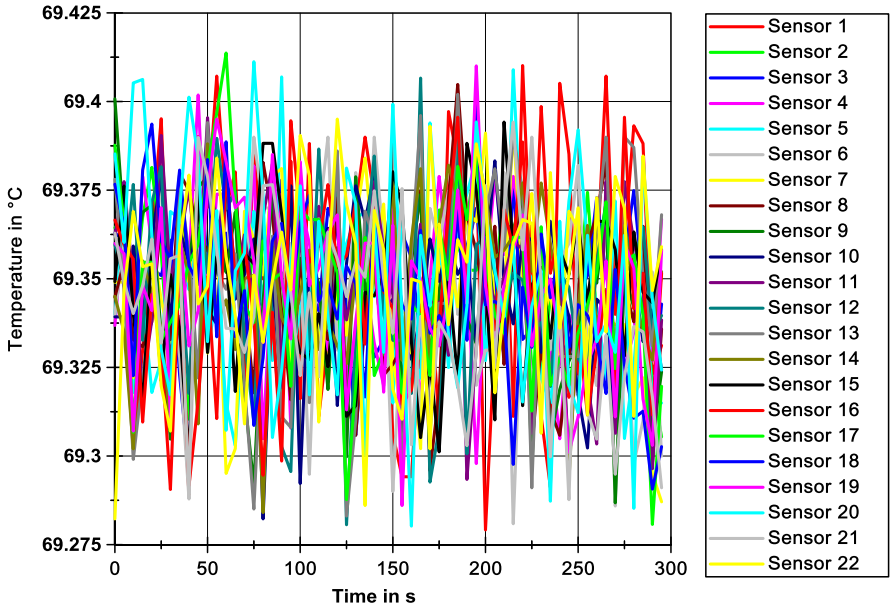

Figure 4.14: Sensor correlation after calibration

After the calibration, the initial sensor difference was reduced to ±0.07 K. This value was derived for several temperature levels and various experiments. Hence, the uncertainty for the temperature sensors was assumed ±0.07 K.

Based on this calibration process, the standard deviation (Equation 4-7), variance (Equation 4-8) and confidence level (Equation 4-9) can be calculated:

$$s = \left(\frac{1}{n-1} \sum_{i=1}^{n} (x_i - \bar{x})^2 \right)^{0.5} \qquad \text{Equation 4-7}$$

The variance is derived by the following equation:

$$s^2 = \left(\frac{1}{n-1} \sum_{i=1}^{n} (x_i - \bar{x})^2 \right) \qquad \text{Equation 4-8}$$

The confidence level is defined by:

$$\mu = \bar{x} \pm t \frac{s}{\sqrt{n}} \qquad \text{Equation 4-9}$$

Table 4.9 comprises the statistic parameters for the 22 sensors.

Table 4.9: Standard deviation, variance and confident level of all 22 sensors

Sensor	s	s^2	μ_{95}
1	0.03485551	0.00121491	0.00900415
2	0.01993654	0.00039747	0.00515017
3	0.01908969	0.00036442	0.0049314
4	0.02286956	0.00052302	0.00590785
5	0.02461456	0.00060588	0.00635863
6	0.02865777	0.00082127	0.00740311
7	0.02476428	0.00061327	0.00639731
8	0.02445231	0.00059792	0.00631672
9	0.02488392	0.00061921	0.00642821
10	0.02061803	0.0004251	0.00532621
11	0.02429222	0.00059011	0.00627536
12	0.02693541	0.00072552	0.00695817
13	0.03066477	0.00094033	0.00792157
14	0.02172594	0.00047202	0.00561242
15	0.02291009	0.00052487	0.00591832
16	0.02655315	0.00070507	0.00685942
17	0.0246766	0.00060893	0.00637466
18	0.02327523	0.00054174	0.00601264
19	0.02432536	0.00059172	0.00628392
20	0.0309042	0.00095507	0.00798342
21	0.02616676	0.0006847	0.00675961

22	0.02651339	0.00070296	0.00684915

The overall standard deviation, variances and the confidence level are shown in Table 4.10.

Table 4.10: Overall standard deviation, variances and confident level (n = 1320)

Sensor	**s**	**s^2**	**μ_{95}**
1 to 22	0.02542859	0.00064661	0.0013753

5 Analysis of the mechanical behaviour of an all-round supported absorber

A technical challenge of a sealed interspace is the pressure change in the cavity and the thermal deformation of the absorber during collector operation, resulting in a mechanical load on the absorber, the edge bond and the glazing. As the absorber is less rigid and hotter than the glazing, the absorber experiences the largest deformation.

To keep the collector design simple, neither an interspace pressure below ambient pressure nor an additional expansion tank were considered in this research.

The mechanical behaviour of a statically over-determined (hyper-static) absorber was simulated taking the thermal elongation of the absorber and the dependent pressure into account. Furthermore, the qualities of a geometrically non-linear and a geometrically linear finite element model were discussed and compared. A physical model of an all-round fully adhesive supported absorber was set up and investigated in laboratory tests. Ultimately, the validated model was used for a parameter study of an optimised absorber design for a hermetically sealed collector with a fully adhesive edge bond.

An overview of finite element simulation and its principles can be found in Klein (2007), Jung and Langer (2013), Gebhardt (2011) or Braess (2010).

5.1 Review of conducted research in this field

Vestlund et al. (2012b) discussed the movement and mechanical stresses in sealed solar collectors at ambient pressure. The authors used a basic finite element model to examine the behaviour of the sealed collector and its components. A sheet-pipe absorber was modelled as a tray connected at its edges to the glazing. The connection between absorber and glazing was modelled as if there were a rigid support. In real applications, an adhesive bead is used to achieve a sealed cavity, which also allows deformation. In addition, only a quarter of the absorber was analysed and a symmetrical deformation was assumed.

The parameter studies were conducted using a gas temperature range of 300 to 500 K, but the thermal expansion of the components was ignored,

including that of the absorber. Vestlund et al. (2012b) justified this by calculations that showed only a minor influence in the volume change compared to the volume change due to the pressure rise. Unfortunately, these calculations were not explained further and so the decision to ignore thermal expansion of the absorber is questionable.

It should be noted that Vestlund et al. did not mention in their publications whether geometrical non-linearity effects were included. Considering the results of the finite element analysis of Vestlund et al. it is possible that a geometrically linear model was used.

Vestlund's model validation is problematic. It was not explicitly mentioned how the validation was carried out, nor was the named reference accessible. In addition, the author's own laboratory tests (Riess et al. 2013) showed a deviation to the results of Vestlund et al.

Neither the behaviour of the adhesive edge bond nor the thermal expansion of the absorber was studied in the research conducted by Vestlund. Furthermore, there was no distinction between the use of a geometrically linear or non-linear model. In fact, the used approach was not mentioned. This may be regarded as a weakness since these factors have a considerable influence on the deflection of the absorber and should therefore be included in studies.

5.2 Implementation of a finite element collector simulation model

Modelling and constraints

Initially, an absorber model was set up in the finite element programme ANSYS Workbench (mechanical). The model is composed of a harp absorber made out of aluminium, an adhesive edge bond and the glazing (Figure 5.1).

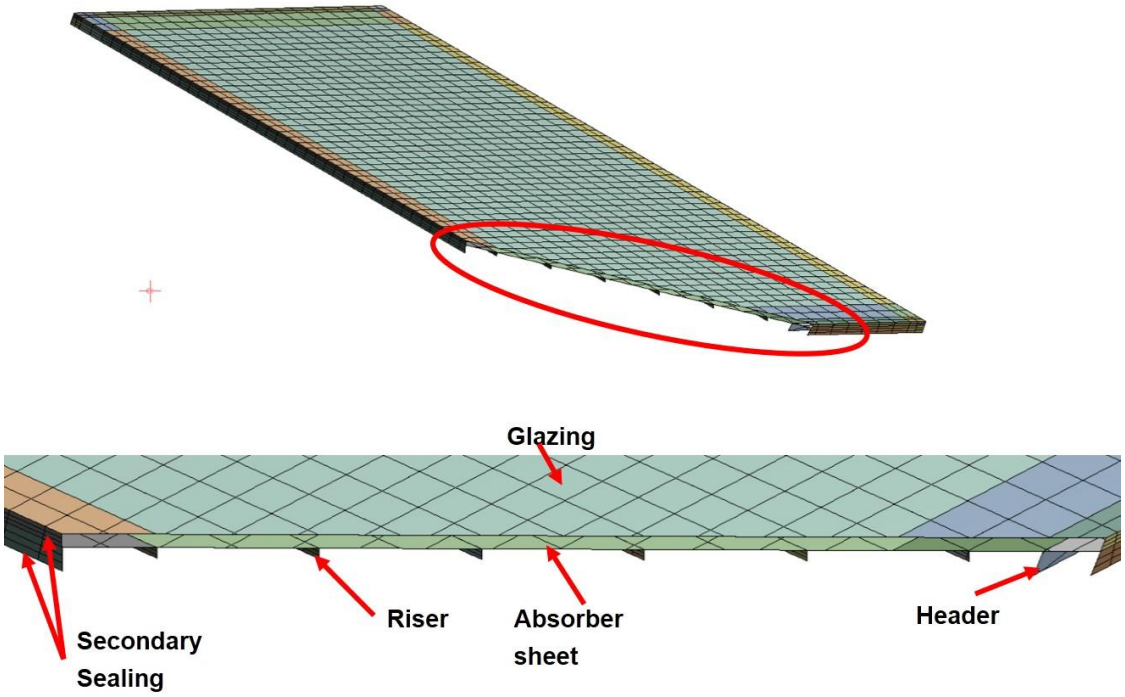

Figure 5.1: Detail view of the finite element model

The model was built up in a CAD environment as a 3D surface model and implemented in the FE programme. During the research, it became clear that it was necessary to model two absorber types – an 'ideal' shaped absorber and a 'real' shaped absorber. The idealised absorber shape was assumed to be a perfect plane parallel to the glazing without any initial deflections. By contrast, for the real shaped absorber the initial deflections of the collector prototype's absorber used in the laboratory testing were taken into account. The shape of the absorber's initial deflection were taken in laboratory testing. The procedure is described in chapter 4.4.

Figure 5.2 shows the element size, the support and the connection type between the components.

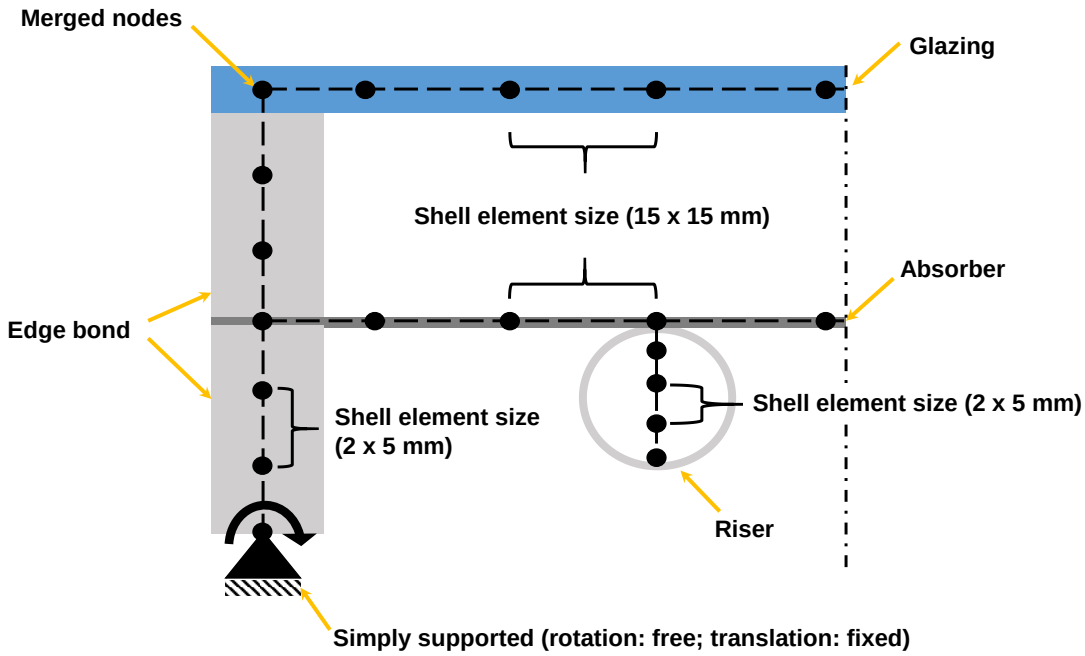

Figure 5.2: Schematic cross section of the FE model

The edge bond is divided into two sections. The upper part connects the absorber and the glazing whereas the lower part connects the absorber and the back plate. In particular, the components were connected via merged nodes. An element size of 2 x 5 mm for the edge bond as well as the piping, i.e. riser and header, had an element size of 2 x 5 mm. The absorber and glazing were meshed with elements of the size 15 x 15 mm. This mesh is shown more in detail in Figure 5.3.

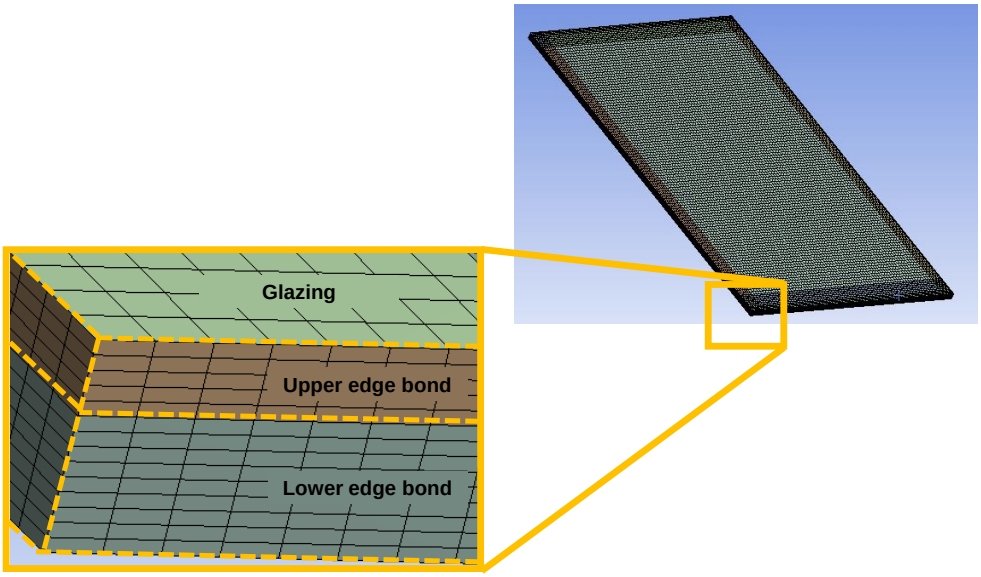

Figure 5.3: Detail view of the mesh of the edge bond and the glazing

In the simulation, the insulated back plate was not modelled. Therefore, the lower edge of the edge bond was simply supported, i.e. rotationally degree of freedom is not fixed whereas the translation is fixed. The elements used for the FE model were shells. The elements lie in the neutral plane of each component. It is assumed that there is no material plasticizing, i.e. linear material behaviour was used. Finally, the earth's gravitation field was taken into account for a collector inclination of 45°.

To ensure an acceptable mesh quality, a mesh refinement study was conducted. Therefore, the idealised absorber was meshed with different element sizes and the expansion volume was computed (Table 5.1).

Table 5.1: Results of the mesh size study for the idealised absorber with a pressure load of 50 Pa

Variant	Elements	Nodes	ΔV_{exp} in litre	Deviation in %
1	33,935	33,984	7.86	0
2	22,992	23,081	7.95	+1.1
3	13,550	13,614	7.91	+0.6
4	5,943	6,001	7.98	+1.5
5	1,730	1,770	7.45	-5.2
6	591	640	3.95	-49.7

The applied mesh consisted of 33,935 Elements and 33,984 nodes (Figure 5.3 and variant one in Table 5.1). For this study, the idealised absorber was meshed with six different meshes whereas the mechanical load was kept steady at 50 Pa. For all the variants, the expansion volume was calculated and compared. Even with variant four, ΔV_{exp} varies to the applied mesh by only +1.5 %. A significant change was detected for a very coarse mesh (variant five in Table 5.1) with 1,730 elements and a deviation of -5.2 %. It was assumed that the chosen mesh size is sufficient to conclude on the absorber's expansion volume.

The ambient conditions, collector parameters and material properties can be seen in Table 5.2.

Table 5.2: Boundary conditions and parameters used in the finite element simulation.

Ambient conditions	
Pressure in kPa	100
Temperature in K	295
Material properties	
Elastic modulus in GPa – Glazing	70
Poisson's ratio – Glazing	0.23
Elastic modulus in GPa – Aluminium	70
Poisson's ratio – Aluminium	0.33
Thermal expansion coefficient in 1/K – Aluminium	$23 \cdot 10^{-6}$
Elastic modulus in MPa – Edge bond	2.83
Poisson's ratio – Edge bond	0.415
Geometric parameters	
Glazing thickness in mm – Tempered glass	3.2
Absorber thickness in mm – Aluminium	0.5
Absorber length in mm	1825
Absorber width in mm	1100
Fin width in mm – w_{fin}	109
Outer diameter in mm – Riser	8
Wall thickness in mm – Riser	0.4
Outer diameter in mm – Header	18
Wall thickness in mm – Header	0.8
Edge bond thickness in mm	10

Simplifications

In reality, a temperature gradient exists along the flow of the fluid in the absorber during collector operation or from collector bottom to top in stagnation. Measurements showed that this gradient is small (Figure 5.4).

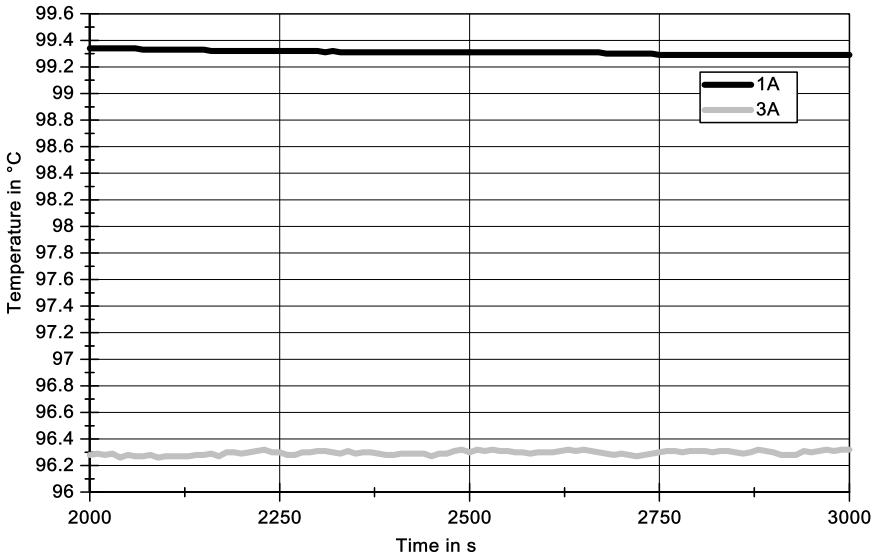

Figure 5.4: Temperature difference of about 3 K in the middle axis of the absorber between top (1A) and bottom (3A) during a measurement deflection under the solar simulator

Figure 5.5 shows the sensor position on the absorber back.

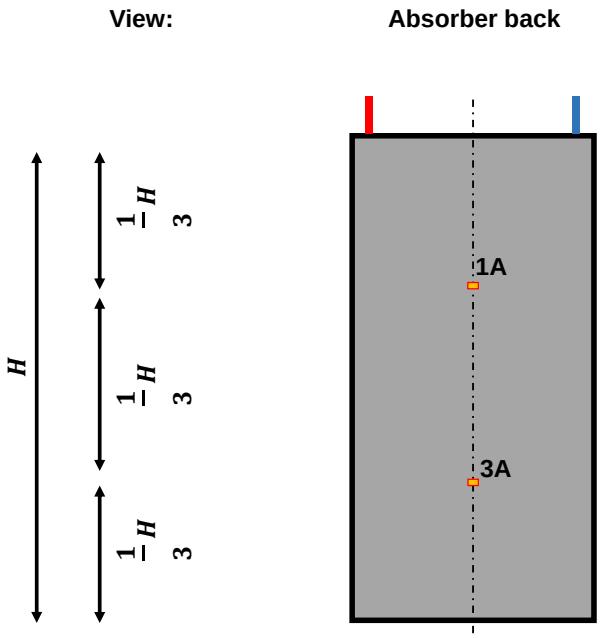

Figure 5.5: Sensor position of 1A and 3A on the absorber (harp) back

The measured gradient of 3 K is considered to be small and, thus, the finite element model refers to a uniform absorber temperature.

The piping was modelled as rectangular beams. This is justified since the beam section modulus and height are the same as the original risers and headers. Eventually, this leads to the same flexural behaviour and maximum stress. Figure 5.6 and the following calculation clarifies this approach.

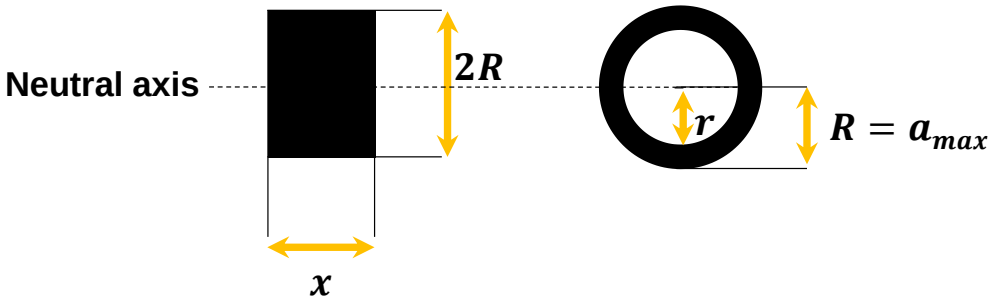

Figure 5.6: Parameters of the substitution of an annulus by a rectangular beam

If the 2nd moment of area of the beam and the annulus are equalled, the beam width x can be derived as follows:

$$J_{\blacksquare} = J_{\odot}$$

$$\frac{x\,(2R)^3}{12} = \frac{\pi}{4}(R^4 - r^4)$$

$$x = 3\frac{\pi}{8} \cdot \frac{R^4 - r^4}{R^3} \qquad \text{Equation 5-1}$$

As the distance to the neutral axis of both geometries are identical, the section modulus can be expressed by:

$$W = \frac{J}{a_{max}} = \frac{J}{R} \qquad \text{Equation 5-2}$$

Hence, the annulus can be substituted by a rectangular beam without changing the mechanical behaviour.

The junctions between header and riser were not modelled in this research; however, in this joint high stress levels are reached. Considering a collector life of 20 years or more, the stresses in these soldered or welded joints should be analysed. To retain correct stress dimensions, only the joint with its welded seam

needs to be modelled with solid elements. Subsequently, the sectional forces can be applied as a load on this model. The sectional forces could be computed using a model similar to the one used in this thesis. To provide a collector function throughout the lifetime, it is important to consider fatigue – especially of the absorber and edge bond. Theses aspects should be brought to attention in a further detail study.

In the simulation, sufficient space between absorber and insulation is assumed, to ensure an unimpeded absorber deflection (Figure 5.7).

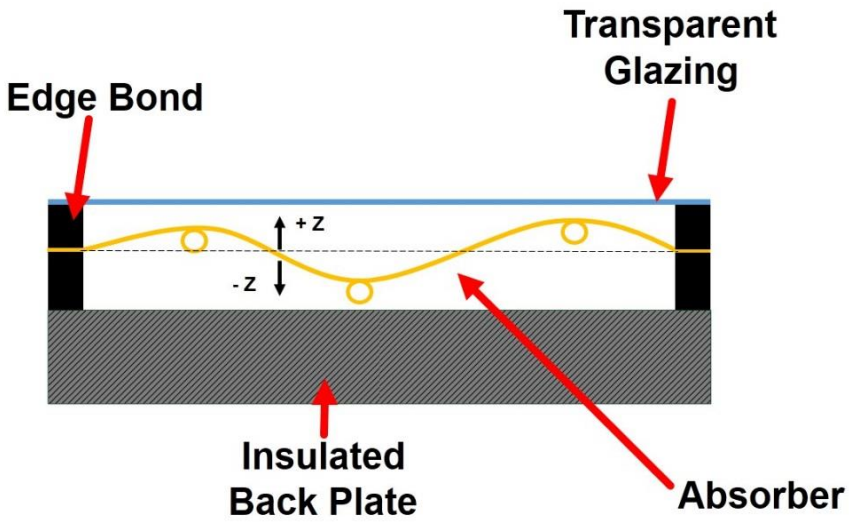

Figure 5.7: Visualisation of the absorber movement

Due to the relatively low temperature of the glazing and its smaller thermal expansion coefficient, the lengthening of the glass has no major effect on the mechanical behaviour of the absorber. The elongation of the glazing with a length of 2 m for a temperature rise of 40 K would be less than 0.6 mm. The chosen glazing material properties are the ones for a single pane of safety glass.

Since the absorber is all-round supported and the thermal expansion of the absorber is considered as well as its initial shape, plate buckling can result, which might cause asymmetric deflections. Hence, a complete absorber was implemented in the finite element programme. If only the pressure change were analysed, a symmetry axis could have been used to reduce the total number of nodes, thus accelerating the computation.

Aluminium has been chosen for the absorber sheet and the piping, as it is likely that aluminium absorbers are going to replace more costly copper absorbers in

the future. There are some advantages of copper compared to aluminium. The thermal expansion coefficient of copper is 28 % less than that of aluminium. This leads to a lower temperature elongation compared to aluminium and, thus, to a less temperature-driven deflection. Collector constructions with an aluminium absorber sheet and copper piping are especially sensitive to thermal stress because of their different thermal expansion coefficient. The deflection of a conventional absorber, (i.e. non-hyper-static), is described by Föste et al. (2013b).

5.3 Comparison of geometrically linear and non-linear approaches

A linear finite element model calculates the deformation based on the initial stiffness matrix during the complete procedure. By contrast, by using a geometrically non-linear finite element model the change of the stiffness according to the current deflection is considered (Figure 5.8).

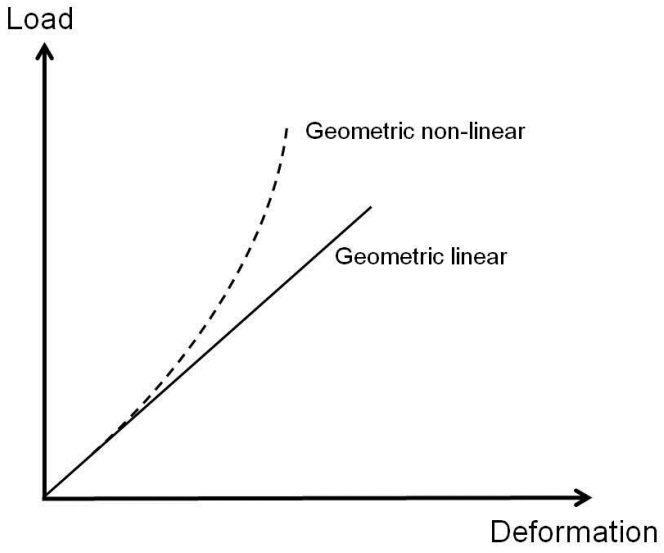

Figure 5.8: Comparison of the geometric linear and non-linear approach

Hence, using a linear FE model for problems with ‘large’ deformations will give inaccurate estimations of either the load or deformation.

The mechanical behaviour of the absorber can best be modelled using plate theory. In relevant publications in this field, rules can be found regarding the use of a geometrically linear or non-linear model (Klein 2011); (Raecke 2013).

Feldmeier (1984, 1996) analysed the mechanical behaviour of gas-filled insulated glazing units, which have a layout similar to the proposed collector design. By simulation and testing, Feldmeier proved that at deflections exceeding the components' material thickness, an error of more than 100 % occurs. As soon as the deflection exceeds the plate thickness the linear Kirchhoff plate theory becomes inaccurate. To simplify the design of IGU and to avoid failure in their design, the norm for overhead glazing limits the deformation of the exposed pane to its material thickness resulting in a higher safety factor but also an oversizing of the product.

The author's own data from simulation and laboratory testing on the physical collector showed that in the case of an all-round supported absorber the maximum deformation is 20 times larger than its thickness. Thus, a simulation model is needed that includes the effect of geometric non-linearity.

5.4 Model validation

To validate the finite element simulation two physical models were constructed and used to analyse the mechanical behaviour at certain collector operation points. In particular, the expansion volume and the shape of the deflected absorber were measured and compared to the simulation results. One of the physical models was equipped with a differential pressure transmitter allowing tests with a sealed and opened interspace. The tests were carried out using a solar simulator.

To measure the real deflection of the fully adhesive supported absorber the back plate and insulation of this collector were removed. Subsequent to this, a matrix of 323 measuring points was applied on the absorber back side.

It was assumed that there is only a movement in the z-axis of the absorber. The z-coordinate of the measured points was recorded twice for each test run – at ambient conditions and in the collector operation state. To measure the point displacement in the z-direction a digital vernier caliper was used which was fixed on a supported traverse, assuring a constant zero level. By measuring ΔV_{exp} and $T_{glazing}$, the pressure change can be calculated. For further details, please see chapter 4.4.

There are some uncertainty factors in the measurement method, which influence the calculated volume expansion of the absorber. As the absorber thickness is only 0.5 mm, there will be always some sporadic buckling. Another element of uncertainty is the measurement method itself. However, throughout the work a precise optical metrology was used to validate the accuracy of the manually recorded displacements. The comparison showed a good accordance giving an uncertainty margin of 0.5 mm. These factors result in a total deviation of ± 1 litres in the volume determination (see also chapter 4.4).

The expansion volume was deduced by the relative z-displacement of the 323 points multiplied by the absorber surface.

The coordinates measured with the vernier caliper were rounded to the nearest 0.1 mm. The absorber temperature and glazing temperature were taken at 2/3 of the height and in the middle of the absorber.

5.5 Simulations results

Initially, the dependency between the pressure change and ΔV_{exp} was analysed for the idealised absorber (Figure 5.9).

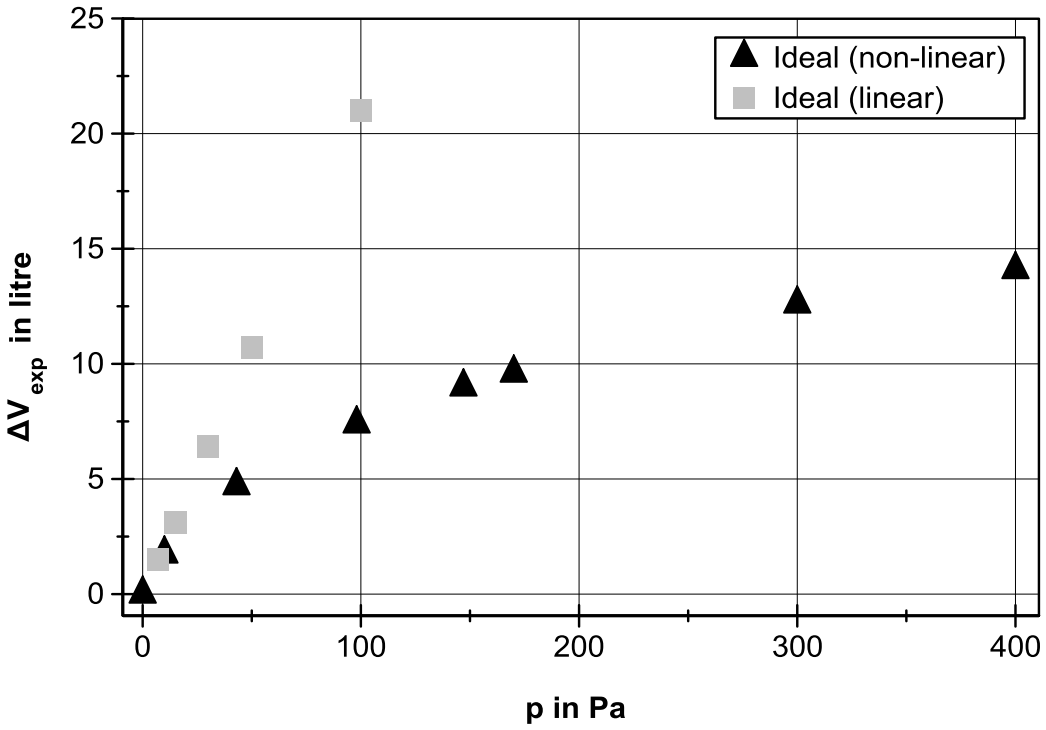

Figure 5.9: Dependency between pressure load and expansion volume

The pressure was varied between 0 and 400 Pa. Figure 5.9 shows the increasing absorber rigidity of the geometrically non-linear model with higher pressure loads. For comparison the same study was conducted with a geometrically linear model. At very small deflections the approach of a geometrically linear model is in good agreement with the geometrically non-linear model.

Figure 5.10 shows the deflection curve taken from the middle axis of the absorber in longitudinal direction.

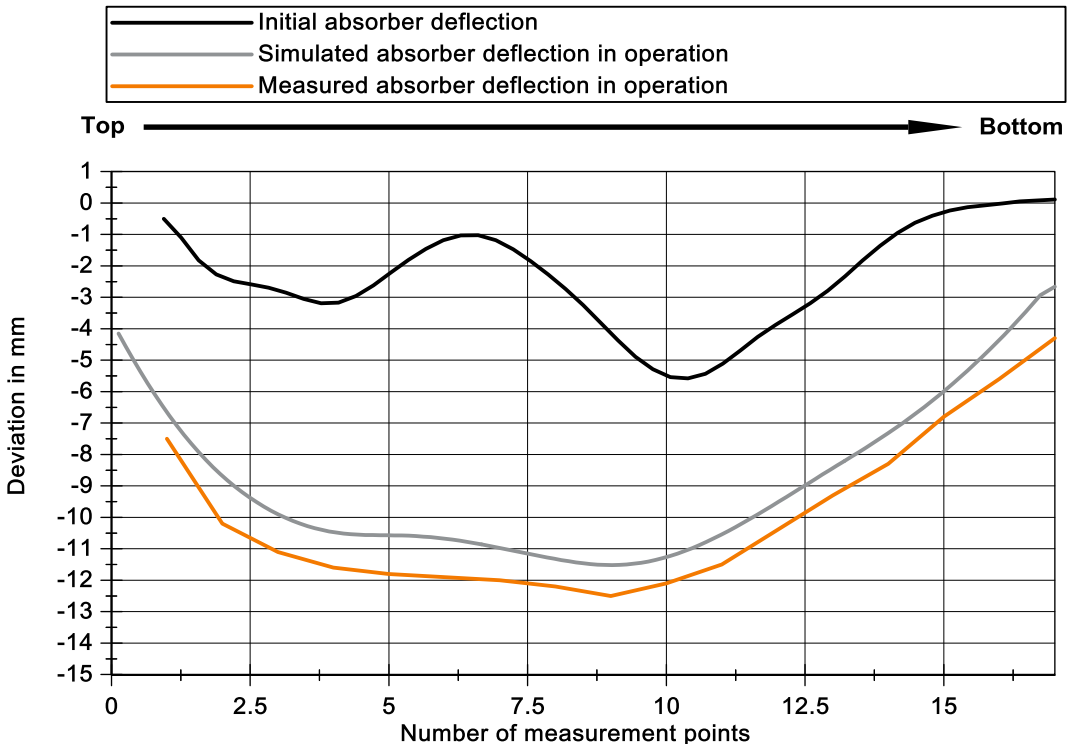

Figure 5.10: Initial (black), simulated (grey) and measured (orange) deflection curve from the middle axis of the absorber in longitudinal direction

The black curve is the initial absorber deflection, which was measured with the digital calliper. The grey line resulted from simulation results of the absorber model with the initial distortions (real shaped absorber) whereas the orange line is the manual measured absorber deflection. Both lines, grey and orange, were derived for the identical collector operation point.

The shape of the simulation results is in a good correlation with the laboratory results. However, the results obtained by laboratory tests are showing a less rigid behaviour than the simulation results. In Figure 5.11 the solution of the FE model is shown.

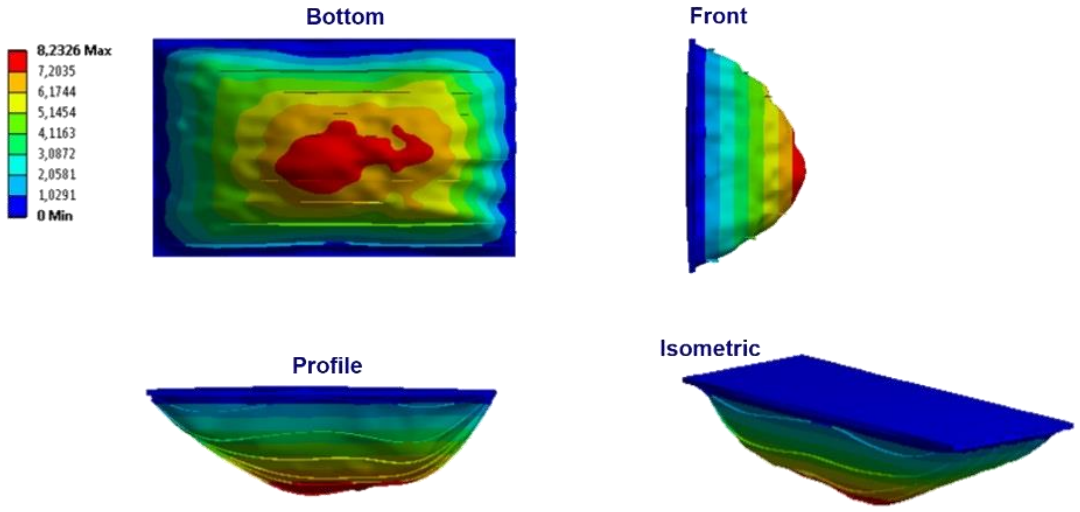

Figure 5.11: Overview of the simulated absorber deformation in mm (twentyfold magnification; example)

Overall, the idealised absorber shows a less rigid behaviour than the real absorber, as tested in the laboratory. In this model only the initial deflections were implemented, the pre-stresses in the material caused by the welding were not included. This factor could be one of the main reasons for the deviation.

Figure 5.12 shows the dependency of the change of the expansion volume and the absorber temperature and mean gas temperature.

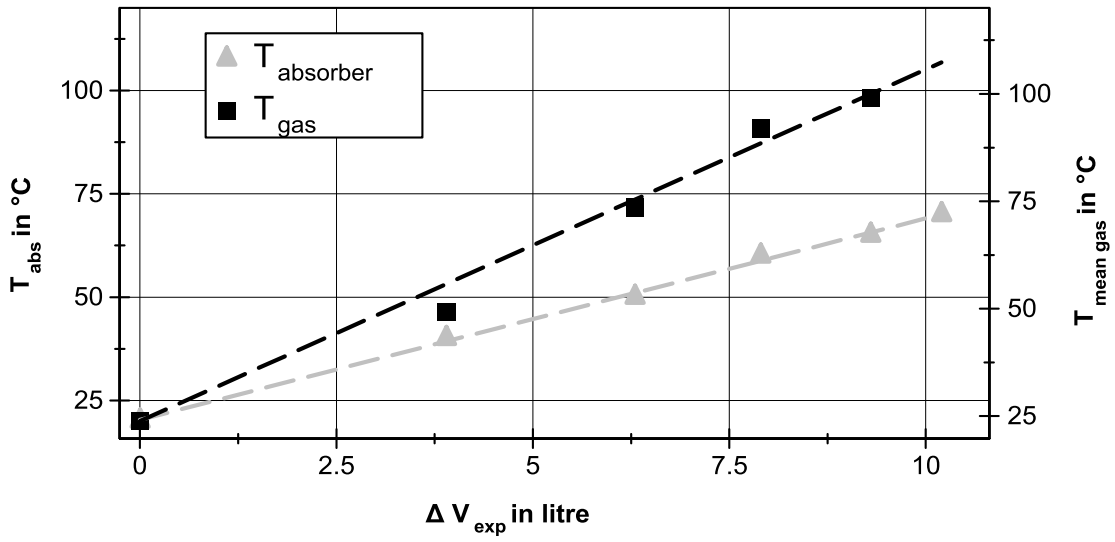

Figure 5.12: Dependency of the change of the expansion volume and the absorber temperature and mean gas temperature

By knowing the ambient conditions, the overpressure and the corresponding expansion volume, it is possible to calculate the mean gas temperature in the collector in this operation point: By laboratory testing, an expansion volume of about 7 litres was computed for a pressure rise of 170 Pa. By applying the ideal gas law, this corresponds to a mean gas temperature of at least 367 K. The mean gas temperature is assumed to be midway between the absorber temperature and glazing temperature. Therefore, T_{abs} is significantly higher than the mean gas temperature during normal collector operation. However, at a temperature rise of only 74 K the absorber elongates by about 2.9 mm. This length variation is accommodated by a deflection in the z-axis as the absorber is constrained on all four edges. In the simulation, the absorber was heated from ambient conditions up to a uniform absorber temperature of 367 K. At this state, an extra volume of about 12 litres was computed, and this was caused purely by the thermal expansion of the absorber.

This leads to the assumption that the thermal expansion of the absorber is actually the driving factor and not the gas expansion. In fact, the expansion volume caused by the thermal elongation could compensate to an extent for the tendency towards overpressure. Eventually, the assumptions on the pressure change and thermal absorber elongation made from the simulation and testing could lead to the following behaviour:

- The collector, which is in the beginning at ambient condition ($T_{abs} = T_{amb}$, $p_{diff} = 0$ Pa), is exposed to an irradiation, e.g. by the sun or a solar simulator.
- This energy input leads to an immediate temperature increase of the absorber.
- Driven by this temperature increase, the all-round supported absorber starts to elongate.
- As the absorber is supported along all edges, the initial absorber shape is magnified. This can result in a sheet deflection towards the glazing or away from it. In the testing and simulation, the initial enclosed volume between absorber and glazing was enlarged. Depending on the initial absorber shape it is possible that either a negative or positive pressure sets in.
- Assuming a growth of the enclosed volume (ΔV_{exp}), the pressure drops and a negative pressure occurs. This is owed to the fact that the absorber sheet heats up faster than the enclosed gas volume.

- At the same time, the gas heats up and expands. However, the gas temperature rise sets in delayed compared to the rise of the absorber temperature.
- By the gas expansion, the pressure in the cavity rises.
- Once the absorber temperature cools down to ambient condition, the gas temperature will follow. Consequently, the pressure difference is equalled again.

This assumption was strengthened by laboratory tests with the collector prototype (see chapter 0, Figure 5.14).

It has to be checked whether this circumstance is applicable for all hermetically sealed collector types. Furthermore, it is interesting which collector parameters can be used as design criteria to achieve a controlled absorber deflection. However, unlike stated in literature that means in the interspace a pressure below ambient pressure can occur.

For the edge bond, a basic stress analysis was conducted. In particular, the von Mises yield stress and the shear stress were calculated by the FE model. The absorber was in a typically operation point with a mean absorber temperature of 80 °C. For the von Mises yield stress, a maximum value of 0.2 MPa at the absorber long side was calculated (Figure 5.13).

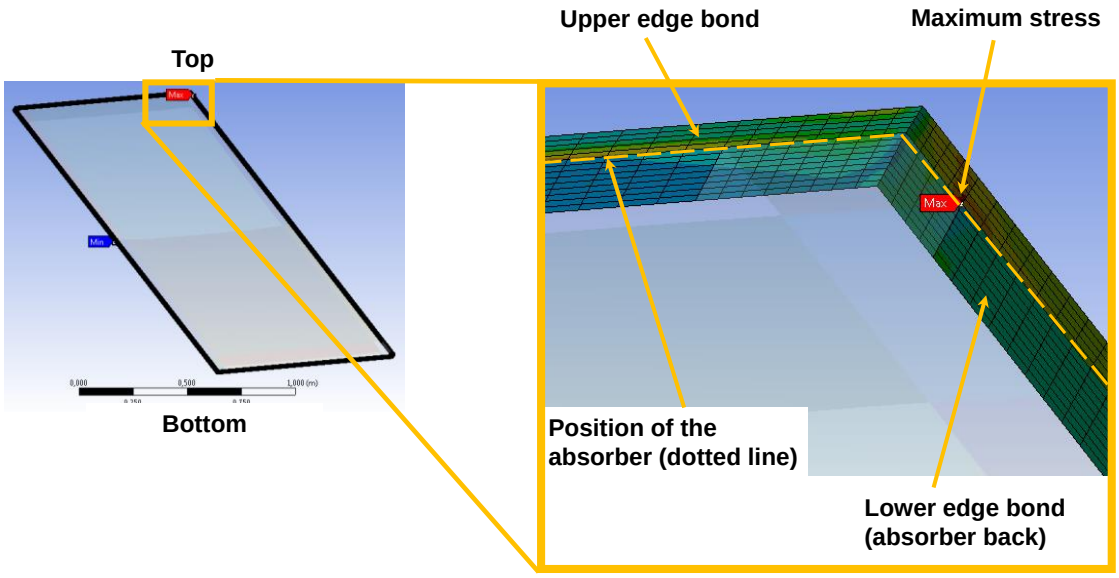

Figure 5.13: Detail view of the von Mises yield stress on the edge bond

According to the adhesive's tensile strength of 2.85 MPa, this computed value is seen as uncritical. The same applies for the shear stress analysis. A shear stress of only 4,348 Pa on the long side was computed, which is compared to the maximum shear stress of 0.15 MPa rather small.

Yet in further research studies, there needs to be a more detailed stress analysis conducted for all the collector components. This should include solid elements instead of shell elements and a fine mesh. Beyond that, further temperature dependent material data for the adhesive is needed to conclude on the precise stress level. Finally, a higher temperature of up to 200 °C should be simulated in combination with a thermal shock test, i.e. sudden cooling of the edge bond.

5.6 Laboratory testing

In particular, three kinds of tests were carried out with the physical model. First the model was loaded by pressurising the interspace. In a second test only the thermal elongation at ambient pressure was measured. Finally, both loads were superposed, i.e. the collector was equipped with a pressure transmitter and sealed at ambient conditions.

Figure 5.14 is in agreement with the results obtained by the FE simulation.

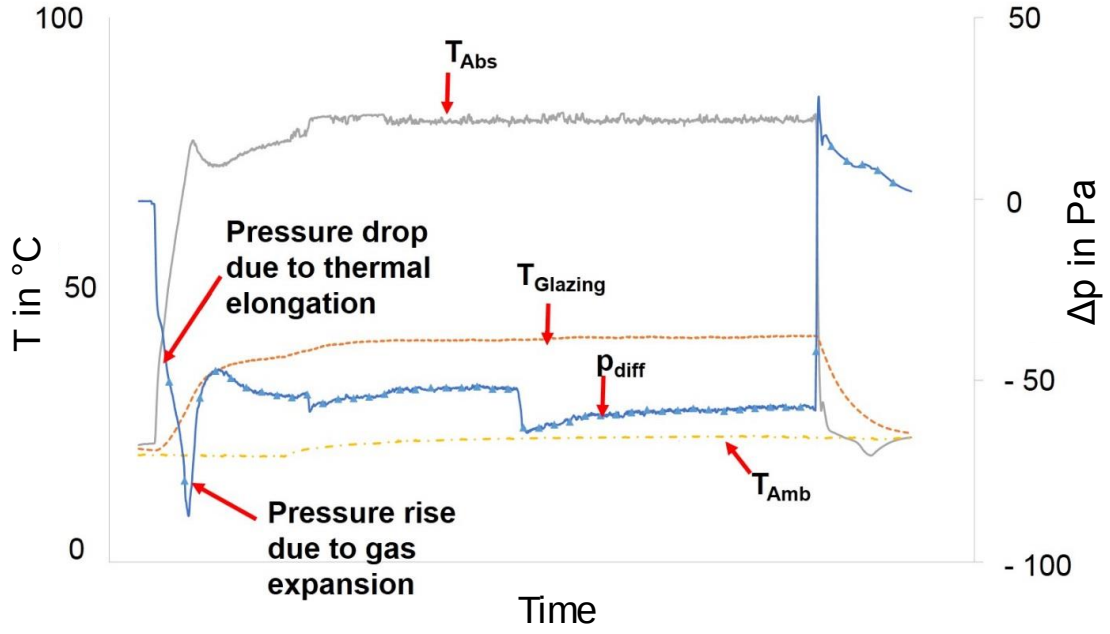

Figure 5.14: Pressure change during a test run with sealed interspace

The pressure change is at first related to the absorber temperature. As T_{abs} rises the pressure drops because of the volume expansion caused by the thermal elongation of the absorber. After some time, the gas in the interspace heats up and the negative pressure decreases. At the end of the test run, the pressure rises again as the absorber cools down and less expansion volume is available. Finally, the pressure is again at ambient conditions.

Figure 5.15 shows the correlation between the ideal absorber (plane parallel) and the real shaped absorber with its initial distortion, which were both used in the simulation, as well as the measured deflection of the actual prototype for a pressure between 43 and 170 Pa.

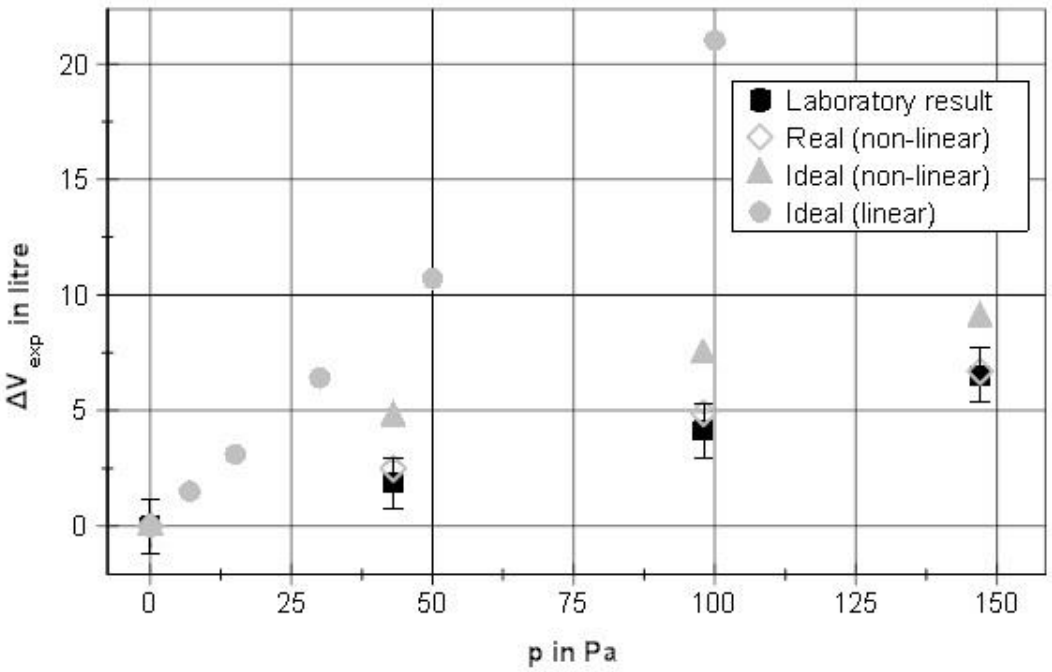

Figure 5.15: Comparison of the simulation results and results obtained by laboratory testing

The graph shows a significant deviation between the ΔV_{exp} of the ideal absorber and the laboratory results. In reality the absorber has an initial deflection, which dominates the deformation. A main cause of this is the welding process during the absorber production as the material is pre-stressed by structural changes. To obtain a better correlation between simulation and measurement the initial deflection of the absorber was taken into account for the FE model. In fact, this implementation is in a very good agreement with the laboratory results.

5.7 Summary

The key finding of this simulation results from an analysis of the mechanical behaviour of an absorber that is all-round supported by a fully adhesive edge bond. As a result of this research, a physical model of a fully adhesive bonded flat plate solar collector has been created. A finite element model of the absorber was implemented and compared with test results collected in laboratory tests. Two different finite element models (geometrically linear and non-linear) were investigated. The pressure change as well as the thermal elongation of the absorber for a temperature difference of 80 K was taken into account.

For an absorber that is all-round supported an elastic edge bond was modelled. An idealised support, such as a linear support, might not reflect the real mechanical behaviour.

The results show that the model including geometric non-linearity is much closer to the reality. By contrast, using geometrical linearity will lead to an oversizing of the components, which increases costs.

It was shown that thermal elongation cannot be omitted in such simulations. In fact, the expansion volume created by the thermal elongation dominates the pressure change. For the prototype, a pressure below ambient was found, which shows that the pressure variation can occur in both directions. By adjusting parameters, e.g. absorber thickness, edge bond width or gap size, the pressure variation (negative or positive) could be influenced. These influencing parameters have to be studied more in detail.

The mechanical behaviour of the real shaped absorber in simulation is almost identical to the behaviour measured in the laboratory tests. It can be assumed that the simulation model itself is correctly set up regarding the material parameters and constraints. The only difference between the ideally shaped absorber and the real shaped absorber is the initial deflection. Therefore, it is concluded that the model of the idealised absorber can be used for further simulation studies. This is an important result as the initial deflection of every absorber differs.

Even though, the absorber deflection of the physical model was to the ‘back’, the absorber could have shown a deflection towards to the glazing as its deformation is strongly dependent on the initial deflection. An interspace pressure below ambient will reinforce this behaviour. For this design, it is important to prevent an uncontrolled deflection.

6 Thermal analysis of a hermetically sealed collector

The key function of a solar flat plate collector is generating useful heat. This fact makes the thermal analysis an essential part in the design approach of a new type of solar collector. In this section, published literature about collector modelling is discussed, the applied numerical simulation model is presented, the importance of the convective heat transfer in solar collectors is analysed, simulation results are compared with laboratory results and different approaches for the calculation of the convective heat transfer are compared and evaluated. Finally, the simulation model is validated by test results.

Vestlund et al. (2009) set up a thermal model based on heat transfer formulae to analyse the performance of a gas-filled flat plate collector at ambient pressure. This simulation study included a sensitivity analysis of the convective heat transfer calculated by the widely used approach after Hollands et al. (1976) as well as an efficiency prediction of a gas-filled collector. Their results showed a superior collector efficiency compared to a conventional solar collector: For a typical collector operating temperature for space heat support systems with a mean fluid temperature of 60 K above T_{amb}, an increase in the efficiency of about 5 % for an argon filled collector was simulated. However, with rising collector operating temperatures, this efficiency difference between conventional and gas-filled collector increases further. Vestlund et al. (2009) derived an improvement in efficiency for T_{mean}-T_{amb} = 100 K of more than 10 %.

Beside the inert gases, Vestlund et al. (2009) analysed carbon dioxide as a gas filling but it proved to be of no interest as the collector performance is similar to that of air. The authors' concluded that gas-filled solar collectors at ambient pressure are enabling higher efficiencies and a thinner collector design. Yet, further analyses are needed to determine the mechanical behaviour of the collector (Vestlund et al. 2009). In 2012, a study was published on the thermal and mechanical performance of gas-filled collectors at ambient pressure (Vestlund et al. 2012a, 2012b). These papers are a combined analysis of the thermal efficiency and mechanical behaviour of a sealed flat plate collector at ambient pressure. Beside the thermal model, a finite element model to discuss the mechanical loads in certain collector operation points enhanced the studies.

Vestlund et al. (2012a) conducted a simulation study to evaluate the material saving potential. In this approach, the absorber thickness was reduced, at the

same time the fin width was increased, resulting in fewer risers. The parameters were changed until the efficiency was at least on the level of a conventional collector. According to Vestlund et al. (2012a), an absorber mass reduction of 75 % would be feasible. This was achieved by using fewer risers and very thin absorber sheets down to 0.1 mm.

As a consequence of simplifications inherent in their mechanical study and the fact that a validation of the results with prototype was not feasible, a possible higher convection loss remained unconsidered. The presented results in this thesis were compared with outcomes from other scientific publications (Bartelsen et al. 1993, Föste 2013 and Eismann 2015) and show that the calculation of the convection after Hollands et al. (1976) tend to underestimate the convective heat transfer in collectors. Hence, it was desirable to investigate the collector efficiency of a gas-filled collector and in particular the convection losses via the top in such collectors more in detail.

6.1 Modelling approaches of solar collectors

There have been many contributions to the modelling of flat plate solar collectors. In the early 1940s, Hottel and Woertz (1942) analysed the thermal performance of flat plate solar collectors. The authors presented an analytical calculation approach for the collector efficiency. In 1958, their analytical approach was refined by Tabor (1958). Based on the equation of Hottel and Woertz, Tabor suggested a new convective heat transfer coefficient, analysed the emissivity between the glazing and the hemisphere and discussed an approach to calculate edge losses in a collector. In the same year, Hottel and Whillier (1958) published a linear efficiency model. Cooper and Dunkle (1980) introduced a non-linear flat-plate collector model whereas the efficiency is plotted in dependence of the difference between ambient temperature and the mean fluid temperature to the solar irradiation. Klein et al. (1974) presented their investigations on the transient collector behaviour and pointed out the differences to a steady state collector model. The collector simulation model was refined by two heat capacities resulting in a two-node model. Matuska and Zmrhal (2008) as well as Koo (1999) published a collector simulation model that can be downloaded and used without a license fee. By changing certain geometrical and physical parameters – such as the backside insulation thickness or the number of the front covers – the

collector efficiency is calculated. The mentioned models are sophisticated and established simulation approaches and most suitable to predict the efficiency of a collector. A drawback of those approaches is that the component temperatures are not available. In the case of a hermetically sealed flat plate collector with a fully adhesive edge bond, new materials are being used. Moreover, the adhesive is by its nature sensitive to high temperature loads, i.e. temperature magnitude, period and occurrences. Against this backdrop, it was essential to analyse the thermal loads on the components beside the collector efficiency. Finally, the freeware simulation software is not capable of simulating a gas-filled cavity. As a consequence, the simulation model by Reiter et al. (2013, 2014, 2015) was adapted for the conducted thermal analysis.

6.2 Simulation models for gas-filled solar collectors

For the thermal modelling and system simulation tasks within this thesis, MATLAB and Simulink with its open-source toolbox CARNOT was used. In principle, the simulation work is divided in a collector analysis using a C-based numerical collector model in MATLAB and a system simulation in Simulink. The collector physics are described in the C-based code and can be compiled in an S-function. This S-function compiles the collector properties and can be implemented as a ‘collector block’ in a solar system simulation in Simulink. Figure 6.1 shows the methodology of the simulation in this thesis.

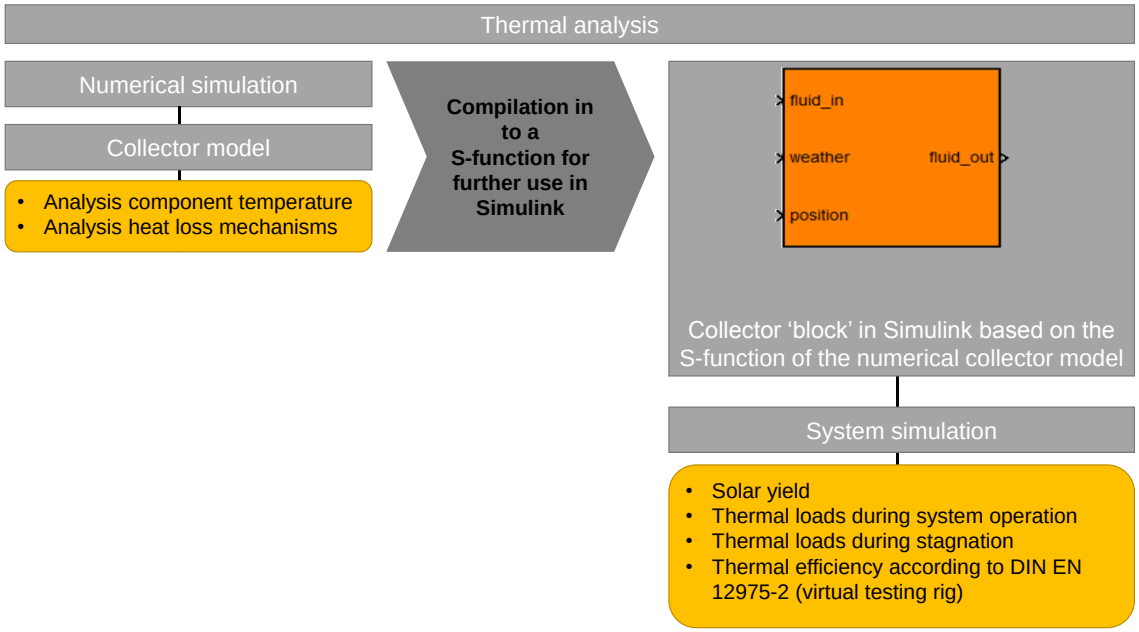

Figure 6.1: Schematic approach for the component and system simulation for a gas-filled solar collector

The numerical collector model was used to derive collector details in steady-state, e.g. component temperatures or the magnitude of heat loss mechanisms. These results are based on the collector's specifications, such as fin width, heat conductivity of the insulation or the parameters of the selective coating. However, to analyse the thermal loads in a solar system, the numerical collector needs to be embedded in a system simulation. The system simulations were conducted in Simulink. Therefore, the numerical collector model was compiled and implemented as a collector block in Simulink.

In the upcoming subchapter, the model is described in brief. Further information on the used equation and coherences can be found in Reiter et al. (2013, 2014, 2015).

6.2.1 Numerical collector model

Figure 6.2 shows the ten-node model of the numerical collector with its energy fluxes.

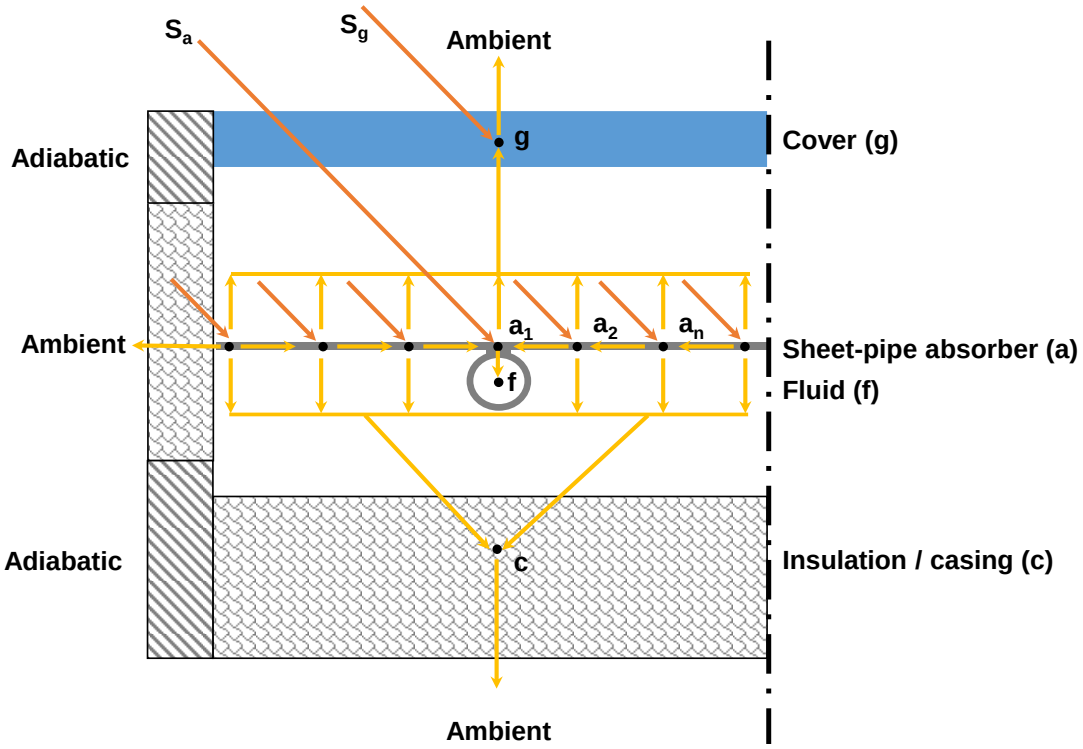

Figure 6.2: Schematic cross section of the ten nodes in the collector model including the energy fluxes

The equations 6-1 to 6-5 describe the energy balances in the numerical model.

Cover (g)

$$m_g c_g \frac{dT_g}{dt} = S_g + \dot{q}_{a1-g} + 2\sum_{a=2}^{4} \dot{q}_{a-g} - \dot{q}_{g-amb}$$ Equation 6-1

Absorber (a_1)

$$m_{a1} c_{a1} \frac{dT_{a1}}{dt} = S_{a1} + 2\dot{q}_{a2-a1} - \dot{q}_{a1-f} - \dot{q}_{a1-g} - \dot{q}_{a-e}$$ Equation 6-2

This node (a_1) includes the base fin and the riser pipe.

Absorber (a_n)

$$m_{an} c_{an} \frac{dT_{an}}{dt} = S_{an} + \dot{q}_{an+1-an} - \dot{q}_{an-a1} - \dot{q}_{an-g} - \dot{q}_{an-c} - \dot{q}_{a-e}$$ Equation 6-3

Fluid (f)

$$m_f c_f \frac{dT_f}{dt} = \dot{m}_f c_f * \left(T_{in} - T_f\right) + \dot{q}_{a1-f}$$ Equation 6-4

Casing (c)

$$m_c c_c \frac{dT_c}{dt} = \dot{q}_{a1-c} + 2\dot{q}_{a2-c} + 2\dot{q}_{a3-c} + 2\dot{q}_{a4-c} - \dot{q}_{c-amb}$$ Equation 6-5

Based on the stated energy fluxes the collector's thermal behaviour is described.

Figure 6.3 shows a schematic workflow of the numerical model and the heat transfer mechanisms calculated.

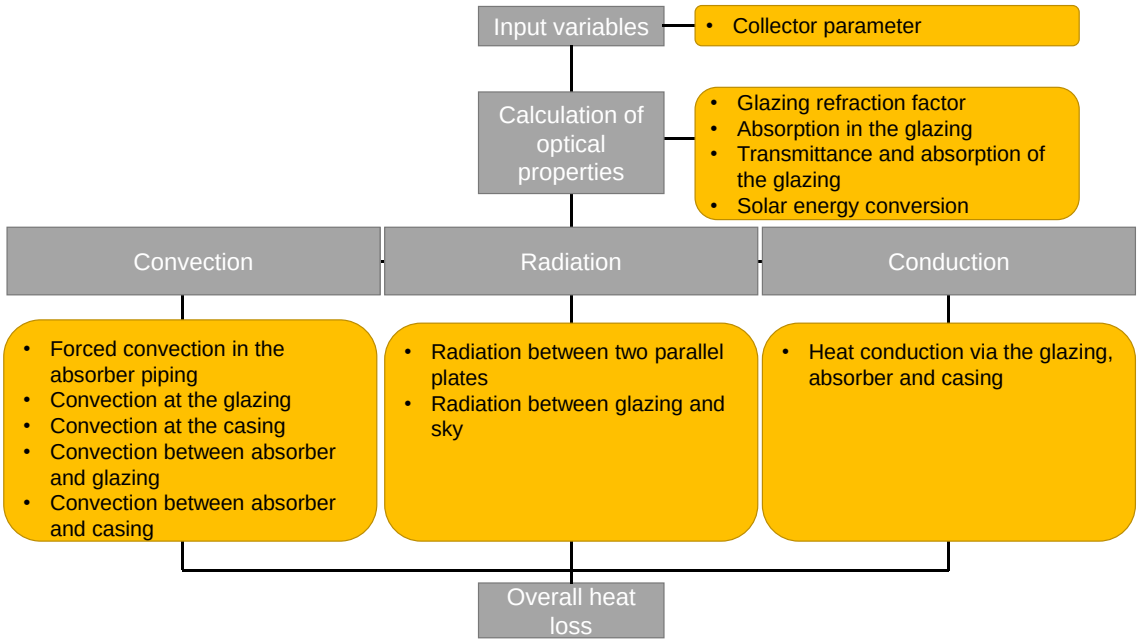

Figure 6.3: Schematic illustration of the calculated heat loss mechanisms in the numerical collector model

The used equations are based on fundamental coherences and can be looked up in Reiter (2015). Solely, the convection between absorber and glazing was modified within this thesis. This heat loss is further described in chapter 6.2.4.

6.2.2 System simulation

Simulink is a simulation tool that allows a drag and drop based coding via graphical blocks. Frequently used blocks, such as fundamental operations, are already included in the Simulink library by default. Further and more specific blocks can be created by so-called S-functions. These blocks are connected by vectors and combined to a complete simulation model, e.g. solar thermal system.

The collector's equations are embedded in a C-based code and are implemented in Matlab as an S-function. An S-function is a description of a component or system, e.g. flat plate collector, written in a high-level language, such as C. The functions are compiled and serve as a dynamically linked subroutine, e.g. in a Simulink simulation. Therefore, the collector S-function is linked with necessary input data, like fluid data, collector orientation and weather conditions.

Figure 6.4 shows the collector block that is used in the Simulink simulation.

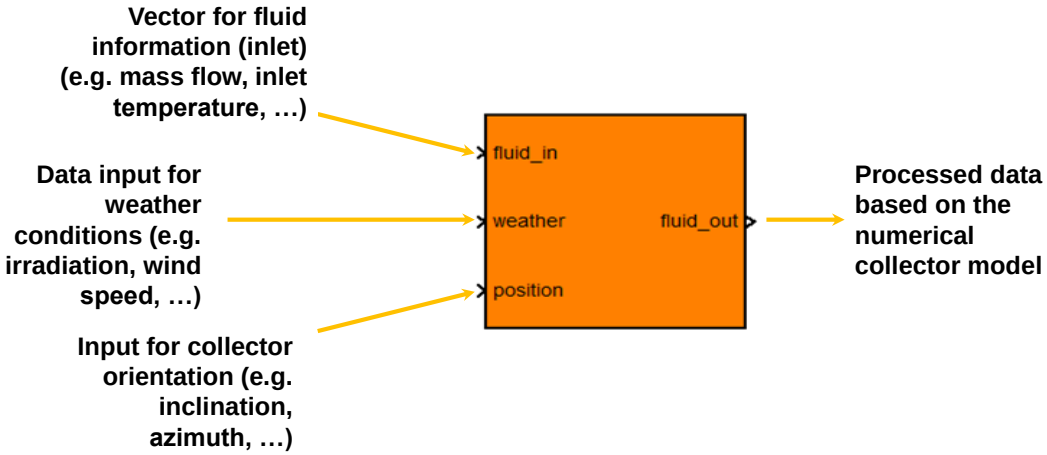

Figure 6.4: Highest layer of the collector block in Simulink

In this thesis, two different Simulink models were used to analyse the solar yield and component loads during normal operation as well as a stagnation test stand to determine the maximal loads. Figure 6.5 shows the solar system in the simulation environment Simulink.

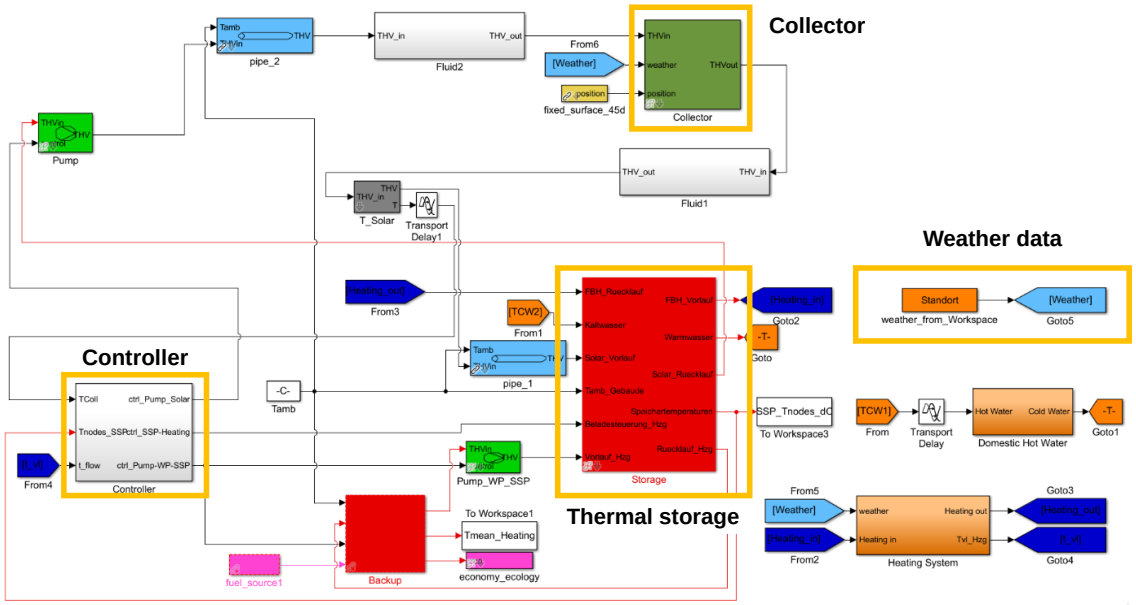

Figure 6.5: Block chart in Simulink of a solar thermal system

The determination of the thermal loads during stagnation were conducted using the Simulink model shown in Figure 6.6. The results are compiled in chapter 6.7.

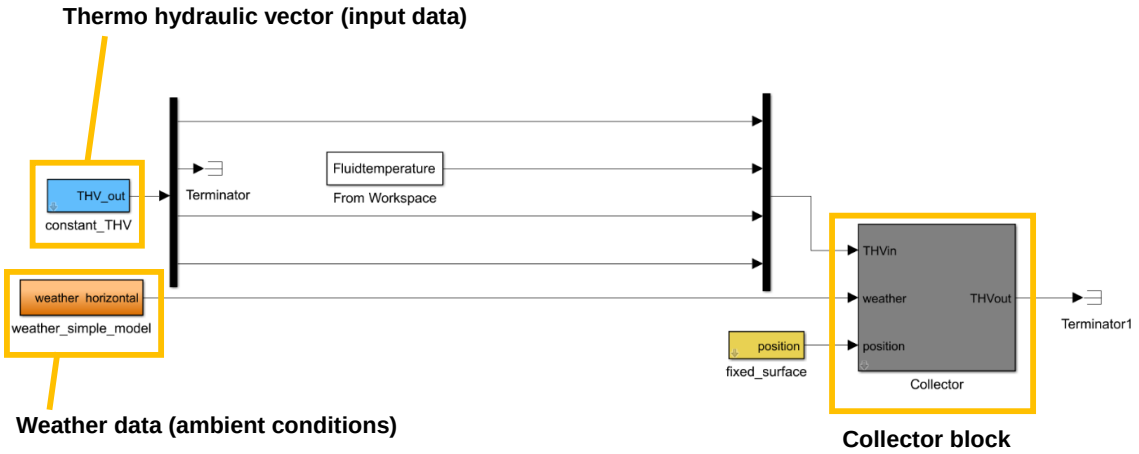

Figure 6.6: Block chart in Simulink of the virtual testing rig to derive e.g. thermal collector loads

Initially, the adapted collector model was set up for the development of full polymeric collectors and, hence, the temperature loads were in the focus of Reiter's research (2013, 2014, 2015). The simulation model was found to be most

suitable as in this approach a new type of adhesive – which is, ultimately, a polymeric component – is used and it was possible to adapt the model for gas-filled solar collectors.

6.2.3 Simplifications

The simplifications of the simulation model can be looked up in Reiter et al. (2015). Further simplifications for a hermetically sealed flat plate collector were not drawn as the stated ones were sufficient.

6.2.4 Modelling

The principal equations used in this model can be found in Reiter et al. (2015) and are, therefore, not further described. However, the convective heat transfer between absorber and glazing was modified.

Reiter et al. (2014, 2015) used an approach to calculate the convective heat transfer between absorber and glazing from Matuska and Zmrhal (2009). The authors used a combination of different convection theories to achieve a wide range of application – e.g. different collector inclinations from 0° to 90°. In this approach the widely used convection theory according to Hollands et al. (1976) was applied at first. During the research program, it turned out that there is a considerable discrepancy between the applied theory and the laboratory testing results – in particular for a solar collector with an all-round supported absorber. As the convective heat transfer between absorber and glazing in this approach is essentially affected, this heat transfer is discussed more in detail.

Finally, different gases than air were implemented. Table 6.1 shows the properties of the used inert gases.

Table 6.1: Overview of the used gases for the thermal simulation (Stephan 2010)

Gas	Abbreviation	Thermal conductivity in W/mK	Heat capacity* in J/kgK
Air	Air	0.0262	1,005
Argon	Ar	0.0179	524
Krypton	Kr	0.00949	248
Xenon	Xe	0.0055	160

The change of the material properties such as viscosity or density depending on the present gas temperature were approximated by polynomials and can be found in the VDI Heat Atlas (Stephan 2010).

Convective heat transfer

The heat transfer between absorber and glazing is due to a combination of radiation and convection. The radiation loss is dependent on the temperature difference between absorber and glazing and by the emission coefficient of the absorber and the glazing. As mentioned, this heat mechanism plays only a minor role since the selective absorber coating is, nowadays, a common feature of a flat plate collector. Equation 6- expresses the convective heat transfer coefficient:

$$h_c = Nu \cdot \frac{\lambda}{d}$$ Equation 6-6

The Nusselt number is the ratio of convective to conductive heat transfer across a fluid layer. In the end, this equation is very similar to the one of pure heat conductance except that the Nusselt number is used as a sort of loss multiplier (Nu > 1) for the convective heat loss.

The Nusselt number is depending on the Rayleigh number, which is another dimensionless number. This parameter describes the ratio of buoyancy and viscosity forces and is multiplied by the ratio of momentum and thermal diffusivities, i.e. Prandtl number. The free convective heat loss is influenced by the medium in the gap, the gap size or the characteristic length – i.e. the distance between absorber and glazing – and the temperature difference between absorber and glazing.

For free convection, the Rayleigh number is calculated by the multiplication of the Grashoff number and the Prandtl number:

$$Ra = Gr \cdot Pr = \frac{\rho \cdot c_p \cdot \beta' \cdot d^3 \cdot g \cdot \Delta T}{\lambda \cdot \nu}$$ Equation 6-7

However, natural convection is also affected by the inclination and the shape factor of the enclosure, i.e. length divided by the width (Figure 6.7).

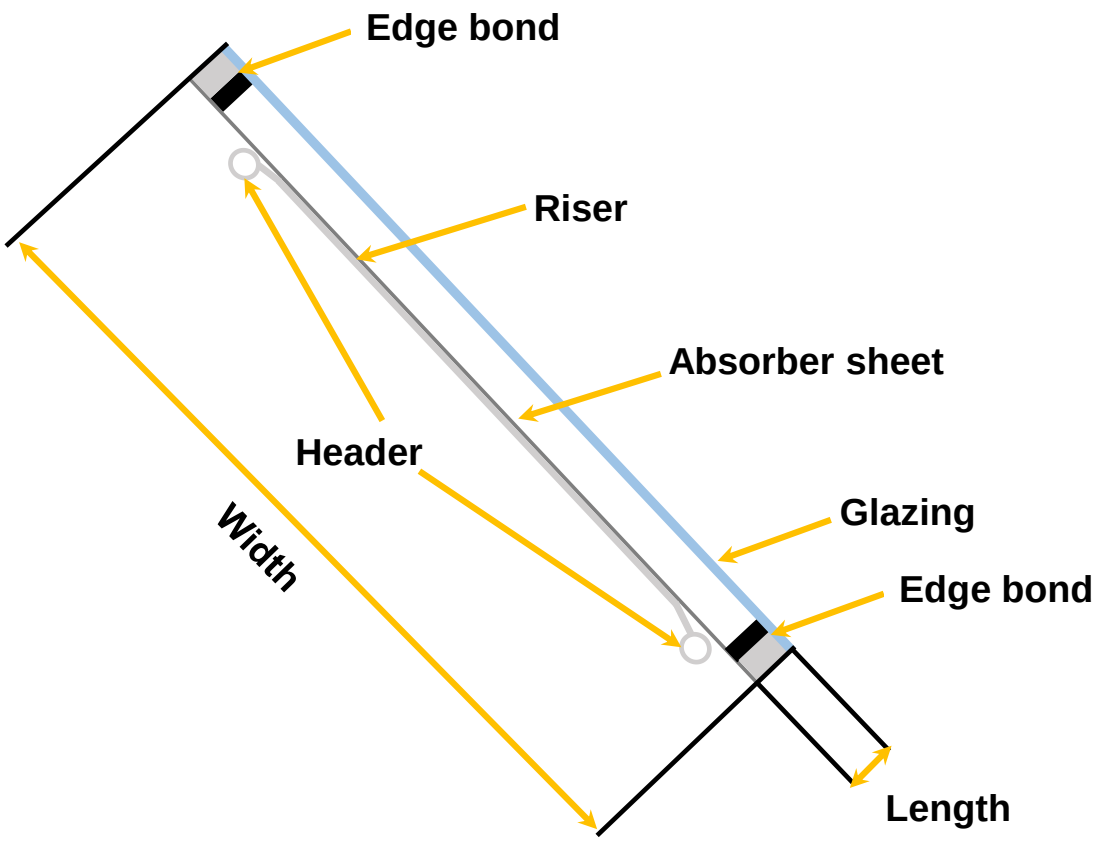

Figure 6.7: Schematic cross section of a collector with an edge bond and definition of W (width) and L (length)

According to Hollands (1976), the shape factor for inclined layers can be ignored for values smaller than 20. The ratio of length to width in the here discussed approach ranges between values of 1,000 to 2,000. Hence, the shape factor for inclined layers was ignored.

6.2.5 Convective heat transfer in flat plate collectors and rectangular gaps

Hottel and Woertz (1942) reviewed different research studies on the convective heat transfer, which were more or less linked to solar thermal application but still seemed applicable for flat plate solar collectors. The authors derived a constant c, which is dependent on the collector or rather the plate inclination. Ultimately, this factor is a numerical value determined by experimental data. Hottel and Woertz compared established c values from Fishenden and Saunders (1932) and Wilkes (1937) and found a considerable deviation of up to 50 % for the same parameter. Hence, Hottel and Woertz defined an own value for c in laboratory tests. Based on the work of Hottel and Woertz, Tabor (1958) corrected the c value by own experimental results. According to Tabor, Hottel and Woertz chose a non-adequate value for their cover emissivity; eventually, resulting in an underestimation of c. Another milestone was made from Hollands et al. (1976) by their analysis of free convective heat transfer across inclined air layers, which is up to date, a widely used approach for the calculation of the convective heat transfer in solar collectors. Hollands et al. (1976) validated the calculation of the Nusselt number by experimental data:

$$Nu = Nu_{con} + Nu^{+}_{conv,\ I} + Nu^{+}_{conv,\ II} \qquad \text{Equation 6-8}$$

With the convention that the terms $Nu_{conv,\ I}$ and $Nu_{conv,\ II}$ are only used for positive values.

The constant term ($Nu_{con} = 1$) in Equation 5-3 stands for the heat conduction, which is always active. $Nu_{conv,\ I}$ and $Nu_{conv,\ II}$ represent the terms for the convective heat transfer and are only in use according to their critical Rayleigh number:

- $Nu_{conv,\ I}$: $Ra_{\Phi} \geq 1{,}708$
- $Nu_{conv,\ II}$: $Ra_{\Phi} \geq 5{,}830$

Equations 6-9 to 6-11 expresses the calculation of the Nusselt number after Hollands et al. (1976):

$$Nu_{con} = 1 \qquad \text{Equation 6-9}$$

$$Nu_{conv,\ I} = 1.44 \cdot \left[1 - \frac{1{,}708}{Ra \cdot cos\phi}\right] \cdot \left(1 - \frac{sin^{1.6}(1.8\phi) \cdot 1{,}708}{Ra \cdot cos\phi}\right) \left[\left(\frac{Ra \cdot cos\phi}{5{,}830}\right)^{\frac{1}{3}}\right] \qquad \text{Equation 6-10}$$

$$Nu_{conv,\ II} = \left[\left(\frac{Ra \cdot cos\phi}{5{,}830}\right)^{\frac{1}{3}} - 1\right] \qquad \text{Equation 6-11}$$

In their apparatus, two plain parallel uncoated copper plates were used whereas one of them was cooled and the other heated with air as medium in between the plates. The boundaries were shielded from the environment by aluminium foil maintaining a linear temperature gradient between the two plates and achieving a radiative shield. This testing rig was put into a vacuum chamber in order to vary the pressure as the Rayleigh number is pressure dependent. This resulted in a variation of different gap sizes (distance between the plates) without making physical changes on the apparatus. The heat flux was measured in a square of 130 mm edge length in the central area of the lower plate. Finally, the complete testing rig was rotatable to the horizontal to measure the heat transfer under different inclinations. According to Hollands et al. (1976), the equation is valid for inclinations between $0° \leq \phi \leq 60°$.

The convective heat transfer is amongst other parameters affected by the inclination angle of the collector. However, the inclination effect was not of interest within this research program. Hence, a standard inclination for testing and simulation of 45° was defined. For a wider variety of inclination angles different approaches have to be used to cover an angle variation between $0° \leq \phi \leq 90°$. Further information can be found in El Sherbiny (1982), Wright (1986), Bartelsen (1999) and ISO 15099 2003 (2003).

In Figure 6.8 the correlation between convective heat loss and the gap size according to the theory of Hollands et al. (1976) for different inert gases is shown.

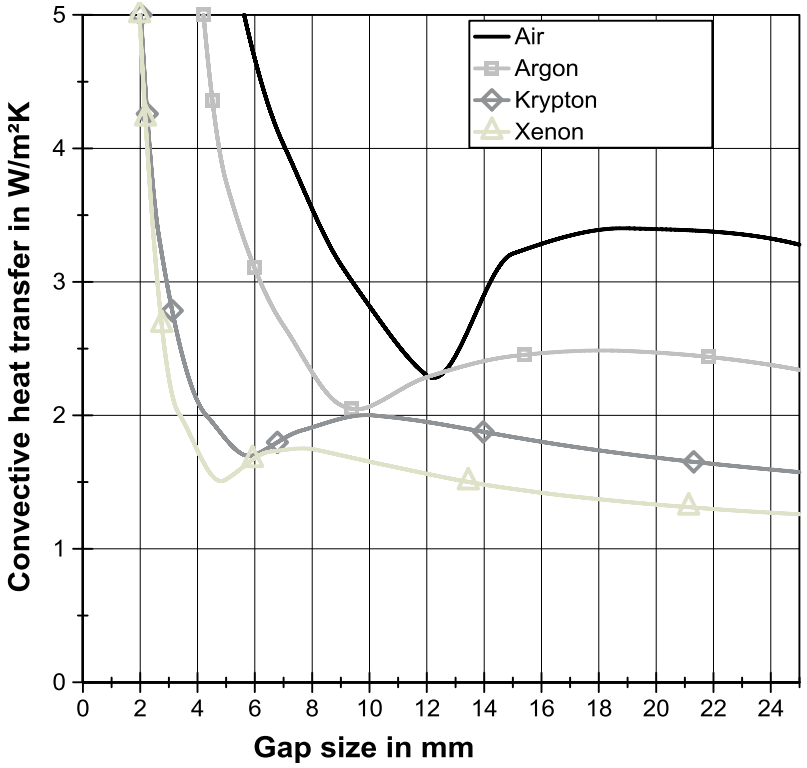

Figure 6.8: Convective heat transfer for different gap sizes and inert gases for T_m - T_{amb} = 60 K and an inclination of 45 ° based on Equation 6-8

All simulated gases are showing a similar curve shape: For increasing gap sizes the heat transfer coefficient decreases to a local minimum. The local minimum indicates the region where Nu = 1 is or very close to it, i.e. transition area between heat conductance and convection. This point is depending on certain parameters such as the inclination angle, the temperature difference T_{abs}-$T_{glazing}$ or on the physical properties of the inert gas. If the gap size is further increased, the heat loss between absorber and glazing reaches a local maximum. With further increasing gap sizes, the curve flattens again. Xenon as filling gas has the lowest convective heat transfer with the local minimum at smallest plate spacing followed by krypton, argon and finally air.

Within this research work, it was favourable to achieve a short distance between absorber and glazing. On the one hand, a shorter distance between absorber and glazing reduces the adhesive costs, which cannot be ignored, as those are a considerable part of the total collector costs. On the other hand, a lower convective heat loss might be achievable by adjusting the gap size to the transition region between conduction and convection, i.e. Nusselt number is still 1 or very close to 1 (Figure 6.9).

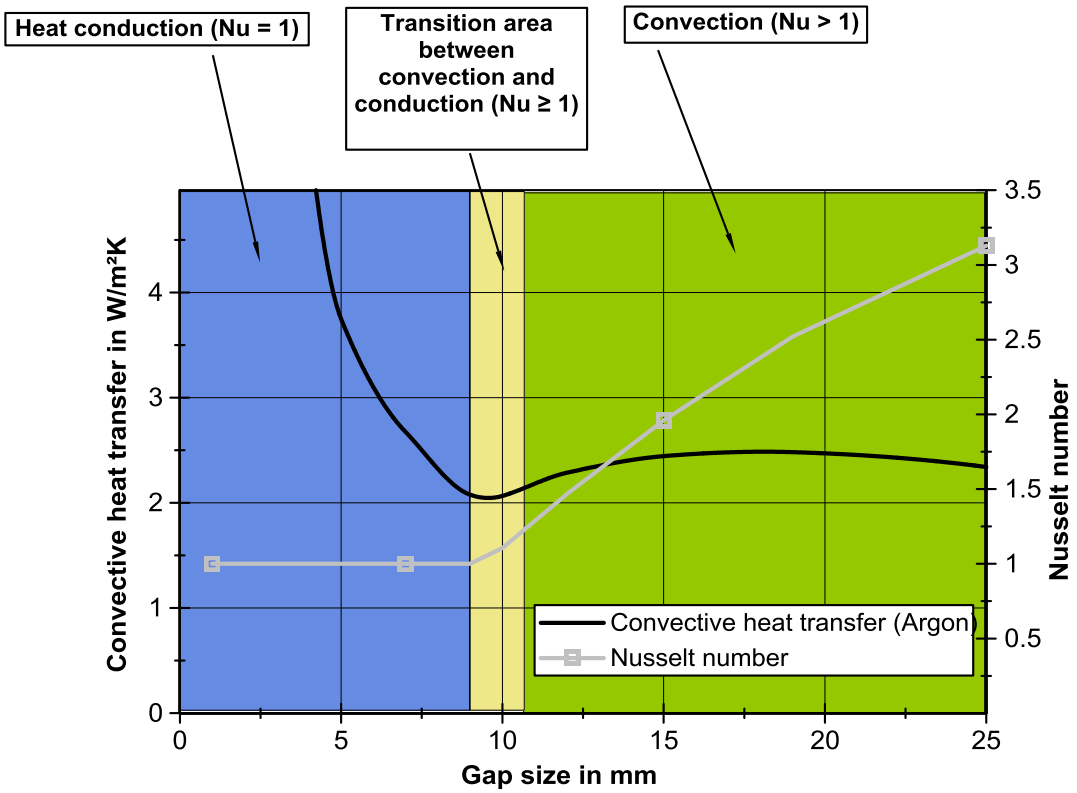

Figure 6.9: Different regimes of heat transfer between absorber and glazing with argon at atmospheric pressure

Furthermore, it needs to be considered that less volume is enclosed between absorber and glazing and, thus, a lower mechanical load is applied on the collector components due to the pressure change. Conventional flat plate collectors are designed to have a gap size between 25 to 35 mm whereas in this approach an absorber glazing distance at first of 10 mm for argon was intended. In a later stage of this work gap sizes of up to 20 mm were as well considered and analysed. Even though xenon and krypton are allowing very short spacing distances in comparison to argon or air, those inert gases are of no practical interest. Whilst krypton is by a factor of 100 times more expensive than argon, xenon is even more costly than krypton. An argon filled interspace with a gap size of 15 mm for an aperture area of 2 m² causes costs of about 0.06 €. In theory, krypton enables a shorter distance between absorber and glazing cutting the filling costs down to about 3.5 €. However, the results in this research program showed that it is not rational to achieve shorter gap sizes than 15 mm with conventional sheet-pipe absorber due to the unpredictable absorber deflection (see chapter 6.3.1, 6.6.1 and 7.3). Beyond that, whether higher filling costs can

be justified by a cost-equally increase in efficiency needs to be investigated in a system simulation. This is further discussed in chapter 9.

Consequently, argon was chosen as a filling gas in this approach whereas air served as the main reference. However, krypton was used in some considerations as a further reference to argon and air. Xenon was of no further interest due to its uneconomic pricing and very limited availability.

6.3 Validation approach based on the convection theory after Hollands et al. (1976)

The efficiency tests of the prototype were conducted on the institute's own indoor solar simulator according to the standard DIN EN 12975-2 (2006). During the complete research programme all parameters relating to the collector efficiency were referenced to the aperture area – unless otherwise stated.

Even though deviations between simulation results and measured efficiency curves were expected, the deviations were surprisingly high. Figure 6.10 shows the simulated efficiency curve and the tested efficiency conducted on an indoor solar simulator. The collector parameters are found in Table 6.2.

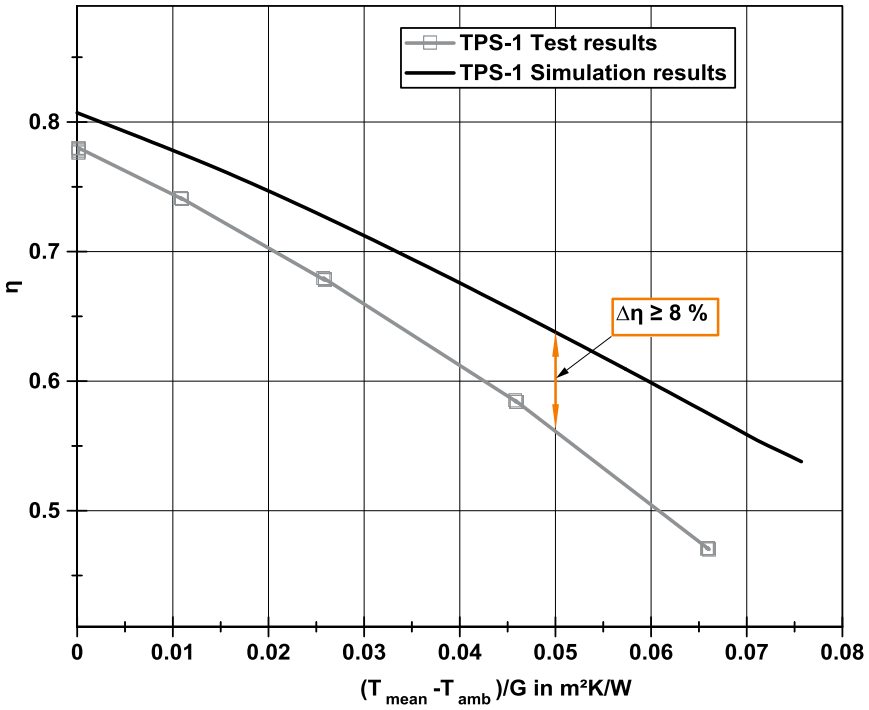

Figure 6.10: Comparison between the first simulation model result of a hermetically sealed and gas-filled collector (convection theory according to Hollands et al. 1976) and the measured collector efficiency of the corresponding experimental collector showed an absolute deviation for T_{mean} - T_{amb} = 0.05 m²K/W of 8 %.

Table 6.2: Measured collector parameters of the prototype TPS-1

Collector	**TPS-1**
η_0	0.782
a1 in W/m²K	3.215
a2 in W/m²K²	0.023
Aperture area in m²	1.9
Initial gap size in mm	10
Insulation thickness (back) in mm	40
Insulation thickness (side) in mm	--
Absorber type	Sheet pipe
Absorber piping	Harp
Material absorber sheet	Al
Material absorber piping	Al
Gas filling	Ar
Bonding absorber sheet ⇔ piping	Laser welded
Number of risers	10
Fin width in mm	110

The simulated efficiency curve shows a higher performance over the complete operating range. Close to η_0 the deviation between the curves is only 2.4 %. The parameter η_0 stands for the zero loss coefficient, there is also the plate efficiency factor F' contributing to this value and, thus, the collector heat loss is affecting this parameter as well. With rising collector working temperatures, the deviation between the two curves increases. For a typical working point of a space heating supporting solar system of $(T_{mean} - T_{amb}) / G = 0.05$ m²K/W the deviation is more than 8 %. Reiter et al. (2015), however, validated the simulation model for a conventional collector with a double-harp absorber and a gap size of 30 mm. According to their results, the model showed a good correlation between laboratory testing and simulation results. Within this research study, the simulation model code was only modified in terms of the convective heat transfer, smaller gap sizes and gas fillings. Consequently, it can be concluded that the deviation is rather an underestimation of the actual convective heat loss or a failure in the experimental setup than an error in the model code. At first, it seemed plausible to examine the experimental setup to exclude possible mistakes. As the institute's solar simulator is regularly checked by testing the same reference collector, it was ensured that the test rig was not faulty. Consequently, the collector was further analysed. The gas concentration of the prototype was measured thrice – right after its production, two hours later and 24 h after the production. All measurements gave values well over 95 % argon concentration. The collector test was conducted 36 h after the production. It can be, therefore, concluded that still a high argon concentration (> 90 %) was left in the interspace. However, several observations were made on the absorber. As described in chapter 7, the thin absorber sheet showed a considerable deflection during collector operation. Instead of the intended 10 mm gap between absorber and glazing a mean distance between the two plates of only 6 mm was measured. Throughout the research program, it turned out that the initial absorber shape has a significant impact on the absorber deflection. This is a further evidence that the thermal induced expansion effect dominates the pressure effect. If it were the other way round, one would expect the gap to grow with temperature. This means, absorber areas that had already a shorter distance than 10 mm to the glazing are getting even closer during collector operation and vice versa.

6.3.1 Impact of the convective heat transfer (according to Hollands et al. (1976)) depending on the gap size on the collector efficiency

Those absorber deflections were only very hard to spot by a visual inspection through the glazing due to the dark absorber coating and the glass reflections. Thence, holes were drilled through the back of the insulated back plate to conclude on the actual distance of the absorber to the glazing. This was possible as the collector dimensions, e.g. glass thickness and total collector height, were known and measurable. This investigation led to the result that the absorber deflection was the main cause for the difference in the collector efficiency prediction. Figure 6.11 clarifies the impact of a small deviation in the gap size on the convective heat transfer and the collector efficiency for collectors with a small gap size, i.e. within the transition area between heat conduction and convection.

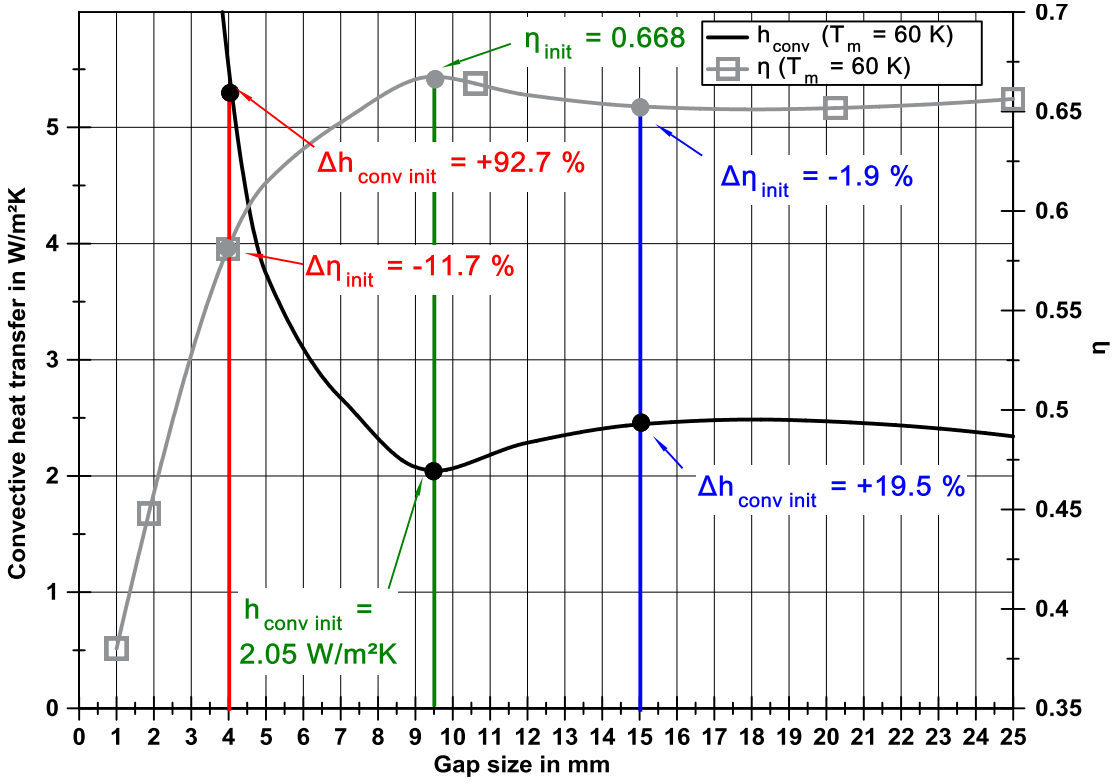

Figure 6.11: Simulated change of collector efficiency depending on the gap size after the convection theory of Hollands et al. (1976) for T_m - T_{amb} = 60 K

For a mean fluid temperature difference of 60 K and argon as gas filling, the local minimum in the convective heat transfer is at 9.5 mm. If the gap size is decreased

by only 5.5 mm the convective heat transfer is increased by almost 93 %. Ultimately, this corresponds to an efficiency loss in this typical working point of 11.7 %. In contrast to this, an increased interspace of 5.5 mm to 14 mm is followed only by a slight increase of the convective heat loss of 19.5 %, which leads to an efficiency loss of less than 2 %. The absolute values are compiled in Table 6.3.

Table 6.3: Compilation of the change in collector efficiency and the convective heat transfer for different gap sizes in absolute values at T_m-T_{amb} = 60 K

Mean collector fluid temperature difference in K	60
Initial gap size in mm	9.5
η_{init} at 9.5 mm gap size	0.668
h_{conv} in W/m²K at 9.5 mm gap size	2.05
η_{init} at 4 mm gap size	0.55
h_{conv} in W/m²K at 4 mm gap size	3.95
η_{init} at 15 mm gap size	0.649
h_{conv} in W/m²K at 15 mm gap size	2.45

However, the interaction between absorber deflection and convective heat transfer cannot be implemented in to the applied thermal collector model. In turn, this aggravates the model validation as the initial absorber deflection is different for each sheet-pipe absorber and, thus, the top heat loss differs from absorber to absorber.

6.3.2 Summary

The first approach to validate the simulation model was not successful. This was owed to the distinctive absorber deflection that – in combination with a short gap sizing – led to a significant increase of the top heat loss. As the absorber behaviour is not foreseeable, it cannot be implemented in a simulation model. A computational fluid dynamic simulation considering the initial absorber shape and its magnified shape at higher collector operation temperature would be interesting. Unlike to the applied analytical approach, the Nusselt number is not averaged along the absorber but calculated locally. This should result in a more precise prediction of the overall convective heat transfer between absorber and glazing. Such a simulation study was not conducted as it did not match the time scope of this research project. However, it remains questionable whether it is possible to derive a universal conclusion for short gap sizes as the absorber deflection depends on its initial shape and differs for each absorber.

Due to the mechanical deflections of a sheet-pipe absorber, it is doubtful whether a precise prediction of the convective heat loss for such short distances between absorber and glazing is feasible. Furthermore, it is problematic if not impossible to adjust the gap to the local minimum of the convective heat transfer for this type of collector, i.e. conventional sheet-pipe absorber, which is attached to the glazing via a fully adhesive edge bond. A more accurate heat loss prediction might be possible if the absorber would be constrained or reinforced to avoid a mechanical deflection. The following measures could contribute to a more predictable sheet buckling during collector operation:

- An array of flexible clips or springs attached to the back of the collector, which holds the absorber to a certain position in the collector casing
- An optimised sheet structure reinforced by e.g. beadings to add more rigidity, which results in less deflection but also higher stress on the seal (cf. chapter 8)
- Spacers between the absorber and glazing to avoid an absorber deflection towards the glazing

To tackle this problem and validate the simulation model in this thesis, another set of prototypes with a wider spacing between absorber and glazing and different absorber types were produced and tested. For the model validation, for one of

those prototypes the convective heat transfer in the gap was measured (cf. chapter 6.4).

Eventually, four other experimental collectors were built. Table 6.4 comprises the parameters of those models.

Table 6.4: Tested parameters of the second series of the prototypes

Collector	**TPS-AlCu**	**TPS-CuCu**	**TPS-RB15**	**TPS-RB20**
η_0	0.815	0.84	0.879	0.88
a1 in W/m²K	3.19	4.03	3.315	3.275
a2 in W/m²K²	0.009	0.017	0.020	0.016
Aperture area in m²	1.8	1.8	1.86	1.86
Absorber type	Sheet pipe	Sheet pipe	Roll bond	Roll bond
Absorber piping	Double-harp	Double-harp	Double-harp	Double-harp
Material absorber sheet	Al	Cu	Al	Al
Material absorber piping	Cu	Cu	Al	Al
Gas filling	Ar	Ar	Ar	Ar

In contrast to the first prototypes, two collectors of the second batch were equipped with roll bond absorbers. This absorber type was already available in

the late 1980s but vanished due to corrosion and coating problems from the market. In 2011, a Finnish collector producer brought this absorber type back to the market. The absorber consists of two aluminium sheets, which are brought together by a roll bonding process. On the contact surface of the metal sheets the fluid channels are painted with a certain liquid called ‘stop-off’. The applied liquid avoids the bonding in these areas and ensures the formation of the channel structure. Subsequently, to the roll bonding the channels are shaped by air inflation. There are several advantages to this absorber design. On the one hand, it is close to a volumetric absorber that results in high heat removal factors of up to 0.97 whereas conventional sheet-pipe absorber are ranging between 0.88 and 0.95 (Treikauskas 2005). On the other hand, the thicker metal sheet is easier to handle on the IGU production line and is by far more rigid than a sheet-pipe absorber. The roll bonded results in a more predictable absorber deflection during collector operation.

For the validation of the simulation model the collector TPS-AlCu20 was used.

6.4 Discussion of different convection theories

Bartelsen et al. (1993) measured with their own experimental collector under various inclinations the convective heat transfer between absorber and glazing down to gap sizes of 15 mm and compared the results to the measurements published by Hollands et al. (1976). Their results showed a 25 to 60 % higher convective heat loss than the results computed according to Hollands et al. (1976). According to the authors, the main cause of this deviation results from the non-isothermal temperature distribution of the absorber. The experiments were conducted for gap sizes between 15 to 105 mm. The typical local minimum of the convective heat loss was not detected. It was left open whether a local minimum exists in a flat plate collector; however, it was not observed in this study.

Föste (2013) measured the convective heat loss of a collector with a double-glazing unit. In his approach, a collector prototype was equipped with temperature sensors along the glass panes and the absorber. Subsequently, the absorber piping was filled with hot water (T_{fluid} > 150 °C) and the temperature difference between inlet and outlet was measured to conclude on the total collector heat loss. The test was conducted without solar radiation and the hot water inlet was

on the collector upper side. This results in a different temperature profile as the heat flux is from the fluid to the absorber. This might lead to a different convection pattern compared to the normal collector operation (Föste 2013). By the measured temperatures on the absorber and the glazing, Föste concluded on the heat flux and compared his results with calculated values derived by the Hollands' equation. His results showed a deviation of the convective heat loss coefficient between the values derived by the literature and the measured results. The values differ by up to 32 % for the measurement between absorber and glazing unit and up to 15 % in the glazing interspace. A different convection model by Buchberg (1976) did not show a better accordance than that of Hollands. For a wide range of the Rayleigh numbers, Föste's (2013) results were in a better correlation with the results after Hollands et al. (1976) than that after Buchberg (1976). As a conclusion, the author suggests an amplification factor for the convective heat loss. Consequently, Föste conducted further tests on the heat loss testing rig and determined a factor for his simulations.

Recently, Eismann (2015) published an extended correlation for the convective heat transfer in the cavity between absorber and glazing. In his study, 22 standard collectors were modelled based on the specifications provided by the producer or test reports. As the common convection correlations were stated for isothermal plates, Eismann's focus was to extend the Hollands' equation for the convective heat loss for non-isothermal absorbers with a high selective coating. This is in particular of interest as the equation from Hollands is only valid for Rayleigh numbers of up to 10^5. The Ra number, however, is by a factor of three higher in the case of coated absorber surfaces (Eismann 2015). A coated absorber surface reduces the radiation losses because of a lower emissivity. Therefore, the absorber temperature rises and results in a higher temperature difference between absorber and glazing. This leads to an increase of the Rayleigh number and, thus, in an increased convective heat loss.

In his approach, Eismann extended the convection equation according to Hollands to cover a range of Rayleigh numbers of up to 10^6 by fitting it to the equation of ElSherbiny et al. (1982). This results in a better accordance for selective coated absorber surfaces. Furthermore, the equation was enhanced by two additional parameters – R_c as a correction factor and C as a further fitting coefficient:

$$Nu = Nu_{con} + Nu_{conv;I} + Nu_{conv,\ II} \qquad \text{Equation 6-11}$$

$$Nu_{con} = 1 \qquad \text{Equation 6-12}$$

$$Nu_{conv;I} = 1.44 \cdot \left(1 - \frac{1{,}708}{Ra \cdot cos\phi + 1{,}708 \cdot R_c}\right) \cdot \left(1 - [(sin1.8\phi)]^{1.6} \cdot \frac{1{,}708}{Ra \cdot cos\phi + 1{,}708 \cdot R_c}\right) \qquad \text{Equation 6-13}$$

$$Nu_{conv,\ II} = \left[\left(\frac{Ra \cdot cos\phi + 5{,}830 \cdot R_c}{5{,}830}\right)^{0.39} - 1\right] \cdot (1 + C \cdot R_c) \qquad \text{Equation 6-14}$$

The dimensionless correction factor R_c was used by Eismann (2015) to represent the thermo physical properties as well as the collector's operation state. This parameter can be set to values varying between 0 and 1; whereas $R_c = 0$ reduces the extended equation from Eismann to the equation of Hollands. With $R_c = 1$, the critical Ralyleigh numbers become 0. For the third term (Equation 5-10) of his equation, Eismann introduced a further correction term. This was necessary to adjust the predicted Rayleigh numbers to the measured ones.

Eismann's calculation of the constant C suggests a value of 0.29 with a useable spectrum of ±0.17. Hence, possible values range between 0.12 and 0.46 for C (Figure 6.12).

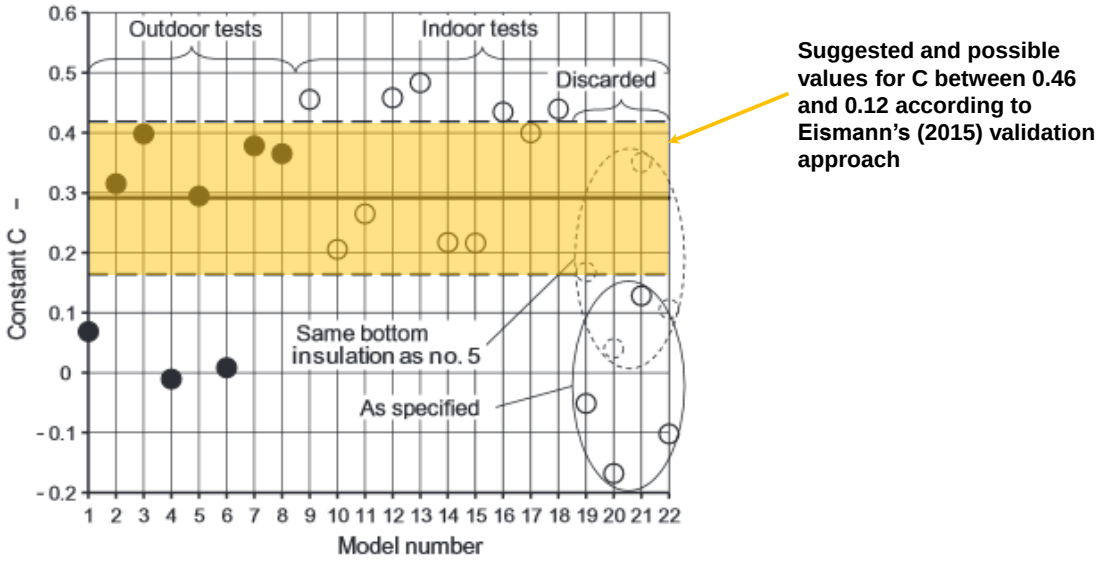

Figure 6.12: Comparison of calculated C values for different collector tests (cf. Eismann (2015))

For the here conducted calculation C was set to 0.46 whereas R_c was 1, which showed the best accordance.

To decide whether Eismann's approach is suitable for this research programme and to validate the own simulation model, the simulation model was extended by his equation and the convective heat transfer in the gap was analysed in laboratory tests.

6.5 Model validation

An experimental test was set up in which the convective heat transfer between absorber and glazing was measured. Therefore, the collector TPS-AlCu20 was – in addition to the already applied 55 mm thick mineral wool on the collector back – further insulated on the back as well as on the side with polystyrene. In principle, a trough was made out of 80 mm thick polystyrene (λ = 0.038 W/mK). The mineral wool and the additional polystyrene insulation resulted in a calculated U-value for the collector insulation of 0.26 W/m²K (before: 0.62 W/m²K):

$$U = \frac{1}{R_n} = \frac{1}{\frac{d_1}{\lambda_1}} + \cdots + \frac{1}{\frac{d_n}{\lambda_n}}$$ Equation 6-15

This was done to eliminate the conductive heat losses via the collector edges and the back. Consequently, the convective heat losses between absorber and glazing as well as the radiation losses of the absorber remained. The latter cannot be eliminated and need to be considered in the calculation. To conclude on the thermal collector losses, the collector was equipped with temperature sensors (thermocouples; Type T). Figure 6.13 shows the temperature sensor positions on the collector.

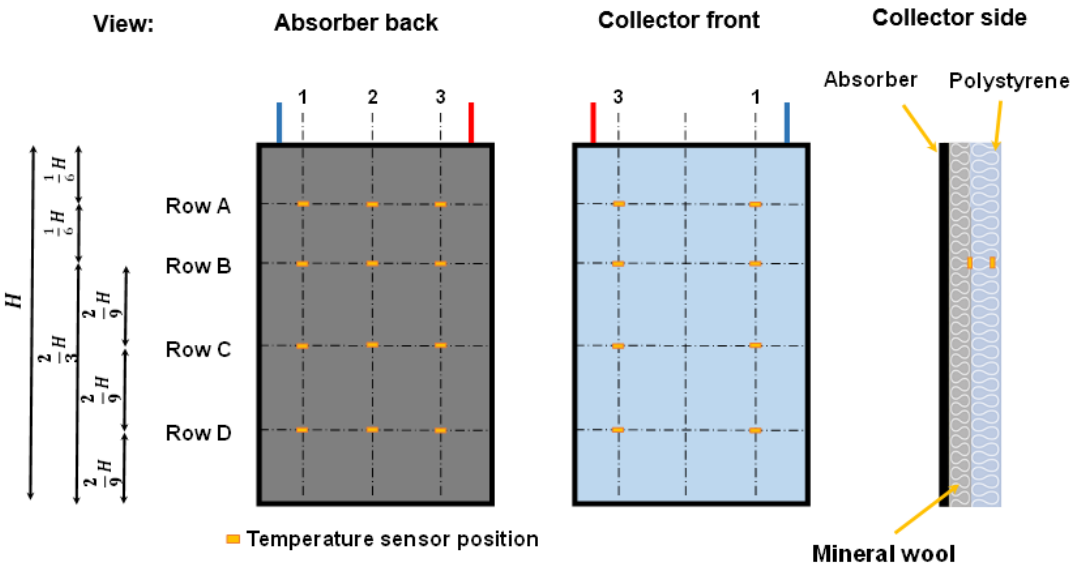

Figure 6.13: Sensor positions on the experimental collector

To shield the sensors from radiation, the sensors were attached on the collector components with an aluminium duct tape.

The prototype was put under the solar simulator to determine the efficiency for certain collector inlet temperatures, i.e. 70, 80 and 89 °C. The institute's solar simulator is not designed for the operation of higher inlet temperatures than 95 °C due to safety reasons as the outlet temperature of the water might exceed the boiling temperature. The solar simulator is equipped with two pyranometers, a magnet-inductive flow meter and two matched RTD sensors to log the collector inlet and outlet temperature (for details see chapter 4). Figure 6.14 shows the schematic setup of the test equipment.

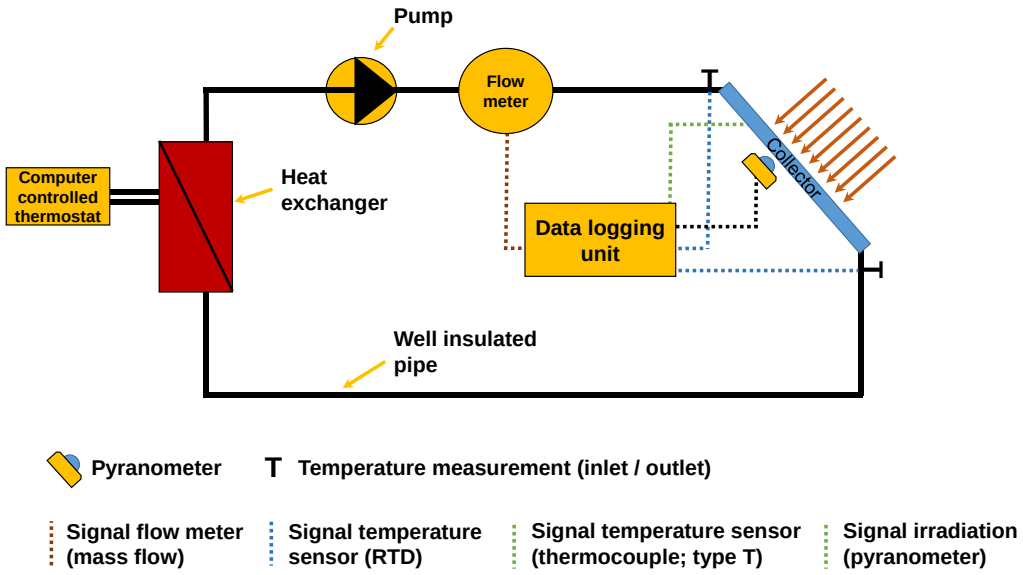

Figure 6.14: Schematic setup of the test equipment

The energy irradiated on the collector from the lamp array was subtracted from the measured collector performance to conclude on the thermal collector losses, i.e. the convection and radiation losses.

The irradiated power from the solar simulator on the absorber is defined by

$$\dot{q}_{irr} = \eta_0 \cdot G \cdot A \qquad \text{Equation 6-16}$$

With η_0 measured on the solar simulator according to DIN EN 12975.

The subtraction of $\dot{q}_{irr}$ and the useful heat results in the collector heat loss:

$$\dot{q}_{loss} = \dot{q}_{irr} - \dot{q}_{use} \qquad \text{Equation 6-17}$$

with

$$\dot{q}_{use} = \dot{m} \cdot c_p \cdot (T_{outlet} - T_{inlet}) \qquad \text{Equation 6-18}$$

The conduction loss via the back insulation and the radiative absorber loss is calculated based on the collector temperature measurements, the ambient temperature and the known physical collector properties. The sidewall losses are neglected, as the collector side surface is small compared to the collector's aperture area. Beyond that, the collector sides are very well insulated and, thus, considered as adiabatic. Table 6.5 summarises the data used for this calculation.

Table 6.5: Used parameters for calculating the convective heat transfer

Emission coefficient absorber	0.06
Gap size in mm	0.018
Zero loss efficiency	0.813
Ambient temperature in °C	26
$\lambda_{mineral\ wool}$ in W/mK	0.038
$t_{mineral\ wool}$ in mm	55
$\lambda_{polystyrene}$ in W/mK	0.038
$t_{polystyrene}$ in mm	80
Heat conductance surface in m²	1.8

Measurements with inlet temperatures below 70 °C ended in a too small heat loss that resulted in high measuring uncertainty.

The author's own experimental convection loss calculations were compared to the results according to the equations of Hollands (1976) and Eismann (2015) (Figure 6.15).

Table 6.6 comprises the calculated values for the convective heat loss values.

Table 6.6: Comparison of the calculated and measured convective heat transfer coefficient

Inlet temperature in °C	70	80	89
Raø	6288	7109	7901
$h_{c\ hollands}$ in W/mK	1.86	1.973	2.068
$\Delta h_{c\ laboratory}$ in %	21.3	23	26.5
$h_{c\ eismann}$ in W/mK	2.269	2.368	2.454
$\Delta h_{c\ laboratory}$ in %	-0.9	2.5	7.8
$h_{c\ laboratory}$ in W/mK	2.364	2.562	2.813
Measured convection loss in W	193	243	304

The convective heat transfer $h_{c\ hollands}$ was calculated using the equations 5-4 to 5-7 whereas $h_{c\ eismann}$ was derived from the equations 5-7 to 5-10. The values for $h_{c\ laboratory}$ were calculated based on the following procedure:

$$\dot{q}_{conv} = \dot{q}_{irr} - \dot{q}_{use} - \dot{q}_{rad} - \dot{q}_{cond} \qquad \text{Equation 6-19}$$

Whereas $\dot{q}_{rad}$ and $\dot{q}_{cond}$ were calculated based on fundamental equations:

$$\dot{q}_{rad} = \varepsilon \cdot \sigma \cdot A \cdot (T^4_{mean\ abs} - T^4_{mean\ g}) \qquad \text{Equation 6-20}$$

$$\dot{q}_{cond} = \boldsymbol{\lambda} \cdot A \cdot d \cdot \frac{1}{T_{mean\ abs} - T_{back}} \qquad \text{Equation 6-21}$$

With σ as the Stefan-Boltzmann constant (5.67 * 10^{-8} W/m²K⁴) and $T_{back} = T_{amb}$. The mean absorber temperature was averaged from the measured temperatures of the applied absorber sensors. The same applies for the mean glazing

temperature. The mean gas temperature was assumed to be midway between the mean absorber and mean glazing temperature.

Figure 6.15 represents the comparison between the measurement results and the simulated values of the convective heat loss.

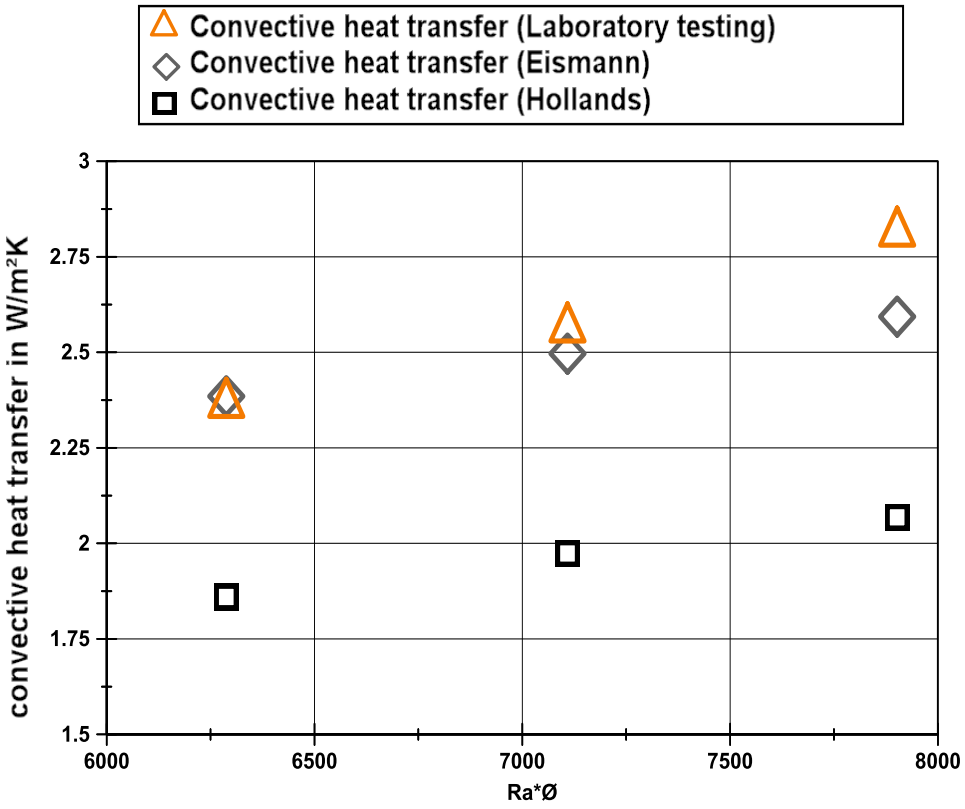

Figure 6.15: Comparison of the calculated heat transfer according to Eismann and Hollands et al. and the own test results

The author's experimental results differ clearly from Hollands' approach but the measured deviations are in a similar range with the results obtained by Bartelsen et al. (1993) and Föste (2013). Beyond that, the results for the convective heat loss are in good accordance with the values from Eismann. The measured points with an inlet temperature of 70 °C and 80 °C are differing only -0.9 % and 2.5 % from the values derived by Eismann's approach whereas the value for the point with an inlet temperature of 89 °C differs by 7.8 %. Based on this experimental setup the used collector model was enhanced by the extended convection equation (Equation 5-5). Figure 6.16 shows the tested results and the simulated efficiency curve according to Eismann's and Hollands' approach of the collector TPS-AlCu20.

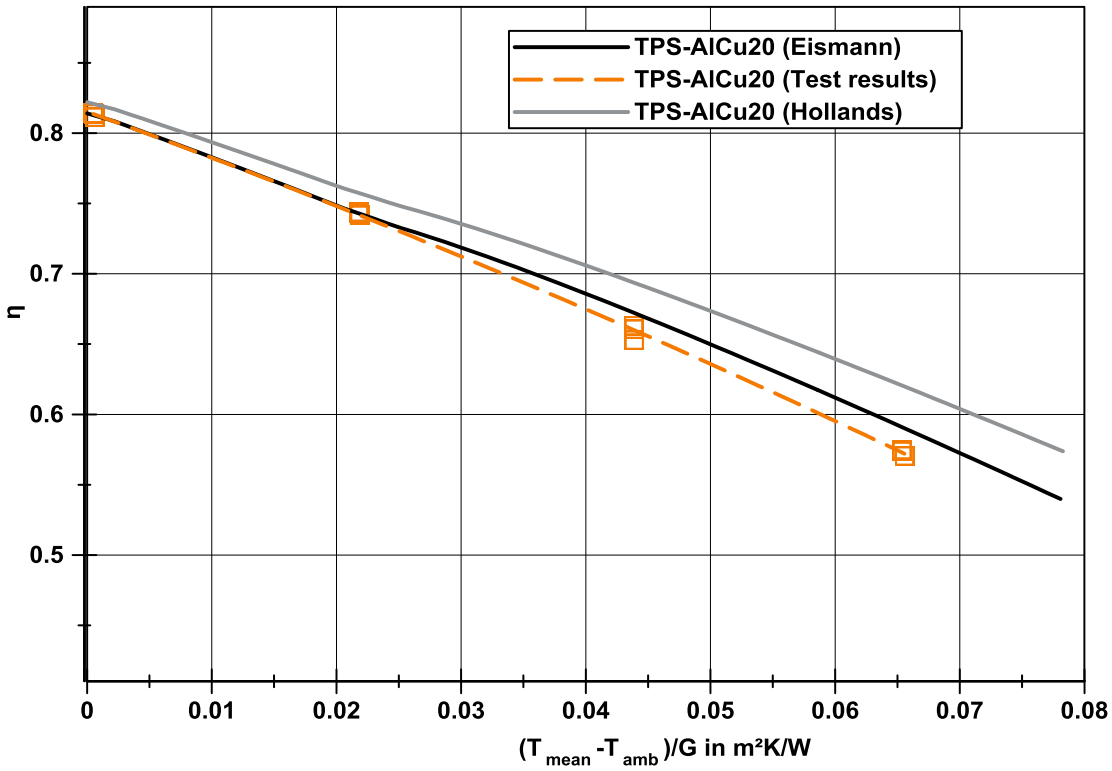

Figure 6.16: Model validation by comparison of the measured and simulated collector efficiency with a calculation approach according to Eismann (2015) and Hollands et al. (1976)

For the typical operation point of 0.05 m²K/W the deviation of the simulated values are 7.5 % (Hollands) and only 3 % (Eismann). The deviation of the complete collector operation range is derived by the subtraction of the measured values from the simulated values (Figure 6.17).

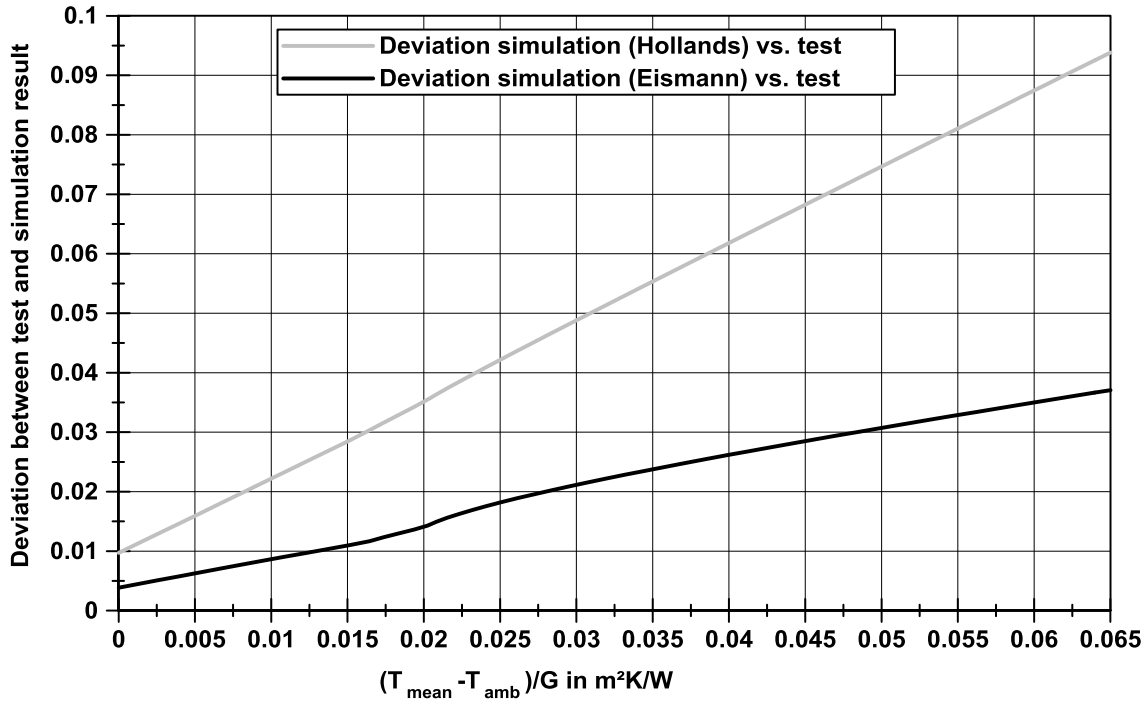

Figure 6.17: Deviation between simulation and measurement results

The smallest deviation for the Hollands' approach is about 1 % in the region of the zero loss efficiency. This is owed to the impact of the plate efficiency factor F' that affects this value as the zero loss efficiency is defined by

$$\eta_0 = F' \cdot \tau \cdot \alpha \qquad \text{Equation 6-22}$$

As the total collector losses are included in F' and the convection losses are slightly different, a rather small deviation exists. However, with increasing operation temperatures the deviation gets more obvious. For an ordinate value of 0.065 m²K/W the difference is almost 9.5 %. The extended correlation after Eismann shows only a deviation of 0.5 % for values close to η_0 and 3.5 % at max for higher operating points. The deviations with increasing temperature ranges were also observed in the own conducted convective heat loss measurement. As the mean collector gap size varies, the convective losses differ as well. This behaviour is not included in an equation.

Beside the satisfying results of the efficiency comparison, the measured component temperatures showed as well a good correlation to the simulated results. In this second test setup, the prototype TPS-AlCu20 without the additional polystyrene insulation was equipped with the sensors according to Figure 6.13

and put under the solar simulator. The collector's absorber and glazing temperatures were measured for three different inlet temperatures (70, 80 and 89 °C). During this steady-state test, the average insolation was 881.7 W/m² with a mean wind speed across the glazing of 2.5 m/s and an ambient temperature of 24.9 °C. In addition to the varying inlet temperatures, a further measurement series in dry stagnation (I = 879.8 W/m²; v_{wind} = 2.5 m/s) was conducted. Finally, the measured temperatures for absorber and glazing were averaged and compared with the simulation results (Table 6.7).

Table 6.7: Comparison of the collector component temperatures in dry stagnation derived by simulation and in laboratory testing

	Stagnation		**T_{in} = 70 °C**		**T_{in} = 80 °C**		**T_{in} = 89 °C**	
	Test	**Sim**	**Test**	**Sim**	**Test**	**Sim**	**Test**	**Sim**
Absorber temperature in °C	194.9	193.2	81.4	82.1	90.3	90.9	98.3	98.2
Deviation in °C	- 1.7		+ 0.7		+ 0.6		+ 0.1	
Glazing temperature in °C	58.5	58.3	35.6	33.9	36.9	35.9	38.5	37.8
Deviation in °C	- 0.2		- 1.7		- 1.0		- 0.7	

Reiter et al. (2014) published similar deviations of 2 to 3 % in terms of the efficiency and about + 1 K for the component temperatures. Föste (2013) documented an efficiency difference of about 1 % between simulation and measurement in his research programme after adjusting the convective heat transfer by an amplification factor. Freeware collector software, such as CoDePrO (Koo 1999) or Kolektor 2.2 (Matuska and Zmrhal 2009), are showing for a reference collector that was tested under the institute's solar simulator a deviation of 3 to 4 %. Overall, the implementation of the extended convection theory by Eismann (2015) led to a very good correlation between measurement and simulation results.

Summary

The laboratory tests for the convective heat loss are showing a slight difference to the simulated results with Eismann's extended equation. It is likely that this caused by a concatenation of measurement uncertainties:

- The influence of the applied thermocouples is small because of the calibrated sensors (see chapter 4). This error ranges in the region of 0.001 W/m²K. Consequently, error bars for the thermocouples were neglected. A further reason for the deviation could be linked with the used material parameters. A minor change in the heat conductivity given for the insulation material of +0.002 W/mK leads to a considerable deviation of the derived convective heat transfer coefficient of up to 0.287 W/m²K. It could be possible that the heat conductivity is higher than stated by the insulation producer. Furthermore, the heat conductivity might rises with the collector operation temperature and, thus, a higher conductive heat loss exists.
- Another uncertainty factor could be caused by the optical parameters of the absorber and glazing, i.e. emissivity coefficient as well as absorptance. A change of the absorber's emissivity coefficient of -0.05 leads to a maximum deviation of the convective heat transfer coefficient of 0.05 W/m²K.
- In addition to this, the absorber deflection affects the measurement in an unpredictable way. This is an issue with all-round supported absorbers with small gap sizes (10 to 20 mm) as the thermal elongation leads to a more distinctive sheet deflection than in collector configurations with an absorber resting on the insulation.

In the end, several errors contribute to the deviation, which were observed in this measurement. However, the results of the stagnation test and the efficiency test strengthen the fundamental statement:

The presented results confirm that the values for the convective heat loss in flat plate collectors according to Eismann's approach are producing more realistic results than that of Hollands et al. (1976). Therefore, for future collector analyses, it is plausible to use the extended equation. It would be preferable to conduct further convective heat loss measurements for hermetically sealed collectors – especially for smaller gap sizes down to 10 mm. The tested experimental collector

TPS-AlCu20 had a mean gap size of 18 mm. It is very likely that during the highest inlet temperature, the absorber deflection reduced the gap size and the convective heat loss increased. Those processes are not predictable and always applying the measurements with an uncertainty. As both component temperatures and the efficiency curve are in a good correlation with the simulation it is concluded that the simulation model is working properly and the simulation results are valid.

6.6 Parameter study and efficiency analysis of a gas-filled collector

In this subchapter, different collector configurations were modelled, simulated and compared to results of similar research studies. The conducted simulations are based on the collector specifications as shown in Table 6.8.

Table 6.8: Used collector parameters within the simulation study

Aperture area in m²	1.84
Absorber type	Sheet-pipe
Absorber piping	Double-harp
Material absorber sheet	Al
Material absorber piping	Cu
Absorption absorber	0.95
Emission absorber	0.05
Transmission glazing	0.94
Emission glazing	0.94
Thermal conductivity Al in W/m²K	235.0
Thermal conductivity Cu in W/m²K	390.0
Thermal conductivity mineral wool in W/m²K	0.035
Thermal conductivity glass in W/m²K	0.84
Glass thickness in mm	3.2
Thickness absorber sheet in mm	0.5
Fin width in mm	99
Outer diameter riser in mm	7
Absorber length in mm	1,857
Absorber width in mm	990
Insulation thickness in mm	50
Gap size in mm (unless stated otherwise)	18
Gas filling	Ar / Kr

6.6.1 Parameter study

Figure 6.18 shows the convective heat transfer depending on the gap size for a hermetically sealed collector with argon and krypton in the interspace for a collector operation point of 0.05 m²K/W.

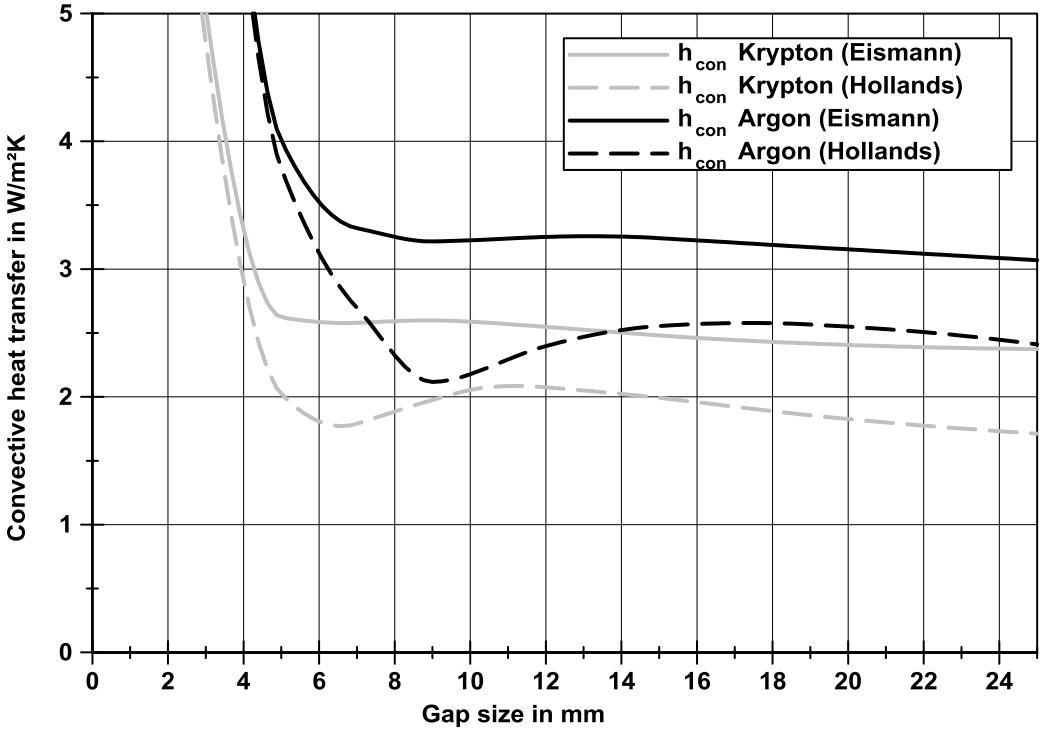

Figure 6.18: Convective heat transfer coefficient for various gases according to Eismann (2015) and Hollands et al. (1976) depending on the gap size for a collector operation point of 0.05 m²K/W

As a consequence of the extended Hollands et al. (1976) correlation, the convective heat transfer after Eismann (2015) differs not only in the dimension but also in the curve shape. The local minimum in the transition region is not existent; however, the change of the convective heat transfer coefficient depending on the gap size is smaller than the calculation approach after Hollands et al. (1976). For gap sizes of less than 8 mm (argon) and 6 mm (krypton), both curves are following an similar exponential increase of the convective heat transfer. In the light of a convective heat loss reduction, these findings lead to the result that a gap size adjustment in the transition region is neither practical nor feasible. Furthermore, by applying the correlation after Hollands et al. (1976), an underrated convection loss and a wrong collector

design parameter for the gap size is chosen. Figure 6.19 shows this effect for argon and krypton filled collectors with a gap size between 5 to 20 mm.

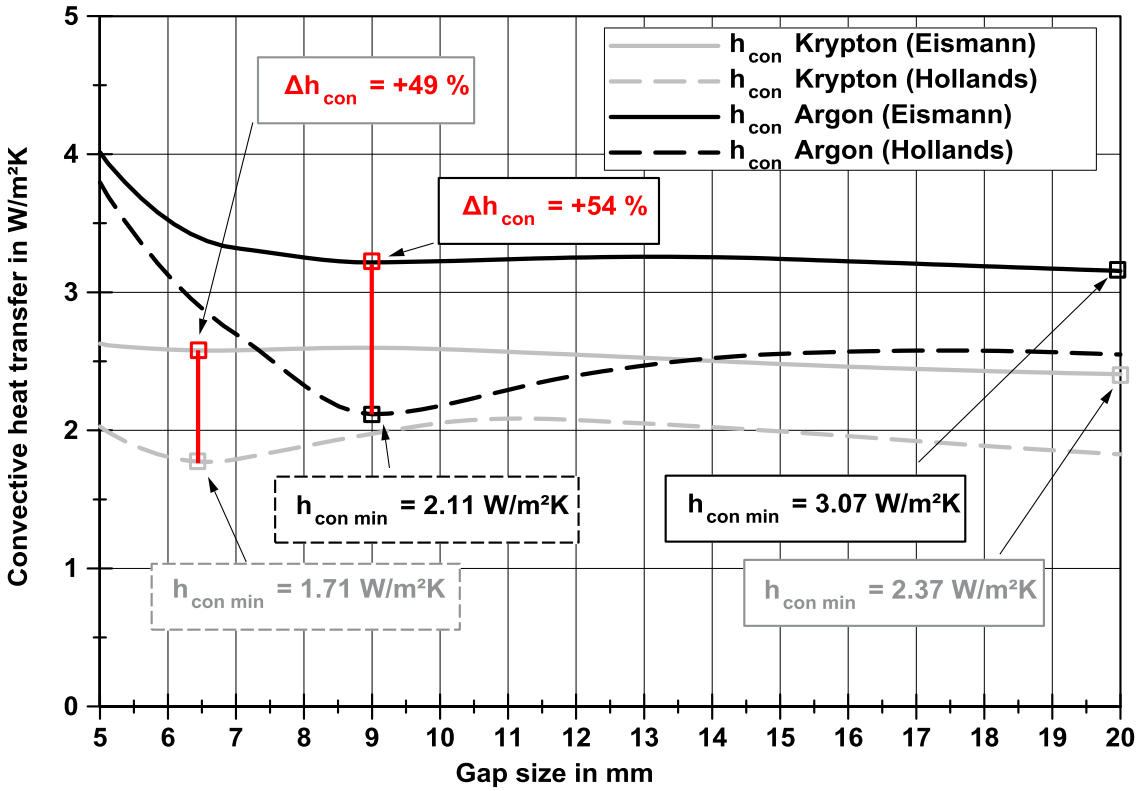

Figure 6.19: Comparison of the minima values of the convective heat transfer coefficient depending on the gap size (between 5 to 20 mm) for a collector collector operation point of 0.05 m²K/W

If the construction boundaries require a collector design in between the priorities of the smallest gap size and the lowest convective heat loss, the original correlation will lead to a smaller gap size than necessary. However, due to the absorber deflection in operation, the losses are magnified, as the absorber buckles and reduces the already small gap between absorber and glazing. For the approach after Eismann (2015), the absolute rise of the convective heat transfer is less problematic as the curve differs only marginally with the gap size. In fact, the smallest heat loss for the shown range is at a gap space of 20 mm. Hence, shorter gap sizes are showing no considerable benefit.

Figure 6.20 compares the collector efficiency and convective heat transfer for an argon, krypton filled and vented collector.

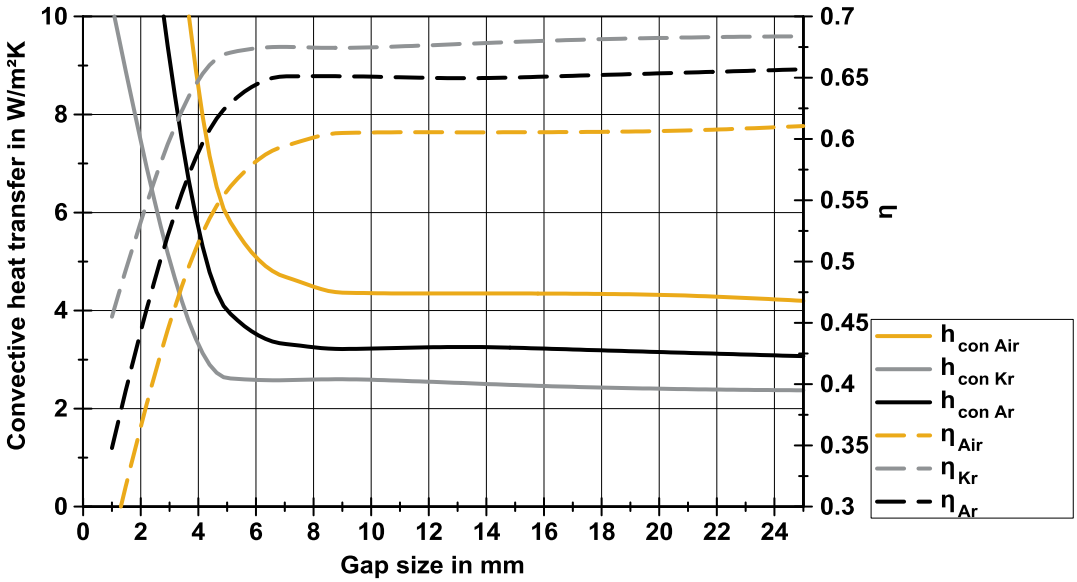

Figure 6.20: Comparison of the convective heat transfer in a hermetically sealed collector for air, argon and krypton for an operating range of $(T_{mean} - T_{amb})/G = 0.05$ m²K/W

Figure 6.19 and Figure 6.20 are showing that a gap size between 15 to 20 mm is a practical design point for a hermetically sealed collector. Within this gap size range, neither the convective heat loss nor the efficiency varies significantly. Furthermore, the distance between absorber and glazing is big enough to allow an absorber deflection towards the glazing; however, this should be minimised and if possible prevented. In literature on hermetically sealed and gas-filled collectors a gap size of about 8.6 mm for argon, 5.7 mm for krypton and even 3.9 mm for xenon filled cavities are recommended (Vestlund et al. (2012a)). Due to the mechanical behaviour and the initial absorber shape, it is doubtful that such small distances are practical. The mechanical bending in an all-round supported absorber is not predictable and, thus, a case study is conducted for an optimised absorber structure that allows a foreseeable deflection (cf. chapter 8). Ultimately, this could lead to an application of smaller spacing.

As a result, for the latter batch of experimental collectors a gap sizing of 15 and 20 mm was chosen.

6.6.2 Efficiency analysis

Derived by the parameter study above, a simulation based efficiency comparison for a gap size of 20 mm between gas-filled collectors (krypton, argon) and the identical but vented collector was conducted.

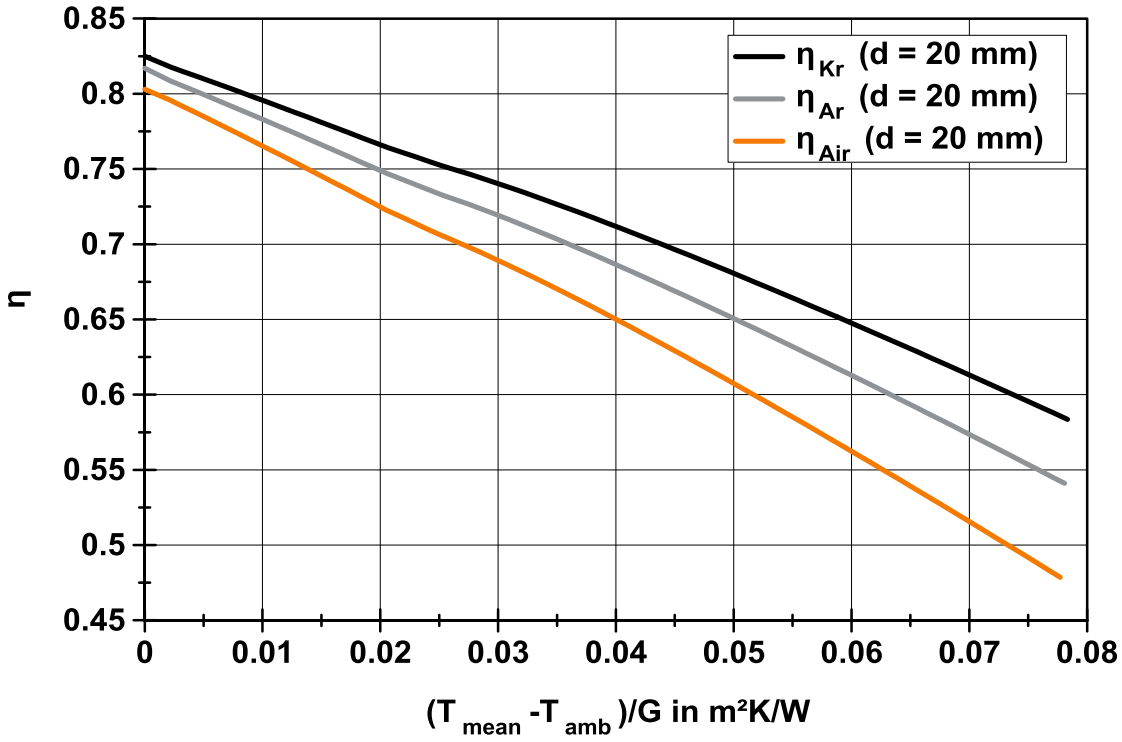

Figure 6.21: Efficiency comparison of an argon and krypton filled and vented collector with a gap size of 20 mm (convection theory according to Eismann (2015))

The collector setting with the krypton filling outperforms the two other simulation results over the complete temperature range. For an ordinate value of 0.05 m²K/W, the efficiency difference between the krypton and vented collector results in a 7.2 % higher performance whereas the second gas-filled collector version (argon) lacks 3 % compared to the krypton variant but outperforms the vented collector by 4.3 %.

Vestlund's approach was to compensate the simulated efficiency boost by a material reduction in the absorber; however, the material savings in the absorber are smaller than predicted. Vestlund et al (2012a) analysed possible material savings in the absorber to the point where the gas-filled collector simulation model showed a similar performance as a vented collector.

For an efficiency comparison between the results according to Vestlund et al. (2012a) and the own simulation results, the gap size was adjusted accordingly to the simulation parameters of Vestlund et al. (2012a). The version 'AlCu8.6' represents a conventional and market available sheet-pipe absorber (Table 6.8) whereas 'Ref Vestlund' is an, in terms of the material use, optimised sheet-pipe absorber. Figure 6.22 compares the efficiency of an optimised simulation variant by Vestlund et al. (2012a) with the author's own results. The collector specifications of the reference can be looked up in Table 6.9.

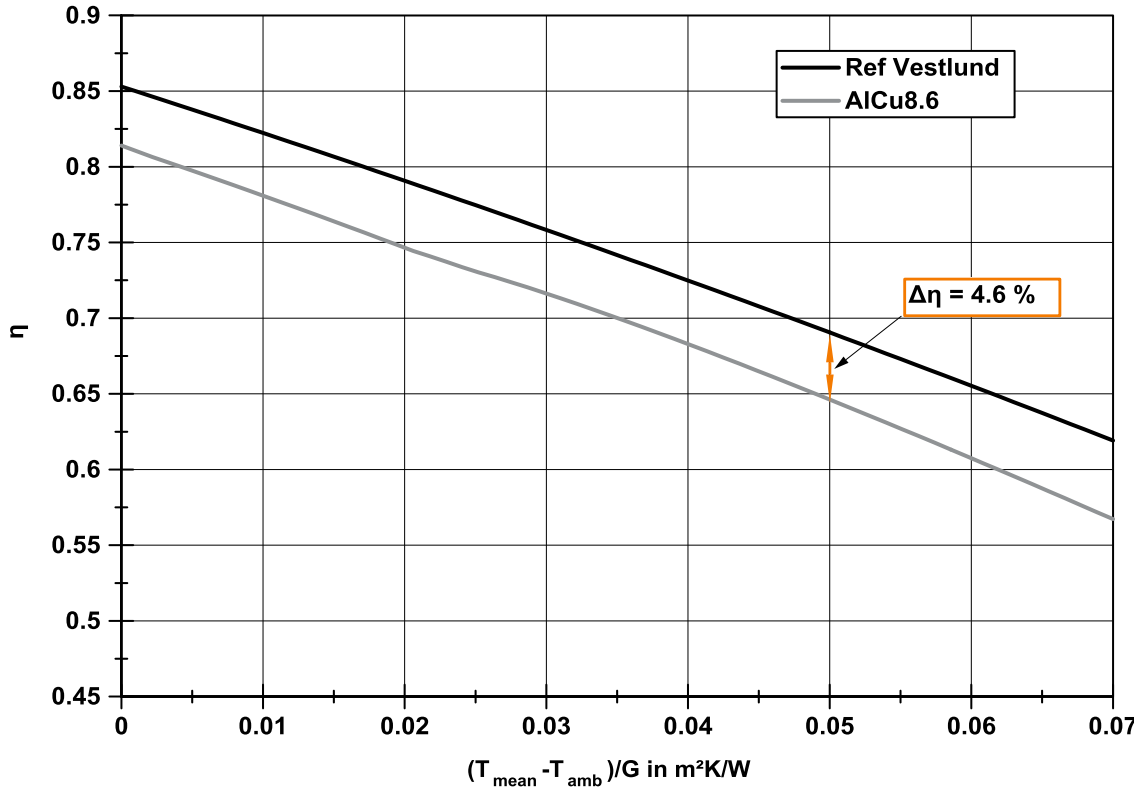

Figure 6.22: Efficiency comparison between a collector version by Vestlund et al. (2012a) and an own configuration

Table 6.9: Applied collector parameters (cf. Vestlund et al. 2012a)

Parameter	**Ref Vestlund**	**AlCu8.6**
Zero loss efficiency η_0	0.853	0.815
Linear loss coefficient a_1 in W/m²K	3.02	3.19
Quadratic loss coefficient a_2 in W/m²K²	0.00458	0.009
Gas-filling	Ar	Ar
Gap size in mm	8.6	8.6
Absorber material	Al	Al
Piping material	Cu	Cu
Absorber thickness in mm	0.5	0.5
Fin width in mm	144	99

The efficiency curves are showing a deviation over the complete collector operation range. It needs to be noted that the version ‘Ref Vestlund’ has a tube-to-tube distance, i.e. fin width, of 144 mm. This results for a typical 2 m² sized absorber with only seven risers. In contrast to this, the version ‘AlCu8.6’ has a fin width of 99 mm, which corresponds to ten risers. In particular, the fewer risers are affecting the heat removal factor F’ and, hence, are lowering the efficiency. In the case of ‘Ref Vestlund’ the decrease of F’ is still compensated by the reduction of the convective top heat loss – according to the convection theory of Hollands et al. (1976). This leads to a difference of about 4.6 % for the collector operation point of 0.05 m²K/W. If both absorbers would be identical, this difference would be significantly higher. An own more precise modelling of the ‘Ref Vestlund’ was impeded due to lacking collector specifications.

6.6.3 Summary

The predicted efficiency of gas-filled collectors calculated by Vestlund et al (2009, 2012a) was not achieved in this research programme due to higher convection losses. In fact, the performance improvement of an argon gas-filled collector compared to a well-designed vented flat plate collector is small. This leads to the consequence that an absorber material reduction of up to 25 % (Vestlund et al. 2012a) will be either smaller or results in a poor efficiency. Still, as shown in Figure 6.21, the gas-filled collectors outperform a vented collector, which, ultimately, indicates a potential to tap cost savings by reducing the material in a sheet-pipe absorber and adjust the performance on a level of a vented collector. Such an approach needs to be analysed from a thermal, mechanical and production-technical point of view. At first, a methodology to identify the optimum between absorber costs and efficiency needs to be analysed. Based on this algorithm, the collector parameters need to be derived before the mechanical behaviour of the cost optimised absorber is investigated. In case that a thin aluminium absorber sheet (t_{sheet} < 0.3 mm) is used, the current absorber manufacturing process might need to be optimised.

6.7 Collector temperature loads during system operation and annual yield

Beside the analyses of the collector's efficiency, a system simulation in Carnot (Hafner et al. 1999) and a simulation of the maximum temperature in dry stagnation were carried out. Therefore, the introduced collector model was embedded in a system simulation to investigate the following:

- the magnitude and occurrences of thermal loads during a normal system operation in Germany
- the maximum temperature during dry stagnation
- the solar yield for a heating system with a hermetically sealed and gas-filled collector referenced to a heating system with a conventional vented collector

6.7.1 Assumptions and boundary conditions

In order to give confidence in the performance of the adhesive chosen, it was necessary to analyse both the magnitude and duration of periods of high thermal load. For the evaluation of the component loads two distinctive temperature limits, which are used in the polymeric material sciences, can be utilised – the short-term service temperature (T_{sts}) and the long-term service temperature (T_{lts}). According to Dominighaus (2012) and Biron (2013), the short-term service temperature represents the maximum temperature that causes no considerable material damage. The T_{lts} of a polymer stands for the temperature at which a material sample is still capable of 50 % of its initial material properties taken at ambient conditions, e.g. tensile strength, after an exposure to either 20,000 h in hot air or 10,000 h in hot oil ISO 175 (2010). The material supplier defined the T_{sts} for the modified butyl sealant (primary sealing) to be 150 °C. The maximum duration for T_{sts} is not known as the material is still in a prototype phase; however, this period can vary between minutes and hours. Temperatures exceeding the 150 °C will lead to an accelerated ageing of the adhesive and, thus, needs to be kept to a minimum. The simulation results serve as an indication of occurring temperature loads for adhesives in solar collectors. The service temperatures of the thermoplastic spacer are compiled in Table 6.10.

Table 6.10: Used temperature limits for the thermal load of the primary sealing

Material	Short-term service temperature in °C	Long-term service temperature in °C
Modified butyl	150 °C	100 °C

The primary sealing is vulnerable to high thermal loads (> T_{sts}) and high thermal loads over a long-lasting period. In case that this temperature is exceeded the ageing is accelerated, which, ultimately, either ends in a delamination between adhesive and absorber, losses of its sealing property or a combination of both effects. Moreover, the high temperatures lead to a softening of the spacer, which can be critical in certain operation points, i.e. internal or external shocks (cf. chapter 7.4.2). Unlike the primary sealing, the secondary sealing is capable to withstand 200 °C over several hours. Its application in solar collectors is already widespread, e.g. to fix the glazing on the casing. Consequently, the use of this adhesive is seen uncritical and not further analysed within this thesis.

For this evaluation, a typical solar thermal system for a single-home in Germany was chosen and implemented in MATLAB / Simulink. The house is equipped with a solar system consisting of 14.4 m² collector aperture area with a 1,000-litre buffer storage. During times of insufficient solar yield, a 15 kW oil heating boiler supplies the floor heating system and the domestic hot water production with thermal energy. During a year, a heat energy demand of 16,239 kWh needs to be covered, of which 2,539 kWh is used for domestic hot water preparation and 13,700 kWh for space heating.

Table 6.11 contains the system details, which were used for the simulation study.

Table 6.11: Applied parameters in the system simulation

Location	Wurzburg (Germany)
Building	Single-family house
Annual heat energy demand in kWh	16,239
Space heating in kWh	13,700
Domestic hot water in kWh	2,539
Heating	Floor heating
Furnace	Oil (15 kW)
Domestic hot water storage volume in litre	130
Buffer storage volume in litre	1,000
Installed solar collector aperture area in m²	14.4
Collector azimuth	South
Collector parameter TPS-AlCu20	
Zero loss efficiency	0.815
Linear heat loss coefficient in W/m²K	3.19
Quadratic heat loss coefficient in W/m²K²	0.009
Collector parameter reference collector	
Zero loss efficiency	0.815
Linear heat loss coefficient in W/m²K	3.52
Quadratic heat loss coefficient in W/m²K²	0.012
Mass flow in l/m²h	40

To conclude on the fin temperature distribution of the absorber, four points in an equidistant distance were implemented in the simulation model (Figure 6.23).

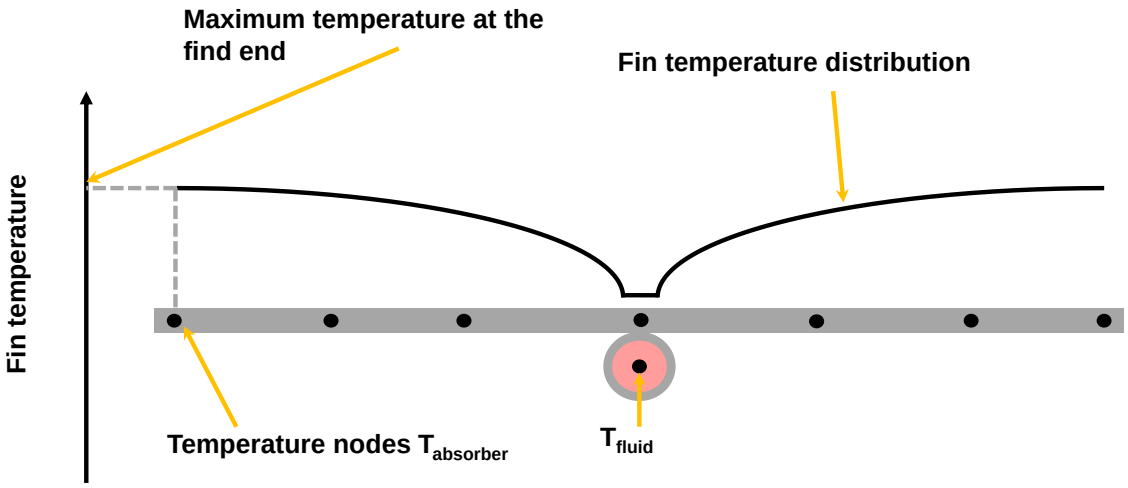

Figure 6.23: Schematic cross section of the simulated temperature positions on an absorber fin

Since the maximum temperature occurs at the fin end (Duffie and Beckman 2009) and the edge bond was applied in this region, these absorber temperatures were analysed for the thermal load on the primary sealing. However, the edge bond temperatures are slightly lower than the simulated absorber temperatures due to higher edge losses. Nevertheless, it is assumed that this effect is negligible because of the thick side insulation (20 mm) and the relatively small edge surface.

Two regions on the double-harp sheet-pipe absorber were chosen to simulate the maximum temperatures (Figure 6.24).

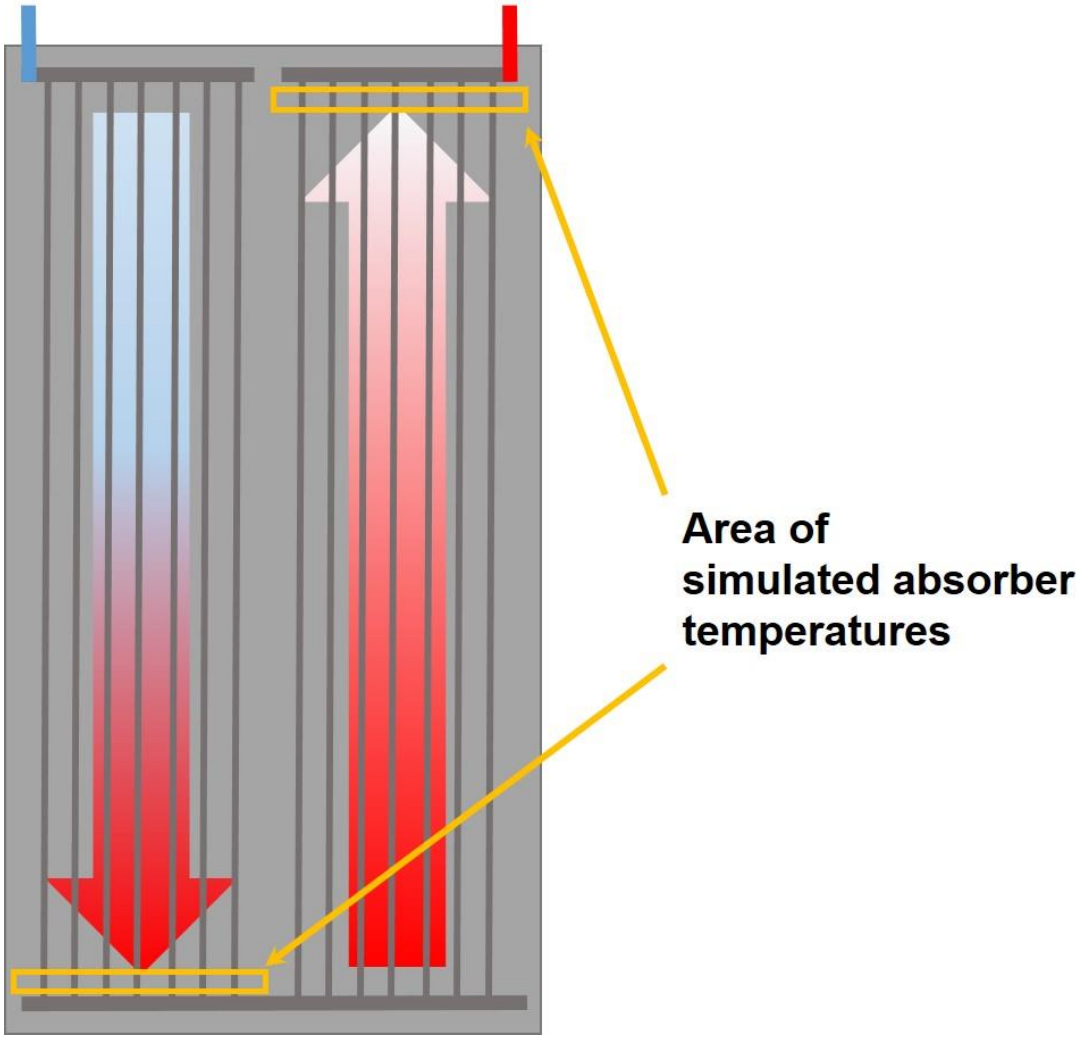

Figure 6.24: Positions of the simulated absorber temperatures

The first temperature points were calculated at the end of the first side of the double-harp absorber whereas the second simulated temperature position was close to the collector outlet. By this approach, maximum temperatures for each absorber side were considered.

6.7.2 System simulation results of the initial collector setting ‘TPS-AlCu20’

The gas-filled collector generated in this simulation has an annual yield of 5,745 kWh, which equals a solar fraction of 35 %. Compared to the vented reference collector, the gas-filled collector produced 180 kWh more heat during the year. Despite the higher collector efficiency, the additional annual yield of the

argon filled collector is minimal compared to a commercially available vented collector. The same collector version with krypton instead of argon generates 5,890 kWh per annum, which corresponds to a 365 kWh higher energy output than the vented reference collector. This corresponds to a specific annual yield of 409 kWh/m²a for this collector type; however, krypton causes about 12 € per collector more costs for the gas-filling compared to argon. Solely based on the increase of the collector efficiency and improvement of the system performance, future collector development should combine further positive features, e.g. lower degradation or lower costs, to be successful on the market. This is further discussed in chapter 9.

Beside the discussion of the profitability, the thermal loads during a normal system operation are of importance to make utilisation of the adhesive technique feasible. Figure 6.25 shows the maximum temperatures that occurred during a regular system operation throughout the year.

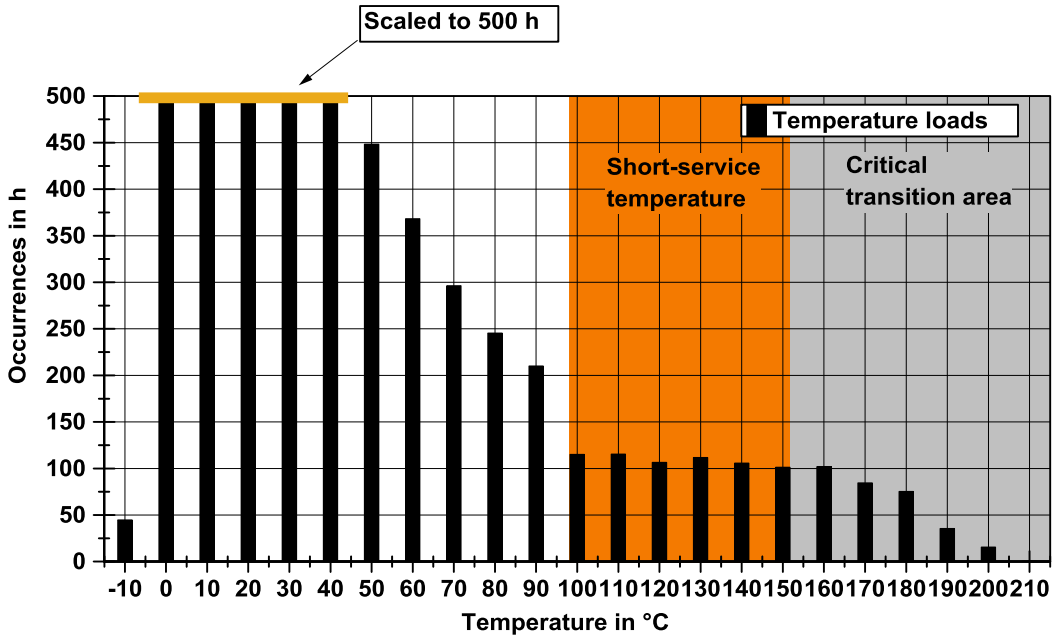

Figure 6.25: Annual temperature occurrences and magnitude during system operation (for better illustration the maximum occurrences in hours was set to 500The system controller shuts down the collector operation at a buffer storage temperature of 95 °C. Hence, it was assumed that absorber temperatures above 100 °C are indicating collector stagnation. The orange-inked area represents the short-term service temperature whereas the grey area indicates a critical temperature range for the

adhesive with accelerated ageing. Idle times in this region need to be avoided or kept to a minimum.

In this case, a dwell time for an absorber temperature between 100 to 150 °C of 656 h and 314 h for temperatures above 150 °C were detected. This means during 3.6 % of the complete collector operation time, the short-term service temperature was exceeded. However, the higher temperatures, e.g. > 200 °C, are degrading the adhesive more than temperatures close to 150 °C. The whole temperature range was between -13 °C and up to 207 °C corresponding to a thermal load amplitude of 220 °C. Unlike the high temperatures, the very low temperatures do not cause an ageing effect. In what dimension the temperature magnitude and periods that are exceeding T_{sts} are affecting the material ageing needs to be thoroughly tested. Outdoor testing results showed that exposure times of up to nine months in permanent dry stagnation led to fatal material failure of the edge bond and visible damages on the absorber and glazing (cf. chapter 7.3 and 7.4).

For the identical collector setting an evaluation of the maximum temperature loads was conducted. To derive the stagnation temperature values, a virtual stagnation test stand was implemented in Simulink. The collector model was built in a virtual test stand and is fed with boundary conditions (mass flow, insolation, wind speed …). For the stagnation simulation, the mass flow was set to 0 m³/h for different levels of irradiation and wind speed.

The maximum temperatures were then calculated by extrapolating the simulation values according to the DIN EN ISO 12975. Table 6.12 constitutes the simulated temperatures values while in dry stagnation as well as the extrapolated figures conforming to the standard.

Table 6.12: Maximum absorber temperatures in dry stagnation derived by simulation for a gas-filled collector (argon) at 3 m/s wind speed

Simulated values **G = 880 W/m²; T_{amb} = 29 °C**	196 °C
Extrapolated climate class A **(G = 1000 W/m²; T_{amb} = 30 °C)**	220 °C
Extrapolated climate class B (sunny) **(G = 1100 W/m²; T_{amb} = 40 °C)**	230 °C

As the current material composition is not capable to withstand such high loads without an accelerated ageing, possibilities to reduce the maximum temperatures need to be investigated. From a collector point of view, several countermeasures for a temperature reduction are conceivable: High absorber temperatures during operation exceeding 110 °C could be lowered by adding a heat sink on the absorber edge. The drawback of this measure would be a lower efficiency. Depending on the heat sink geometry, it will affect the collector heat loss more or less and, thus, this measure should be analysed by simulation and testing. It is debatable whether this measure lowers the stagnation temperatures to an acceptable level for the adhesive. Promising in this context seems the application of overheating protections, which are in a focus for the application in polymeric collectors. These measures range from thermotropic layers on the glazing (Resch and Wallner, 2009) to a specially designed increase of certain collector loss mechanisms, e.g. adjusting absorber coatings for higher radiation losses and lower absorption (Marty et al. 2008) as well as active cooling (Tigi 2015). Reiter (2014) included an excerpt of these measures in a system simulation to evaluate the impact for polymeric collectors. Based on his results and with focus on keeping the complexity and, thus, the costs down, two possible measures to reduce the thermal loads were considered:

- reduction of the absorption coefficient by a different absorber coating
- reduction of the back side insulation

In terms of investment costs for the countermeasure and its impact, the two analysed approaches are the most appropriate one.

6.7.3 System simulation results of the version ‘TPS-AlCu20’ with an increased emissivity of the absorber coating

A market available absorber coating with a reduced absorption and an increased emission coefficient for infrared radiation was chosen as a compromise to a non-selective absorber. Table 6.13 shows the specifications of the selected coating and two other typical coatings as comparison.

Table 6.13: Specifications of typical coatings used in the collector industry

			Ref_coa
Layer type	TiNxOy	Cermets	Ni-NiO
Substrate	Cu	Cu	Al
Aboprtion coefficient α	0.95	0.95	0.96
Emission coefficient ε	0.05	0.05	0.1
Coating method	Physical vapour deposition	Sputter	Sputter

For this simulation study the coating ‘Ref_coa’ was selected to lower the thermal loads. As an alternative, a non-selective coating in terms of black paint was dismissed due to too high losses. This seems more suitable for polymeric collectors that can justify the lower efficiency by significantly reduced component costs (Reiter 2014). Table 6.14 contains the simulated temperature values with the coating ‘Ref_coa’.

Table 6.14: Maximum absorber temperatures in dry stagnation derived by simulation for a gas-filled collector (argon) with an increased thermal emissivity (ε = 0.1 instead of 0.05) at 3 m/s wind speed

Simulated values **G = 880 W/m²; T_{amb} = 29 °C**	179 °C
Extrapolated climate class A **(G = 1000 W/m²; T_{amb} = 30 °C)**	201 °C
Extrapolated climate class B (sunny) **(G = 1100 W/m²; T_{amb} = 40 °C)**	211 °C

In contrast to the high selective coating, the maximum absorber temperature is reduced by 17 °C down to 179 °C. Yet, this temperature still exceeds the adhesive service temperature by almost 30 °C.

Figure 6.26 shows the impact of the annual thermal loads during operation.

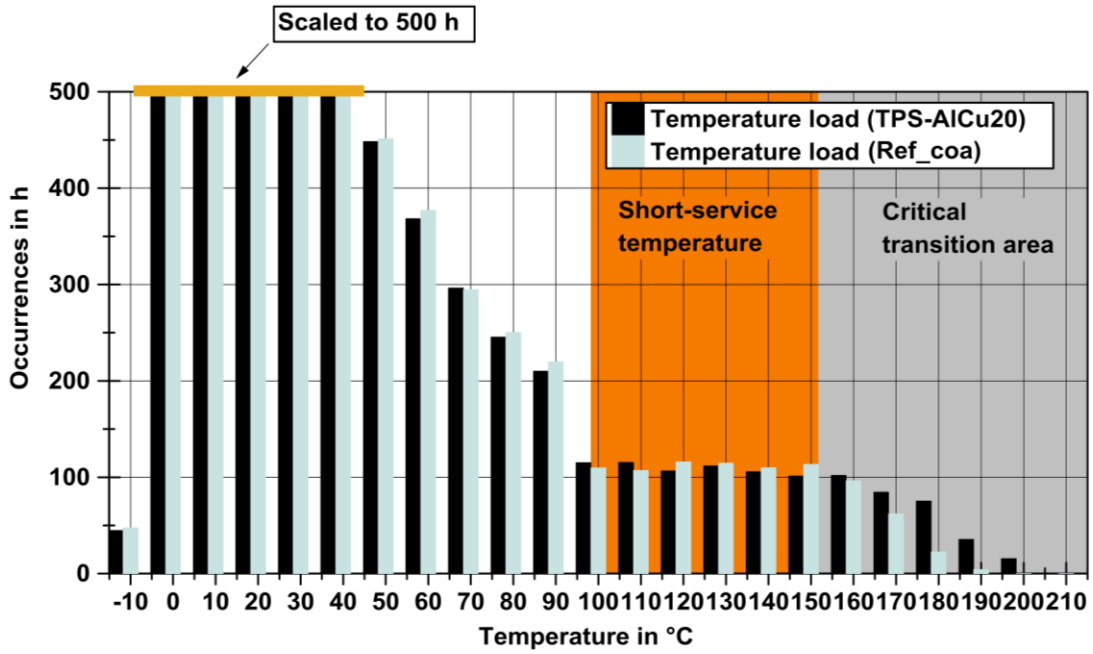

Figure 6.26: Simulated annual temperature occurrences and magnitude during system operation for a collector with a Ni-NiO absorber coating (Ref_coa)

The period during which absorber temperatures reached more than 150 °C was cut down to 185 hours, which corresponds to a reduction compared to the initial collector setting of 55 % or 230 h. The change of the absorber coating affects the collector's efficiency parameter as well. A lower efficiency is derived (Figure 6.27) that ranges depending on the collector operation point between 1.7 % at the zero loss coefficient η_0 to 2.4 % lower at 0.07 m²K/W (Figure 6.27).

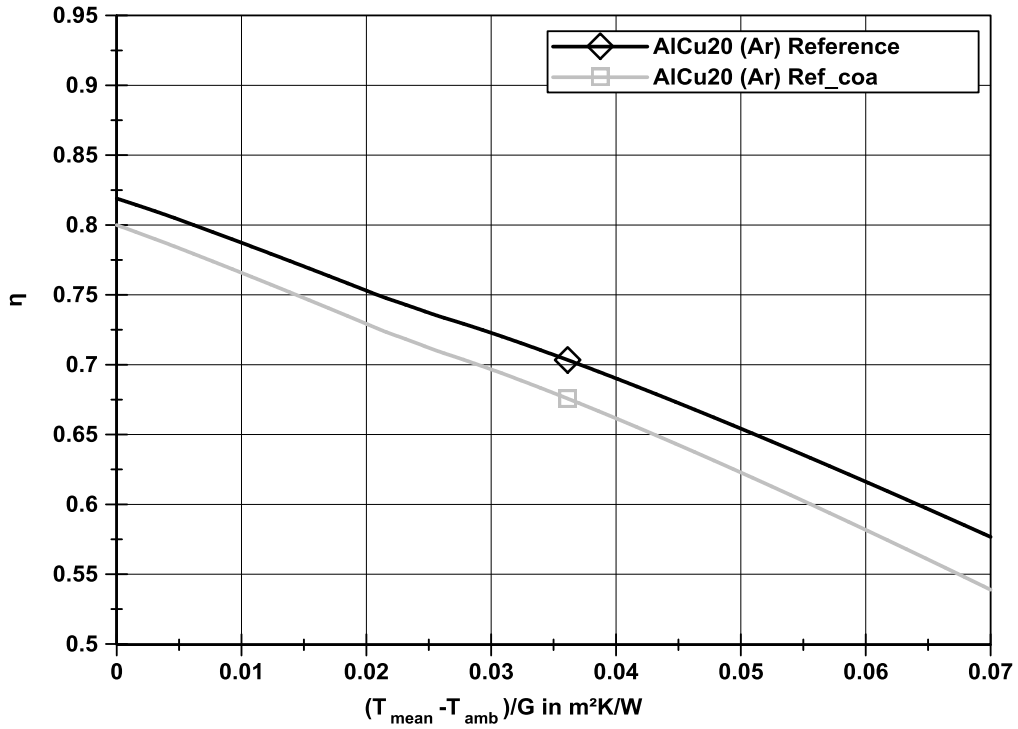

Figure 6.27: Simulated efficiency comparison of the reference collector (Al-Cu, 20 mm spacing, high selective coating) and an identical collector with a different absorber coating

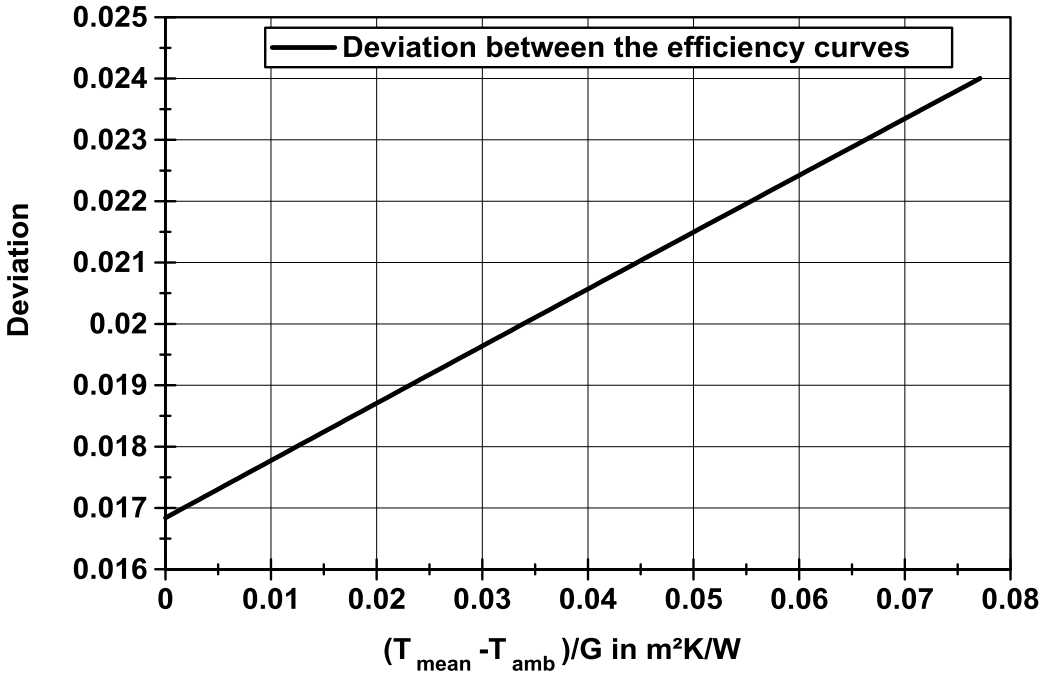

Figure 6.28: Deviation between the two simulated efficiency curves depending on the collector operation point

In comparison to the initial collector setting, the annual yield was reduced by 9.4 % to 5,205 kWh and 5.8 % or 320 kWh compared to the vented reference collector.

6.7.4 System simulation results of the version ‘TPS-AlCu20’ with a reduced backside insulation

The reduction of the insulation thickness leads to a higher collector loss via the back and to a lower stagnation temperature and, thus, to a reduced collector efficiency as well (Figure 6.30). Within this case study, a backside insulation of 30 mm was chosen as the collector efficiency is still at a similar level as a vented solar collector.

Table 6.15 shows the derived stagnation temperatures for the collector setting with the reduced insulation thickness.

Table 6.15: Maximum absorber temperatures in dry stagnation derived by simulation for a gas-filed (argon) collector with reduced backside insulation (30 mm instead of 50 mm) at 3 m/s wind speed

Simulated values **$G = 880\ W/m^2$; $T_{amb} = 29\ °C$**	185 °C
Extrapolated climate class A **($G = 1000\ W/m^2$; $T_{amb} = 30\ °C$)**	207 °C
Extrapolated climate class B (sunny) **($G = 1100\ W/m^2$; $T_{amb} = 40\ °C$)**	217 °C

With a stagnation temperature of 185 °C, the maximum temperature was lowered by 11 °C compared to the initial setting of the gas-filled collector. In contrast to the version with the higher emissivity, a 17 °C reduction in stagnation temperatures is prevailing.

Figure 6.29 shows the temperature magnitude and occurrences during the normal collector operation throughout a year.

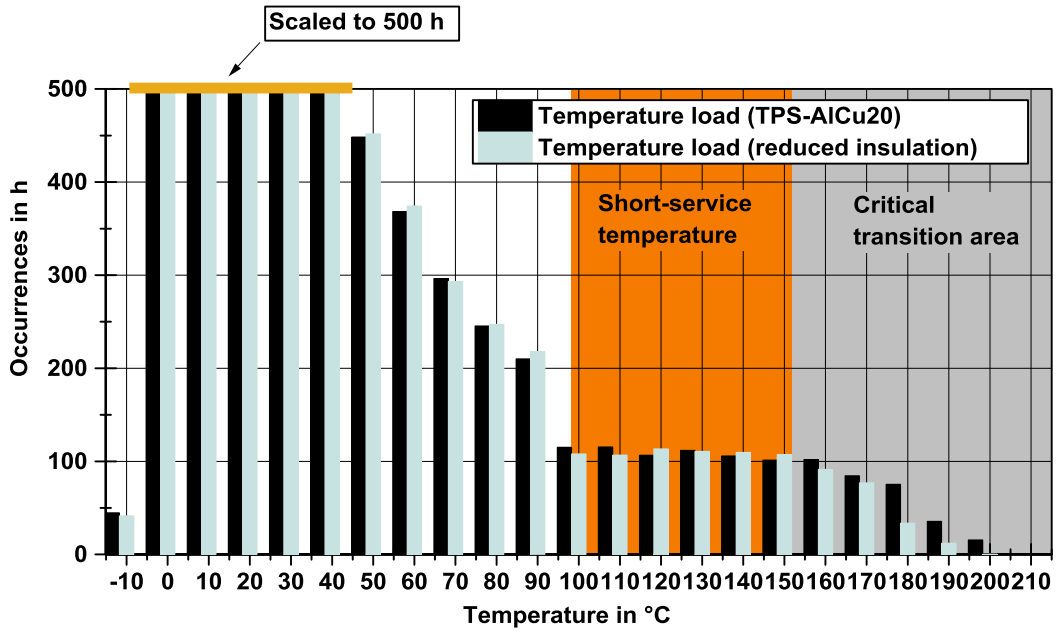

Figure 6.29: Simulated annual temperature occurrences and magnitude during system operation for a collector setting with reduced backside insulation (30 mm)

The 150 °C-limit was transcended by 214 hours whereas a dwell time within the short-service temperature of 656 hours were computed. Yet, this version leads to reduced dwell time for temperatures above 150 °C by 48 % compared to the initial collector setting ‘TPS-AlCu20’ but keeps the collector by 29 hours longer in the critical transition area than the configuration with the Ni-NiO coating (Ref_coa).

As a result of the reduction of the insulation thickness from 50 mm down to 30 mm, an efficiency decrease for an ordinate value of 0.05 m²K/W of 1.7 % is simulated (Figure 6.30).

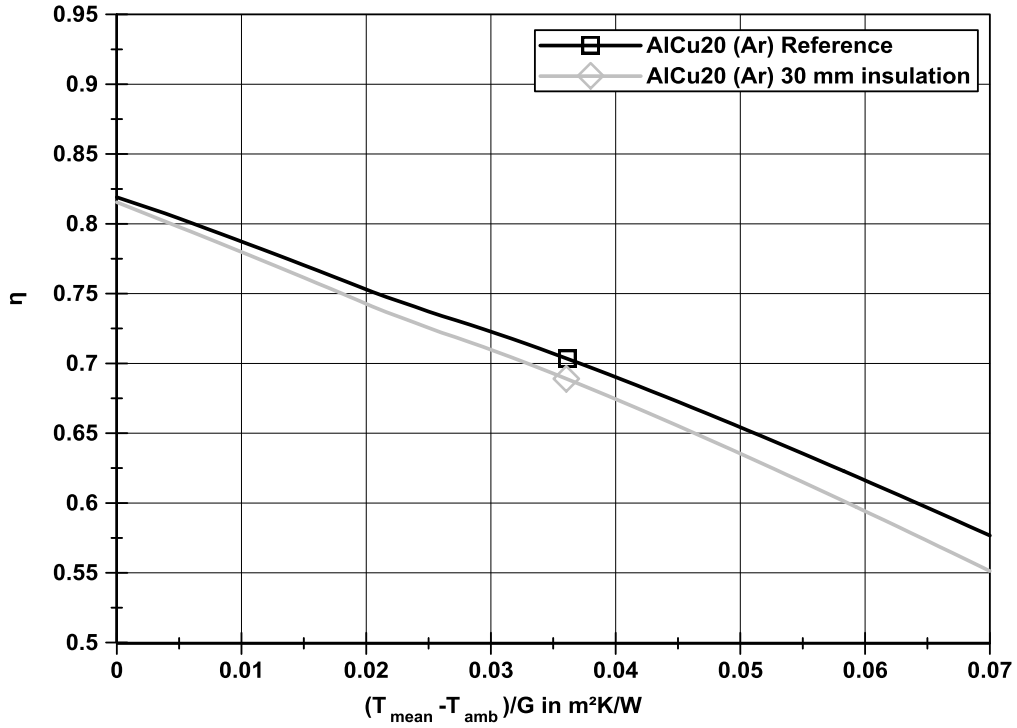

Figure 6.30: Efficiency comparison of the reference collector and an identical collector with reduction insulation (30 mm instead of 50 mm)

The deviation depending on the collector operation range between the two collector settings varies from 0.5 to 2.7 % (Figure 6.31).

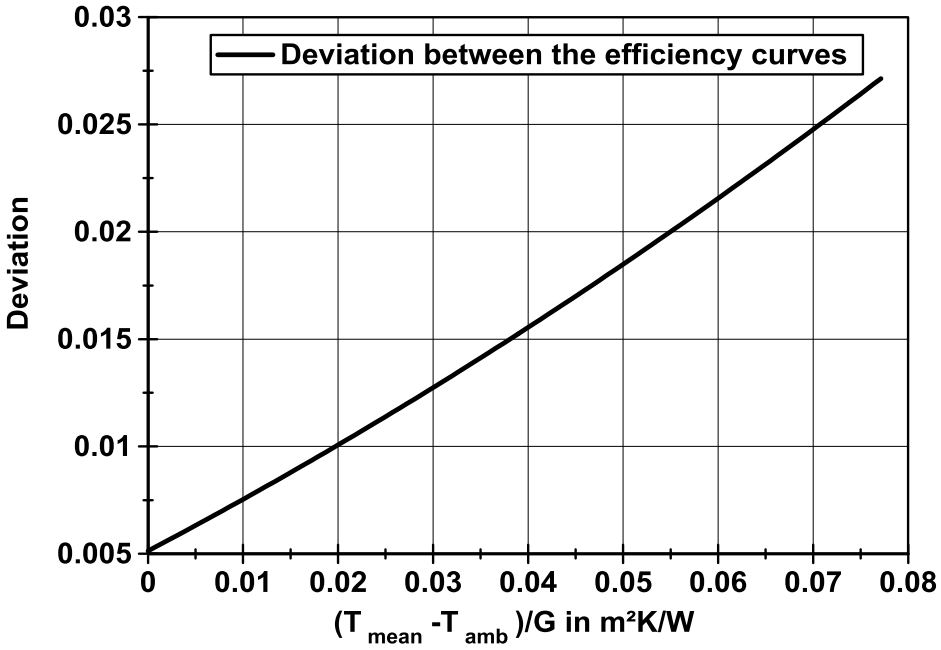

Figure 6.31: Deviation between the two simulated efficiency curves depending on the collector operation point

Compared to the collector version with the modified absorber coating, a similar annual yield for this collector type of 5,207 kWh was simulated. This equals a 5.8 % lower annual yield than the vented collector and 9.4 % less useful solar energy than the collector ‘TPS-AlCu20’.

Table 6.16 comprises the system simulation results referenced to the initial collector setting ‘TPS-AlCu20’ and to the market available vented collector.

Table 6.16: Compilation of the simulation results of the variants

	TPS-AlCu20	**TPS-AlCu20 with increased emissivity**	**TPS-AlCu20 with reduced backside insulation**	**Reference collector (vented)**
Dwell time T_{abs} ≥ 100 ≤ 150 °C in hours	656	671	656	-
Dwell time T_{abs} ≥ 150 °C in hours	314	185	214	-
Dwell time (≥ 150 °C) reduction compared to TPS-AlCu20	-	41 %	32 %	-
Annual yield in kWh	5,745	5,205	5,207	5,525
Difference of annual yield compared to TPS-AlCu20	-	-9.4 %	-9.4 %	-3.8 %
Difference of annual yield compared to reference collector (vented)	+4.0 %	-5.8 %	-5.8 %	-

6.7.5 Summary

It was not the intention of the author that this thesis should focus on the identification of the most suitable overheat protection. The case study on the thermal loads was conducted to show that certain design options are available to lower the maximum collector temperatures. Ultimately, the reduction of the temperature loads by the applied measures are considerable and can contribute to an increase of the adhesive lifetime. The applied measures are simple to implement, as no additional or expensive hardware is necessary. For the version with the reduced backside insulation, a cost advantage could be expected as 40 % less mineral wool is used; however, in terms of total figures, this would be only about 1.8 € per collector. The maximum efficiency loss of both collector versions is smaller than 3 %. Yet, this corresponds to a reduced system performance of up to 5.8 % compared to the reference collector. As this difference is small, the lowered system performance needs to balance this drawback by other aspects, such as a lower investment or other significant advantages over vented collectors – e.g. less absorber degradation. A gas-filled collector with krypton instead of argon could balance the loss in the annual yield but, at the same time, the thermal material loads would increase.

The limited thermal capability of the primary sealing is the most vulnerable point of this new collector type and needs to undergo a thorough evaluation. Hence, a further optimisation of the material is practical – whether this is possible in the scope of the limits of certain chemical processes needs to be analysed by material science experts. In any case, the measures need to be evaluated in field tests to derive results on the material ageing.

7 Prototype testing and manufacturing

In this chapter the testing and manufacturing of a hermetically sealed flat plate collector is discussed as there is only limited published literature available on such a collector type. The results can be used for a further utilisation of both the applied production technology and the discussed collector design.

In the upcoming subchapter, the production of an experimental collector is presented as proof of concept of the adapted mass production technique. Beyond this, the mechanical behaviour of both collector versions with both a sheet-pipe and roll bond absorber were analysed in comprehensive indoor and outdoor testing. For each test series, an efficiency test before and after the exposure in dry stagnation was conducted.

7.1 Overview of experimental collectors and performance

In total three generations of physical prototypes were built throughout this research program. Table 7.1 shows the specifications of the six collectors with a fully adhesive edge bond.

Table 7.1: Overview of the measured collector parameters according to DIN EN 12975-2

Collector	**TPS-1**	**TPS-2**	**TPS-AlCu**	**TPS-CuCu**	**TPS-RB15**	**TPS-RB20**
η_0	0.782	0.788	0.815	0.84	0.879	0.88
a1 in W/m²K	3.215	3.474	3.19	4.03	3.315	3.275
a2 in W/m²K²	0.023	0.021	0.009	0.017	0.020	0.016
Aperture area in m²	1.9	1.9	1.8	1.8	1.86	1.86
Gap size in mm	10	10	20	15	15	20
Insulation material	Mineral wool (λ = 0.035 W/mK)					
Insulation thickness (back) in mm	40	40	55	55	55	55
Insulation thickness (side) in mm	--	--	20	20	20	20
Absorber type	Sheet pipe	Sheet pipe	Sheet pipe	Sheet pipe	Roll bond	Roll bond
Absorber piping	Harp	Harp	Double-harp	Double-harp	Double-harp	Double-harp
Material absorber sheet	Al	Al	Al	Cu	Al	Al
Material absorber piping	Al	Al	Cu	Cu	Al	Al
Gas filling	Ar	Ar	Ar	Ar	Ar	Ar

The collector ‘TPS-CuCu15’ was destroyed during the preparation of the second efficiency test in which a deflection measurement would have been conducted. This was very unfortunate as this collector was expected to show a lower deflection because of the absorber material pairing – copper sheet and copper piping due to the same thermal elongation coefficient.

A reference collector was used as a benchmark for the efficiency tests of the physical prototypes. There was one market available gas-filled flat plate collector available. Unlike the protoypes, this collector type was equipped with a stainless steel spacer, which was glued between absorber and glazing and, thus, functions as a gas tight sealing. Beside this collector, a vented collector was used as a further reference. Table 7.2 comprises the collector specifications.

Table 7.2: Collector parameters of the reference collectors

Collector	**Ref1 (sealed)**	**Ref2 (vented)**
η_0	0.832	0.815
a_1 in $Wm^{-2}K^{-1}$	4.06	3.52
a_2 in $Wm^{-2}K^{-2}$	0.01	0.012
Aperture area in m²	2.09	1.8
Gap size in mm	20 to 25	25 to 30
Insulation material	Mineral wool	Mineral wool
Insulation thickness (back) in mm	50	50
Insulation thickness (side) in mm	10	10
Absorber type	Sheet-pipe	Sheet-pipe
Absorber piping	Double-meander	Double-harp
Material absorber sheet	Cu	Al
Material absorber piping	Cu	Cu
Gas filling	Argon	-

Figure 7.1 shows the measured efficiency comparison of three TPS-collectors and the reference collector Ref1.

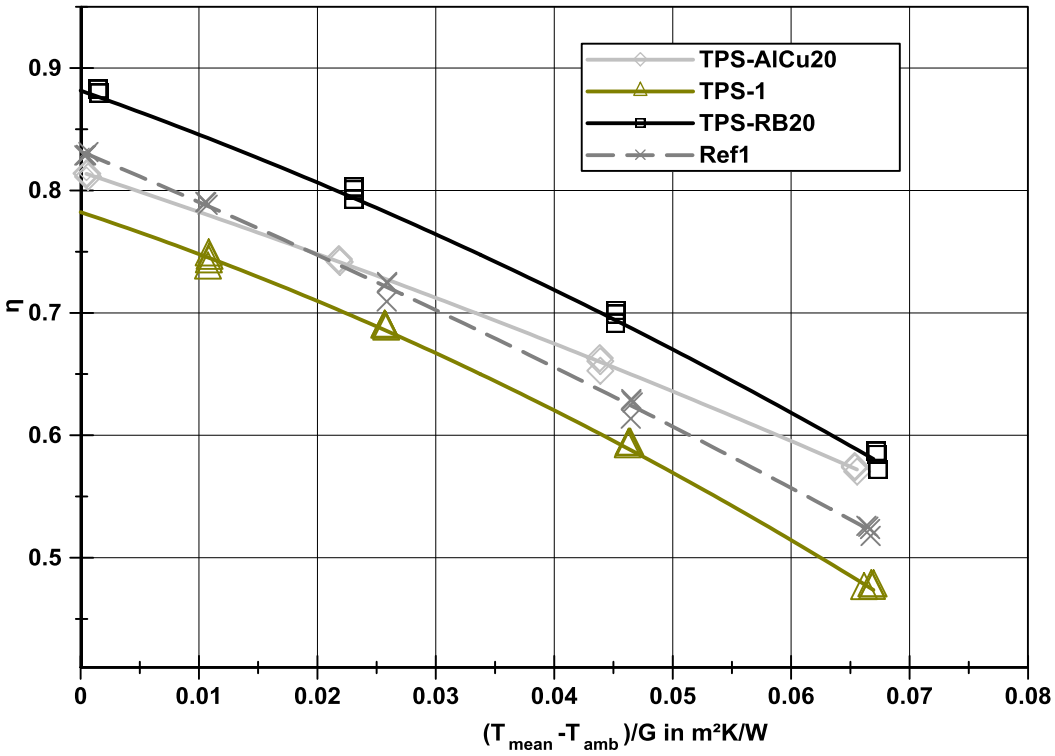

Figure 7.1: Measured collector efficiency of three different experimental collectors and a reference collector according to DIN EN 12975-2

The first experimental collector (TPS-1) showed a rather poor efficiency in this comparison. Two reasons were identified for this:

- Instead of the 10 mm adjusted gap size the mean distance between absorber and glazing was 6 mm,
- The absorber deflected towards the glazing and this effect magnified the thermal losses.

In contrast to this, the second collector set with a sheet-pipe absorber (TPS-AlCu20) was at least as good as the commercially available collector with a stainless steel spacer. The best efficiency was measured for the hermetically sealed collector with a roll bond absorber. For the typical collector operation point of 0.05 m²K/W the TPS-RB20 outperforms the reference collector by an efficiency increase of 7 %.

Figure 7.2 comprises the calculated efficiency curves of the collectors TPS-AlCu20, a simulated gas-filled collector by Vestlund et al. (2012a) and a

conventional vented flat plate collector (Ref2 (vented)). The specifications of the reference collector according to Vestlund et al. (2012a) are compiled in Table 7.3.

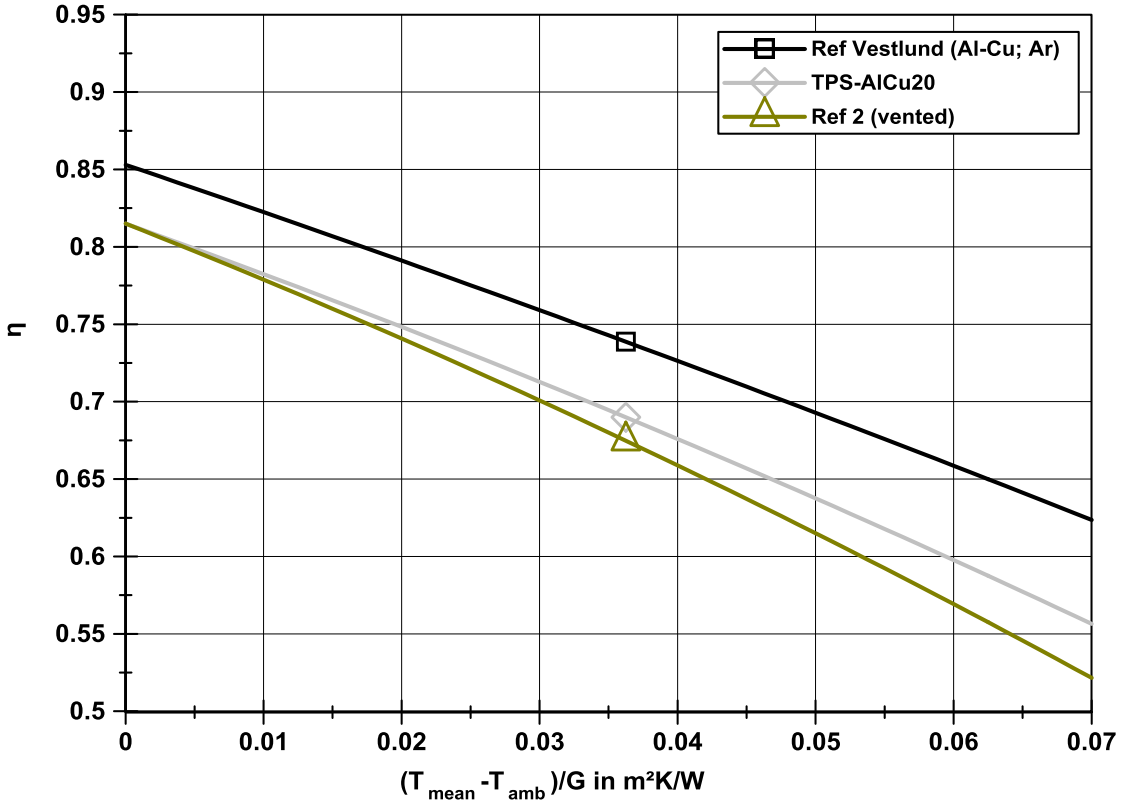

Figure 7.2: Comparison of the calculated efficiency curve of two reference collectors (based on the results of Vestlund et al. (2012a) and a commercially available vented solar collector) and the experimental collector TPS-AlCu20

Table 7.3: Overview of the collector specifications used in the efficiency comparison

Parameter	Ref Vestlund	TPS-AlCu20	Ref 2 (vented)
Zero loss efficiency η_0	0.853	0.815	0.815
Linear loss coefficient a_1 in W/m²K	3.02	3.19	3.52
Quadratic loss coefficient a_2 in W/m²K²	0.00458	0.009	0.012
Gas-filling	Ar	Ar	Vented
Gap size in mm	8.6	20	>30
Absorber material	Al	Al	
Piping material	Cu	Cu	
Absorber thickness in mm	0.5	0.5	
Fin width in mm	144	99	

The author's own measured results fall short of expectations compared to the results of Vestlund et al. (2012a). In their study, Vestlund et al. (2012a) derived the collector efficiency of a hermetically sealed, Al-Cu sheet-pipe absorber with argon and an 8.6 mm gap size by their simulation model. The collector 'Ref 2 (vented)' is a commercially available vented collector with an identical absorber as was used in the experimental collector TPS-AlCu20. The efficiency difference between Vestlund's results and the results presented in this thesis varies over the operating range between 3.8 to 6.7 % (Figure 7.3).

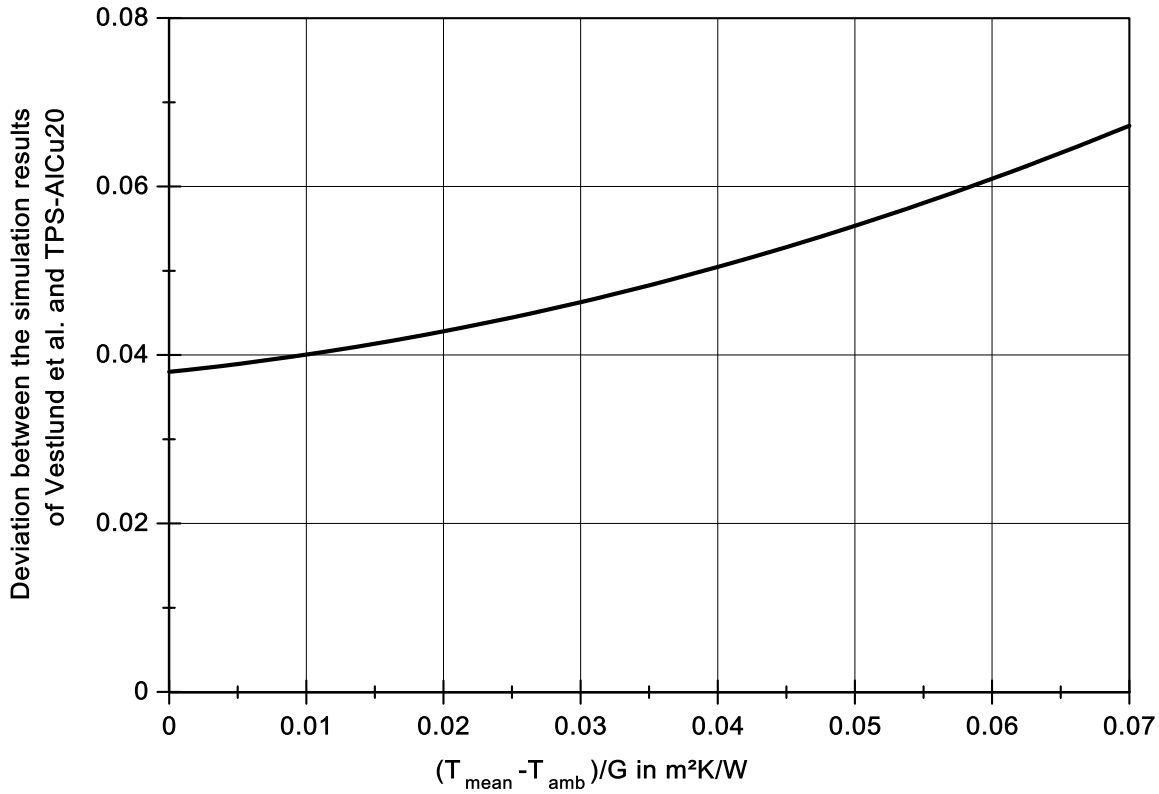

Figure 7.3: Deviation between the own results based on the collector TPS-RB20 and the simulation results of Vestlund et al. (2012a)

Vestlund et al. (2009, 2012a) used in their simulation study the convection theory based on the equation after Hollands et al. (1976), which leads to an underestimation of the convective heat loss in solar collectors. Hence, the simulation results are overestimating the efficiency of a gas-filled collector. The results in this research programme show that a gas-filled solar collector with an interspace of 8.6 mm will suffer even higher losses as a result of the mechanical absorber deflection.

7.2 Exemplary production of a prototype

The exemplary production of a prototype is described in brief to give the reader an idea of the production method and to document the proof of concept.

Figure 7.4 shows the setup of the production line with its stations.

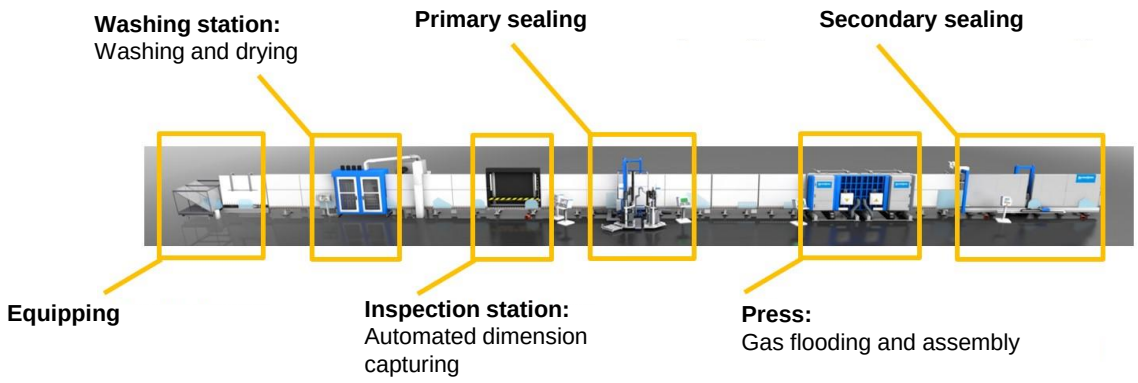

Figure 7.4: Stations of the adapted production technology (cf. Bystronic)

First, the collector glazing is put on the production line and is, subsequently, cleaned, automatically inspected and directly transferred to the press. As the absorber sheet is only between 0.3 and 0.5 mm thick, the sheet-pipe absorber was put in a jig for stabilisation (Figure 7.5).

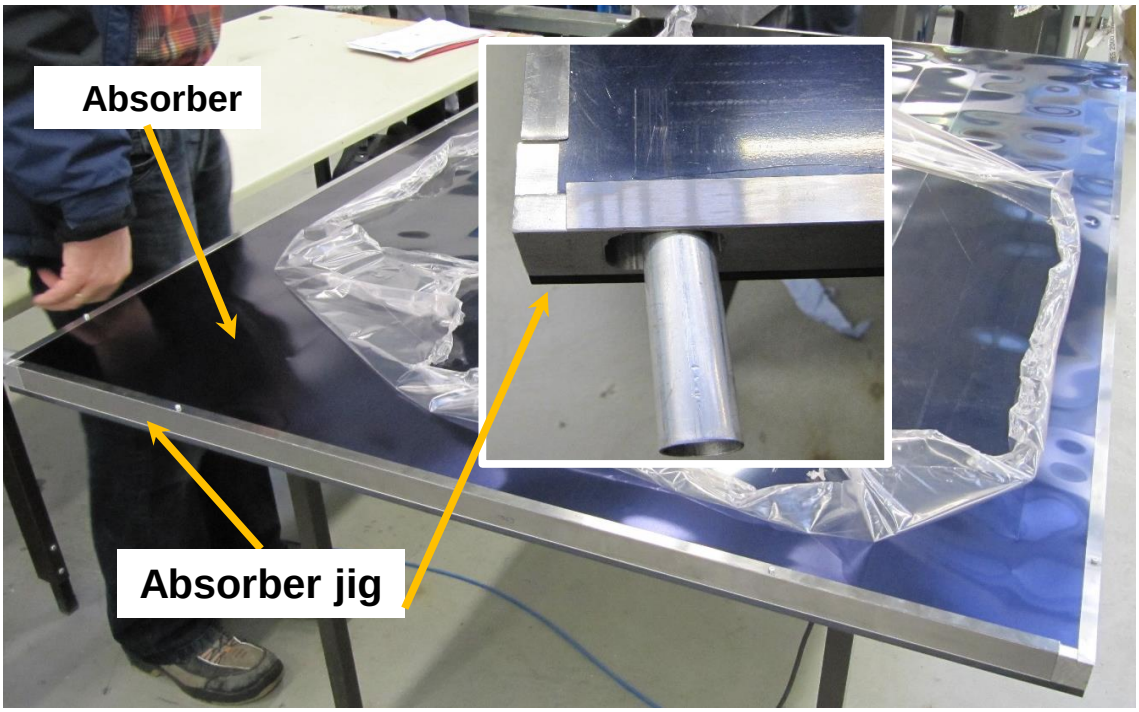

Figure 7.5: Sheet-pipe absorber fixed in a jig for better handling

A handling on the assembly line without a jig is possible but, due to the minor component rigidity, might lead to damage during the transport on the roller conveyor, the adhesive application or the pressing.

Once the absorber is vertically brought on the roller conveyor an air stream keeps the component distanced to the wall of the production line and enables a frictionless transfer to the next assembly stations. The absorber is then transferred to the first production step – the TPS applicator. A numerical controlled robot applies the thermoplastic with a nozzle along the absorber edges. This adhesive functions as a spacer between absorber and glazing and as a sealant to achieve a gastight cavity. By adjusting the adhesive application height, the gap size is set.

A crucial aspect of the application is the gastight closure between the start and end of the thermoplastic material: The robot starts the process by applying the adhesive on the absorber in a sloping upward movement. Once the nozzle reaches the programmed application height, the adhesive is applied in a laterally movement on the absorber edges. The robot registers its starting coordinates at the end of the application procedure and seals the closure at the end of this work step. Figure 7.6 clarifies this procedure.

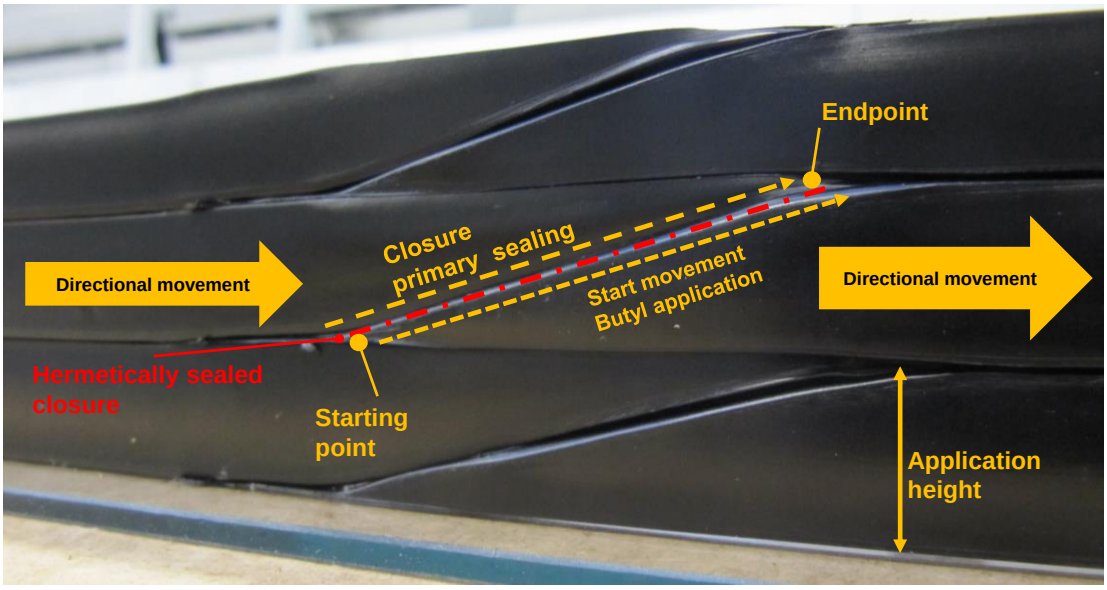

Figure 7.6: Explanation of the hermetically sealed closure

Somewhat problematic is the fact that the butyl is applied with a temperature of about 150 °C on the thin absorber sheet. Due to the high temperature difference between adhesive and absorber, the absorber sheet edges tend to buckle. However, the adhesive must be planar in contact with the absorber sheet to assure a gas tightness. A fully adhesive edge bond can compensate this deflection – unlike a hermetically sealed collector with a solid spacer, such as a stainless steel spacer. This was another reason that a solid spacer was not further taken into considerations of the proposed collector design. In Figure 7.7 a cured primary sealing was removed from the absorber to show the contour plot of the deflected absorber edge. For a better comparison, a stainless steel spacer was put on the deflected primary sealing surface to show the magnitude of the deformation.

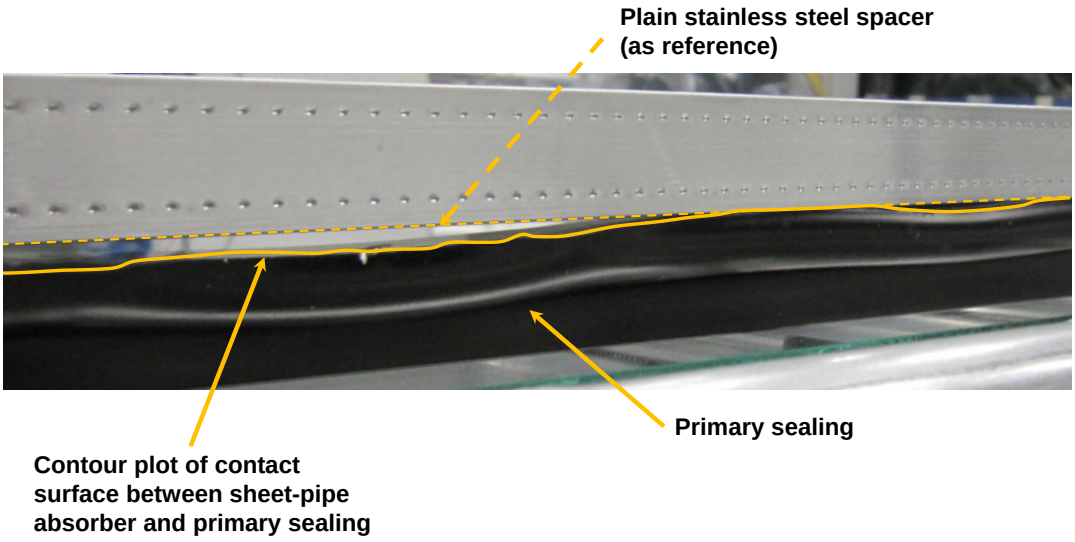

Figure 7.7: 'Negative image' of the absorber deflections due to adhesive application of a removed edge bond (plain stainless steel spacer as reference)

The next-to-last production step is the pressing in which the absorber is assembled to the glazing via the thermoplastic spacer. Simultaneously during this pressing process, the cavity between the two components is flooded with an inert gas: One side of the press primes the solar glazing, which is already positioned in the device (first step), so that the absorber can be moved in this station. The press is closed and a bendable plate in the press opens two opposing corners of the glazing by depression. A nozzle floods then the cavity until a sensor at the upper corner detects at least a 95 % filling degree. Finally, the glazing corners are put back on the adhesive and the components are pressed. Figure 7.8 shows the assembled group of the sheet-pipe absorber, primary sealing and glazing.

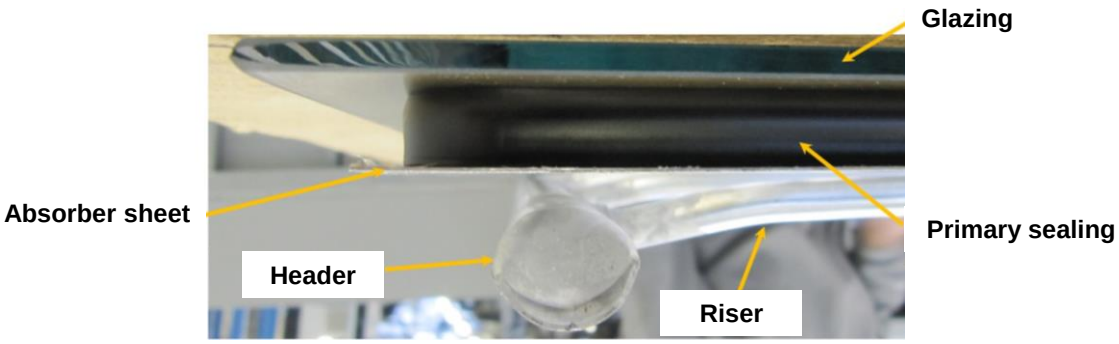

Figure 7.8: Assembly group glazing and absorber

In the last step the secondary sealing is applied. This silicone based adhesive is necessary to stabilise the sealant as the butyl itself has only a minimal mechanical stability.

For later prototypes, a roll bond absorber was used. The production process happened in an identical way as described. However, this type of absorber was favourable from a production-sided point of view as of the better handling due to a higher rigidity.

Summarising, the highly automated production technique for insulation glazing units was successfully applied for the assembly of a hermetically sealed flat-plate collector with a fully adhesive edge bond. A cycle time of 60 s can be achieved if the application of the secondary sealing is conducted automatically. In case of a solar collector with a framed collector box, it would be necessary to assemble the collector box in a separate production step. For the second batch of prototypes a polymeric trough was used.

To evaluate the new collector design in terms of durability and lifetime expectancy, several prototypes were tested. The collectors were equipped with multiple sensors, such as a differential pressure sensor, and tested on indoor and outdoor testing rigs. The main aim was to analyse the absorber deflection and its consequences on the components, the magnitude of the pressure changes in the interspace and the change of efficiency before and after the exposition tests in dry stagnation. Finally, the edge bond was analysed and in the case of the TPS-RB 20 the gas concentration was documented.

7.3 Experimental collectors with sheet-pipe absorber

In the first production series, two different prototypes (TPS-1 and TPS-2) were produced without a conventional casing. One of the collectors was equipped with an insulated back plate (Figure 7.9) whereas the other absorber, basically, was put in between two glass panes and insulated with mineral wool (Figure 7.10).

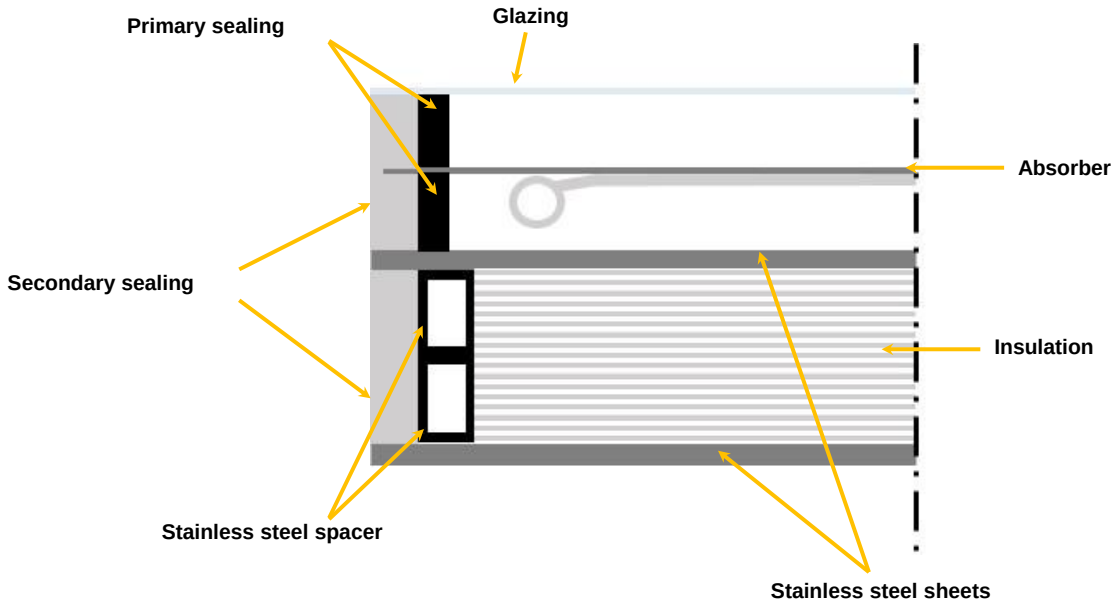

Figure 7.9: Schematic cross section of the experimental collector TPS-1

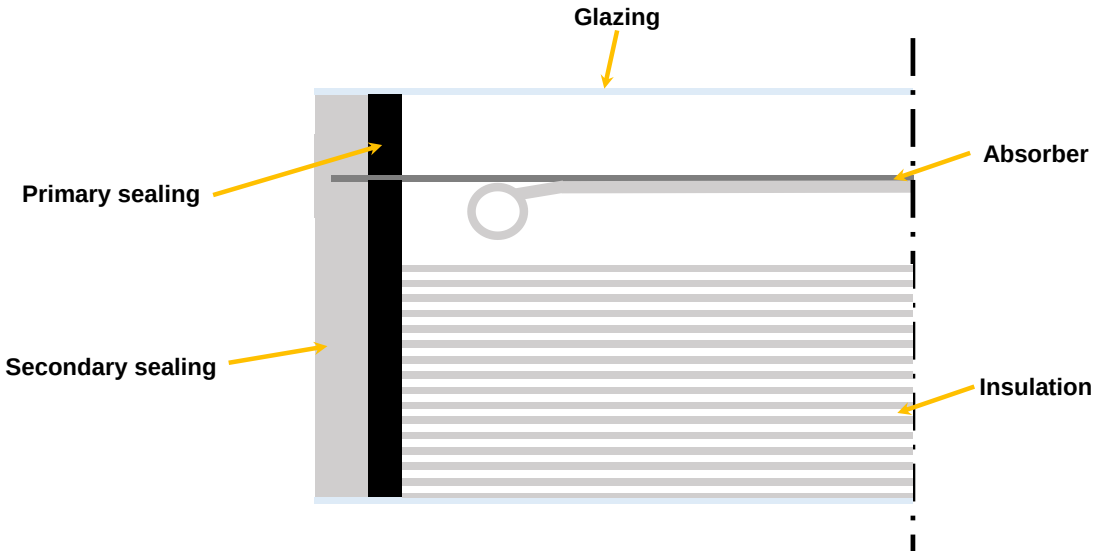

Figure 7.10: Schematic cross section of the experimental collector TPS-2

The approach of the insulated back plate came along with advantages in the production but showed unsatisfying aspects during the collector operation. Lacking a rigid body, the experimental collector suffered from a high deflection on the collector's long side. However, this can be overcome by a further design optimisation. More adverse is the high amount of adhesive used for this approach that, ultimately, prevents a further utilisation due to the high material costs of the primary sealing. Both aspects are applying as well for the full-glazed collector. The economic evaluation is discussed in detail in chapter 9.

7.3.1 Results of the experimental collector TPS-1 and TPS-2

Very little research has been published on the thermal and mechanical behaviour of collectors with small gap sizes. As in this research program collectors with gap sizes of only 10 mm were produced, it was logical to investigate the collector more in detail to derive a basis for further scientific activities or developments. An essential part of the analysis was the observation of the absorber deflection in different operation points. Those results were partly used for the mechanical model validation and can be further used for design optimisation of the absorber. Figure 7.11 shows the initial absorber shape of a hermetically sealed collector with a full aluminium harp absorber (TPS-2).

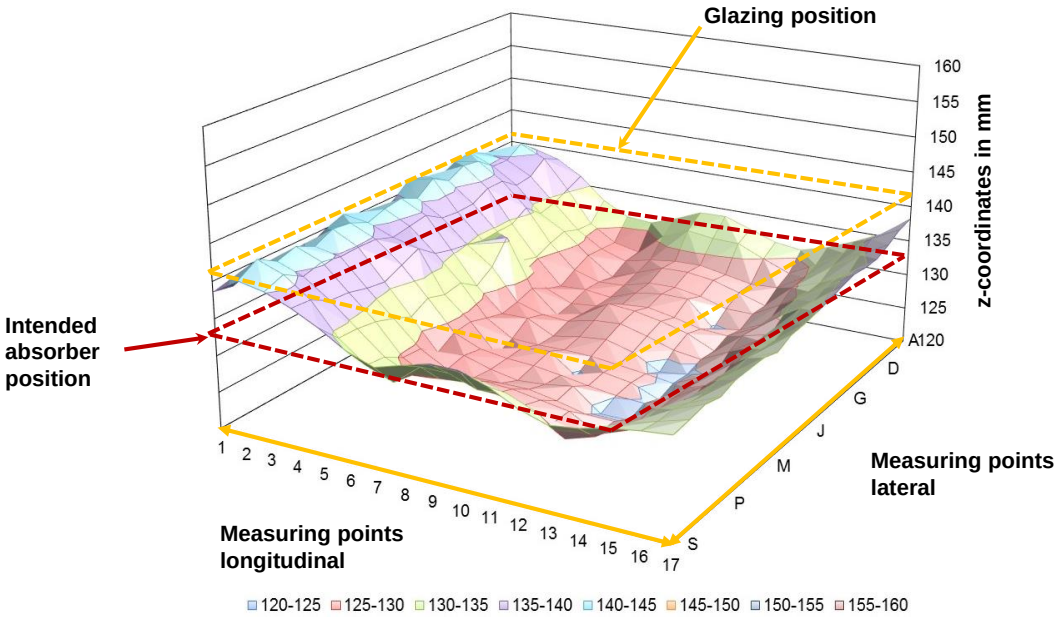

Figure 7.11: Measured absorber shape of a full aluminium harp absorber at ambient conditions

The deviation from the intended position (red dashed line) is up to ±9 mm. At a first glance, this seems rather small but compared to a gap size of just 10 mm it is a deviation of 90 %. In the area of the measuring points 2 to 4 (longitudinal), the gap size was less than 1 mm (cyan inked area in Figure 7.11). As this measurement was conducted subsequently to the collector production, a possible reason to this deviation is the absorber production itself, e.g. the welding processes. The support and the handling of the absorber during its production contributes as well to the absorber shape. In this view, an analysis of the absorber production process is of interest but was not conducted within this research program. In particular, the simulation of the welding process in a finite element model reveal indication of possible welding induced material pre-stresses. It is likely that such material stresses are affecting the absorber shape. The assembly on the IGU production line has probably no or just a minor effect as the absorber gets fixed in a jig, which avoids mechanical deflections. Yet, thermal induced buckling was observed during the application of the primary sealing along the absorber edges. As the material is applied with about 150 to 160 °C, the thin absorber sheet experiences a temperature gradient of at least 120 °C. In this context, it is plausible to design the absorber jig to allow a compensation of the thermal elongation.

Beside the reduced collector efficiency due to the shortened interspace, these areas are critical for the lifetime expectancy of the glazing and the absorber. The collector was in dry stagnation exposed to a solar energy of about 2,900 MJ between June and January. During this period, the collector was visually inspected at least once a week to document incidents. At the end of the exposure (last third), damage on the absorber coating was visible (Figure 7.12).

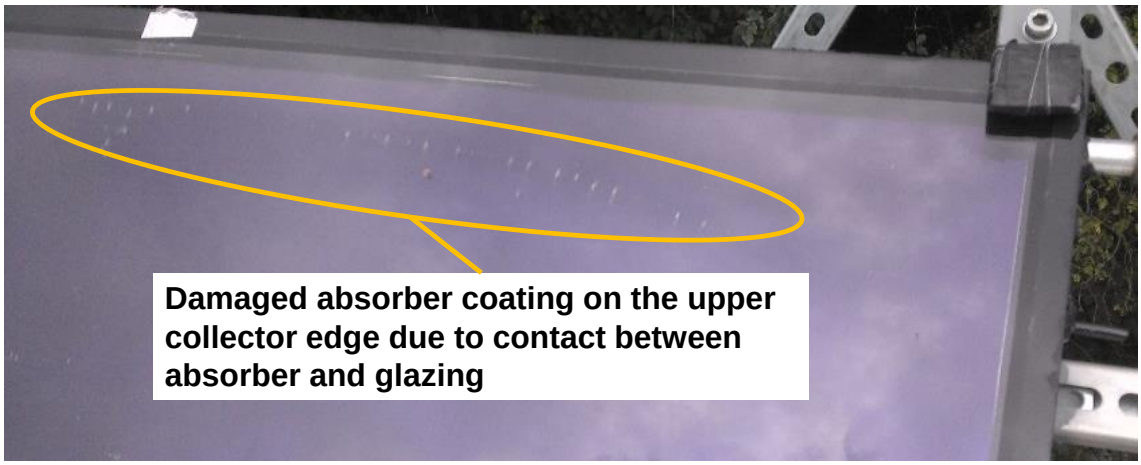

Figure 7.12: Absorber deflection exceeded gap size and resulted in a damaged absorber coating in the upper end of the collector

The damage pattern was only observed for collectors equipped with a sheet-pipe absorber. Even though this happened during abnormally extended periods of dry stagnation, it cannot be excluded that similar damage would occur in a normal operating solar system during stagnation. Furthermore, under certain conditions, it is possible that the glazing could be damaged or even destroyed: On a clear day with low ambient temperature and high solar insolation, the absorber heats up, deflects towards the glazing and, eventually, touches it. Caused by the high thermal gradient between absorber and glazing, thermal stress is imprinted on the glazing, which can lead to a shattering of the glazing.

In the end of September, separations between primary sealing and absorber as well as blistering were detected (Figure 7.13).

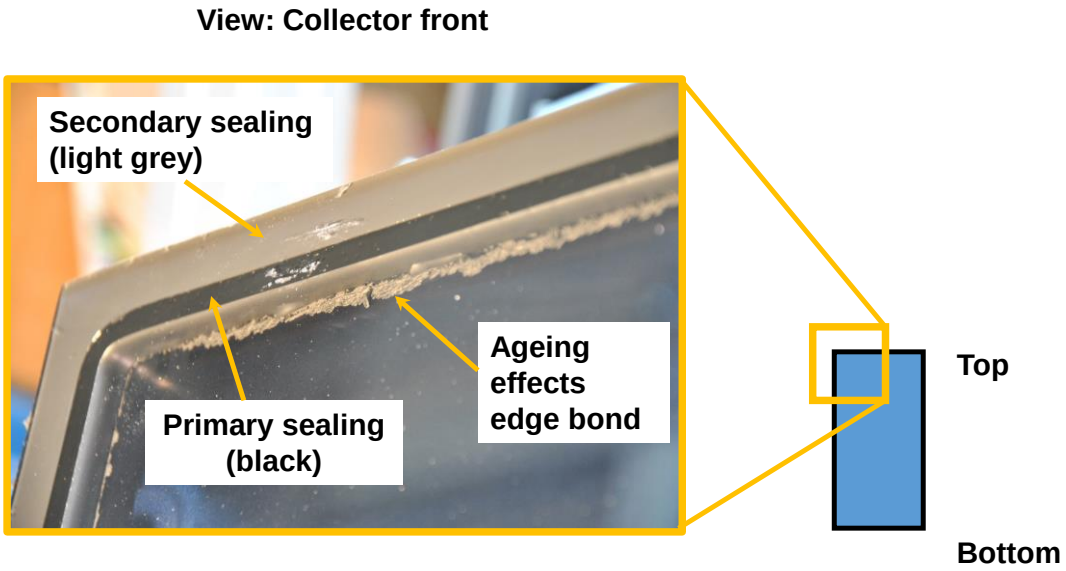

Figure 7.13: Separations of the edge bond due to absorber movement after exposure test on the upper collector side (TPS-1)

It is more than unfortunate that it was not possible to determine the gas concentration during this exposition test. It is likely that at this time – at the latest – the edge bond had no more sealing properties and the argon filling had vanished. This assumption is strengthened by the post exposure efficiency tests of this collector (Figure 7.14). However, no fogging effects on the glazing occurred for the prototypes with sheet-pipe absorbers and the absorber deflections stayed reversible.

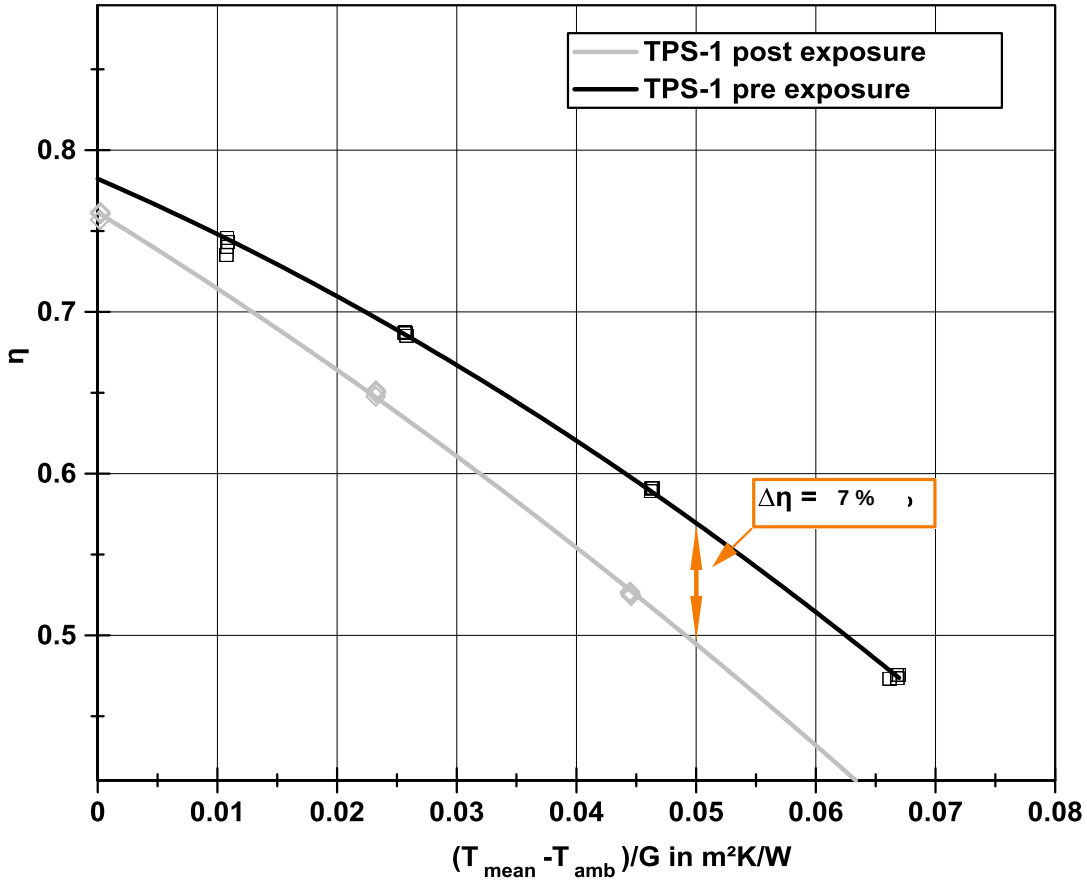

Figure 7.14: Measured collector efficiency before and after the exposure in dry stagnation of the collector TPS-1

An efficiency loss at 0.05 m²K/W between pre and post exposure of 7 % (absolute) was measured. This is caused by the superposition of the optical degradation and both thermal and mechanical material degradation of the absorber and edge bond. The latter two led to a leakage in the primary sealing and, thus, to an increased convective heat transfer from the absorber to the glazing as the argon dissipated. To ensure that there was no argon left in the interspace two holes on the opposing collector corners were drilled through the edge bond and another efficiency test was conducted after a 48 h idle time. The test showed the same result as the efficiency test right after the exposure. This leads to the conclusion that there was certainly no argon left at the end of the exposition test. However, the exact moment of the edge bond leakage remains in this case unknown.

The prototype TPS-2 was only tested under the solar simulator and used for indoor absorber deflection measurements. As different pressures were manually

applied in the interspace, the sealed edge bond was opened and the argon filling was replaced by air. To analyse the effect of the gas filling in the cavity, the collector's efficiency was tested with and without the inert gas filling on the institute's solar simulator. Figure 7.15 shows the comparison of the measured efficiency between the argon filled and the vented collector version with an initially adjusted gap size of 10 mm.

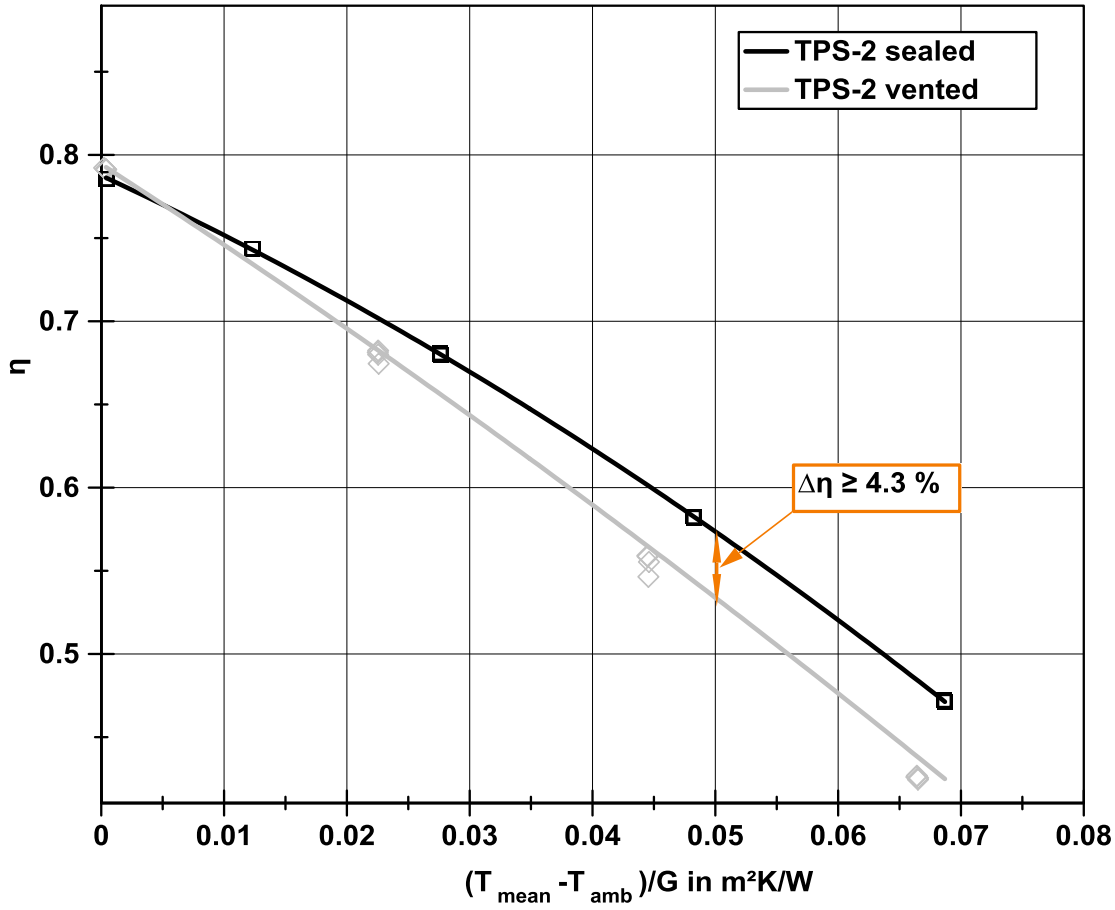

Figure 7.15: Collector efficiency comparison of TPS-2 between a hermetically sealed interspace (argon filled) and a vented interspace according to DIN EN 12975-2

For T_{mean} - T_{amb} of 0.05 K/m²W an absolute efficiency reduction of 4.3 % was measured. The efficiency difference in thermal simulations of a gas-filled and an identical non-gas-filled collector ranged as well in this region (ca. 4 to 5 %).

7.3.2 Summary sheet-pipe absorber

The drawbacks of a conventional sheet-pipe absorber in a hermetically sealed flat plate collector are considerable for collectors with small interspaces. The difficulties are caused by the absorber deflection leading to damages on the absorber and glazing. Beyond that, the absorber deflection, in particular, towards the glazing leads to an efficiency loss. The lower convective heat transfer of the inert gas cannot compensate the latter. However, since tests were carried out over a relatively short duration, this does not mean that the absorber might not suffer fatigue during its design life.

Critical was the ageing of the edge bond – especially of the primary sealing. Once the separations between primary sealing and absorber occurred, it can be concluded that, at this point, the inert gas volatilised. The two experimental collectors TPS-1 and TPS-2 were the first collectors with a fully adhesive edge bond produced. Albeit the used IGU sealing was already modified for higher temperatures (T_{design} = 120 °C), it was back then not exhausted to its full potential. In the later prototypes, a further optimised adhesive was applied and, subsequently to the tests, analysed in a material science laboratory (chapter 7.4). Those collectors were equipped with additional sensors in the edge bond to document the temperature loads. There were in total nine temperature sensors (sensor type: PT100) placed on the absorber of the collector TPS-1. During the early phase of the exposure, the sensors gradually broke down and leaving too few data for a valid evaluation. As the complete collector was sealed, it was not possible to exchange the sensors. Consequently, a permanent temperature load log was not possible.

To overcome the problems of the absorber deflection an absorber design that deflects in a predictable way needs to be analysed. This would allow smaller gap sizes in such collector types, higher efficiency during operation and less degradation. This aspect is brought attention to in chapter 8.

7.4 Experimental collectors with roll bond absorber

The two collector models TPS-RB15 and TPS-RB20 were equipped with multiple temperature sensors on the absorber, glazing and the edge bond. This time thermocouples (type T) for high temperature applications (more than 250 °C) were used to avoid sensor failures. The experimental setup TPS-RB20 was tested according to the standard DIN EN 12975-2 on its efficiency before and after the exposure in dry stagnation. The other collector model, TPS-RB15, passed several efficiency tests before and after the exposure in dry stagnation. After a first efficiency test under the solar simulator, a differential pressure transmitter was installed to measure the interspace pressure change during the exposure. Through a hole in the edge bond, the measuring device was connected to the cavity between absorber and glazing. Subsequently, the area around the pressure tube was sealed again. Figure 7.16 and Figure 7.17 show the temperature sensor position of the both prototypes.

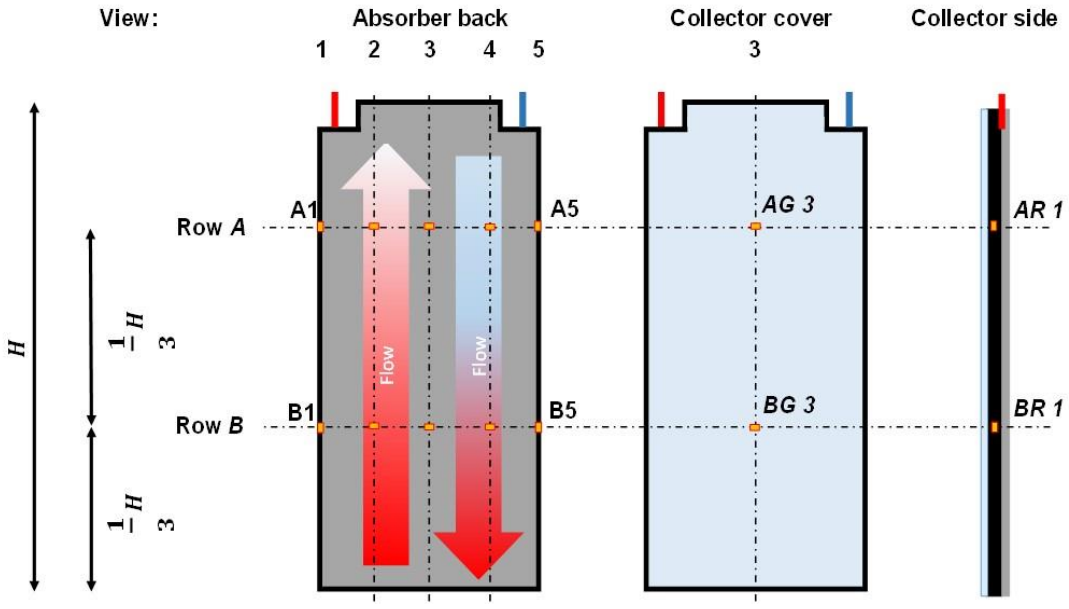

Figure 7.16: Sensor positions on the experimental collector TPS-RB15

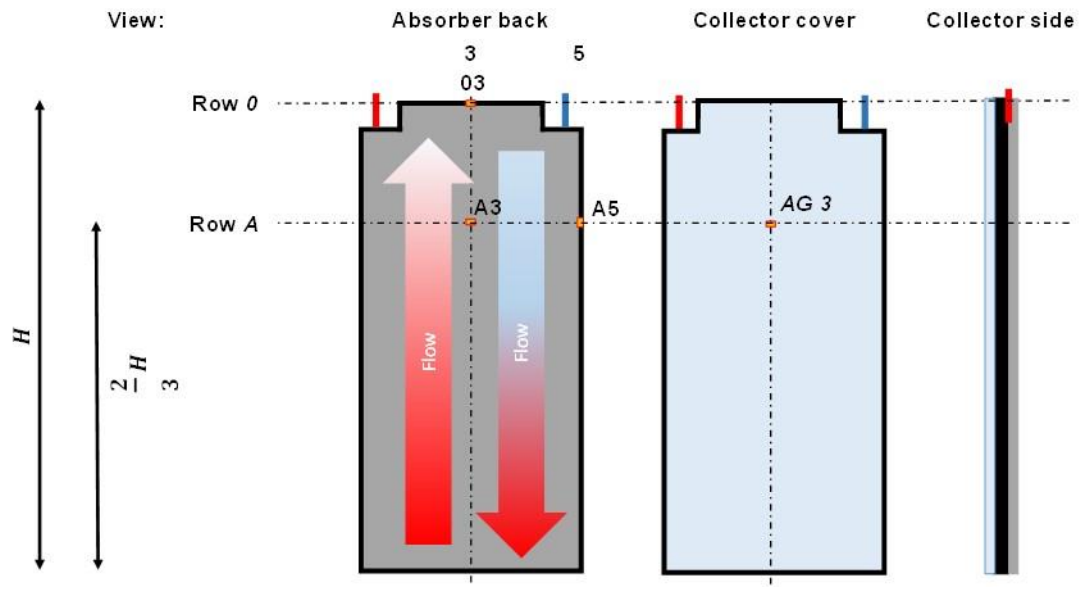

Figure 7.17: Sensor positions on the experimental collector TPS-RB20

The edge bond temperatures were logged by applying two sensors on the absorber bottom side underneath the area of the adhesive application. Beyond that, two further sensors were embedded directly in the primary sealing of the collector.

Four position sensors were used on the absorber back side to track the magnitude of the absorber deflection during the stagnation. These sensors were used to conclude whether the sheet deformation is irreversible or reversible and to get information on the deflection range and frequency. The sensors were installed in equidistant distances on the longitudinal axis of the absorber. As the assembly group ‘absorber-glazing’ was put in a polymeric trough, the sensors had to be mounted on the outside of the collector box. During the exposure, one of the position sensors broke down due to spray water.

7.4.1 Results of the experimental collector TPS-RB15

Figure 7.18 comprises the temperature load occurrences during a seven-week exposure for the sensors in the edge bond. As the lower temperatures are not causing significant material ageing, the graph’s time scale was set to a maximum of 80 h to allow a closer look on the higher temperatures. The red bar indicates that temperature idle times above 80 h occurred.

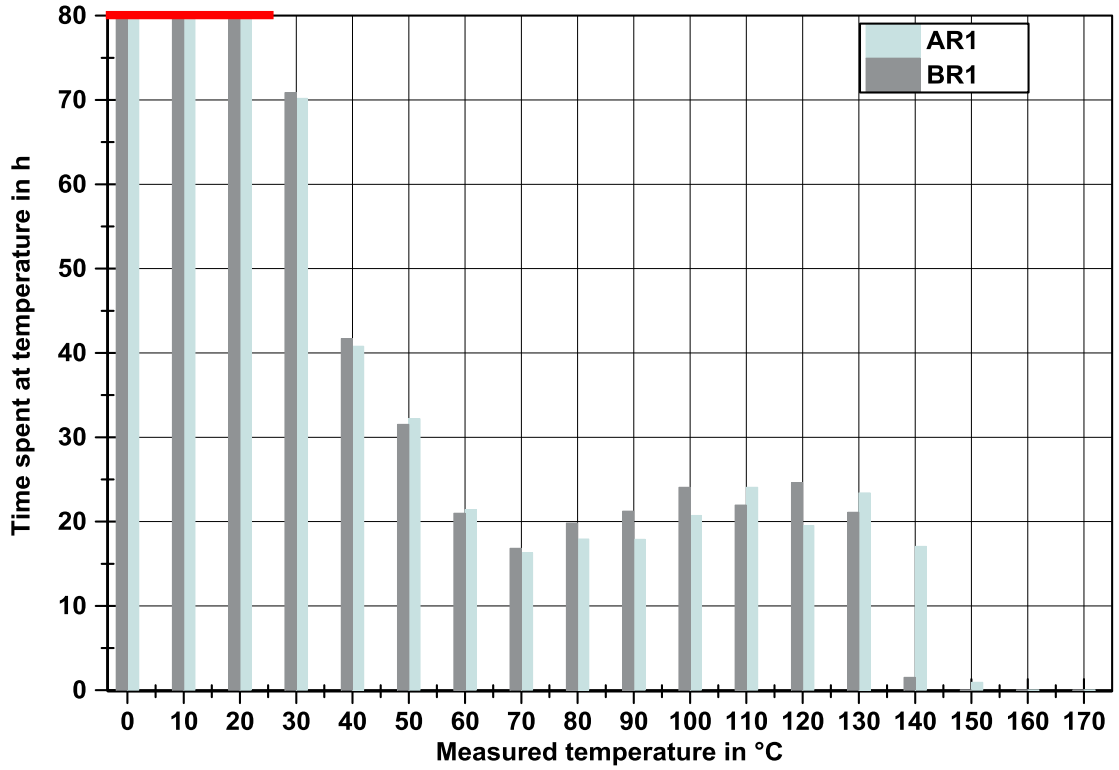

Figure 7.18: Temperatures loads of the edge bond during dry stagnation (TPS-RB15)

The graph shows the temperature gradient of the absorber alongside axis. The sensor AR1 logged 140 °C for a period of about 20 minutes whereas BR1 was only two minutes exposed to this temperature. The occurred maximum temperatures in the edge bond are still in the range of the short-term design temperature area. However, for regions with a higher solar insolation or higher ambient temperatures than Germany the temperatures will reach a critical value causing an accelerated material ageing.

Figure 7.19 shows the comparison of the measured temperatures at A1 and AR1.

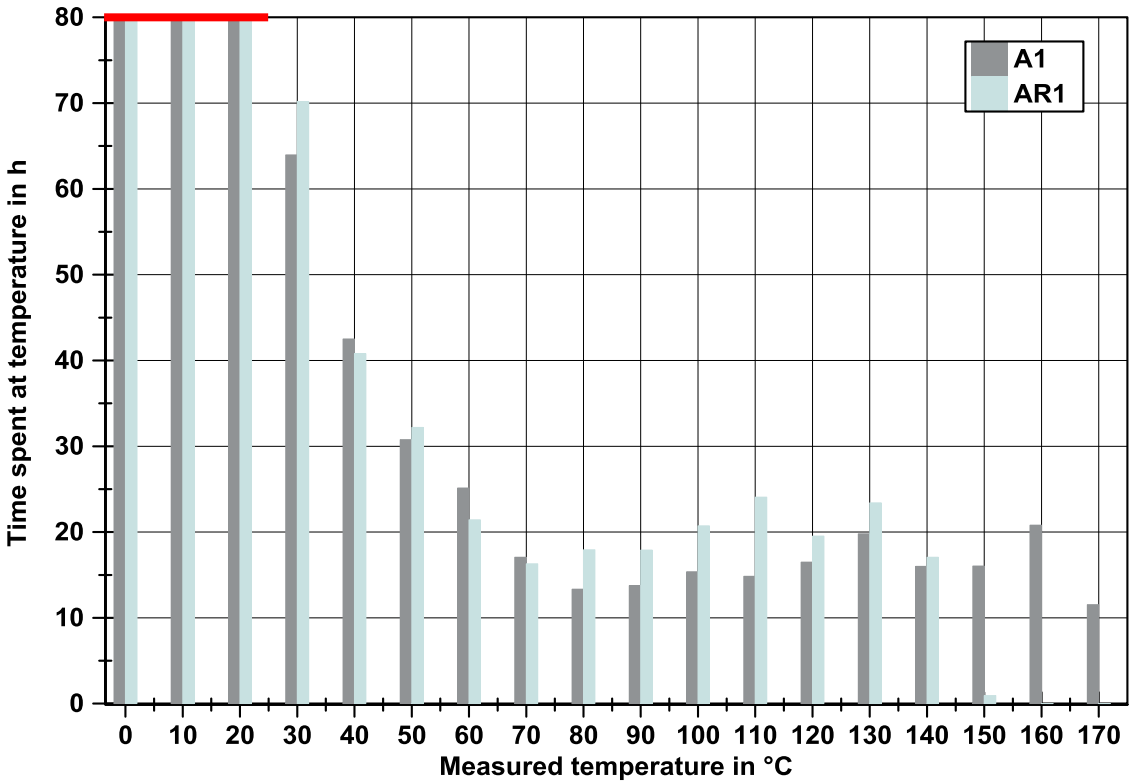

Figure 7.19: Measured temperature loads in the edge bond and underneath the contact surface (absorber bottom side) between absorber and edge bond

Compared to the other sensors A1 and B1 on the absorber bottom side underneath the edge bond, the temperatures are higher, i.e. a maximum temperature of 170 °C (A1) occurred. The sensors AR1 and BR1 were applied in the middle of the edge bond height about 7 mm above the absorber surface. This, in turn, indicates a good insulation behaviour of the thermoplastic spacer.

Nevertheless, the high temperatures were logged on the contact surface between absorber and edge bond and, thus, the edge bond experienced at least in the lower layer critical temperatures. To what extent the material ageing is accelerated needs to be investigated in a close cooperation with the material supplier. In any case, it is recommendable to analyse constructive counter-measures to lower the maximum temperature in the edge and alongside the contact surface between absorber and adhesive. Stagnation is not only a problem if the collector is already installed in a space heating system but also while installing large collector fields, e.g. in district heating networks.

The pressure change in the cavity during extreme collector operations (e.g. stagnation) for the further development were of interest. Figure 7.20 shows the measured pressure values and occurrences in hours during the stagnation.

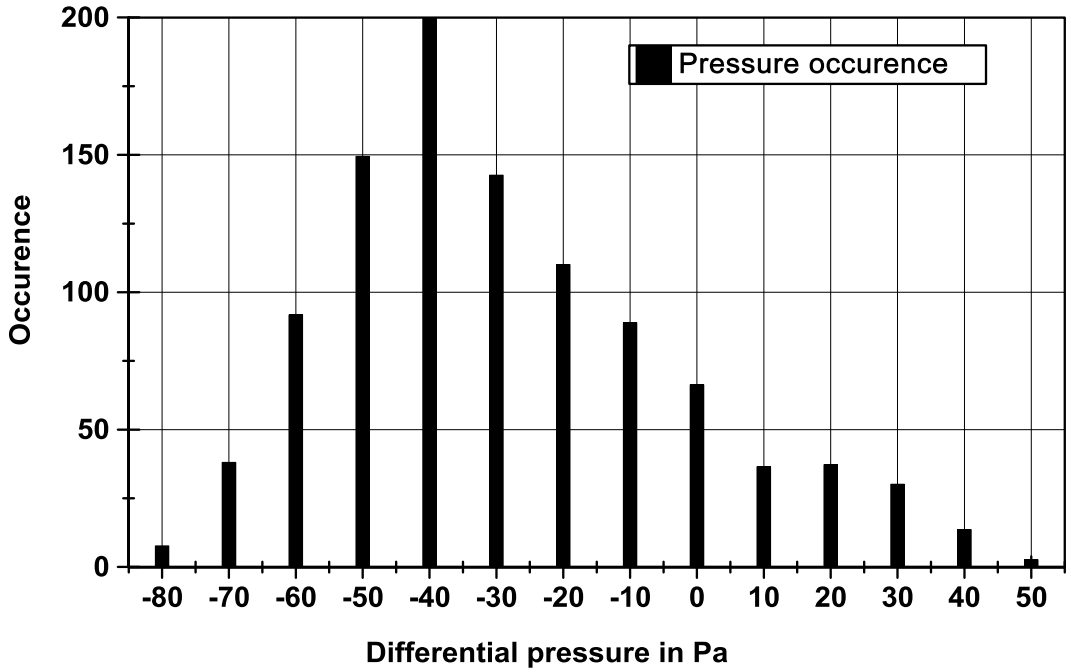

Figure 7.20: Measured pressure and occurrences in the cavity during exposure in dry stagnation

The pressure difference of 0 Pa represents the initial state, i.e. the ambient conditions in the laboratory as the pressure sensor was installed. Even though an overpressure of 50 Pa was detected in the cavity, a depression of 40 Pa (200 h) prevailed. This pressure corresponds to a force on the glazing and absorber of about 80 N.

A total pressure range of 170 Pa was logged whereas the extreme values ranged from -100 Pa to +70 Pa. Within this range, neither the glazing, the absorber nor the edge bond showed damages or fatigue due the pressure variation. This was also observed during the laboratory tests for the validation of the FE model as different pressures were induced in the cavity manually.

During the exposition, the behaviour between absorber temperature, differential pressure and absorber deflection was analysed (Figure 7.21).

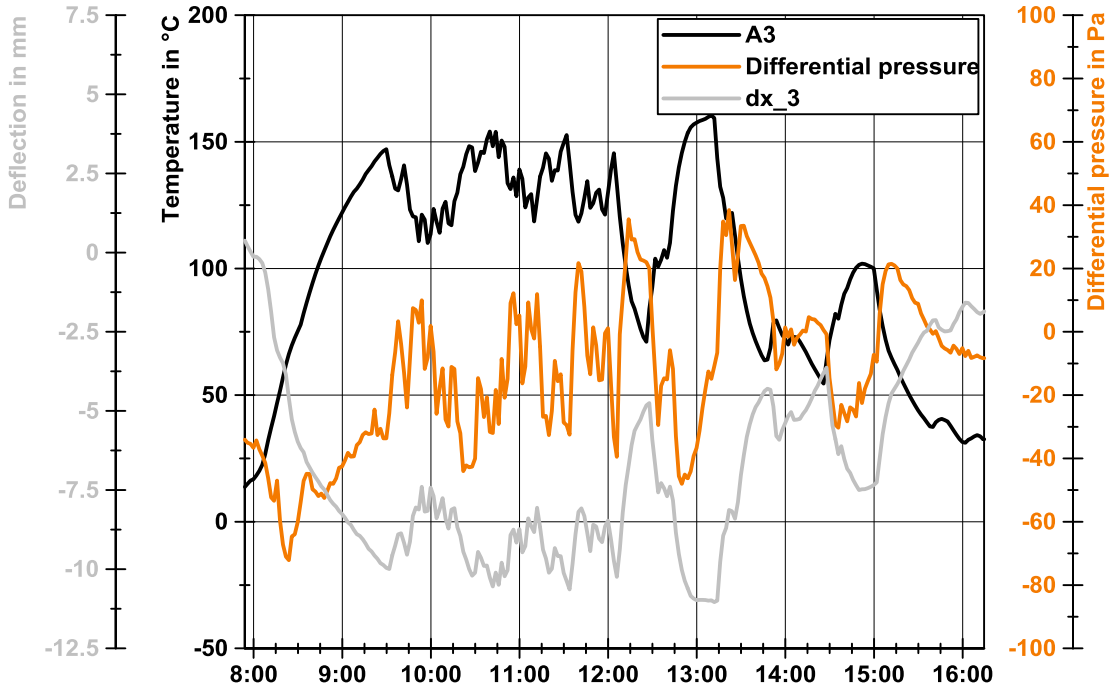

Figure 7.21: Typical coherences in a hermetically sealed flat plate collector between absorber temperature, differential pressure and deflection (positive values indicate a deflection into the direction of the glazing)

As soon as the absorber temperature (A3) rises, the pressure (orange line) in the cavity decreases (from 8:00 to 8:30 am). This is owed to the thermal elongation of the absorber that heats up once the irradiation increases. At the same time, the absorber deflects towards the back of the collector casing. The absorber deflects towards the glazing (between 9:30 and 10:00 am) as the absorber cools down and, thus, the pressure rises. An opposed behaviour between absorber temperature and pressure as well as absorber deflection can be observed: the higher the absorber temperature the higher the absorber deflection and the lower the pressure gets. Once the absorber temperature cools down due to shading or cloudy weather, e.g. at 12:00 pm, 1:15 pm or 3:00 pm, the behaviour of the absorber temperature and deflection is just opposed whereas the differential pressure follows with some delay.

During the complete stagnation procedure, a total deflection range of 20.3 mm with the extreme values between -14.5 to +5.8 mm was logged. The most frequent deflection of the roll bond absorber during the exposure was close to the intended gap size – between 1 to 5 mm towards the glazing (Figure 7.22).

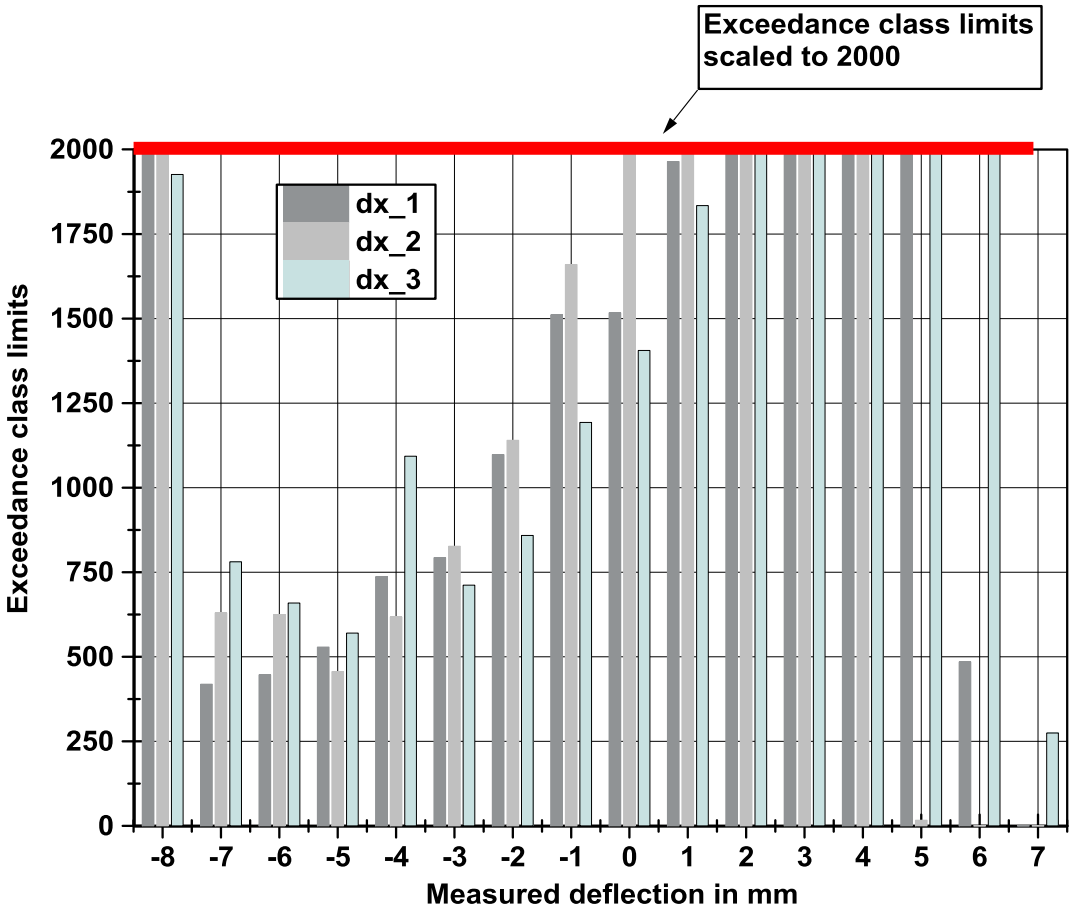

Figure 7.22: Measured deflection distribution throughout the exposure

In few cases, the absorber area around dx_3 came as close as 8 mm to the glazing. However, the sensors dx_1 and dx_2 shortened the 15 mm gap by 6 mm and 4 mm. Neither a contact between absorber and glazing nor an irreversible absorber deflection was ascertainable in an experimental collector with a roll bond absorber. The fact that the most frequent deflection was towards the glazing was caused by the weather condition. In particular, the cold temperature and low irradiation between February and March led to this behaviour (Figure 7.23).

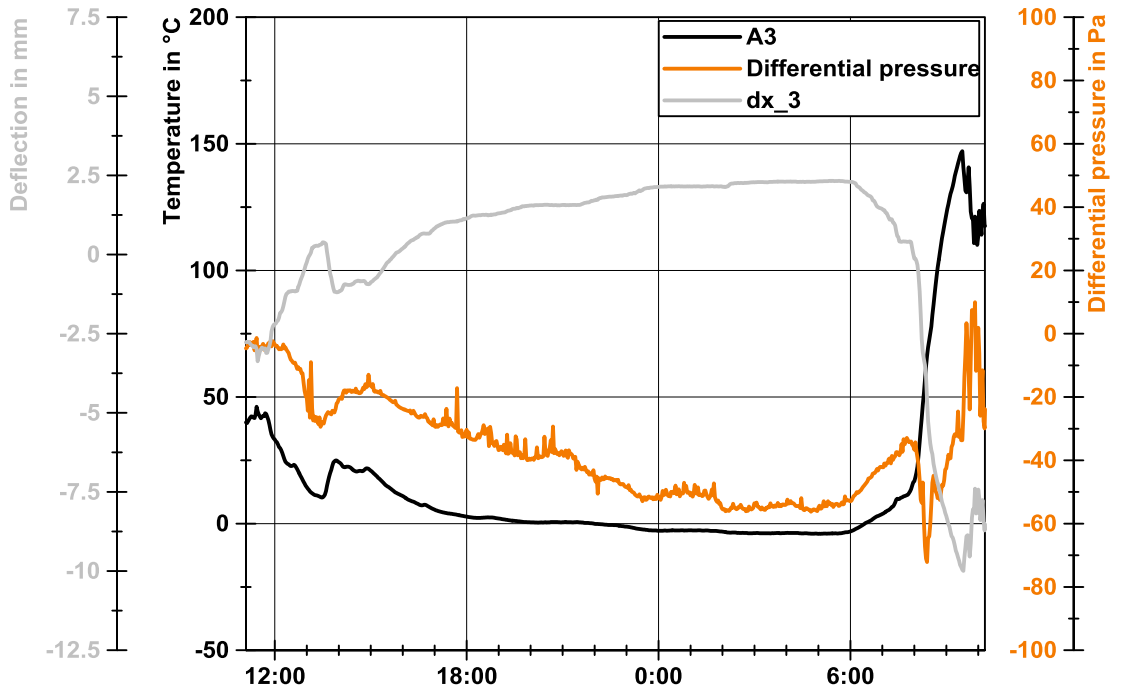

Figure 7.23: During cold nights the absorber deflects towards the glazing due to gas and metal sheet contraction

The graph shows a typical weather condition in February with ambient temperatures close to 0 °C. As there was no irradiation at this time, the absorber temperature is close to the ambient temperature. Hence, the absorber experiences no thermal elongation. The gas volume in the cavity cools down and contracts. Driven by the gas depression the absorber deflects towards the glazing. However, future collector designs need to consider both effects for the choice of a suitable gap size – the gas depression, e.g. during cold nights, and the thermal elongation during collector operation.

According to the material producer, the primary sealing is sensitive to low pressure; however, this is only a factor if the depression exceeds 200 Pa for longer periods.

The question arises which other parameters are affecting the pressure in the interspace of a hermetically sealed collector. These aspects are well analysed for insulated glazing units, e.g. by Feldmeier (2012). According to Feldmeier (2012), suboptimal parameters in IGUs that are magnifying the mechanical loads induced by pressure variations are:

- a wide interspace between the glass panes
- thick glass panes
- an asymmetric setup of the glass panes interspace
- small edge lengths (< 600 mm)
- small glazing dimensions
- increase of altitude above sea level

In this view, it would be of interest whether the stated parameters are appropriate for a collector with a similar edge bond and an inert gas filling in the interspace and, if so, to what extent. Usually, the glass pane thickness in solar collector does not exceed 4 mm whereas 6 mm thick glass panes are common in an IGU. Insofar, this criterion is of small interest in the design of a hermetically sealed solar collector with an adhesive edge bond. An asymmetric setup of the interspaces can be excluded as well if it is a typical flat plate collector. However, there are other approaches for solar collectors analysed whereby the frame is completely substituted by a transparent cover in the front, an adhesive edge bond and a transparent cover on the collector back, similar to the TPS-2 or Leibbrandt and Schabbach (2014). For those applications, an asymmetric setting of the glass panes and, thus, the induced mechanical loads are becoming a more dominant role. The edge lengths and the smaller sizes are again of a minor importance for solar collectors. Prevailing is a gross collector area of about 2 to 2.5 m² with a typical shortest edge length of more than 1000 mm. The gap size in solar collectors are larger than in a triple insulated glazing (12 mm) unit and in a similar range of double glazing units (24 mm). However, it is doubtful that this insight is one-to-one applicable for solar collectors as the absorber 2nd moment of area is smaller than that of a 3.2 or 4 mm strengthened glass pane. In fact, laboratory results show that the glazing deflection during collector operation was in the linear range, i.e. less than the glass thickness. Beyond that, the thermal expansion of the absorber leads to an additional expansion volume and, thus, the pressure is reduced. These aspects show that the pressure variation in solar collectors with an adhesive edge bond is less critical than for

insulated glazing units. Ultimately, no critical pressure was detected within in this research programme. It is plausible to extend the tests for a different variation of collector sizes, e.g. very small sizes to large-area collectors of up to 15 m² gross area. Unfortunate is the fact, that such an analysis will be costly as for each analysis several experimental collectors need to be produced. Even more important in this matter is the use of finite element simulation model to keep the quantity of tests on a rational level.

7.4.2 Results of the experimental collector TPS-RB20

The second prototype, TPS-RB20, ran through an efficiency test, a stagnation test and an exposure in dry stagnation with a subsequent internal shock test. All tests were performed according the valid standard DIN EN 12975-2. As a leakage in the edge bond after the internal shock test was detected, the test procedure was stopped and another efficiency test was conducted. Table 7.4 comprises the determined stagnation temperature of the collector TPS-RB20.

Table 7.4: Measured and extrapolated collector temperatures according to DIN EN 12975-2

Sensor	**A3**	**A5**	**O3**	**AG 3**
Measured value **I = 932 W/m²; T_{amb} = 30 °C**	203 °C	190 °C	182 °C	78 °C
Extrapolated climate class A **(I = 1000 W/m²; T_{amb} = 30 °C)**	212 °C	199 °C	191 °C	81 °C
Extrapolated climate class B (sunny) **I = 1100 W/m²; T_{amb} = 40 °C)**	236 °C	222 °C	213 °C	95 °C

The sensors showed a maximum absorber stagnation temperature of 203 °C whereas the sensors A5 and O3, which were applied on the absorber bottom side in the area of the primary sealing, measured up to 190 °C. Even though the temperature sensor was not applied in the edge bond, it is certain that the short-term design temperature of the primary sealing was exceeded. As this modified

sealing material is still in testing up to now, no ensured experience on its durability is available. Neither is a maximum time span for the short-term design temperature known. If the short-term design temperature is permanently exceeded the material ageing is accelerated. This means that the butyl adhesive will lose its properties, such as the adhesion to the absorber or the gas tightness. In contrast to the experimental collectors with a sheet-pipe absorber, an optical deficiency occurred which was a side effect of the edge bond leakage. Figure 7.24 shows a large-area deposition on the inner side of the glazing after the internal thermal shock test.

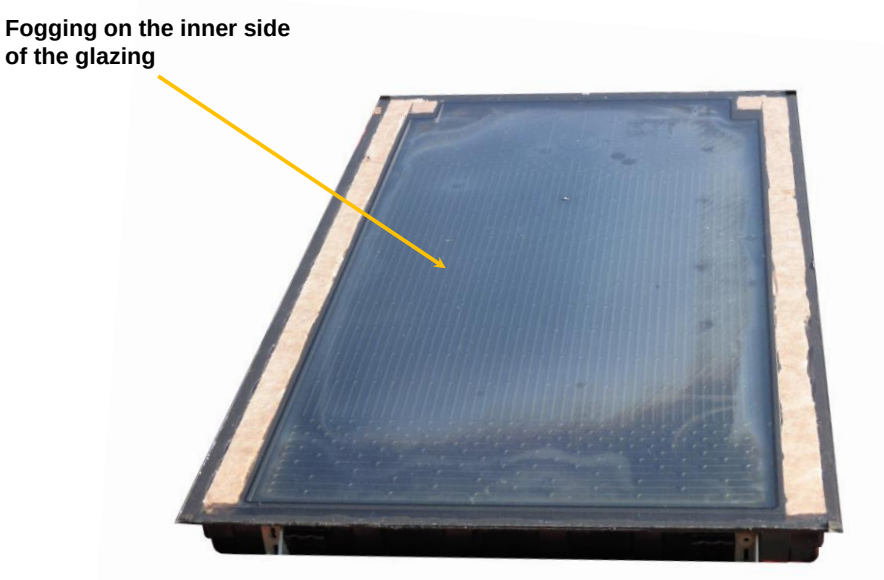

Figure 7.24: Fogging on large-areas of the inner glazing side after the internal thermal shock test

A visual inspection showed a clear fog on the inner side of the glazing. In some spots outside of the sealed cavity, a greasy film on the inner side of the glazing was detected. There are three possible reason to the fogging:

- a chemical reaction between adhesive and absorber or absorber coating,
- degassing of the adhesive – either primary or secondary sealing,
- degassing of the insulation material (under the assumption of a leaking edge bond).

The collector was shipped to the material producer to analyse the cause of the fogging in their chemical laboratory. According to the material analysis report (Koemmerling 2014), the cause of the fogging on the inner side of the glazing is either a contamination (ester resin) that deposited a temperature induced film on

the glazing or by diffusion of chemical vapours from the secondary sealing through the edge bond leakage. The latter reason seems, according to the material experts, more likely. This film, however, has no negative effects on the efficiency nor on the collector lifetime but can be seen as an aesthetic flaw.

Subsequently to the chemical analysis, the adhesion between the edge bond and the absorber was analysed by a peel-off test. The test was conducted for the adhesion between edge bond and glazing, edge bond and absorber as well as between primary and secondary sealing. Figure 7.25 shows the adhesion surfaces of the edge bond and the glazing and absorber.

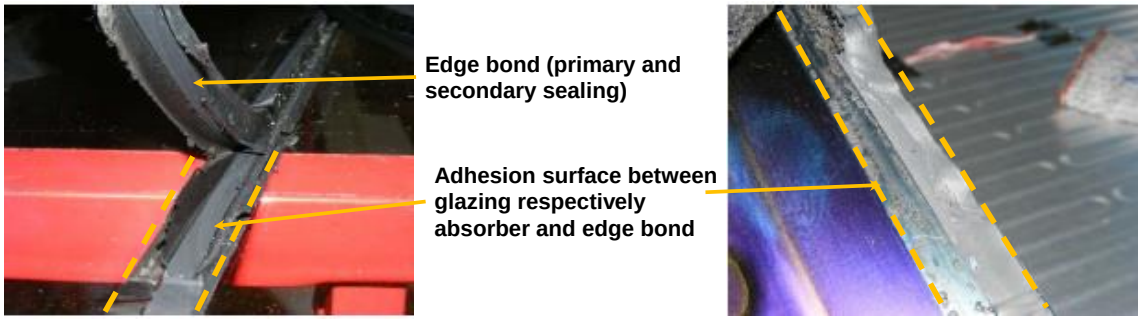

Figure 7.25: Peel-off test proven the material's full mechanical capacity after the exposure (cf. Koemmerling 2014)

In all cases, the full mechanical capacity (adhesion strength) was verified. The exact leakage spot in the edge bond was not identified. The leakage was probably caused by two superimposed effects – a suboptimal, i.e. three-dimensional absorber structure and the high temperature gradient between absorber and edge bond during the internal shock test, which led to a sudden sheet contraction. The precise test procedure of the internal shock test is described in the standard (DIN EN 12975-2).

The header tube geometry of the roll bond absorber avoids an optimal edge bond contact in this area because of its three-dimensional structure (Figure 7.26).

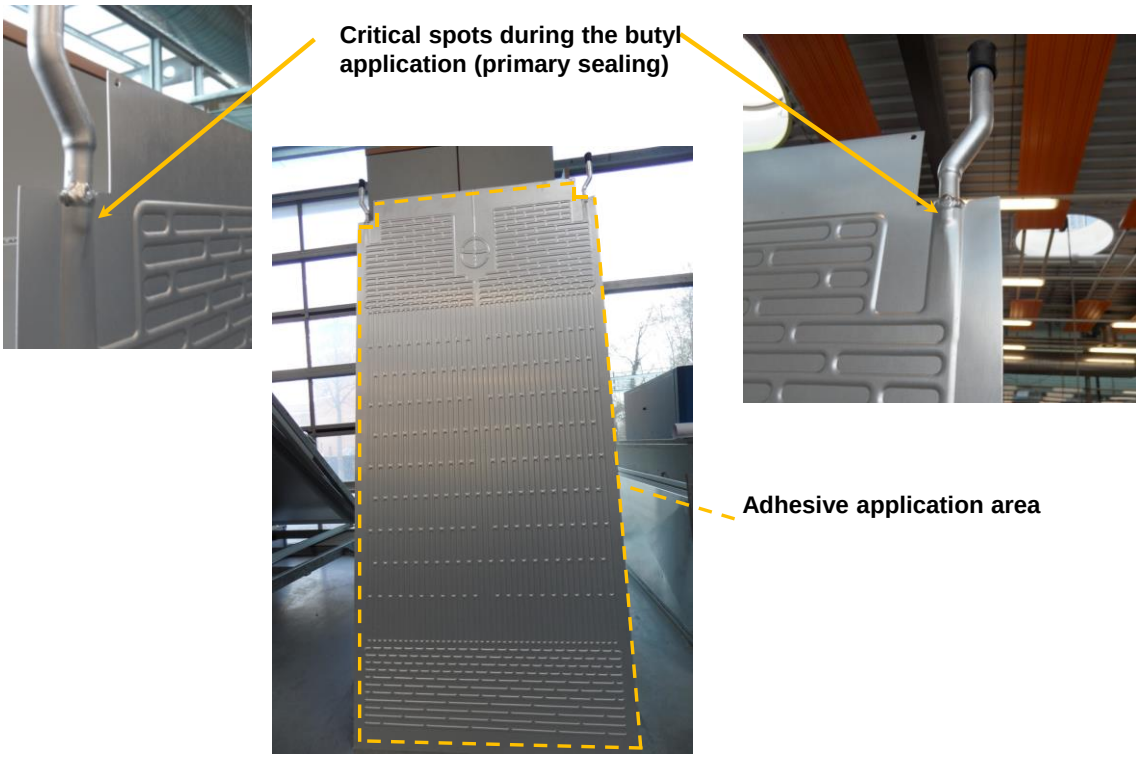

Figure 7.26: Problematic adhesive area due to three dimensional absorber structure

As the TPS applicator was not designed to move in the z-axis, a faulty adhesive application in the area of the header tubes might be a consequence. Furthermore, the pressing procedure could damage the brazed joints between tube and sheet or lead to a squeezed flow passage.

Consequently, if a leakage occurs it is likely to happen in this area. The sudden injection of cold water in an internal shock test during stagnation leads to a temperature-induced contraction of the absorber sheet. This is critical for the edge bond as the adhesive gets soft due to the high temperature. The metal sheet is cooled down in a short time whereas the adhesive is still hot due to its good insulation properties. By the sheet contraction, mechanical stress is applied on the absorber supports, i.e. adhesive edge bond. The stress probably exceeded the capability of the material, which might have led or at least contributed to the leakage. In particular, this seems to be a problem of the rather rigid roll bond absorber geometry as no similar problems occurred with a sheet-pipe absorber. The assumption that the internal shock test caused the leakage is supported by a gas concentration measurement during the test procedure (Figure 7.27).

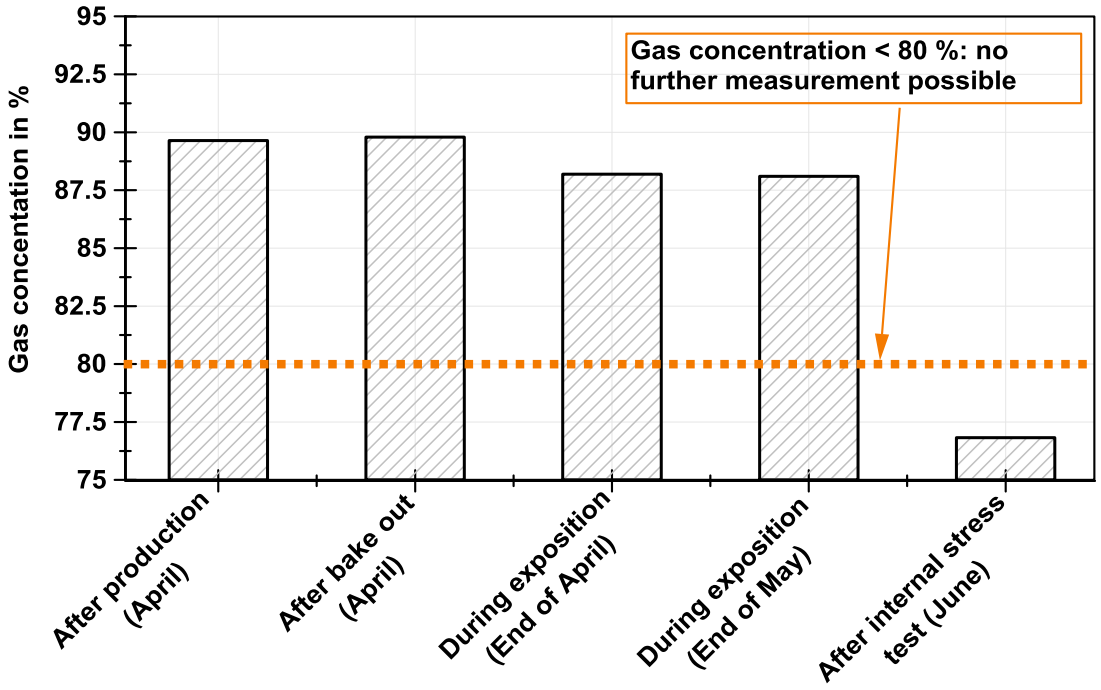

Figure 7.27: History of the gas concentration during the test procedure

The used measurement device is only reliable for gas concentrations of at least 80 % or above. Once the gas concentration drops below 80 % only a qualitative comparison is possible. Based on several measurements during the exposure and the internal stress test a leakage was proven. However, until end of May the argon concentration was steady and the measurements showed filling degrees of more than 87 %.

After the leakage was determined, an efficiency test was conducted to conclude on the impact of the gas leakage on the collector performance. Figure 7.28 shows the collector efficiency before and after its exposure.

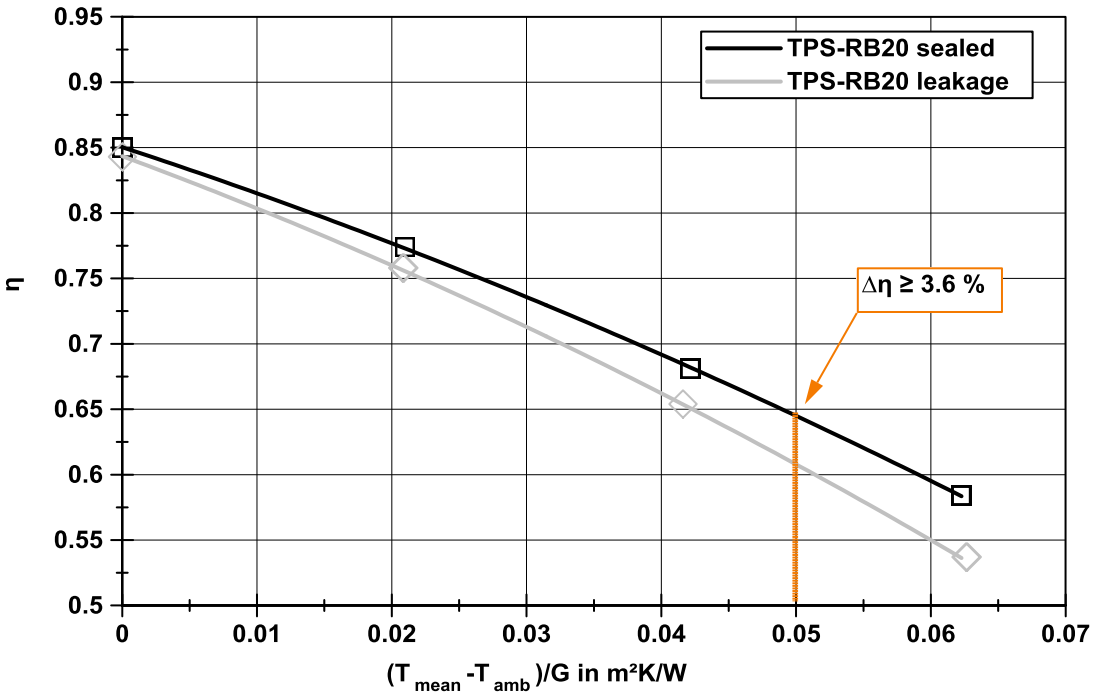

Figure 7.28: Comparison of the collector efficiency before and after the leakage

The tests showed an efficiency reduction for 0.05 m²K/W of 3.6 %. This corresponds to the results of the TPS-2, which was about 4 % for the same ordinate. This efficiency increase is rather small and cannot justify solely this type of collector design.

7.4.3 Summary

Beside the advantages in the production of a hermetically sealed flat plate collector, the roll bond absorber is with its current design only partly suitable for this type of collector. In coordination with the roll bond absorber manufacture's, a plane absorber surface facing towards the glazing would be possible to produce (CGA, SavoSolar 2014). This would allow an optimal adhesive application and pressing around the header tube and welding seams. More critical are the high mechanical loads on the edge bond caused by the rigid metal sheet. It is essential to conduct further analyses of the edge bond by means of a finite element simulation. In this simulation, different mechanical load situations, such as internal or external shock tests, should be simulated. Consequently, the adhesive edge bond needs to be modelled in detail, which is probably one of the biggest challenges in this attempt. Laboratory tests are inevitable to validate obtained

simulation results. Both results can be used to optimise the current absorber design and find an optimal edge bond geometry.

In general, a well-designed system or specific optimisation of the absorber to avoid long periods of stagnation would lower the risk of material fatigue as well.

8 Mechanical simulation study

As shown in the previous chapters, the mechanical behaviour of a collector with a fully adhesive edge bond has a significant impact on the collector efficiency and its lifetime. The current sheet-pipe absorber design is, however, not fully suitable for the here described collector design due to the arbitrary absorber deformation. Instead of a more or less chaotic deflection a predictable mechanical deflection to the collector back, i.e. increasing gap size, would be favourable. A complete prevention of a deflection is seen as a suboptimal approach as it causes high stress in the absorber and especially in the edge bond, which might lead to accelerated fatigue of certain components. In any case, an absorber displacement towards the glazing should be prevented.

The following parameters can be considered to affect the mechanical behaviour of the absorber:

- absorber type,
- absorber material,
- absorber sheet thickness,
- absorber piping,
- sheet structures (beadings).

The influence of a different absorber type was investigated in laboratory tests by means of a roll bond absorber and is not part of this simulation study.

During the research programme, different absorber materials were used in the experimental collectors. This variation is limited as nowadays most often absorber with an aluminium sheet and a copper piping are used. The reasons to this are, on the one hand, lower costs compared to full copper absorbers and, on the other hand, no corrosion problems during the collector lifetime. Nevertheless, all material pairings were considered in the simulation study.

A main reason for the buckling is the thin absorber sheet. This assumption can be traced back to the critical buckling load $\sigma_{critical}$ of a simplified absorber, i.e. without piping. If the value $\sigma_{critical}$ is exceeded for a component, buckling will occur. To calculate $\sigma_{critical}$ this equation can be used:

$$\sigma_{critical} = k * \sigma_E \qquad \text{Equation 8-1}$$

whereas σ_E is defined as

$$\sigma_E = \frac{\pi^2 * E}{12(1-\nu)^2} * (\frac{t}{b})^2 \qquad \text{Equation 8-2}$$

Figure 8.1 shows typical k-factors according to different support versions.

Load case	p	q	k_{min}
	0.0	0.0	
	0.425	0.0	0.425
	0.57	0.125	1.28
	2.00	1.0	4.0
	2.50	5.0	6.97
	2.27	2.45	5.4

Figure 8.1: k-factors for different load cases (Klein 2013)

For the described problem, a value of 6.97 was chosen as it is fixed all-round the absorber edges. Based on the k-factor and the equation $\sigma_{critical}$ can be derived. Table 8.1 comprises the critical buckling load for a copper and aluminium absorber sheet.

Table 8.1: Calculation of the critical buckling load for a simplified absorber sheet

Material	**Copper**	**Aluminium**
Young's modulus in MPa	125,000	70,000
Poisson's ratio	0.35	0.33
Thickness in mm	0.3	0.5
Width in mm	1,000	
Length in mm	2,000	
k-factor	6.97	
2nd moment of area in mm4	2.25	10.42
$\sigma_{critical}$ in MPa	0.073	0.112

For both absorber sheets a very low buckling load of only 0.073 MPa and 0.112 MPa is derived. This indicates that such a thin sheet is likely to buckle already at low mechanical loads.

Concerning the absorber sheet thickness, it was plausible to use the common absorber sheet thicknesses between 0.5 mm (aluminium) and 0.25 mm (copper). Usually, aluminium absorbers come along with a thicker sheet to substitute the lower heat conductivity compared to copper. According to absorber manufacturers, thin aluminium sheets (t_{sheet} < 0.5 mm) are causing problems during the welding process that are – at least in the moment – not of interest to overcome (Rohde 2012). Hence, this was a factor that was not changed in this study.

Laboratory tests showed that the absorber piping has a considerable impact on the absorber deflection. In particular, the double-meander showed due to its divided temperature sections a different deflection behaviour (Figure 8.2).

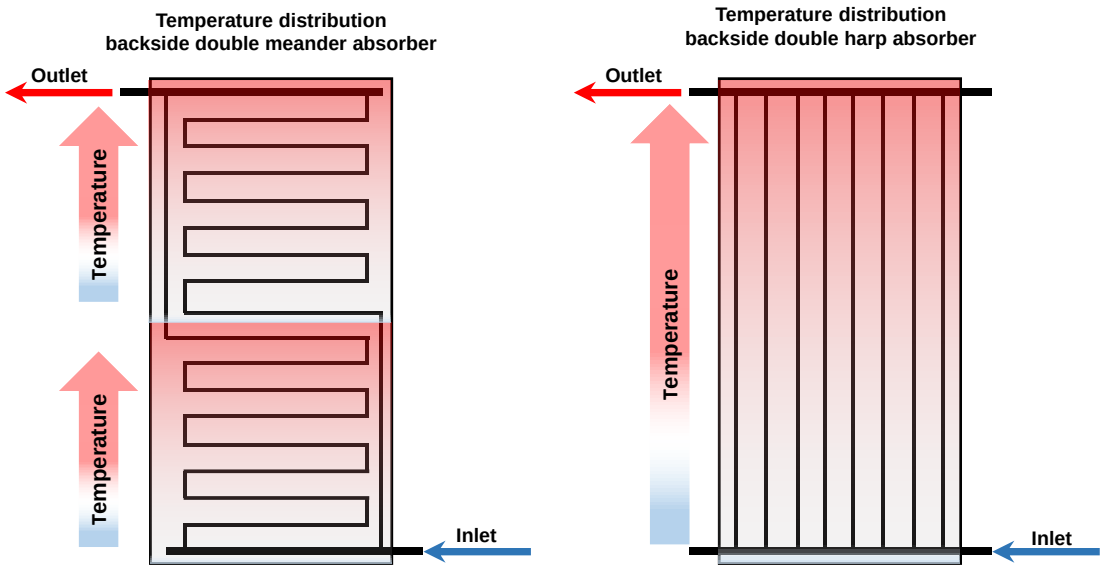

Figure 8.2: Scheme of the temperature distribution of a double-meander and harp absorber in longitudinally direction

The temperature distribution in the double-meander splits the absorber deflections in to a lower and upper part – according to the absorber piping.

Figure 8.3 shows the deformation plot of a double meander absorber whereas Figure 8.4 shows the deflection of a harp absorber. Both measurements were conducted with an absorber temperature of 97 °C. The absorber temperature was measured at two-thirds of the total absorber height on the upper part in the middle of an absorber fin.

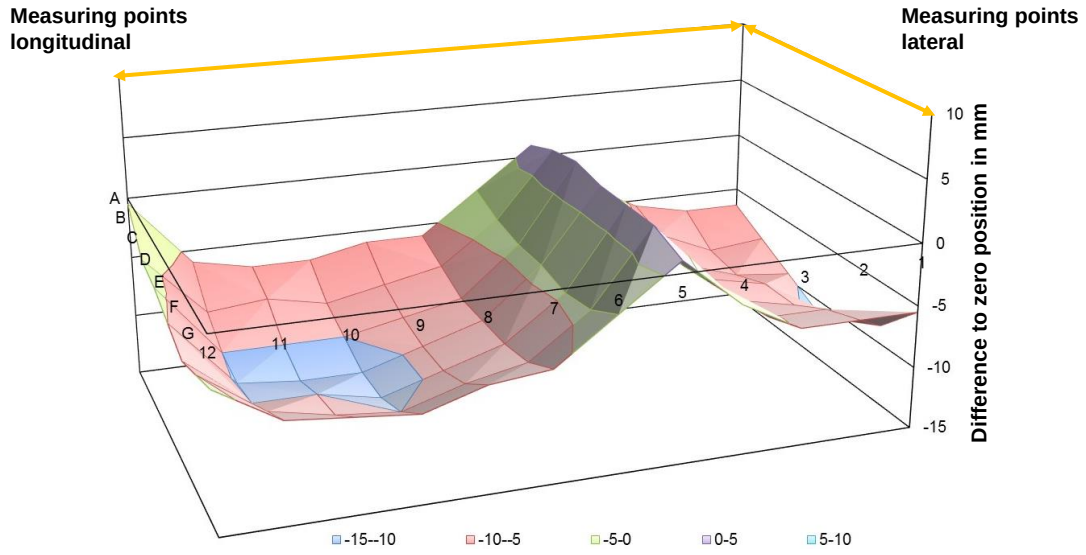

Figure 8.3: Measured absorber deflection of a double-meander absorber (Cu-Cu)

Distinctive in this measurement was that the divided temperature distribution splits the deflection in to a lower and upper part with its border in the middle of the absorber.

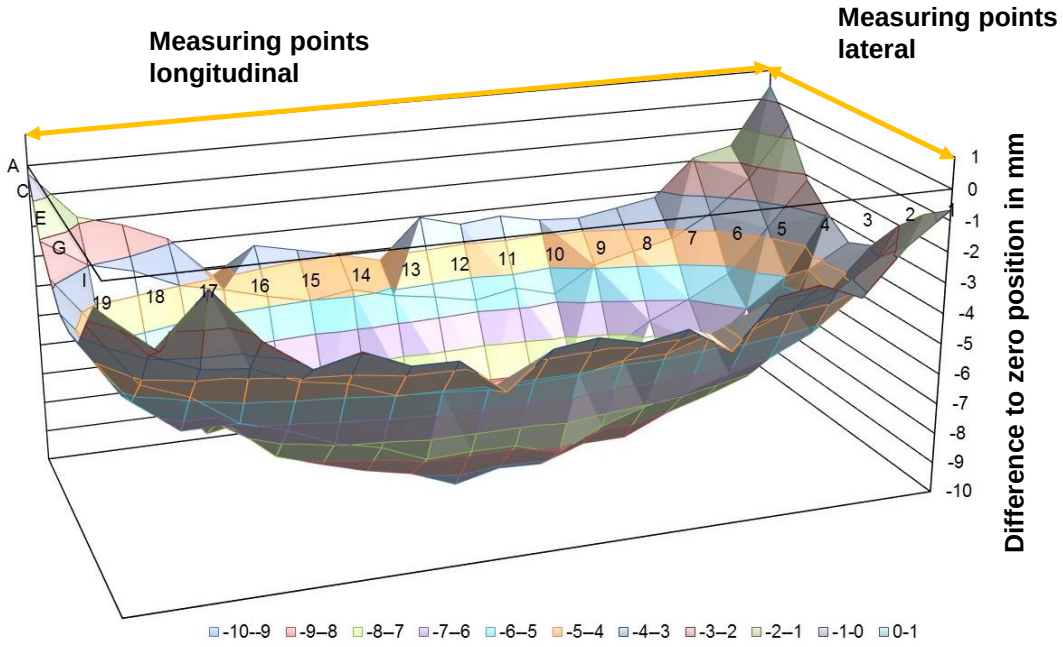

Figure 8.4: Measured absorber deflection of a harp absorber (Al-Al)

From a structural mechanic point of view, both a meander and double-meander piping is more favourable than a harp absorber. This can be deduced from the basic deflexion equation of a double supported beam, as the maximal deflection rises with the beam length. Hence, it is advantageous to keep the beams, i.e. risers, short and exclude harp piping from the mechanical case study.

A focus was put on an optimised structure in the absorber sheet. During the production process, it turned out that an increased stiffness for sheet-pipe absorbers would be favourable as the handling during the production process is easier as well as the adhesive application on the absorber edges. Above that, a reinforced absorber structure allows a smaller deflection and under certain circumstances a more predictable absorber deflection. Another synergy is given by the fact that thinner metal sheets with a higher stiffness due to the bracing can be used for the absorber. This, in turn, results in lower material costs. However, to make use of this approach the current absorber welding technique needs to be further analysed and adapted to thinner metal sheets. In this approach, the influence of a bracing in terms of beadings were analysed in a finite element model. Instead of beadings, additional ribs and beams on the absorber could be

used for stiffening the absorber. Compared to beadings that can be deep drawn during the production process the attachment of additional ribs and beams is more effortful. Despite this, an additional weight is added to the absorber and the bracing would function as a heat sink, which can cause an extra heat loss on the back of the absorber. The same applies to the possibility of an array with insulated spacer between absorber and glazing. Ultimately, these approaches were not further investigated in this thesis as the drawbacks prevail.

In this thesis, two possible absorber structures concepts were evaluated in a case study to show the potential of the beadings. The analysed structures are an example type. However, there might be even more suitable structures possible. The design studies are discussed in the upcoming subchapters.

8.1 Absorber bracing by beadings

Figure 8.5 shows a cross section of a trapezium beading with its important parameters.

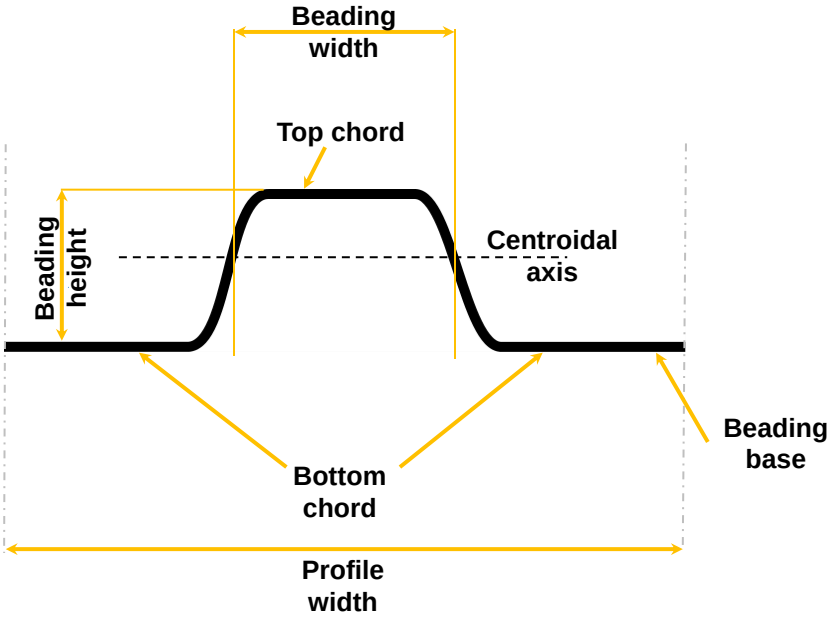

Figure 8.5: Components of a box beading

The beading leads to an offset of the barycentre from the neutral axis and increases the magnitude of the Steiner's theorem. Consequently, the 2nd moment of area and, thus, the section modulus is increased, which in turn results in a higher stiffness. Figure 8.6 clarifies this fact.

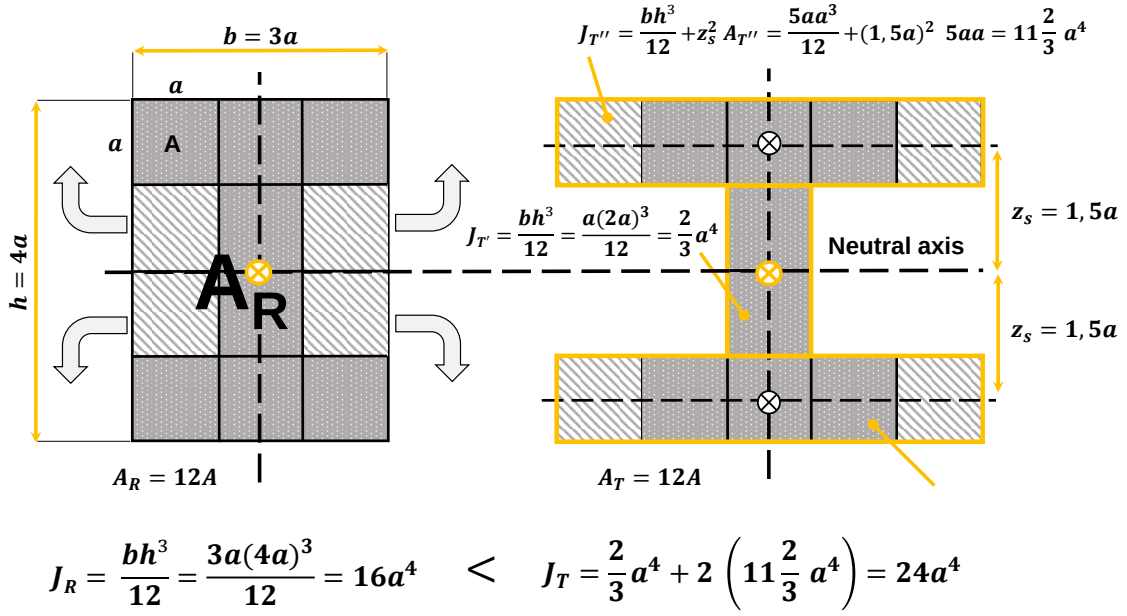

Figure 8.6: Comparison of the 2nd moment of area of a rectangular cross section and an I-beam with an identical cross sectional area

The value z_s describes the distance between the partial centres of gravity to the centre of gravity. Steiner's theorem states that the 2nd moment of area increases with the second power of distance from its centre of gravity and, thus, the beading height plays an important role in the design of such. Consequently, this indicates that the beading type 'R' comes along with the highest increase of the 2nd moment of area as the Steiner's theorem is maximised (Figure 8.7).

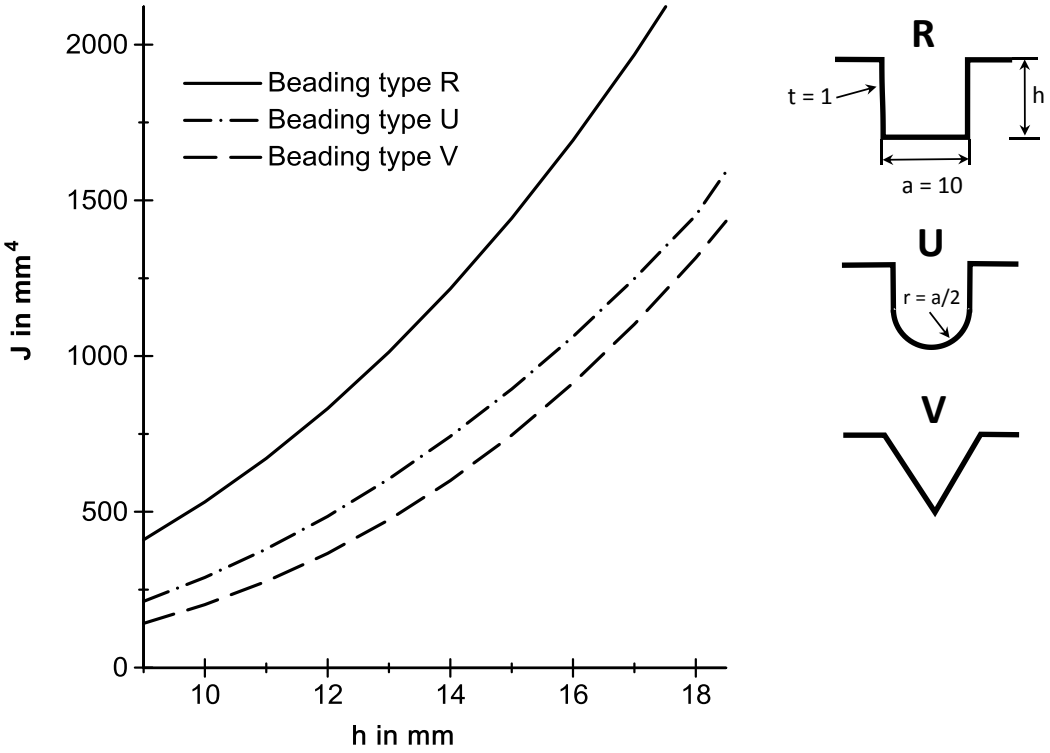

Figure 8.7: 2nd moment of area of different beading geometries depending on the beading height and geometry

For the further conducted studies, the beading type ‘R’ was chosen due to its higher 2nd moment of area.

Beside the beading geometry, certain design guidelines for metal sheets with static loads need to be followed (Klein 2013):

- preferred axis of inertia in metals sheet need to be avoided
- unstiffened sheet edges need to be avoided
- rectangular workpieces should be braced by circular structures and vice versa
- nodal points of beadings and intersecting beadings are to be avoided
- linear beadings are to be conducted along the sheet edges
- each imaginary cross section through the workpiece should intersect with a beading

Beside the beading geometry and the design guidelines, another major design aspect is represented by the beading degree φ of the metal sheet. This value is defined as the relation between the top and bottom chord area to the initial metal

sheet surface. For the deduction of the optimal beading degree, an extreme value determination of φ can be conducted.

The beading degree is as

$$\varphi = \frac{A_{top\ chord}}{A_{top\ chord} + A_{bottom\ chord}} \qquad \text{Equation 8-3}$$

With the convention that

$$A = A_{top\ chord} + A_{bottom\ chord} \qquad \text{Equation 8-4}$$

Follows

$$(1 - \varphi) = \frac{A_{bottom\ chord}}{A} \qquad \text{Equation 8-5}$$

The sheet area centroid is weighted by its subareas and can be expressed by the following equation:

$$S_z = \frac{1}{A_{total}} \cdot \sum_{i}^{n} A_i * z_i \qquad \text{Equation 8-6}$$

In the discussed beading application, there are only two subareas – the area of the top and bottom chord. If Equation 7-7 is applied by inserting the subareas, it results in

$$S_z = \frac{(A_{bottom\ chord} \cdot 0 + A_{top\ chord} \cdot h)}{A_{top\ chord} + A_{bottom\ chord}} = \frac{\varphi \cdot A_{top\ chord} \cdot h}{A_{top\ chord} + A_{bottom\ chord}} \qquad \text{Equation 8-7}$$
$$= \varphi \cdot h$$

The value of the Steiner's theorem for the top and bottom chord is

$$J_{bottom\ chord} = S_z^2 \cdot A_{bottom\ chord} \qquad \text{Equation 8-8}$$

$$J_{top\ chord} = (h - S_z)^2 \cdot A_{top\ chord}$$

$$J_{Steiner} = J_{top\ chord} + J_{bottom\ chord}$$

$$J_{Steiner} = S_z^2 \cdot A_{bottom\ chord} + (h - S_z)^2 \cdot A_{top\ chord}$$

S_z is substituted by

$$J_{Steiner} = (\varphi \cdot h)^2 \cdot A_{bottom\ chord} + (h - \varphi \cdot h)^2 \cdot A_{top\ chord}$$

The term of $A_{top\ chord}$ and $A_{bottom\ chord}$ is expressed by φ and A

$$J_{Steiner} = (\varphi \cdot h)^2 \cdot A(1 - \varphi) + (1 - \varphi)^2 \cdot h^2 \cdot A \cdot \varphi \qquad \text{Equation 8-9}$$

$$J_{Steiner} = \varphi^2 h^2 A - \varphi^3 h^2 A + \varphi h^2 A + \varphi^3 h^2 A - 2\varphi^2 h^2 A = \varphi h^2 A - \varphi^2 h^2 A$$

$$J_{Steiner} = (-\varphi^2 + \varphi) \cdot h^2 A$$

To deduce the optimal beading degree the term is differentiated

$$J'_{Steiner} = (-2\varphi + 1) \cdot h^2 A \qquad \text{Equation 7-10}$$

Subsequently, the term is analysed on its extreme value

$$J'_{Steiner} = 0 = (-2\varphi + 1) \cdot h^2 A \qquad \text{Equation 7-11}$$

$$2\varphi = 1$$

$$\varphi = 0{,}5$$

Deduced by this extreme value analysis, the highest value for the Steiner's theorem is achieved if 50 % of the total sheet is in the top chord and bottom chord area. As a simplification, the risers and header tube geometry was neglected. However, the absorber piping displaces the centroidal axis towards the negative z-axis. The effect on the beading degree is dependent on the position of the risers and beading height.

The given design guidelines for beadings, e.g. beading degree, and the design restrictions of a sheet-pipe absorber resulted in two promising beading geometries.

8.2 Outlook on an optimised absorber structure

The conducted study is meant to provide an idea of the potential for absorber structures with beadings to reduce the mechanical deflection. The basis for this case study is the finite element model introduced in chapter 4. However, instead of an absorber with a harp piping, a double-meander piping was modelled as the laboratory tests and the shorter risers showed a more preferable mechanical behaviour.

By following the stated design guidelines for beadings and to satisfy the criteria of the optimal beading degree φ, two promising approaches were developed. Moreover, the absorber piping limits the beading design, as beadings are only possible between the fins of two riser tubes.

Figure 8.8 shows the two derived and analysed beading structures with their geometrical parameters for a sheet-pipe absorber with a double-meander piping.

Version	Total absorber area in m²	Total beading area in m²	Beading degree	Beading parameters		View (absorber bottom)
				Height in mm	Beading quantity	
Rec_bead	2	1	50 %	8	11	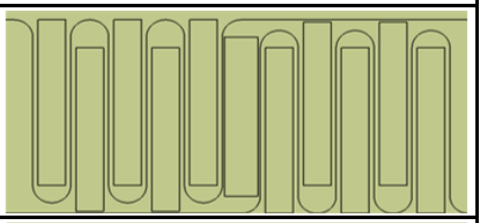
Curv_bead		0.879	44 %	8	11	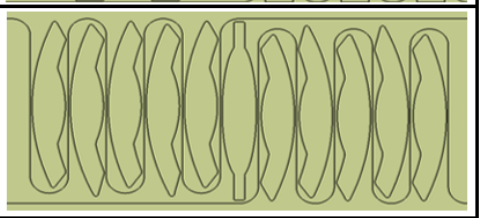

Figure 8.8: Overview of the parameters of the analysed absorber structures with rectangular and curved beadings

Figure 8.9 shows one of the absorber types with double-meander piping and a promising beading structure.

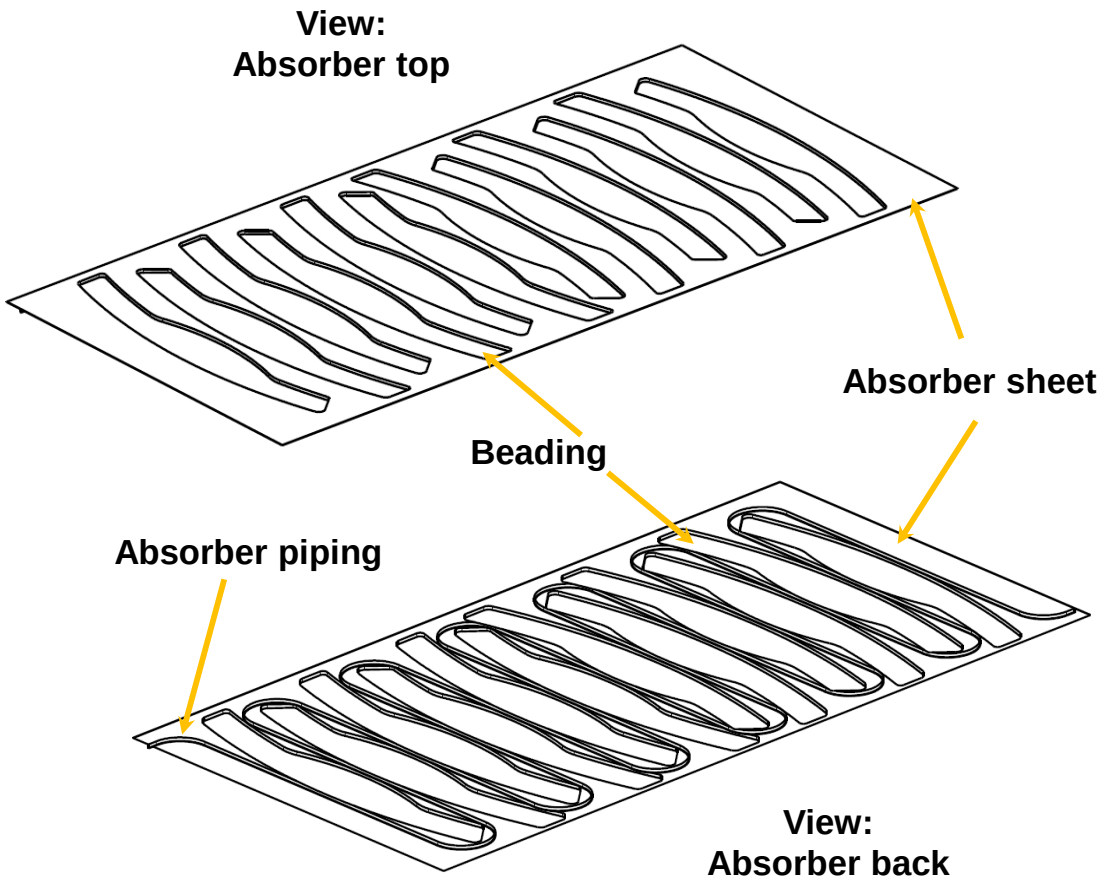

Figure 8.9: Isometric view of the absorber with the curved beading structures

For this analysis, a beading height of 8 mm was assumed. An increased beading height was neglected due to the challenging production process. The number of beadings is a result of the geometrical absorber properties as the beading needs to be between two risers. This is essential to ensure that the riser could be welded on the absorber sheet. If this criterion would be omitted, different beading structures could be possible as well. However, these solutions could have a drawback in the thermal efficiency as of the deteriorated heat exchange between sheet and riser.

The two structures ‘Rec_bead’ and ‘Curv_bead’ were analysed more in detail and a parameter study considering different material pairing were conducted. In particular, only a constant overpressure of 20 Pa was applied on the reinforced structure. For all variations, the maximum deflection and the resulting expansion volume were computed. For reason of better comparison, a conventional sheet-

pipe absorber with a sheet thickness of 0.5 mm (aluminium) and 0.25 (copper) and a double-meander piping was used.

Table 8.2 comprises the deflection maximums and expansion volumes for the conventional sheet-pipe absorber with a pressure of 20 Pa.

Table 8.2: Overview of the maximum deflection and expansion volume for the reference absorber

	Material sheet	Material piping	Load type	Applied pressure in Pa	Maximum deflection in mm	Expansion volume in litre
Ref	Aluminium	Aluminium	Overpressure	20	1.44	1.64
	Aluminium	Copper			1.16	1.36
	Copper	Aluminium			1.79	2.22
	Copper	Copper			1.55	1.98

Table 8.3 shows the simulation results for an overpressure of 20 Pa for the different absorber settings.

Table 8.3: Overview of the maximum deflection and expansion volume depending for the two versions and different material pairings

	Material sheet	Material piping	Load type	Applied pressure in Pa	w_{max} in mm	Reduction Δw_{max} compared to 'Ref'	V_{exp} in litre	Reduction ΔV_{exp} compared to 'Ref'	Relative change ΔV_{exp} of to 'Ref'
Rec_bead	Aluminium	Aluminium	Overpressure	20	0.43	-1.01	0.55	-1.09	-66%
	Aluminium	Copper			0.41	-0.75	0.52	-0.84	-62%
	Copper	Aluminium			1.23	-0.56	1.62	-0.60	-27%
	Copper	Copper			1.18	-0.37	1.55	-0.43	-22%
Curv_bead	Aluminium	Aluminium	Overpressure	20	0.76	-0.68	0.92	-0.72	-43%
	Aluminium	Copper			0.72	-0.44	0.87	-0.49	-36%
	Copper	Aluminium			1.68	-0.11	2.06	-0.16	-7.2%
	Copper	Copper			1.55	0.0	1.93	-0.05	-2.5%

Based on the simulation results the following conclusions can be drawn:

- Despite the higher Young's modulus of copper, a Cu-Cu absorber comes along with a higher deflection and a bigger expansion volume than a configuration with an Al-Al absorber. This is independent from the beading type. Ultimately, this is caused by the 0.25 mm thicker aluminium absorber sheet.
- For the versions with an aluminium piping and a copper sheet both values for the deflection and the expansion volume are bigger than for the versions with a copper piping and aluminium sheet. This, in turn, indicates

that the absorber sheet has a more dominant effect on the deflection and expansion volume than the piping.

- The absorber type ‘Curv_bead’ allows a higher deflection as well as a higher expansion volume than the version ‘Rec_bead’. This is owed to the slightly lower beading degree of the absorber with the ‘curved’ beadings.
- Compared to the reference absorber without beadings, the reinforced structures show a more rigid behaviour as less deflection and less expansion volume is computed. The version ‘Rec_bead’ reduces the ΔV_{exp} by up to 1.09 litre or 66 % compared to the reference absorber. In contrast to this, the ‘Curv_bead’ version reduces the expansion volume by up to 43 % for the Al-Al absorber.
- Within this potential study, the absorber with the rectangular beadings (‘Rec_bead’) showed a higher stiffness. However, a stress analysis needs to be conducted to ensure that the material will not fail during operation.

8.3 Summary

Within this case study, it was shown that beadings in sheet-pipe absorber can contribute to a reduction of the deflection. In fact, compared to the conventional absorber structure a reduction down to 1.01 mm considering the maximum deflection and up to 66 % concerning the expansion volume was shown. It turned out that the absorber sheet has a more dominant effect on the absorber deflection and expansion volume than the piping structure. However, a more rigid structure will increase the stresses on the edge bond and on the absorber components.

The most suitable parameter of the beadings, e.g. beading height, need to be investigated. This needs to be closely linked to a stress analysis of the complete absorber structure to avoid a failure during operation as the mechanical strength could be exceeded.

The conducted study just indicates the potential of further mechanical optimisation measures for sheet-pipe absorbers in terms of mechanical stability. Hence, there is still plenty of research to do in this field. In particular, the design of the edge bond needs to be analysed more in detail, as the change of the stress-strain curve depending on the temperature was not implemented in this work. Another crucial as well as challenging aspect is the stress analysis of the edge

bond and of the absorber components. Moreover, more suitable beading designs can be derived in a more detailed analysis.

As a result of chapter 7.4, internal and external thermal stress tests are a vulnerable point of the edge bond. Consequently, these tests need to be simulated to ensure a durability over the collector lifetime and find an optimisation potential. Once the technical parameters are elucidated, a feasibility study on the production processes of the derived reinforced absorber needs to be conducted. Eventually, this will show details on the cost structure of such an absorber type.

9 Economic analysis of the collector production method

In this economic analysis both the collector production as well as collector component costs were considered depending on the produced annual collector units. The sum of the collector components costs and the production costs were defined as the total collector costs.

A conventional production line with a normal vented flat plate collector was benchmarked to the adapted production technology and the discussed collector design. Overall, three different line concepts of the modified IGU production technology were compared that differ in their automation level and in the investment costs. The used parameters of the reference assembly line for the conventional collector were based on the study of Müller and Zörner (2010). Table 9.1 comprises the used parameters of all four lines.

Table 9.1: Parameters of the adapted production lines and the reference production line

Assembly line	Cycle time in s	Investment costs in Mio. €	Collectors per shift	Collectors per year	Personnel
Low	240	1.2	120	90.000**	8*
Mid	120	1.9	240	180.000**	8*
High	60	2.9	480	360.000**	6*
Conventional	240	1.2	120	90.000**	9*

*Including washing process and packing

**Annual collector production based on a three-shift operation

Figure 9.1 shows exemplary the setup of the concept ‘high’ with a maximised automation level and the concept layout ‘low’ with a minimum of automation.

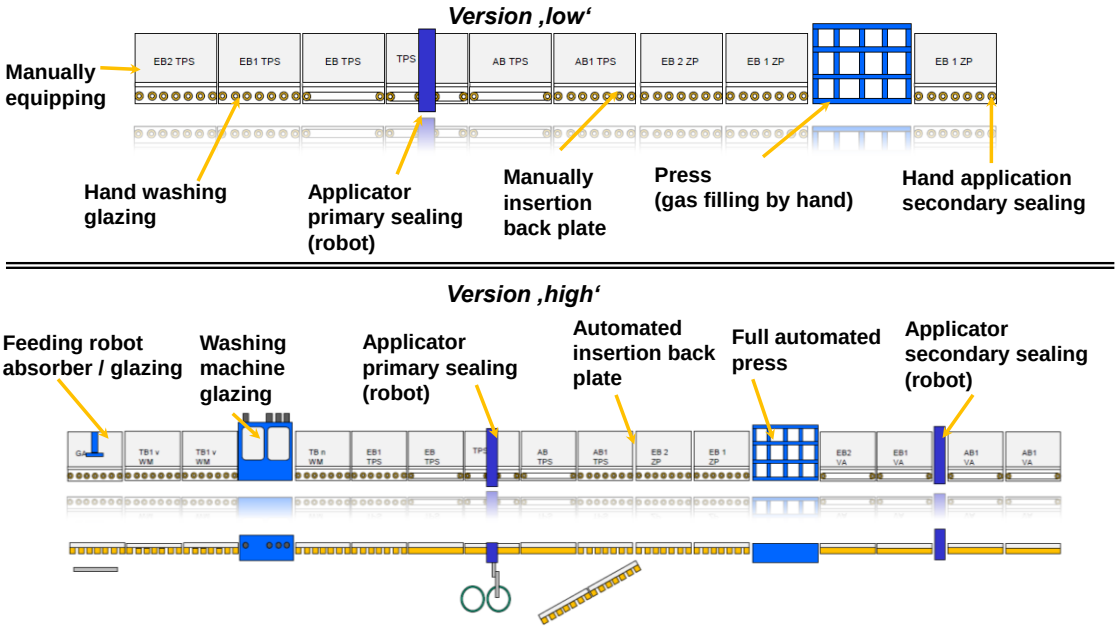

Figure 9.1: Scheme of two possible production lines with a low and high automatization grade

Independently from the grade of automation, the primary sealing needs to be applied by a robot. Production steps such as the component equipping of the line, the cleaning of the front cover, the gas filling of the interspace or the application of the secondary sealing can be done by hand. Consequently, the decrease of the automation level leads to an increase of the cycle time. For the production line concept ‘high’, the plant manufacturer determined a collector cycle time of 60 s. In contrast to this, four minutes are needed to assembly a collector on the low automated line. The cycle times were derived by a simulation model of the plant manufacturer.

As the conventional assembly line has a higher cycle time than the concepts ‘mid’ and ‘high’ it was assumed that multiple conventional lines are used to achieve the same annual collector unit output, i.e. two conventional lines in the case of the concept ‘mid’ and four lines to equal the annual unit output of concept ‘high’. Müller and Zörner (2010) reported that a duplication of collector production lines was a method used by European collector producers to reach a higher annual collector production rate.

Concerning the collector setup, similar boundaries and components for both collector types – conventional and hermetically sealed collector – were taken as a basis. This means the same collector size, insulation material and thickness, casing, glazing and absorber was used. Consequently, both collectors are

varying only in the fact that the TPS collector causes higher adhesive costs than the common type. In Table 9.2 the component costs are shown whereas Figure 9.2 represents the cost structure of the two collector types.

Table 9.2: Component costs of the TPS collector and the reference collector

Collector	**TPS collector**	**Conventional collector**
Absorber (Al-Cu; 1.9 m²) in €	69	
Casing* (Frame; Al) in €	60	
Side and back Insulation (Mineral wool) in €	12	
Total adhesive costs in €	12.5	2
Glazing (uncoated) in €	18	
Miscellaneous (Grommet, down holder, …) in €	1.5	3
Total component costs	173	164

*Including all frame parts, e.g. back plate

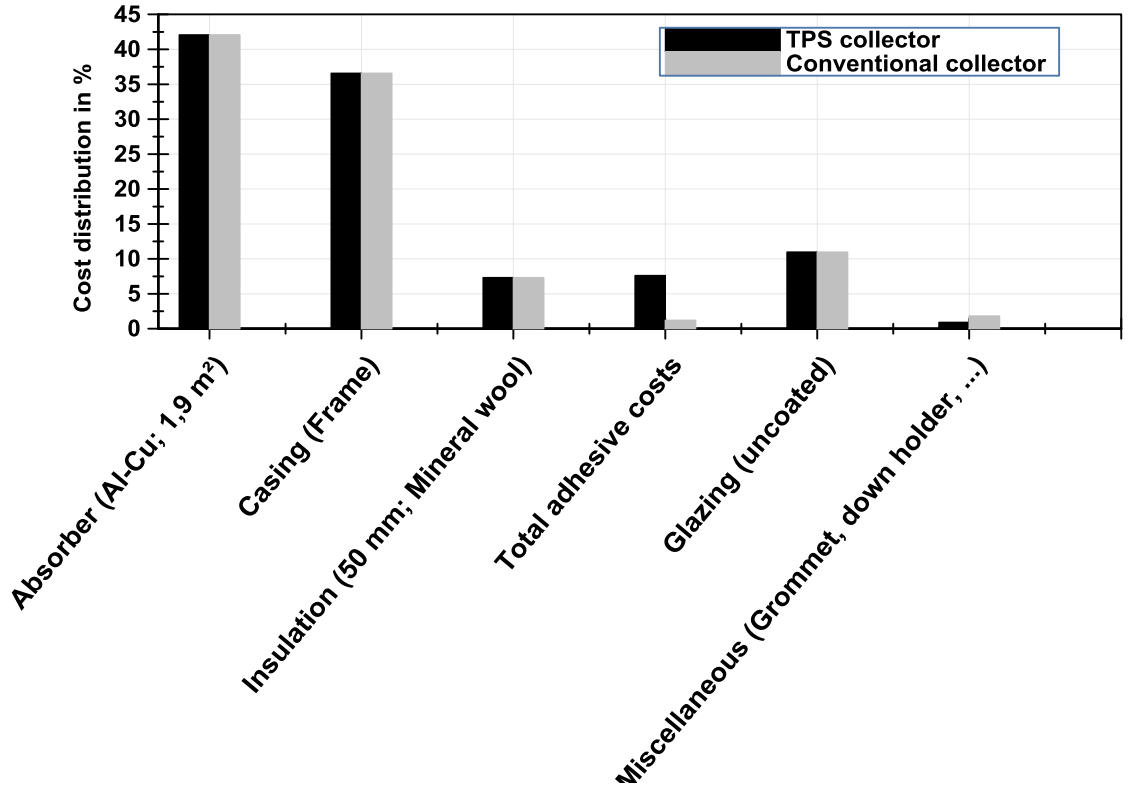

Figure 9.2: Relative costs distribution of the TPS collector compared to the reference collector

By default, three different gap sizes – 5, 15 and 20 mm – were chosen for the hermetically sealed collector. The here presented findings from chapter 4, 6 and 7 showed that for gap sizes smaller than 20 mm an optimised absorber structure is preferable as the braced sheet structures lead to a lower absorber deflection. The adhesive costs for the hermetically sealed collector are distinctively higher. Therefore, it is practical to reduce the application height. An obvious solution to bring down the adhesive costs is a geometrical change of the absorber edges (Figure 9.3).

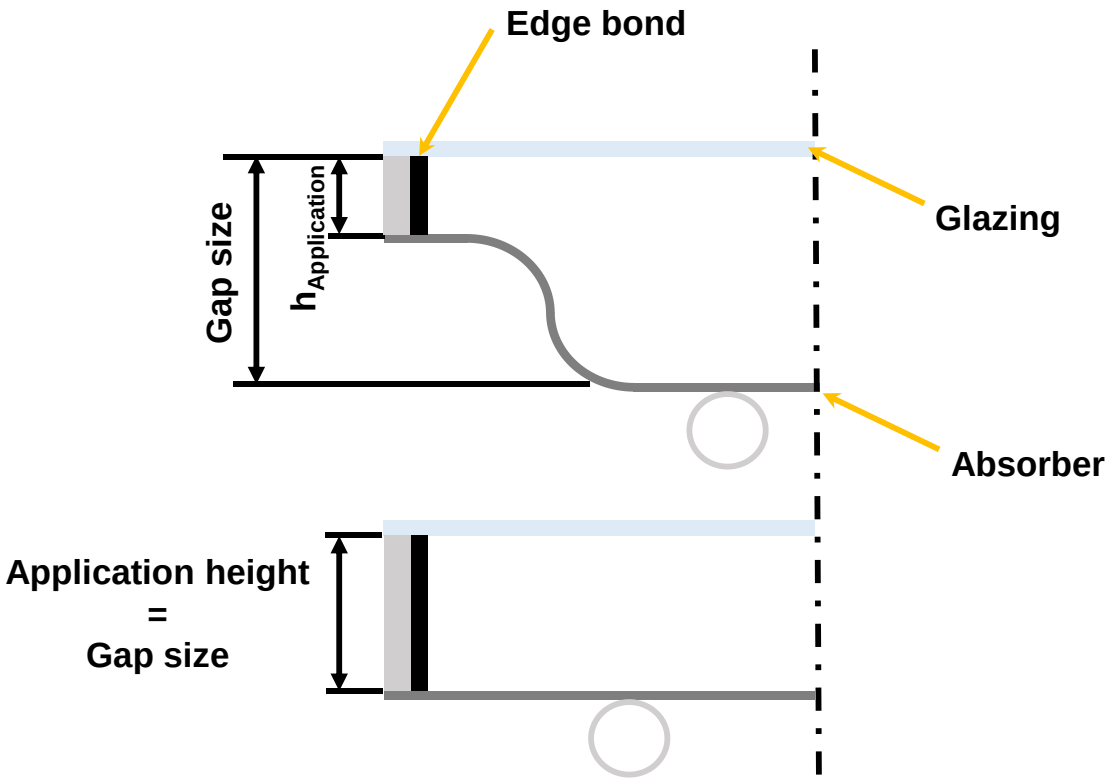

Figure 9.3: Difference between gap size and application height

The upper absorber scheme shows the version with an application height of 5 mm and a gap size of 10 and 15 mm. This geometry can be produced by a deep-drawing process whilst the beadings are formed. The lower scheme, which is ultimately a standard absorber, refers to a gap size of at least 15 to 20 mm. Additional production costs for the modified absorber structure were not taken into account.

Further saving potential could be the material reduction of the absorber for the hermetically sealed collector, which is with 41 % of the total component costs the most expensive collector component. By an aimed weakening of the fin efficiency F', e.g. thinner absorber sheet or fewer risers, the thermal efficiency drops but less material is needed. A material reduction down to an efficiency level of a conventional collector seems plausible but was not analysed.

9.1 Assumptions and simplifications

The detailed costs were provided from the plant manufacturer (Bystronic 2014) as well as from a German collector producer (CitrinSolar 2014). As those figures are not meant to be publicised, a dimensionless ratio was introduced that allows a comparison between the two collector production lines without revealing the specific money sums. Equation 9-1 defines the relative collector costs ϑ:

$$\vartheta = \frac{\gamma_{\text{concept}} - \gamma_{\text{convFPP}}}{\gamma_{\text{convFPP}}} \qquad \text{Equation 9-1}$$

whereas γ represents the actual total collector costs of the production lines.

The collector production costs are divided into fixed costs, labour costs and material costs while the fixed costs include the following factors:

- Investment costs of the production line,
- linear depreciation based on a machine lifetime of five years,
- imputed interests of 6 %,
- maintenance costs (2 % of the total investment sum),
- building occupancy expenses (5 €/m²),
- insurance costs with 0.25 % of the total investment sum.

The following cost positions were omitted:

- Economies of scale,
- energy costs of the production line (electricity, water, compressed air …),
- costs for the marketing and sales department.

It is certain that economies of scale will affect the costs of both collector types with rising sale figures – especially for sale figures of up to 360.000 units a year. However, in the end, this is an individual agreement between the material or component supplier and the collector producer. To avoid a speculative assumption, possible economies of scale are not considered. The energy demand of the production line would be interesting and is actually simple to include but it was not possible to obtain the energy consumption for both production lines due to lacking data. The same applies for the salaries and expenses for the marketing and sales department of the collector producer.

9.2 Results

Figure 9.4 shows the relative collector costs of the three TPS line concepts in comparison with the conventional approach (convFPP) depending on the annual collector units.

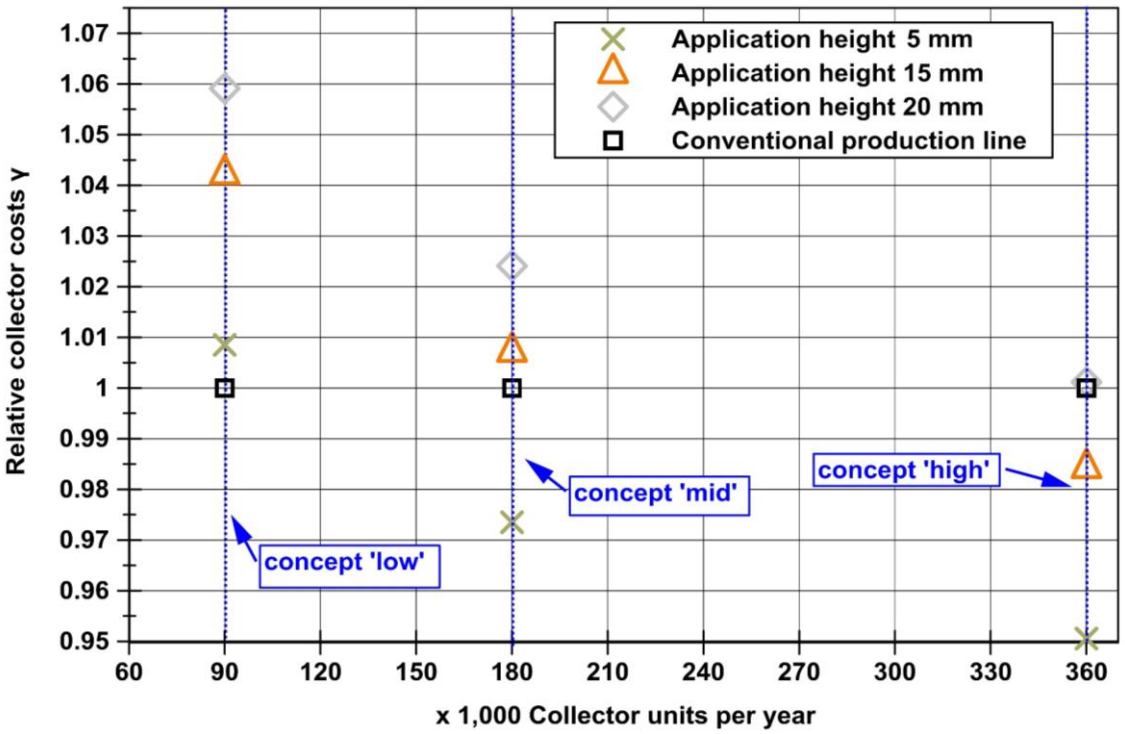

Figure 9.4: Comparison of the profitability of three different concept lines with varying application heights and the reference line depending on the annual collector output

Based on a TPS collector with an application height of 20 mm more than 360.000 collectors per year need to be produced to equal at least the production costs of the conventional collector line. This fact, in turn, shows the high impact of the material costs for the total collector costs. If the adhesive height is cut down to 15 mm the concept ‘high’ is 1.5 % more cost efficient than the conventional production method. This corresponds to a yearly cost saving of about one million € and results in a short payback period for the production line. By reducing the adhesive height by another 10 mm, e.g. optimised absorber edges, to a 5 mm total application height a TPS production line can be operated economically by an annual collector output of 180.000 units for the production line ‘mid’. If the maximum production capacity of the concept ‘high’ is fully used, i.e. 360.000 units a year, 3.4 Mio. €/a are saved in contrast to the conventional assembly lines.

However, the last years showed a struggling collector sales market (Figure 9.5).

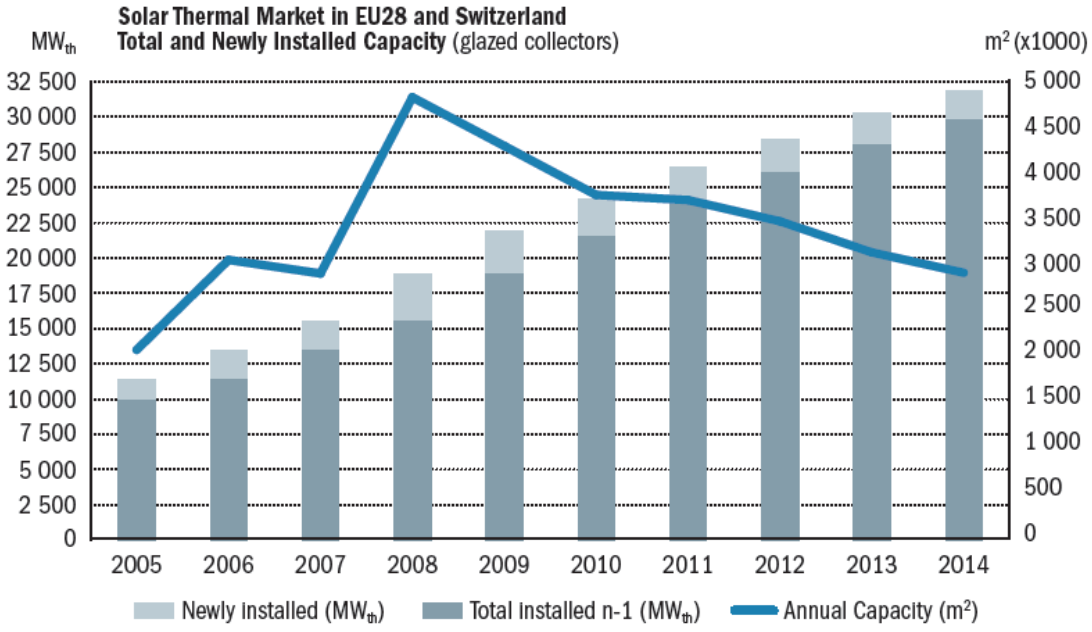

Figure 9.5: Fluctuating development of the solar thermal market in Europe and Switzerland (ESTIF 2014)

Between 2005 and 2008 the sales figures rose and reached a maximum in 2008. Since then, the market is more or less stagnating or even declining. Only a few companies in Europe are producing slightly more than 120.000 collector units per year. Nevertheless, those companies are operating up to two or more assembly lines at a time (Müller and Zörner 2010). In times of declining markets the capacity of the backup lines are not in use. Assuming that the company is keeping the personnel employed during this time, a highly automated production line would be competitive. Figure 9.6 clarifies this aspect for a production capacity use of only 50 %.

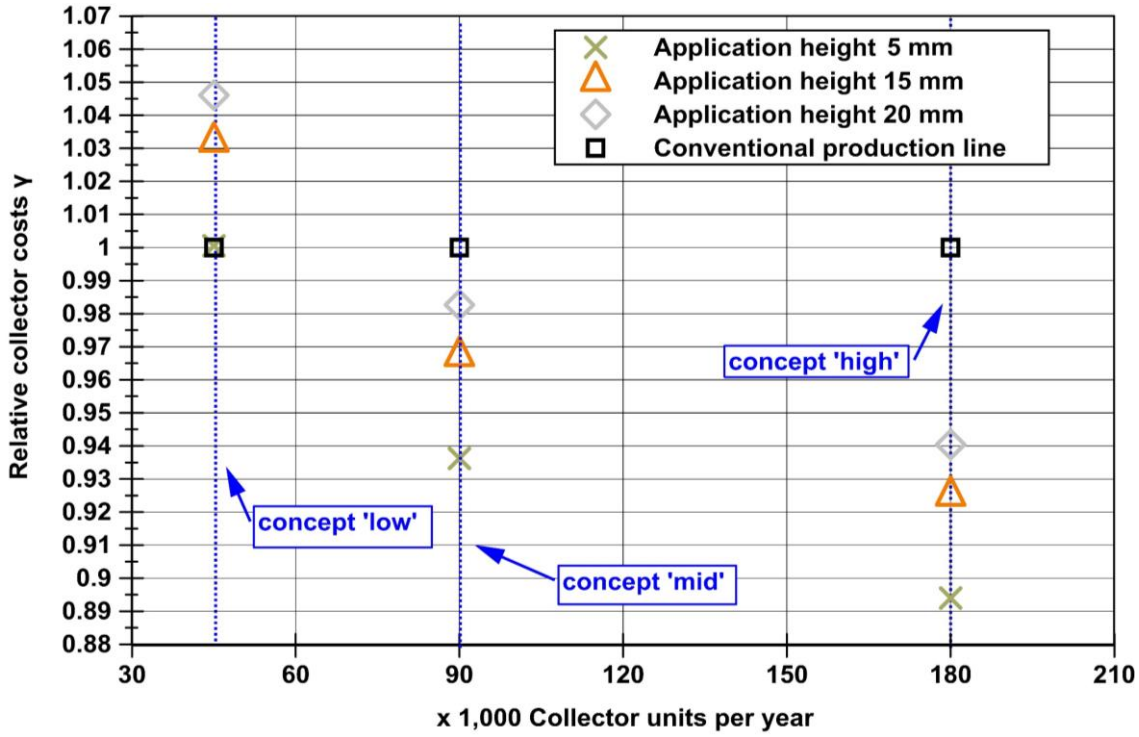

Figure 9.6: Profitability comparison of three different concept lines with varying application heights and the reference line depending on the annual collector output at a production capacity use of 50 %

Compared to the reference line, a maximum saving of 11 % is achieved with the concept ‘high’ whereas the concept ‘low’ with an application height of 20 mm adds 5 % additional collector production costs.

However, it remains to be seen whether a company can keep the production personnel during times of declining markets.

9.3 Summary

The high investment costs of the production line as well as the high material pricing for the adhesive are hurdles for the further utilisation of this technology. Consequently, the aim needs to be a decrease of both investment and production costs of this collector type. A promising approach could be a further material optimisation of the absorber or the insulation. As the efficiency of a hermetically sealed collector is higher than that of a conventional one, there might be potential to reduce the material use in the absorber.

In terms of the production technology, it is questionable whether a price reduction is feasible at all. The machinery for the highly automated production steps causes the high costs and it is unlikely that these costs will decrease in a significant manner. An increase of the collector sales will lead to more solvent collector producers that are capable of investing in such a production line. However, it is currently not foreseeable at what time the collector market starts to increase again. A business strategy that is followed by collector producers is the outsourcing of the production of the hermetically sealed assembly group (glazing ⇔ absorber) to IGU producers. Plenty of these IGU production lines are already operating in Europe and in some cases, the full production capacity is not used for glazing units. On the one hand, the collector producer can avoid high investments costs and on the other hand, the IGU producer can operate the highly automated production line at full capacity. In any case, the collector producer will face higher unit costs for this flexibility.

10 Conclusions

The overall objective of this work was to analyse a collector with a fully adhesive edge bond produced on a highly automated production line. This research focussed on the thermal and mechanical behaviour and the laboratory testing of this collector. Furthermore, an innovative collector production technique for insulated glazing units was introduced and adapted for collector production. Only limited data was accessible on the mechanical absorber deflection – especially in a hermetically sealed collector that superimposes a pressure change in the gas-filled cavity and the thermal absorber elongation. In simulation and laboratory testing, the impact of different calculation approaches, the thermal elongation of the absorber and its interaction with the pressure change in the cavity was discussed. Based on these outcomes, a finite element model has been validated that could be used to optimise some aspects of absorber design under given design conditions. To investigate the thermal performance of gas-filled collectors, an existing collector model was refined in terms of the convective heat transfer, enhanced and validated for the simulation of gas-filled collectors. A parameter study on the gap sizing in collectors was carried out, which shows practical values for this parameter. Subsequently, a simulation on the efficiency of gas-filled collectors was conducted. The results showed that the efficiency uprating is less than predicted by other research studies. As the lifetime durability of the used adhesive is a crucial aspect, the thermal loads on the seal were derived in a system simulation. This work included a study of possible paths for lowering the high thermal loads on the adhesive and, thus, increasing the collector's lifetime. In addition to this, the annual yield of different argon filled collector versions were compared to a vented reference collector. To demonstrate and document the feasibility of producing a solar collector on a highly automated production line for insulated glazing units, the production process was described more in detail. The interaction between absorber deflection, climatic changes and pressure change between absorber and glazing was analysed. During this sequence, the ageing effects of the adhesive and absorber were documented. Finally, the production method was evaluated by means of an economic analysis, which considered the collector construction costs and the total production costs. In comprehensive testing, different absorber types were analysed for the application as an all-round supported absorber with a fully adhesive edge bond.

The findings in this thesis are in line with the research questions stated in chapter 1.3. A detailed summary with conclusions and the contribution to knowledge for each sector are summarised in the following subchapters. Finally, future research questions that appeared during this research are stated.

10.1 Mechanical analysis

The validated finite element simulation of the absorber and the edge bond made a significant contribution to the understanding of the mechanical loads in a gas-filled collector. A comparison of two calculation approaches including geometrical linearity and non-linearity was carried out. As a result, it was concluded that the non-linear approach results in a higher precision – especially with increasing loads. Unlike claimed in recent published literature, the simulation proved that the thermal absorber elongation as well as a flexible edge bond as absorber support has a major impact on the absorber deflection and cannot be omitted. Beside the pressure change, the edge bond and the thermal absorber elongation, the absorber thickness, the absorber piping, absorber type and the initial absorber shape are playing an important part in the design of a gas-filled collector with an all-round supported absorber. Consequently, the absorber deflection is not symmetric and, thus, a complete absorber model needs to be set up as an asymmetric deflection can occur. Finally, in laboratory and outdoor testing the magnitude of the absorber temperatures, absorber deflection and the pressure change in the cavity was documented. The high mechanical deflections exceeded in many cases the gap size of 10 to 15 mm and led to visible damage on the absorber and edge bond. A combination of the permanent high thermal loads and mechanical stress resulted in two cases in a leakage of the edge bond, which, in turn, lowered the collector efficiency. During the complete testing phase, there was no critical pressure rise in the cavity detected – unlike the assumption made by Vestlund et al. (2009, 2012a, 2012b).

The results of the validated simulation model and the derived results from laboratory testing were merged in an improved absorber structure. A conventional sheet-pipe absorber was reinforced by beadings but will put extra stress on the edge seal, potentially causing failure in a similar manner to the collectors tested with roll-bond absorbers. It was shown that the maximum deflection was decreased, which allows a shorter gap size in solar collectors.

10.2 Thermal analysis

In laboratory testing, a considerable deviation between test results and simulation results was identified. Mainly two aspects caused this deviation: On the one hand, the distance between absorber and glazing was intended to be 10 mm. This value was derived by an initial parameter study according to the convective heat transfer equation of Hollands et al. (1976). These values were in accordance with results that can be found in the literature. However, by visual inspection and subsequent measurements, absorber spots were identified that were in contact with the glazing, which led to a significant increase of the top heat loss. On the other hand, own laboratory results and recently published literature showed a significant deviation between simulations and testing results. Therefore, the adapted collector model was enhanced by an extended equation for the convective heat loss. The simulation results according to Hollands et al. (1976) and Eismann (2015) were compared to the measured results of the convective top heat loss. In fact, the simulation results after Eismann (2015) showed a very good accordance to the measurements results by terms of the convective heat transfer, the efficiency curve as well as the component temperatures. The results after Hollands et al. (1976), however, showed a distinctive underestimation between simulation and laboratory testing of up to 30 % for the convective heat transfer coefficient. Based on the outcomes, the extended equation was confirmed and the simulation model validated. According to the simulation model, a parameter study for practical gap sizes in gas-filled collector were identified; however, these values are also applicable for vented solar collectors. An efficiency analysis for a typical (Al-Cu) sheet-pipe absorber with a gap sizing of 20 mm and 50 mm backside insulation was conducted. For better comparison, the results were referenced to a market available vented flat plate collector. It was demonstrated by simulation and testing that the efficiency increase of a gas-filled collector varies depending on the inert gas for a collector operation point of 0.05 m²K/W between 4 to 7 %. As the adhesive is sensitive to high thermal loads, i.e. magnitude and dwell time, a system simulation was set up to conclude on the thermal loads and the annual yield of an argon filled collector.

A permanent exceedance of the adhesive’s temperature limit will result in an accelerated degradation of the sealant. Consequently, delamination between the sealant and the absorber or leakages in the edge bond are likely to happen. As

a result of the simulation and testing results, it is assumed that the current sealant material is not capable to withstand the thermo-mechanical loads in a solar collector over a lifetime of 20 years. Despite of the leakage or delamination of the primary sealing, the collector will be still operable but the efficiency is decreased. Within the thesis, two countermeasures to reduce the thermal loads on the polymeric were analysed: A reduction of the backside insulation as well as an absorber coating with an increased emissivity. These measures were found to be most appropriate due to their simplicity. In the case of the insulation, cost savings could be put to use. The simulation results of both measures showed a notable reduction of the thermal loads; however, the annual yield was as well reduced.

An annual yield for the initial setting of the gas-filled collector 'TPS-AlCu20' of 5,745 kWh was calculated. This corresponds to a specific yield of 399 kWh/m²a and is about 4 % higher than that of the vented reference collector (384 kWh/m²a). For the versions with the reduced insulation and the higher emissivity of the absorber coating an almost identical annual yield of 5,205 kWh/a and 5,207 kWh/a were computed, which is by about 319 kWh/a or 22 kWh/m²a less than that of the reference collector. If krypton instead of argon is used for the initial collector configuration ('TPS-AlCu20') the annual yield is by 6.6 % higher than that of the vented reference collector. In total figures, this equals an energy output per annum of 5,890 kWh and a specific annual yield of 409 kWh/m²a. Adverse are the even higher thermal loads and the higher costs for the inert gas. If the high thermal loads on the adhesive can be solved by constructive measures or material optimisation, a krypton filled collector would be of interest as of the superior efficiency.

Efficiency tests of the prototypes validated the conducted simulation work in this thesis. In the laboratory testing, three collectors were analysed during several exposition tests in dry stagnation in Germany. Important data, such as the pressure change, magnitude of absorber deflection and component temperatures, were gathered and can be used for further development tasks in this field. The sensitivity to sudden temperature change of the absorber, glazing and the edge bond caused by an internal or external shock test is seen as a flaw of this collector type. In particular, during thermal shock tests, the rigid roll bond absorber seems to induce high mechanical stress on the edge bond, which leads to a leakage in the adhesive sealant. This was also indicated by a gas concentration measurement.

10.3 Collector production

The disadvantages of the current flat plate solar collector was summarised. According to the literature review, the suboptimal collector construction impedes a higher automated production. To tackle this problem, an adhesive production technology adapted from insulated glazing units was applied for solar collector production. This production technology allows a high and repeatable quality and enables a hermetically sealed collector construction. Within the approach, a sealed cavity between absorber and glazing was achieved, which was flooded with an inert gas during the assembly process. As a result of the lower convective heat transfer, the efficiency is increased and at the same time negative environmental effects, such as moisture or contaminatnts that lead to a faster component degradation, can be excluded. By the production of different series of prototypes, the feasibility to adapt this production method was demonstrated.

10.4 Economic analysis

Both collector and production method were evaluated in terms of collector costs and production costs. Furthermore, a conventional collector production line and a vented flat plate collector was defined and used as a reference. It turned out that the adhesive costs had a relevant impact on the total collector costs. Consequently, it is necessary to use as little sealant as possible for a hermetically sealed collector to hold the costs down. By changing the absorber geometry, the adhesive material usage could be reduced by up to 75 %. Furthermore, three different subversions of the production line were presented, which differ in the degree of automation and, thus, in the investment costs. The cost saving potential was evaluated depending on the used production capacity, i.e. 50 % or 100 % utilisation, as well as on the output figures. It was shown that the maximum cost saving potential varied between 5 % for a full-utilised production line and up to 11 % for a production line that is only 50 % in use. Yet, to make use of these savings a certain market demand for solar collectors is required. The volatile solar thermal market has as well a negative impact that cannot be neglected as it aggravates the willingness of invest of collector producers. Ultimately, the high investment costs for the machinery and for the adhesive are showing room for further improvement.

10.5 Contribution to knowledge

Recently published research studies dealt with the thermal and mechanical analysis of gas-filled solar collectors. However, these studies did not consider a suitable production method that is capable of assembling collectors using a highly automated production line nor was an appropriate sealing technique for the gas-filled interspace discussed. Moreover, a detailed mechanical simulation of a hermetically sealed flat plate collector with a fully adhesive edge bond accompanied by extensive indoor and outdoor testing was not conducted as well. As a consequence, practical design guidelines for this type of collector have been so far unavailable. In previous research into this type of collector, simplifications in the modelling and the lack of prototype testing have led to an overestimation of the performance of gas-filled solar collectors.

In this research, in-depth analyses of gas-filled collectors with a fully adhesive edge bond for highly automated production contributed to a better understanding of solar collectors. In the following, valuable and novel findings of this thesis are highlighted:

- For mechanical absorber FE analyses, a comparison between the geometrical non-linear and geometric linear calculation approach showed that the use of the latter leads to inaccurate design parameters. This finding is also applicable for conventional (vented) collectors with a sheet-pipe absorber.
- Contrary to findings of previous researchers, the mechanical simulation results showed that the consideration of the thermal absorber elongation is essential for understanding the absorber's mechanical behaviour. For the sake of accuracy, this behaviour should not be ignored in FE simulations. This insight was validated and strengthened by observations made in the laboratory and in field testing.
- Previous research studies solely focussed on an overpressure in the interspace, as the thermal elongation was not considered. Yet, due to the thermal elongation of the metal sheet, the interspace's volume may be enlarged, which leads to a pressure depression. A critical pressure rise, which could damage the collector components, was not observed during the test.

- It has been found that the superposition of the thermal absorber elongation, pressure change and initial absorber shape leads to an unpredictable sheet deflection. However, the absorber shape plays a major role in the absorber deformation as the sheet's initial distortion is magnified during collector operation. Consequently, this can result in a contact between absorber and glazing, which magnifies the top heat loss significantly.
- The absorber piping affects the mechanical behaviour of the absorber, whereas the absorber sheet dominates the mechanical deflection.
- By simulation studies, a reinforced absorber structure with beadings was introduced. This countermeasure can help to induce a more predictable and, thus, favourable deflection behaviour allowing smaller gap sizes in collectors and more cost-effective designs.
  This study indicated room for further improvement.
- During the thermal analysis of gas-filled collectors, simulation and testing confirmed a recently published convection calculation approach from Eismann (2015). At the same time, it was found that a commonly used convection equation for solar collectors underestimates the convective top heat loss.
- Based on the validated simulation results, practical collector design parameters were derived, which are applicable for both gas-filled and vented collectors.
- The performance analysis showed only a moderate improvement in the efficiency and annual yield of gas-filled collectors compared to vented flat plate collectors.
- Different absorber types were analysed for their suitability for collectors with a fully adhesive edge bond.
- A novel production technique used for the assembly of insulated glazing units was adapted for solar collectors.
- Comprehensive prototype testing showed that there is still research needed into suitable sealing materials in gas-filled solar collectors.

10.6 Future research questions

During this work many scientific questions arose that were judged to be out of scope due to their relevance to the aims of the research and the time available.

A very important and challenging topic will be the detailed modelling of the primary and secondary sealing, i.e. edge bond, whose mechanical properties, such as the stress strain curve, are dependent on the temperature. On the one hand, this is necessary as the costs can be cut down if less material can be used. On the other hand, certain effects that a collector is exposed to, e.g. sudden temperature change during stagnation, need to be simulated to conclude on its impact. Not until then, it will be possible to identify further cost reduction.

The discussion of a reinforced absorber structure in this thesis was rudimentary and should be seen as a starting basis for further research in this context. In particular, a more detailed parameter study on the geometrical properties could be conducted to identify suitable values, e.g. for beading dimensions – such as height or radii. Beyond that, the stress analysis in both edge bond and critical absorber joints need to be investigated. This is an essential question as the absorber holds the highest cost share on a collector. Therefore, cost reductions on this component is most promising to save costs.

In this thesis, sheet-pipe as well as roll bond absorbers were used for the prototype. The latter ones showed a superior thermal performance but caused trouble during the exposition test. Hence, if optimisation potential can be identified and applied, this kind of absorber could be more adequate than a sheet-pipe absorber – especially with krypton as gas-filling.

It would be of interest whether the production technique or parts of the collector aspects are usable for polymeric collectors, e.g. a gastight and inert gas-filled cavity on the backside of a polymeric collector to decrease losses. The use of adhesive for polymeric collectors seems practical and it might be possible to assemble such a collector type with the here described production method.

For large area collectors, which are commonly used in solar district heating, the use of krypton could increase the efficiency compared to a conventional large area collector. However, the mechanical loads will be even more critical than in normal sized collectors. Moreover, is it advantageous to combine several

convective heat loss reducing measures in one collector – such as a hermetically sealed and gas-filled double glazed collector?

Instead of sealing the cavity between absorber and glazing, it might be worth to analyse to seal the complete casing instead – similar to the approaches conducted by Buttinger (2009), Shire et al.(2016) and Henshall et al. (2016). However, this will lead to different challenges than in this approach.

The most vulnerable point was the lifetime durability of the sealant. Against this backdrop, it is plausible to conduct further efforts either in the material optimisation of the butyl sealant or in constructive countermeasures.

Finally, further research should be conducted for the convective heat transfer in solar collectors – especially with shorter gap sizes down to 10 mm.

For all of these possible approaches a combined investigation of mechanical and thermal analysis is plausible and recommended.

References

ABDULLAH, A., ABOU-ZIYAN, H., GHONEIM, A. (2003) *Thermal performance of flat plate solar collector using various arrangements of compound honeycomb*. Energy conversion & management, Volume 44, pp. 3093-3112.

ARNOLD, J., CATTON, I. & EDWARDS, D. (1976) *Experimental investigation of natural convection in inclined rectangular regions of differing aspect ratios.* Transactions of the ASME: Series C, pp. 67-71.

BARTELSEN, B., JANßEN, S. & ROCKENDORF, G., (1993) *Heat transfer by natural convection in the air gap of flat plate collectors*. Proceedings ISES Solar World Congress, pp. 267-273.

BARTELSEN, B., KIERMARSCH, M., ROCKENDORF, G. (1999) *Inclination dependency of flat plate collector heat losses*. ISES Solar world congress 1999, Volume III, pp. 72-75.

BEIKIRCHER, T., (2009) *Hocheffizienter Flachkollektor mit Folienisolation und Überhitzungsschutz für höhere Betriebstemperaturen* FKZ: 0329280A. Final report, München.

BEIKRICHER, T., (2010) *Plastic film insulates flat plate collector*. BINE Informationsdienst, projektinfo 08/10.

BEIKIRCHER, T., OSGYAN, P., REUSS, M., STREIB, G. (2013) *Flat plate collector for process heat with full surface aluminium absorber, vacuum super insulation and front foil*. Energy Procedia 48, pp. 9-17.

BENZ, N., BEIKIRCHER, T. & AGHAZEDEH, B., (1996) *Gas heat conduction in evacuated tube solar collector*. Solar Energy, Band 58, pp. 213-217.

BENZ, N., BEIKIRCHER, T. & AGHAZADEH, B., (1996) Aerogel and krypton insulated evacuated flat plate collector for process heat production. Solar Energy, Band 58, pp. 45-48.

BENZ, N., BEIKIRCHER, T., (1999) *High efficiency evacuated flat-plate solar collector for process steam production*. Solar Energy 65, pp. 111-118.

BERNER, J., (2012) *Bending, welding and more*. Sun, Wind & Energy, February, pp. 56-58.

BERNER, J. & EPP, B., (2010) *Finding the right adhesive*. Sun, Wind & Energy, February, pp. 54-58.

BRAESS, D., (2010) *Finite Elemente Theorie, schnelle Löser und Anwendungen in der Elastizitätstheorie.* 5. Hrsg. s.l.:Springer.

BIRON, M. (2013) *Thermoplastics and Thermoplastic Composites*. 2nd Edition. Oxford (GB): Elsevier.

BRANDMAYR, S. D., (2012) *Optimised thermosyphon solar hot water heater - simulation, design and experimental analysis,* De Montfort University, PhD.

BUCHBERG, H., (1976) *Design considerations for solar collectors with cylindrical glass honeycombs*. Solar Energy, Volume 13, Issue 3, pp. 193-203.

BUCHBERG, H., CATTON, I., EDWARDS, D. (1976) *Natural convection in enclosed spaces a review of application to solar energy*. Transaction of the ASME, Series C, Vol. 98-2, pp. 182-188.

BUCHBERG, H., EDWARDS, D. (1976) *Design considerations for solar collectors with cylindrical glass honeycombs*. Solar Energy, Vol. 18, pp. 193-203.

BUTTINGER, F., (2009) *Entwicklung eines konzentrierenden Vakuum-Flachkollektors zur Prozesswärmeerzeugung*. Dissertation, TU München.

BUTTINGER, F., (2010) *Development of a new flat stationary evacuated CPC-collector for process heat applications*. Solar Energy, Volume 85, pp. 1166-1174.

BYSTRONIC GLASS (2014) *TCO production costs calculation tool.* Internal communication.

CANE, R., HOLLANDS, K., RAITHBY, G., & UNNY, T. (1977) *Free convection heat transfer across inclined honeycomb panels*. Transactions of the ASME: Series C, Volume 99-1, pp. 86-91.

CGA ITALIA SNC (CTO), SAVOSOLAR LTD. (CTO) (2014) *Personal communication*

CITRINSOLAR ENERGIE- & UMWELTTECHNIK (CTO) (2014) Personal communication

COOPER, P.I. and DUNKLE, R.V. (1981) *A non-linear Flat-plate collector model*. *Solar Energy*, Volume 26 (Issue 2), pp. 133-140.

CORMACK, D., LEAL, L. & IMBERGER, J. (1974a) *Natural convection in a shallow cavity with differentially heated end walls. Part 2. Numerical solutions.* J. Fluid Mech., Vol. 65, Part 2, pp. 231-246.

CORMACK, D., LEAL, L. & IMBERGER, J. (1974b) *Natural convection in a shallow cavity with differentially heated end walls. Part 3. Experimental results.* J. Fluid Mech., Vol. 65, Part 2, pp. 247-260.

CUCE, E., RIFFAT, S. (2015) *A state-of-the-art review on innovative glazing technologies*. Renewable and sustainable energy reviews, Volume 41, pp. 695-714.

DIN EN 12975-2 (2006) *Thermal solar systems and components – Solar collectors – Part 2: Test metho*ds; German version EN 12975-2:2006. DIN German Institute for Standardization. Berlin (DE): Beuth Verlag GmbH, pp. 16.

DIN EN ISO 175 (2011) *Plastics; Determination of the effects of liquid chemicals, including water; German version EN ISO 175:2010*. ISO International Organization for Standardization. Berlin (DE): Beuth Verlag GmbH.

DUFFIE, J.A. and BECKMAN, W.A. (2009) *Solar engineering of thermal processes*. 3rd Edition. New York (US): John Wiley & Sons.

EATON, C. B., BLUM, H., (1975) *The use of moderate vacuum environments as a means of increasing the collection efficiencies and operating temperatures of flat-plate solar collectors*. Solar Energy 17, pp. 151-158.

EICKER, U. (2003) *Solar Technologies for Buildings*. 1st Edition. Chichester: John Wiley & Sons.

EISENMANN, W., (2003) *Untersuchungen zu Leistungsfähigkeit und Materialaufwand von Sonnenkollektoren mit serpentinen- und harfenartiger Rohrverlegung.* 490 Hrsg. Düsseldorf: VDI Fortschitt-Berichte.

ESTIF (2012) *Solar thermal markets in Europe.* [Online] Available at: http://www.estif.org/fileadmin/estif/content/market_data/downloads/Solar_Thermal_M%20arkets%202012.pdf
[Last access: 10/10/2014]

EL SHERBINY, S. M., RAITHBY, G. D. & HOLLANDS, K. G. T., (1982) *Heat transfer by natural convection across vertical and inclined air layers*. Journal of Heat Transfer-Transactions of the ASME, Band 104, pp. 96-102.

EISMANN, R., (2015) *Accurate analytical modelling of flat plate solar collectors: Extended correlation for convective heat loss across air gap between absorber and cover*. Solar Energy, Volume 122, pp. 1214-1224.

EISMANN, R., PRASSER, H. (2013) *Correction for the absorber edge effect in analytical models of flat plate solar collectors.* Solar Energy, Volume 95, pp. 181-191.

FISHENDEN, M. & SAUNDERS, O. (1932) *The calculation of heat transmission.* His Majesty's Stationery Office, London, pp. 104-120.

FELDMEIER, F., (1984) *Belastung von Isoliergläsern durch Klimaschwankungen*. Fenster und Fassade, pp. 41-52.

FELDMEIER, F., (1996) *Zur Berücksichtigung der Klimabelastung bei der Bemessung von Isolierglas bei Überkopfverglasung*. Stahlbau, Band 65.

FÖSTE, S. (2011) *Grundlagen für selektiv beschichtete Hochleistungs-verglasungen für Flachkollektoren.* Final report GME .

FELDMEIER, F., (2012) Bemessung von Dreifach-Isolierglas, Stahlbau, DOI: 10.1002, Ernst & Sohn.

FÖSTE, S., (2013) *Flachkollektor mit selektiv beschichteter Zweischeiben-verglasung*. Dissertation, Universität Hannover.

FÖSTE, S., GIOVANETTI, F., MÜLLER, S. & ROCKENDORF, G., (2013) *Temperaturbedingte Verformung von Absorbern in hocheffizienten Flachkollektorenf*. *OTTI Symposium Thermische Solarenergie.*

GEBHARDT, C., (2011) *Praxisbuch FEM mit ANSYS Workbench: Einführung in die lineare und nichtlineare Mechanik.* s.l.:Hanser.

GIOVANETTI, F., KIRCHNER, M. & ROCKENDORF, G., (2011) *Entwicklung eines Sonnenkollektors mit transparenter Wärmedämmung zur Steigerung des Wirkungsgrades bei hohen Betriebstemperaturen,* Emmerthal, Final report DBU (FKZ: 27375).

GIOVANETTI, F., KIRCHNER, M., ROCKENDORF, G. & KEHL, O., (2011) *Entwicklung eines Sonnenkollektors mit transparenter Wärmedämmung zur Steigerung des Wirkungsgrads bei hohen Betriebstemperaturen.* Emmerthal, Final report DBU (FKZ: 27375).

GOSWAMI, D. Y., KREITH, F. & KREIDER, J. F., (2000) *Principles of Solar Engineering.* 2. Hrsg. Philadelphia: Taylor & Francis.

HAFNER, B. et al. (1999) *Carnot Blockset Version 1.0 - Conventional and renewable energy systems optimization blockset - User's guide*. Solar-Institut Jülich, Fachhochschule Aachen.

HENSHALL, P., EAMES, P., ARYA, F., HYDE, T., MOSS, R., SHIRE, G.S.F., (2016). *Constant temperature induced stresses in evacuated enclosures for high performance flat plate solar thermal collectors*. Solar Energy, 127, pp. 250-261.

HOLCK, O., KÖHL, M. & BRUNOLD, S., (2003) *Solar collector design with respect to moisture problems*. Solar Energy, Band 75, pp. 269-276.

HOLLANDS, K. G. T., (1965) *Honeycomb devices in flat-plate solar collectors*. Solar Energy, Volume 9, Issue 3, pp. 159-164.

HOLLANDS, K. G. T., (1973) *Natural convection in horizontal thin-walled honeycomb panels*. Journal of heat transfer, Volume 95, pp. 439-444.

HOLLANDS, K.G.T., UNNY, T.E., RAITHBY, G.D. and KONICEK, L. (1976) *Free convective heat transfer across inclined air layers*. Journal of Heat Transfer, Volume 98, Issue 2, pp. 189-193.

HOLLANDS, K. G. T., IYNKARAN, K. (1984) *Proposal for a compound-honeycomb collector*. Solar Energy, Vol. 34, pp. 309-316.

HOTTEL, H. C., WOERTZ, B. B., (1942) *The performance of flat-plate solar heat collector*. ASME Transactions 64.

HOTTEL, H.C. and WHILIER, A., (1958) *Evaluation of Flat-Plate Collector Performance*. In: Trans. of the Conf. on the Use of Solar Energy, 2 (1), pp. 74-76.

DIN EN ISO 175 (2011) *Plastics; Determination of the effects of liquid chemicals, including water*; German version EN ISO 175:2010. ISO International Organization for Standardization. Berlin (DE): Beuth Verlag GmbH.

DIN EN ISO 15099:2003 (2003) *Thermal performance of windows, doors and shading devices – Detailed calculations.* ISO International Organization for Standardization. Berlin (DE): Beuth Verlag GmbH.

JUNG, M. & LANGER, U., (2013) *Methode der finiten Elemente für Ingenieure: Eine Einführung in die numerischen Grundlagen der Computersimulation.* 2. Hrsg. s.l.:Springer.

KALTENBACH, F., (2013) *Transluzente Materialien: Glas – Kunststoff – Metall*. 1. Auflage, Institut für internationale Architektur-Dokumentation GmbH & Co. KG, München.

KESSENTINI, H., ROSER, C., CASTRO, J., ASSENSI, O., CHIHEB, B., (2014) *Three dimensional heat transfer analysis of combined conduction and radiation in honeycomb transparent insulation*. Solar Energy, Volume 105, pp. 58-70.

KLEIN, S., DUFFIE, J.A. and BECKMAN, W.A. (1974) *Transient considerations of flat-plate solar collectors*. *Trans. of ASME: Journal Engineering for Power*, 96A, pp. 109-113.

KLEIN, B., (2007) *FEM - Grundlagen und Anwendungen der Finite-Element-Methode im Maschinen- und Fahrzeugbau.* 7. Hrsg. s.l.:Vieweg.

KLEIN, B., (2011) *Leichtbau-Konstruktion Berechnungsgrundlagen und Gestaltung.* 9. Hrsg. s.l.:Vieweg + Teubner.

KÖMMERLING CHEMISCHE FABRIK GmbH, (2014) Analyse Niederschlag Funktionsmuster THI, Internal report.

KÖHL, M., KÜBLER, V. & HECK, M., (2007) *Optimisation of the micro-climate in solar collectors*. Solar Energy Materials & Solar Cells *,* Band 91, pp. 721-726.

KOO, J.-M. (1999) *Development of a Flat-Plate Solar Collector Design Program*. Published Thesis (Master of Science), University of Wisconsin-Madison.

LEIBBRANDT, P. & SCHABBACH, T. (2014) *CFD-Untersuchungen zu konvektiven Wärmeverlusten in Scheibenzwischenräume mit großem Seitenverhältnis*. OTTI Symposium Thermische Solarenergie.

MARTY, H., BRUNOLD, S., VOGELSANGER, P. (2008) *Überhitzungsschutz mit thermochromen Solarabsorberschichten*. OTTI Symposium Thermische Solarenergie.

MATUSKA, T. & ZMRHAL, V. (2009) *KOLEKTOR 2.2 – reference handbook*. 1st Edition. Prague (CZ): Czech Technical University.

MEYER, B. & MITCHELL, J., (1979) *Natural convection heat transfer in moderate aspect ratio enclosures*. Heat Transfer*,* Band 101, pp. 655-659.

MÜLLER, H. & ZÖRNER, W. (2008) *Kurzstudie Produktionsprozesse für die Deutsche Solarthermie-Technologie Plattform*. Available at: http://www.solarthermietechnologie.de/fileadmin/img/Service/PDF/Studien/st_ag1_prodtech.pdf [Accessed: 27/07/12].

MÜLLER, H. & ZÖRNER, W., (2010) *State-of-the-Art Collector Production - An Overview.* Berlin: SMEThermal 1st Solar Thermal Materials.

NORDGAARD, A., BECKMAN, W.A., (1992) *Modelling of flat-plate collectors based on monolithic silica aerogel*. Volume 49, Issue 5, pp. 387-402.

PLATZER, W. J., (1988) *Solare Transmission und Wärmetransportmechanismen bei transparenten Wärmedämmaterialien*. Dissertation, Universität Freiburg.

REITER, C., TRINKL, C. and ZÖRNER, W. (2013) *Entwicklung eines Kunststoffabsorbers: Strömungsmechanische und fertigungstechnische Gestaltung*. In: *23. Symposium Thermische Solarenergie, Bad Staffelstein (DE), April 2013*. Regensburg (DE): Ostbayerisches Technologie-Transfer-Institut e.V. (OTTI), pp. 40-41.

RESCH, K., HAUSNER, R. and WALLNER, G. (2009) *Phase separated thermotropic layers based on UV cured acrylate resins – Effect of material formulation on overheating protection properties and application in a solar collector*. *Solar Energy*, Volume 83 (Issue 9), pp. 1689-1697.

RAECKE, I., (2010) *Flächentragwerke I/II Elastische Platten, Universität Magdeburg.* [Online] Available at: www.uni-magdeburg.de/ifme/l-numerik/plattenvorlesung.pdf [Last access: 12/9/2013].

RENEWABLES 2016 GLOBAL STATUS REPORT (2016) [Online] Available at: www.ren21.net/wp-content/uploads/2016/06/GSR_2016_Full_Report.pdf [Last access: 10/11/2016]

REITER, C., (2014) *Polymeric Solar-Thermal Flat-Plate Collectors*. PhD, De Montfort University

REITER, C., TRINKL, C., ZÖRNER, W., HANBY, V.I., (2015) *A Dynamic Multinode Model for Component-Oriented Thermal Analysis of Flat-Plate Solar Collectors*. Journal of Solar Energy 2015, pp. 1–16.

RIESS, H., BRANDMAYR, S., ZÖRNER, W. & GREENOUGH, R., (2013) *Analysis of the mechanical behaviour of an all-round fully adhesive supported absorber*. Energy Procedia

RIESS, H., BRANDMAYR, S., ZÖRNER, W. & GREENOUGH, R., (2014b) *A novel production techniqe for flat plate solar collectors with a fully adhesive edge bond*. DOI: 10.18086/eurosun.2014.16.19, EuroSun 2014, Aix-les-Baines.

KOLLEKTORBAU BERLIN KBB, (2012) *Personal communication.*

ROMMEL, M., WAGNER, A. (1992) Application of transparent insulation materials in improved flat-plate collectors and integrated collector storages. Solar Energy, Vol. 49, pp. 371-380.

ROMMEL, M., SCHÄFER , A., SCHMIDT, V. & SCHMITT, Y., (2003) *Entwicklung neuer doppelverglaster Flachkollektoren mit Antireflex-Glas*. OTTI Symposium Thermische Solarenergie.

SHIRE, G.S.F., MOSS, R., HENSHALL, P., ARYA, F., EAMES, P., HYDE, T. (2016) *Development of an efficient low- and medium-temperature vacuum flat-plate solar thermal collector.* Renewable Energy in the Service of Mankind Vol II: Selected Topics from the World Renewable Energy Congress WREC 2014, Berlin, Boston, Springer International Publishing, pp. 859-866.

STEPHAN, P. (2010) *VDI Heat Atlas*. 2nd Edition. Düsseldorf (DE): VDI-Verlag GmbH.

SYMONS, G., (1984) *Calculation of the transmittance-absorptance product of flat plate collectors with convection suppression devices*. Solar Energy, Vol. 33, pp. 637-640.

SVENDSEN, S., (1992) *Solar collector with monolithic silica aerogel. Journal of Non-Crystalline Solids*. Volume 145, pp. 240-243.

SVENDSEN, S., JENSEN, K. I., (1987) *Flat Plate Solar Collector with Monolithic Silica Aerogel*. ISES Solar World Congress, Hamburg.

TABOR, H. (1958) *Radiation, convection and conduction in solar collectors*. Bulletin of the Research Council of Israel, Volume 8C, pp. 155-176.

TABOR, H., (1959) *Radiation, convection and conduction coefficients in solar collectors*. Solar Energy, Volume 3, pp. 155-176.

TABOR, H., (1969) *Cellular insulation (honeycombs)*. Solar Energy, Volume 12, Issue 4, pp. 549-552.

THERMO|SOLAR (2015) *Vakuumkollektor TS 400*. [Online] Available at: http://www.thermosolar.de/site/index.php/kollektortechnik/vakuumkollektor-ts-400 [Last access: 10/07/2015].

TIGI SOLAR (2015) *The honeycomb collector*. [Online] Available at: http://www.tigisolar.com/the-honeycomb-collector.html
[Last access: 13/09/2015].

TREIKAUSKAS, F.-D. (2009) *Development of a volumetric solar thermal absorber.* De Montfort University, PhD.

VEJEN, N., FURBO, S. & SHAH, L. (2004) *Development of 12.5 m² solar collector panel for solar heating plants*. Solar energy materials & solar cells, Volume 84, pp. 205-223.

VESTLUND, J., RÖNNELID, M. & DALENBÄCK, J.-O., (2009) *Thermal performance of gas-filled flat plate solar collectors*. Solar Energy , Band 83, pp. 896-904.

VESTLUND, J., RÖNNELID, M. & DALENBÄCK, J.-O., (2012a) *Thermal and mechanical performance of sealed, gas-filled flat plate solar collectors*. Solar Energy, Band 86, pp. 13-25.

VESTLUND, J., RÖNNELID, M. & DALENBÄCK, J.-O., (2012b) *Movement and mechanical stress in sealed, flat plate solar collectors*. Solar Energy, Band 86, pp. 339-350.

VOSS, K., BRAUN, P. & SCHMID, J., (1991) *Transparente Wärmedämmung - Materialien, Systemtechnik und Anwendung*. Bauphysik, Band 13, pp. 217-224.

WILKES, G. & PETERSON, C. (1937) *Radiation and convection across air spaces in frame construction*. Heating, Piping and Air Conditioning, Vol. 9, p. 505.

WITTWER, V., STAHL, W., PFLUGER, A., GOETZBERGER, J. (1983) *Heat loss mechanisms in transparent insulation with honeycomb structures*. Optical materials and process technology for energy efficiency and solar application, pp. 101-104.

WRIGHT, J. (1986) *A correlation to quantify convective heat transfer between vertical window glazings*. Transactions American society of heating, refrigerating and air-conditioning.